AD NUMBER

AD864279

NEW LIMITATION CHANGE

TO

Approved for public release, distribution unlimited

FROM

Distribution authorized to U.S. Gov't. agencies and their contractors; Critical Technology; 25 NOV 1969. Other requests shall be referred to Naval Ordnance Lab., White Oak, MD.

AUTHORITY

NOL ltr dtd 15 Nov 1971

NOLTR 69-214

MAGNUS MEASUREMENTS ON THE M823 RESEARCH STORE WITH FIXED AND FREELY SPINNING CRUCIFORM STABILIZERS, FREELY SPINNING MONOPLANE STABILIZERS AND SPLIT-SKIRT STABILIZERS

By
Frank J. Regan
John E. Holmes
Mary Ellen Falusi

25 NOVEMBER 1969

NOL

UNITED STATES NAVAL ORDNANCE LABORATORY, WHITE OAK, MARYLAND

NOLTR 69-214

ATTENTION

NOLTR 69-214

MAGNUS MEASUREMENTS ON THE M823 RESEARCH STORE WITH FIXED AND FREELY SPINNING CRUCIFORM STABILIZERS, FREELY SPINNING MONOPLANE STABILIZERS AND SPLIT-SKIRT STABILIZERS

Prepared by:
Frank J. Regan
John E. Holmes
Mary Ellen Falusi

ABSTRACT: The M823 configuration is an instrumented free-fall store used in bomb stability research programs. This report presents the results of Magnus wind-tunnel tests on the basic forebody with fixed and freely spinning cruciform stabilizers, freely spinning monoplane stabilizers and split-skirt stabilizers.

U. S. NAVAL ORDNANCE LABORATORY
White Oak, Silver Spring, Maryland

NOLTR 69-214 25 November 1969

MAGNUS MEASUREMENTS ON THE M823 RESEARCH STORE WITH FIXED AND FREELY SPINNING CRUCIFORM STABILIZERS, FREELY SPINNING MONOPLANE STABILIZERS AND SPLIT-SKIRT STABILIZERS

The purpose of this investigation was to obtain Magnus measurements on the M823 research store fitted with a variety of fixed and freely spinning stabilizers.

This project was performed at the request of the Bureau of Naval Weapons.

The authors wish to acknowledge the assistance rendered by Mr. Roy Dunavant (NSRDC) for wind-tunnel operation, Mr. Roger Milam (NSRDC) for data reduction and Mr. Richard Ogan (NOL) for instrumentation. Wind-tunnel balance design, including model and drive system, was the work of Mr. Eugene Horanoff (NOL).

GEORGE G. BALL
Captain, USN
Commander

L. H. Schindel

L. H. SCHINDEL
By direction

CONTENTS

ILLUSTRATIONS

ILLUSTRATIONS (Continued)

ILLUSTRATIONS (Continued)

ILLUSTRATIONS (Continued)

TABLE

INTRODUCTION

The Naval Ordnance Laboratory (NOL) has been engaged in a cooperative bomb research program with the Royal Aircraft Establishment (RAE) and the Australian Weapons Research Establishment (WRE). This effort was undertaken primarily to ascertain the suitability of six-degree-of-freedom digital computer trajectory programs for predicting the motion of free-fall weapons. A study of this type became feasible with the establishment of the instrumented bomb research program of the Weapons Research Establishment. As a result of joint meetings among representatives of NOL, WRE and RAE a mutual effort was agreed upon. Within the frame work of this agreement, it was NOL's responsibility to make the required wind-tunnel measurements and to perform some of the trajectory computations.

In addition to comparing the digital computer trajectory calculations with data obtained from the instrumented free-fall stores, it was also decided to extend this cooperative effort to a study of less conventional stabilizers. These stabilizers would include freely spinning cruciform tails, freely spinning monoplane tails and split-skirt tails.

This report presents the results of Magnus wind-tunnel measurements of fixed and freely spinning cruciform stabilizers, freely spinning monoplane stabilizers and split-skirt stabilizers. Other reports present static measurements and damping-in-pitch measurements on all configurations.

SYMBOLS

cp	center of pressure
C_m	pitch-moment coefficient, M_y/QSd
C_n	yaw-moment coefficient, M_z/QSd
C_{n_p}	Magnus-moment derivative, $\partial C_n/\partial(pd/2V_\infty)$
$C_{n_{p\alpha}}$	second-Magnus moment derivative, $\partial^2 C_n/\partial(pd/2V_\infty)\partial\alpha$
C_y	yaw-force coefficient, F_y/QS
C_{y_p}	Magnus-force derivative, $\partial C_y/\partial(pd/2V_\infty)$

$C_{y_{p_y}}$	second Magnus-force derivative, $\partial^2 C_y / \partial(pd/2V_\infty)\partial\alpha$
d	reference length, maximum body diameter
F_y	component of aerodynamic force along y axis
F_M	Magnus force vector
l_x, l_y, l_z	unit vectors along the x, y, z axes
M	Mach number
M_M	Magnus-moment vector
M_z	pitching moment, moment about z axis
p	spin rate, of body about body x axis
$\bar{p}$	reduced spin rate, $pd/2V_\infty$
P_0	stagnation pressure
Q	dynamic pressure, $1/2\rho V_\infty^2$
r	distance from center of gravity to center of pressure
R	gas constant for air
R_e	Reynolds number (based upon body length)
S	reference area, $\pi d^2/4$
T	temperature
V_∞	free-stream velocity
X	body axis from center of gravity to body vertex along longitudinal axis of symmetry
y	body axis orthogonal to x axis and normal to angle-of-attack plane
α	angle of attack, angle between x axis and V_∞ vector
ρ	density of free stream
δ	angle of fin cant

DESCRIPTION OF CONFIGURATIONS

Table 1 lists the various configurations which were considered for both wind-tunnel and full-scale free-fall testing. All configurations used the same basic forebody with the exception of the addition, in some cases, of a yaw probe. The main distinction among the various configurations is in the stabilizer. Each shape in Table 1 is designated by a letter. In the case of the cruciform and monoplane stabilizers, the literal designation is followed by a symbol to indicate the angle of fin cant. Thus, Bδ4 refers to a freely spinning cruciform tail with a four-degree fin cant. Whether the monoplane or cruciform stabilizer is used, all fins have identical cant angles.

In this report Magnus wind-tunnel measurements are given for configurations A, B, C and G. Because the making of Magnus measurements is a rather lengthy procedure it became necessary to reduce the number of originally proposed configurations to fit within a tractable test program. Therefore, the originally proposed shapes were reexamined in the light of tactical advantages and possible operational difficulties. Of course, there were also experimental problems - both in wind-tunnel and free-fall tests - that also influenced the final evaluation.

Any test program would have to include the fixed cruciform stabilizer (designated as A) since this configuration is an operational free-fall store. Further, these Magnus data would be added to a large store of static and dynamic (pitch damping and roll damping) data already in existence. The freely-spinning cruciform stabilizers (configurations B) were retained because this stabilizer had previously shown great promise - both in computer simulations and in the free-fall portions of the program - in avoiding yaw-roll resonance problems. In evaluating the fixed split-skirt stabilizers (configurations C and E) it was felt that Magnus measurements, made at a single skirt opening would be sufficient. This stabilizer has the tactical advantage of providing a variable drag capability (by changing the skirt opening) in a single low-drag carriage. However, it was felt that the additional mechanical complexity needed to deploy and lock the skirts would reduce the attractiveness of the split-skirt from an operational point of view. (It also proved impossible to prevent stabilizer fracture under the high spin rates required in a Magnus test.) Thus, the tests were limited to a skirt opening of 10 degrees (configuration C). The freely spinning split-skirt stabilizers (configurations D and F) were examined briefly at the onset of the program and were eliminated because of mechanical complexity. No wind-tunnel models or free-fall stores were constructed.

The freely spinning monoplane stabilizer (configuration G) was tested both in the wind tunnel and in full-scale free fall. This stabilizer is formed from the freely spinning cruciform by removing two opposing panels. This stabilizer has all the advantages of the freely spinning cruciform. The removal of two panels makes this configuration attractive from the point of view of stowage.

Wind-tunnel models of the cruciform and split-skirt stabilizers are shown in Figure 1. The lower figure presents configuration A, or the fixed cruciform stabilizer. The removal of a small set screw in the model permits the tail to freely spin relative to the forebody. The result is the freely spinning cruciform stabilizer or configuration B. Configuration B is converted into configuration G, the freely spinning monoplane, by removing two opposing stabilizer panels and replacing these with blanks.

The upper figure depicts configuration C or, the split-skirt stabilizer at a 10-degree opening. The split-skirt stabilizer may be formed from the fixed cruciform configuration by removing 1.75 calibers of the aft section of the body and replacing this with a cylindrical section of the same length. This cylinder is then split axially into four equal petals. These petals are rotated about a forward hinge line to make the desired angle with the body's axis of symmetry. As has been mentioned, only the petal configuration making a 10-degree angle with the body's center line was tested.

Figures 2 and 3 present some of the dimensional details of the full-scale cruciform and split-skirt stores, respectively. The wind-tunnel models were 3.5 inches in diameter (about 0.18 of full scale).

EXPERIMENTAL METHOD

All Magnus wind-tunnel measurements were carried out in the Naval Ship Research and Development Center's 7 x 10-Foot Transonic Wind Tunnel. This facility is a continuous flow wind tunnel capable of operating up to 1.5 atmospheres, or up to a Mach number of 1.17. Some of the more significant flow capabilities of this facility are presented in Figure 4.

It will be noted in Figure 4 that there are three operational modes for this transonic tunnel. The table given below shows the Mach number capability in each of these modes:

Mode	Upper Mach Number	Total Pressure (atmospheres)
Test Section Vented	0.70	1.0 to 1.5
Settling Chamber Vented	1.00	1.0
Settling Chamber Evacuated	1.17	0.5 to 1.0

The Magnus effect, at least on the forebody, has its origin in the boundary layer (see Ref. (1)). Therefore, it was felt to be essential to test over a range of Reynolds numbers. This requirement, coupled with a Mach number range of 0.60 to 0.95, led to the decision to use the vented and evacuated modes of wind-tunnel operation.

Also contained in Figure 4 is the altitude equivalent of the test conditions. If the atmosphere is assumed to be isothermal and composed as an ideal gas, it is a straightforward matter to show that the equivalent altitude, h, may be expressed as a function of density, ρ, by

$$h = RT_o \ln\left(\frac{\rho_o}{\rho}\right) \qquad (1)$$

where T is temperature, R the gas constant for an ideal gas and the subscript naught refers to reference, or stagnation, conditions.

If the density ratio--Mach number relationship for a diatomic gas is used, Equation (1) becomes,

$$h = \frac{5RT_o}{2} \ln\left(1 + \frac{M^2}{5}\right). \qquad (2)$$

The total temperature condition for the NSRDC facility under evacuated and vented conditions is 535-degrees Rankine.

The most important single instrument used in making successful Magnus measurements is the wind-tunnel balance. In evaluating the design of a Magnus balance it is necessary to consider the nature of the Magnus effect. The Magnus force acts normal to the angle-of-attack plane; or that plane defined by the free-stream velocity vector and the body's longitudinal axis. The Magnus force, therefore, must be measured in the presence of an orthogonal force (normal force) which is at least ten times greater in magnitude. In addition, these measurements must be made on a body which is spinning.

At the heart of the Magnus balance is the Magnus bridge. These bridges are a special gage section designed to measure the low-level Magnus loads, and to make these measurements with low interaction from the orthogonal normal force. The details of the Magnus bridge are shown in Figure 5, which shows a yaw-plane view of the forward-gage section of the Magnus balance. It will be noted that the gages for measuring yaw are mounted on the eccentric columns. These columns are attached to the balance proper by means of pin joints.

Assume that the balance is subject to a yaw (or in this case Magnus) moment such that the upper fibers are in compression. Due to the eccentric loading on the flexure, secondary bending in addition to that imposed on the balance proper will mechanically amplify the elastic distortion due to the Magnus moment. That is, if the bending experienced by a point on the flexure is compared with that at a point on the balance proper, equidistant from the elastic axis, the point on the flexure will be at about a five times greater stress. Because the flexure is attached to the balance by means of a pin joint, there is low yaw-pitch interaction.

In order to make Magnus measurements it is necessary to mount the model on the balance in such a way that the model is free to spin about its longitudinal axis. Torque can come from a pneumatic or electric motor mounted inside the model; or, obtained by canting the model's tail fins.

For the Magnus measurements on the fixed cruciform and split-skirt stabilized configurations, the model was supported at two points by ball bearings. A variable frequency electric motor spun the model about its longitudinal axis. (Figure 6 is an illustration of this support and drive system.) Because of the large contribution from the fins to aerodynamic damping, it was necessary to provide a 3-to-1 speed-reduction gear box. In the case of the split-skirt configuration it was possible to omit the gear box because of the much lower torque requirements. For the freely spinning stabilizer tests, torque was generated by differential fin cant. Because of the versatile model design it was necessary only to release a set-screw in the rear of the model to uncouple the stabilizer from the forebody. The forebody was locked to the balance by replacing the gear box with a dummy unit which keyed the forebody to the balance.

Figures 7 and 8 illustrate the cruciform and split-skirt stabilizer configurations mounted in the NSRDC transonic facility. Figure 9 presents the sting model base geometry for both the cruciform and split-skirt stabilizers. The dimensions given here are for the wind-tunnel models used at NSRDC.

The technique used for making Magnus measurements will be briefly outlined next. After the tunnel flow had been established the model was brought to angle of attack. In the case of the fixed cruciform (configuration A) and split-skirt (configuration D) the electric motor provided the desired spin rate. While the spin rate was held constant (to within 2 percent) the gage readings were sampled 150 times. These readings were then averaged to give a single load measurement. A data point for a given configuration is defined by the triplet of numbers: angle of attack, spin rate and Mach number. This averaged load is then a single data point. The model spin rate is changed successively throughout its range. Once the range of spin rates have been spanned, the angle of attack is changed and the entire procedure is repeated.

A similar approach is used for the freely spinning cruciform (configuration B) and freely spinning monoplane (configuration G) stabilizers. A modification in the order of spin rate, angle of attack and Mach number variation is necessary because the fin cant is used for torque generation. This requires that a single measurement be made at each angle of attack and Mach number. It is necessary to make measurements over the entire Mach number--angle-of-attack range with a freely spinning stabilizer of fixed fin cant. Spin rate will vary somewhat with changes in Mach number and angle of attack due to changes in fin effectiveness and roll damping. The model is then fitted with a fin of geometrically identical planform but a different angle of fin cant. Again measurements are made at all values in the angle-of-attack-Mach number range. In these tests fins having cant angles of 2 and 4 degrees were used.

DATA REDUCTION

The Magnus force, $\vec{F}_M$, will be defined as a force depending upon body spin rate and angle of attack, and acting normal to the plane established by the spin vector, p, and the free-stream velocity vector, $\vec{V}_\infty$. Mathematically this force, $\vec{F}_M$, and its corresponding moment, $\vec{M}_M$, can be expressed as

$$\vec{F}_M = k\left(\vec{p} \times \frac{\vec{V}_\infty}{V_\infty}\right) \tag{3}$$

and

$$\vec{M}_M = k\left[\vec{r} \times \frac{(\vec{p} \times \vec{V}_\infty)}{V_\infty}\right] \tag{4}$$

where k is a scalar constant for a given set of flow conditions; $\vec{r}$ is the vector distance from the center of gravity to the Magnus center of pressure, along the body's axis of symmetry; and, $\vec{p}$ is the spin-rate vector defined along the axis of symmetry.

All forces and moments are referred to the conventional aeroballistic body axis system; that is, an axis system which is fixed to the body and shows all its rotational and translational motion except spin. In this axis system the x axis is forward along the axis of symmetry; the y axis is to the right when the store is viewed along the positive x axis; the z axis completes a right-handed triad. The origin of this axis system is at the moment reference center taken, in this case, to be the body mid-point. Unit vectors along the x, y, z axes will be defined as $\vec{l}_x$, $\vec{l}_y$, $\vec{l}_z$. The wind-tunnel constraints are such that the x, z plane is vertical; and, that this plane contains the flow velocity vector.

Since $\vec{p} = p\,\vec{l}_x$, $\vec{V}_\infty = (V_\infty\cos\alpha)\vec{l}_x + (V_\infty\sin\alpha)\vec{l}_z$, Equation (3) may be rewritten as

$$\vec{F}_M = -k[p\sin\alpha]\vec{l}_y = F_y\vec{l}_y \qquad (5)$$

where the side force, F_y, is equal to $-kpV_\infty\sin\alpha$. This relationship demonstrates that the Magnus force is an odd function of the angle of attack and spin rate. The Magnus moment equation also may be rewritten using the components of the spin-rate and free-stream velocity vectors. That is,

$$\vec{M}_M = -k(pr\sin\alpha)\vec{l}_z = M_z\vec{l}_z \qquad (6)$$

where the yawing moment, M_z, is equal to $-kpr\sin\alpha$. It can be seen from Equation (6) that the Magnus moment is an odd function in center of pressure location, spin-rate and angle-of-attack. For example if the Magnus center of pressure is ahead of the center of gravity, the Magnus moment would be negative (nose to the left).

The yaw-force and yaw-moment coefficients are defined as;

$$\frac{F_y}{QS} = C_y \text{ and } \frac{M_z}{QSd} = C_n \qquad (7)$$

The above coefficients depend upon the body pressure distribution, which in turn depends upon the compressibility, viscosity and unsteadiness of the flow field. To indicate the degree of simulation

of these effects it is necessary to present coefficients as functions of the appropriate similarity parameters.

Since the free-stream velocity is in the vicinity of the speed of sound, it is necessary to regard the medium as compressible. Simulation of compressibility effects is assured by testing at identical free-flight Mach numbers. Also, since the Magnus effect on the forebody originates entirely in the boundary layer, it is necessary to test at the anticipated Reynolds numbers to simulate viscous effects. Finally, since each surface element on a steadily spinning body experiences a cyclically changing flow field, the test must be made at a parameter which matches flow unsteadiness. In Magnus tests this flow unsteadiness parameter is designated as the reduced frequency, $\tilde{p}$. Testing at identical reduced frequencies assures a matching of the flow angularity at similarily located surface elements on geometrically similar bodies. Thus, it will be postulated in a Magnus test that the coefficients must be expressed as functions of Mach number, Reynolds number and reduced frequency, as well as body angular attitude.

If the Magnus force is assumed to be an analytic function of angle of attack and reduced frequency, the yaw-force coefficient can be expanded in a truncated Taylor series in α and $\tilde{p}$, as;

$$C_y(\alpha, \tilde{p}) = C_y(0, 0) + \frac{\partial C_y}{\partial \alpha}\alpha + \frac{\partial C_y}{\partial \tilde{p}}\tilde{p} + \frac{1}{2}\left(\frac{\partial^2 C_y}{\partial \alpha^2}\alpha^2 + 2\frac{\partial^2 C_y}{\partial \alpha \partial \tilde{p}}\alpha\tilde{p} + \frac{\partial^2 C_y}{\partial \tilde{p}^2}\tilde{p}^2\right) \quad (8)$$

where all derivatives are evaluated at α and $\tilde{p}$ equal to zero. Since,

$$C_y(0, 0) = C_y(0, p) = C_y(\alpha, 0) = 0 \quad (9)$$

it follows that all but the cross derivatives vanish. Thus, Equation (8) becomes, as a first approximation,

$$C_y(\alpha, \tilde{p}) \cong \frac{\partial^2 C_y}{\partial \alpha \partial \tilde{p}}\alpha\tilde{p} = C_{y_{p\alpha}}\tilde{p}\alpha. \quad (10)$$

A similar relationship for the moment coefficient, C_n, would be

$$C_n \cong \frac{\partial^2 C_n}{\partial \tilde{p} \partial \alpha} = C_{n_{p\alpha}}\tilde{p}\alpha. \quad (11)$$

The terms on the right in Equations (10) and (11) are the familiar Magnus force and moment derivatives, respectively, for linear aerodynamics. It should be noted that Equations (10) and (11) are compatible with Equations (5) and (6) for small angles of attack.

Before coming to grips with an analytic description of the problem's nonlinearities it is important to recall the methods of data acquisition. Side-force and yawing-moment measurements were made while the body was spinning at a constant rate and at a fixed angle of attack and Mach number. After measurements were made at six discrete spin rates, the angle of attack was changed and the process repeated.

Such a procedure suggests rewriting Equation (7) as,

$$C_y(\alpha,\tilde{p}) = \frac{\partial C_y(\alpha)}{\partial \tilde{p}}\tilde{p} + \frac{1}{2}\frac{\partial^2 C_y(\alpha)}{\partial \tilde{p}^2}\tilde{p}^2 + \frac{1}{6}\frac{\partial^2 C_y(\alpha)}{\partial \tilde{p}^3}\tilde{p}^3 + \ldots, \quad (12)$$

where the derivatives are evaluated at $\tilde{p} = 0$. Equation (12) may be thought of as an expression for C_y as a polynomial in $\tilde{p}$ with the derivatives - or coefficients - as functions of angle of attack.

At the onset of the test program it was hoped that the Magnus effect would be linear with the reduced frequency and, therefore, Equation (12) could be rewritten as

$$C_y(\alpha,\ \tilde{p}) = \frac{\partial C_y(\alpha)}{\partial \tilde{p}}\tilde{p} \quad . \quad (13)$$

In the case of the tests of the split-skirt stabilizer (configuration C) the Magnus force and moments were found to be linear with the reduced spin rate. However, for all other configurations - fixed and freely-spinning cruciform stabilizers - the Magnus effect was nonlinear in the reduced frequency as well as the angle of attack. Thus, in the case of the cruciform configurations it was necessary to present the yaw-force and yawing-moment coefficients as functions of the reduced frequency.

DISCUSSION OF RESULTS

Figures 10 to 110 contain the entire collection of Magnus data obtained on the M823 Research Store. These data include measurements made on the basic fixed cruciform configuration as

well as configurations with the freely spinning cruciform, freely spinning monoplane and the split-skirt stabilizers.

It was mentioned in the previous section that it was not possible to linearize the Magnus moment, in spin rate, except in the case of the split-skirt stabilizer. Thus, it is necessary to express the yaw force and moment as functions of the reduced spin rate.

Figures 10 through 20 present the yaw force as a function of reduced spin rate for Mach numbers of 0.70, 0.85 and 0.95 and over an angle of attack range of from 0 to 20 degrees. Figures 21 through 30 give the yaw-moment coefficient versus reduced frequency over the same range of values. If the reduced spin rate remains below 0.04, it would be possible to linearize the yaw-force and moment measurements. Above a reduced spin rate of 0.06, especially at the higher angles of attack, the nonlinearities in the Magnus force and moment become evident. If the reduced spin rate is thought of as being approximately the angle of attack due to roll rate experienced by a fin panel, a reduced spin rate of 0.06 would correspond to about 3.6 degrees of angle of attack. In examining the static measurements made earlier in the program (see Ref. (2)), it is obvious that the normal force is linear with angle of attack below 20 degrees. Thus, nonlinearities of the Magnus effect with reduced spin rate must be explained through other than static aerodynamics.

Evaluating the trends of Magnus measurements is difficult because of the lack of quantitative understanding of the phenomenon. Two theories for finned bodies have been advanced which deserve at least passing mention here. One is the qualitative theory of Platou (Ref. (3)) and the other is a quantitative theory due to Benton (Ref. (4)). Both of these theories assume that the Magnus effect originates entirely in the stabilizer. In other words, the distortion of the boundary layer on the forebody due to spin rate of the forebody (considered by Martin in Ref. (1)) is ignored.

Platou points to the body-induced flow interference on the leeward fin as the source for the Magnus effect. According to this theory the pressure distribution on the leeward and windward fins acts at right angles to the angle-of-attack plane. Thus, a decrease in the pressure distribution on the leeward fin (due to forebody interference) means that there is a net force on the body which acts normal to the angle-of-attack plane. For a clockwise spin (viewed from the rear) the net force should be to the right (or, in a positive direction).

Benton's theory recognizes that the normal-force vectors on the fins, which are instantaneously perpendicular to the angle-of-attack plane, are not parallel (Ref. (4)). The result is a couple acting to move the body vertex out of the angle-of-attack plane. The sign of the couple is negative; that is, for a positive spin rate, the couple tends to move the vertex to the left. Benton shows that this couple is proportional to the angle of fin cant. The so-called Benton Magnus moment is identical to the yawing moment, due to differential aileron deflection which is familiar to aircraft engineers. Since most of the fixed cruciform Magnus measurements present here are for the A80 configuration (zero fin cant), the application of Benton's theory is not appropriate.

Some of these Magnus measurements may be examined in light of the flow interference hypothesis of Platou. At low spin rates, and at low angles of attack, the yaw moment is negative (see for example Fig. 21 for α = 4.05 degrees). Under the same conditions the side force is also negative. This means that the Magnus center of pressure is forward of the body midpoint (moment reference center). As the reduced spin is increased above 0.06, the Magnus center of pressure moves rearward, causing the moment to become positive. According to the flow interference theory of Platou, the Magnus force is positive to the right. The force on the forebody should be to the left if consistency with measurements made on spin-stabilized weapons (see Ref. (5)) for example) is to be maintained. At higher angles of attack (Figs. 12 and 23), the yaw force is large and negative, while the yaw moment is positive, for small reduced spin rates, becoming negative for the higher reduced spin rates. It appears difficult to make any real evaluation of the flow-interference hypothesis at this point.

A positive yawing moment may be due either to a movement of the forebody center of pressure, rearward, past the moment reference center; or due to a positive force acting at (and due to) the stabilizer rotation. It will be found, subsequently, that when a modification is made to body geometry in the vicinity of the body vertex, such as by the adding of a yaw probe, the sign of the Magnus force (and moment) will change.

It seems that the effect of the forebody on the fins is far more complex than simply causing a velocity defect through a wake. Adding to the above complexity the yaw force changes sign at a Mach number of 0.95 (see Fig. 13).

Figures 31 through 58 present yaw-force and moment measurements over the same angle of attack and reduced spin-rate range. This set of measurements was made at a total pressure of one atmosphere,

and at essentially twice the Reynolds number. In this second set of Magnus measurements the moment is positive up to a Mach number of 0.85 (see Figs. 51 through 53). The Magnus force is still to the left (or negative) so it may be concluded that either the Magnus force (due to the stabilizer) is negative, or that the Magnus force on the forebody dominates. Later, when the freely spinning cruciform measurements are examined it will be seen that the Magnus or yaw force is positive; this seems to support the flow interference theory. However, it will also be shown that the presence or absence of the probe can drastically affect the sign of the yaw force. Thus, it is not possible to entirely resolve even the qualitative contribution of the stabilizer.

One aspect of the problem which can be examined is the relative magnitude of the forebody contribution to the overall Magnus force. One fair assumption might be to regard the forebody flow as unaffected by the flow field of the stabilizer. (The converse would be a worse and, at times, an unacceptable assumption.) The forebody then might be likened to a spin-stabilized projectile.

Reference (5) is a compendium of Magnus measurements on research projectile shapes. For a 7-caliber body at a Mach number of 0.80, an angle of attack of 4 degrees and a reduced spin rate of 0.1, the yaw-force coefficient, C_y, is -0.018. This value might be compared with a value of -0.02 taken from Figure 37. Quite obviously then a large contribution to the Magnus effect on a fin-stabilized configuration comes from the forebody. This points to the inadequacy of explaining the Magnus effect solely in terms of fin-flow interference (Ref. (3)) or fin cant (Ref. (4)).

Attention has been called to the effect of Mach number on the yaw forces and moments. To illustrate this effect Figures 59 through 62 have been prepared from the material given earlier. In these figures the yaw force and moment are presented as direct functions of the reduced Mach number. All of these data were taken from six-degree angle-of-attack measurements. The data in Figures 59 and 60 were measured in a flow of one-half-atmosphere stagnation pressure. In Figures 61 and 62 the flow-stagnation pressure was one atmosphere.

If one accepts the postulate that the Magnus force on the forebody is negative, or to the left (Refs. (1) and (4)), and on the stabilizer positive, or to the right (Ref. (3)), then some interesting conclusions may be drawn from Figures 59 and 60. At the Mach number of 0.70 the net yaw force is negative but the yaw moment is positive. According to the above postulate the forebody Magnus force dominates. Further, this force acts aft of

the mid-point moment reference center if it is to give a positive moment. As the Mach number increases the Magnus center of pressure moves aft. This postulate is entirely consistent with measurements made on finless bodies (Ref. (5)). At a Mach number of 0.85 the Magnus force on the stabilizer had increased. This increase of Magnus force on the stabilizer, with increasing Mach number, is consistent with measurements made on the freely spinning stabilizer. These measurements will be discussed subsequently. Since the forebody and stabilizer forces are nearly equal, but opposite in sign, the result is a negative couple which is being applied to the body. If the forebody force is slightly greater, the net force is negative but considerably reduced in magnitude over the same measurements made at Mach 0.70. As the Mach number increases to 0.95 the Magnus center of pressure for the forebody moves further aft until it nearly coincides with the center of pressure of the stabilizer Magnus force. The Magnus force on the stabilizer has increased further so that it dominates. The result is a positive net force acting on the body; and, since this force acts aft of the moment reference center, the net moment is negative.

In Figures 61 and 62 essentially the same phenomenon is observed. Figure 61 shows that the yaw force is always negative even though it decreases in magnitude as the Mach number increases. The Magnus force on the forebody is recognized as being essentially viscous in origin (Ref. (1)) and, therefore, should increase with increasing Reynolds number. On the other hand, the yaw force on the stabilizer may be described, at least in part, by potential flow methods (Ref. (4)). Thus, the stabilizer would not be expected to be strongly influenced by viscous effects. Speculations, such as those above, are not conclusive; and their resolution must await more definitive experiments.

One of the most unexpected aerodynamic inputs into this cooperative free-fall research program has centered about the addition of a yaw probe at the body vertex. Originally its presence was expected to have negligible effect on the aerodynamic loads. Attention was focused on its presence when free-fall telemetry records of body motion differed markedly from the computer predictions. Subsequently, wind-tunnel measurements were made of the yaw force and moment in the presence and absence of the yaw probe. Figures 63 and 64 indicate the influence of the probe on the A50 configuration at a Mach number of 0.85. Clearly, the addition of the probe changes the yaw force from negative to positive and the moment from positive to negative. No adequate theory from fluid mechanics presently exists to explain this change in sign. A bibliography, summarizing work done in the area of vortex shedding, is given by Reference (6).

Figures 65 through 88 present the yaw force and moments as a function of angle of attack. These figures also present Magnus data on the Aδ2 and Aδ4 configurations.

Figures 89 through 94 present the yaw force and moment on the freely spinning cruciform configurations at Mach numbers of 0.70, 0.85 and 0.95. It will be noted, immediately, that the yaw force is positive - the sign which was predicted by the interference theory. In making these tests the forebody was fixed to the balance and only the stabilizer was allowed to spin freely. There is clearly a decrease in the steady-state spin rate with increasing angle of attack. Also, at small angles of attack the yaw force and moment are weak functions of reduced frequency; but the dependency of load on spin rate increases with angle of attack. Unfortunately, measurements were made at only two fin-cant angles (2 and 4 degrees) so that it is difficult to draw any detailed conclusions regarding the Magnus loads. These freely spinning cruciform measurements had been used earlier, to support speculations based upon the qualitative flow-interference theory. Yet it was shown that, at least in the case of the fixed cruciform stabilized configurations, the presence of the yaw probe drastically changed the Magnus effect. Of course, when Figures 63 and 64 were made the forebody was also spinning. Unfortunately no measurements have been made for the freely spinning cruciform and monoplane configurations without a yaw-meter probe.

Figures 95 through 100 present yaw-force and moment measurements, for the freely spinning monoplane stabilizer, at Mach numbers of 0.70, 0.85 and 0.95. These conditions are identical to those used for testing the freely spinning cruciform (Figs. 89 through 94). It might be of some advantage to compare the freely spinning monoplane and cruciform configurations in order to determine what effect the removal of two opposing stabilizer panels has on the Magnus characteristics. This can be done by comparing the two configurations at (say) a Mach number of 0.70. It will be noted that the Magnus force on the monoplane stabilizer is somewhat larger than half of that for the cruciform stabilizer.

Figures 89 through 100 present yaw-force and moment measurements made on the freely spinning stabilizer. These figures should be accepted only as indicators of trends and relative orders of magnitude. Unfortunately there is only a sparse coverage of the spin range (only two fin-cant angles) and irregular angle-of-attack dependency. For this reason it is felt that further examination of the Magnus characteristics for a freely spinning stabilizer should be carried out before such measurements can be accepted, quantitatively.

Figures 101 through 110 give the Magnus characteristics of the 10-degree split-skirt stabilized configuration at Mach numbers of 0.70, 0.80, 0.85, 0.90 and 0.95. For configurations given earlier in this report the Magnus measurements were presented in terms of the yaw-force and moment coefficients. In the case of the split-skirt stabilizer, the yaw coefficients exhibited sufficient linearity with spin rate so that it was possible to use only the slopes as representative of the Magnus effect. These slopes are called the Magnus force and moment derivatives.

Linearity of the yaw force and moment with spin rate is not too surprising, since at high rotational speeds the configuration appears to be a body of revolution. It is interesting to note that the Magnus force and moment derivatives, when plotted versus angle of attack, have a rather sudden change in slope at an angle equal to near the petal half angle - 10 degrees in this case. If the angle of attack of the weapon was below 10 degrees it would be possible to employ Equation (11) and obtain the second Magnus force and moment derivatives.

CONCLUSIONS

This report has shown that it is possible to make meaningful Magnus measurements on finned configurations at subsonic and transonic airspeeds.

In the operation of this test program certain difficulties were encountered which were not anticipated at the onset of the testing. First, the Magnus effect on finned bodies was found to be nonlinear with reduced spin rate. Initially, it was felt that, based upon linear aerodynamics, the yaw force and moment should be quite linear within the range of reduced spin rates used here. The effect of fin-cant angle was not expected to be as severe as measurements have indicated. Future work should include a comparison between measurements made using the internal drive motor as a power source and with fin cant. The freely spinning body configurations have certain curious behavior characteristics which can be resolved only through more tests using a larger number of fin-cant angles. Further testing should also be done to investigate the effect of forebody protuberances on the Magnus effect. In doing this future work, certainly low-speed flow visualization studies should be made. Finally, an adequate assessment should be made of the theoretical approaches to the Magnus effect problem. Since the flow-interference hypothesis seems promising it is recommended that a fruitful set of experiments might consist of a set of measurements to determine the pressure distribution on a body fitted with a spinning-cruciform stabilizer.

REFERENCES

(1) Martin, John C., "On Magnus Effects Caused by the Boundary Layer Displacement Thickness on Bodies of Revolution at Small Angles of Attack," Journal of the Aeronautical Sciences, June 1957.

(2) Regan, F. J., Falusi, M. E., Holmes, J. E., "Static Wind-Tunnel Test of the M823 Research Store with Fixed and Free Spinning Tails," NOLTR 65-14, 1967.

(3) Platou, A. S., "The Magnus Force on Finned Bodies," BRL Report 1193; Ballistic Research Laboratories, Aberdeen Proving Ground, Maryland, 1963.

(4) Benton, E. R., "Supersonic Magnus Effect on a Finned Missile," AIAA Journal, Vol. II, No. 1, Jan 1961.

(5) Greene, J. E., "A Summary of Experimental Magnus Characteristics of a 7 and 5 Caliber Body of Revolution at Subsonic through Supersonic Speeds," NAVORD 6110, 1958.

(6) Larock, B. E., "Literature Survey on Vortex Formation and Shedding," Technical Note 4061-102, U. S. Naval Ordnance Test Station, China Lake, California, Sep 1963.

TABLE I

CONFIGURATIONS AND STABILIZERS

A. Fixed Cruciform Tail, δ = 0, 2, 4 Degrees

B. Free-Spinning Cruciform Tail, δ = 2, 4 Degrees

C. Fixed Split-Skirt Tail, Skirt Angle 10 Degrees

D. Free-Spinning Split-Skirt Tail, Skirt Angle 10 Degrees

E. Fixed Split-Skirt Tail, Skirt Angle 15 Degrees

F. Free-Spinning Split-Skirt Tail, Skirt Angle 15 Degrees

G. Free-Spinning Monoplane Tail, δ = 2, 4 Degrees

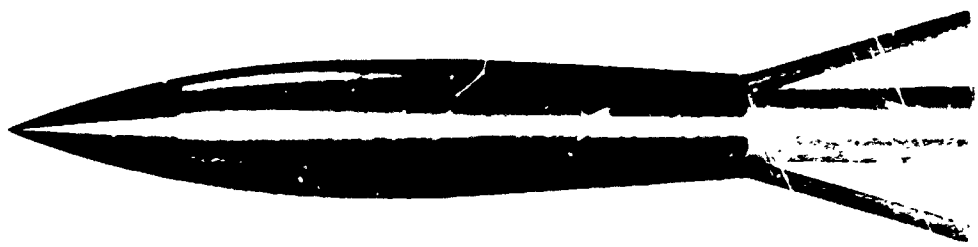

SPLIT SKIRT STABILIZER

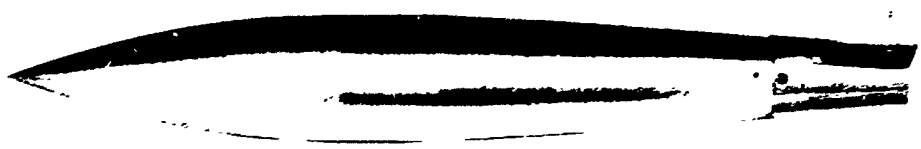

CRUCIFORM STABILIZER

FIG. 1 CONFIGURATIONS OF THE M823 FREE-FALL RESEARCH STORE

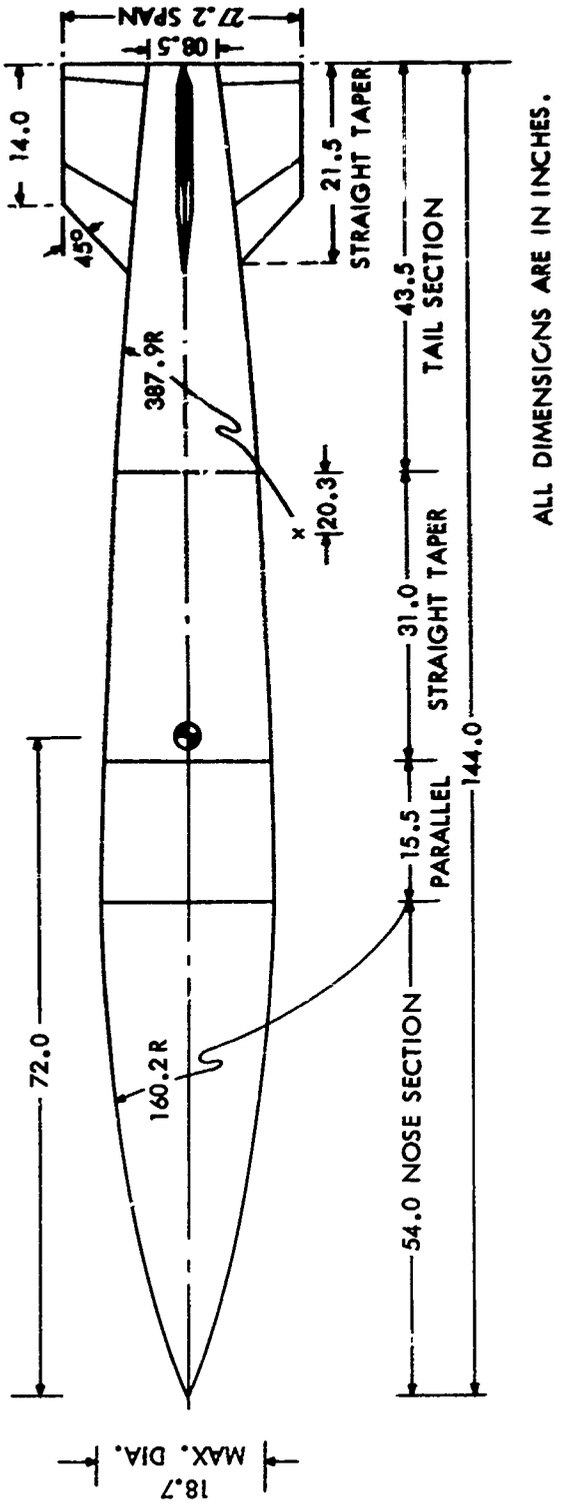

FIG. 2 M823 FREE-FALL RESEARCH STORE WITH A FIXED CRUCIFORM STABILIZER

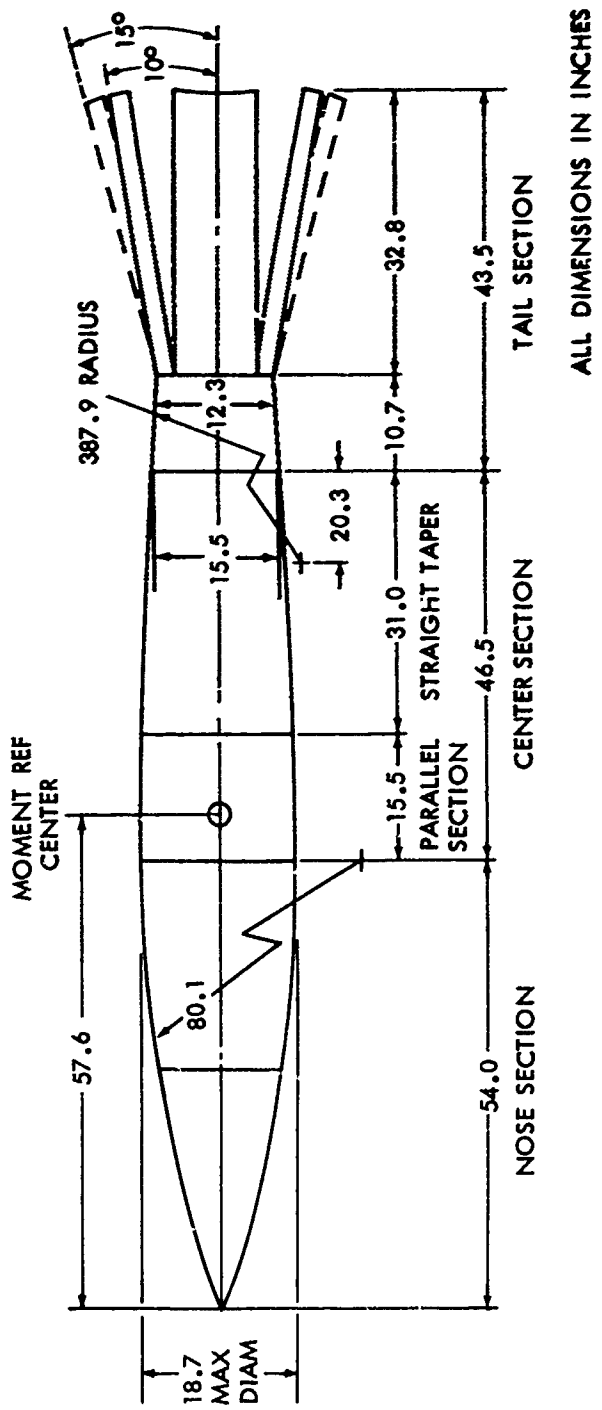

FIG. 3 M823 FREE-FALL RESEARCH STORE WITH A SPLIT SKIRT STABILIZER

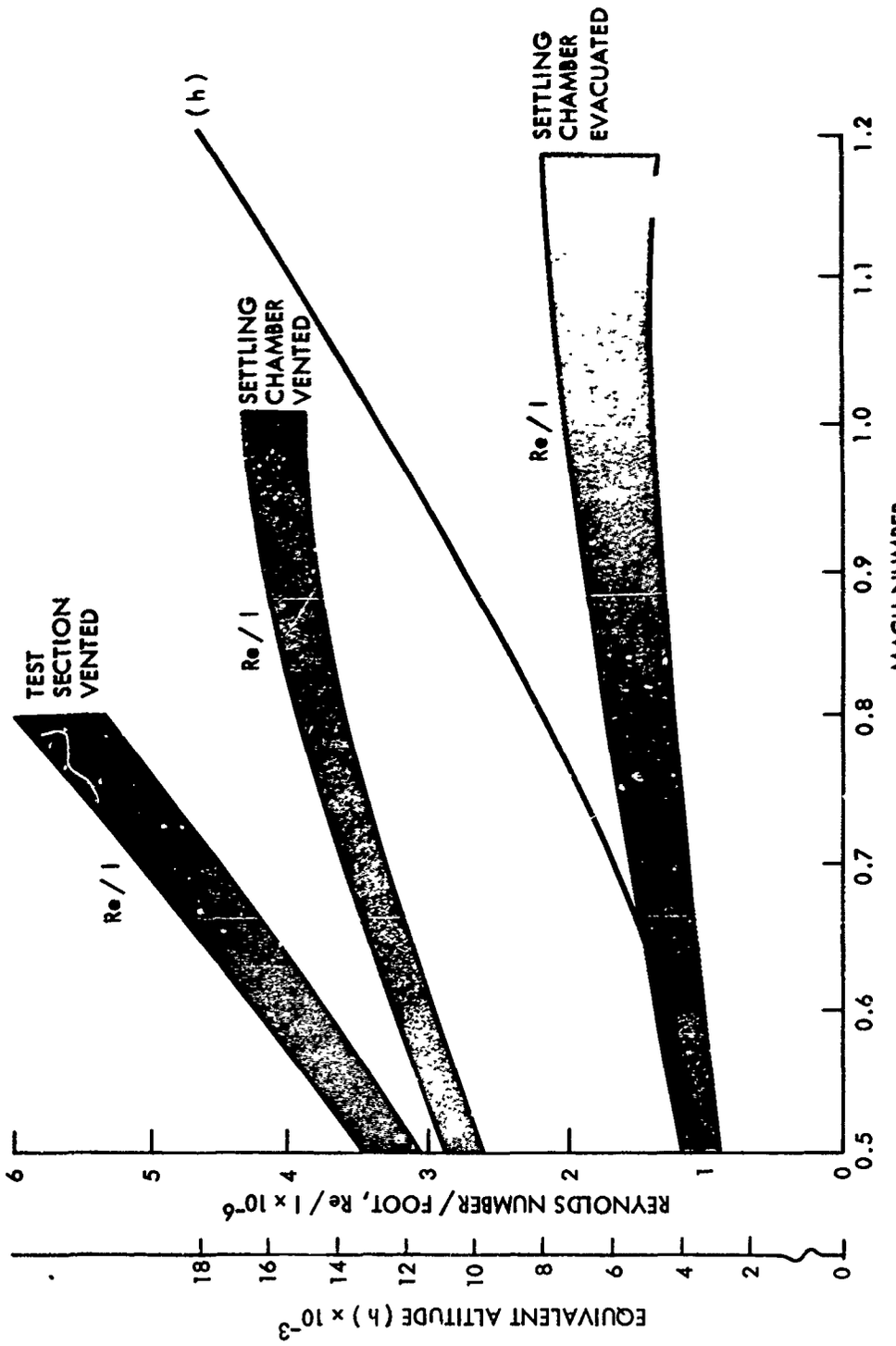

FIG. 4 REYNOLDS NUMBER PER FOOT AND EQUIVALENT ALTITUDE VERSUS MACH NUMBER IN THE NAVAL SHIP RESEARCH AND DEVELOPMENT CENTER 7 BY 10 FOOT TRANSONIC TUNNEL

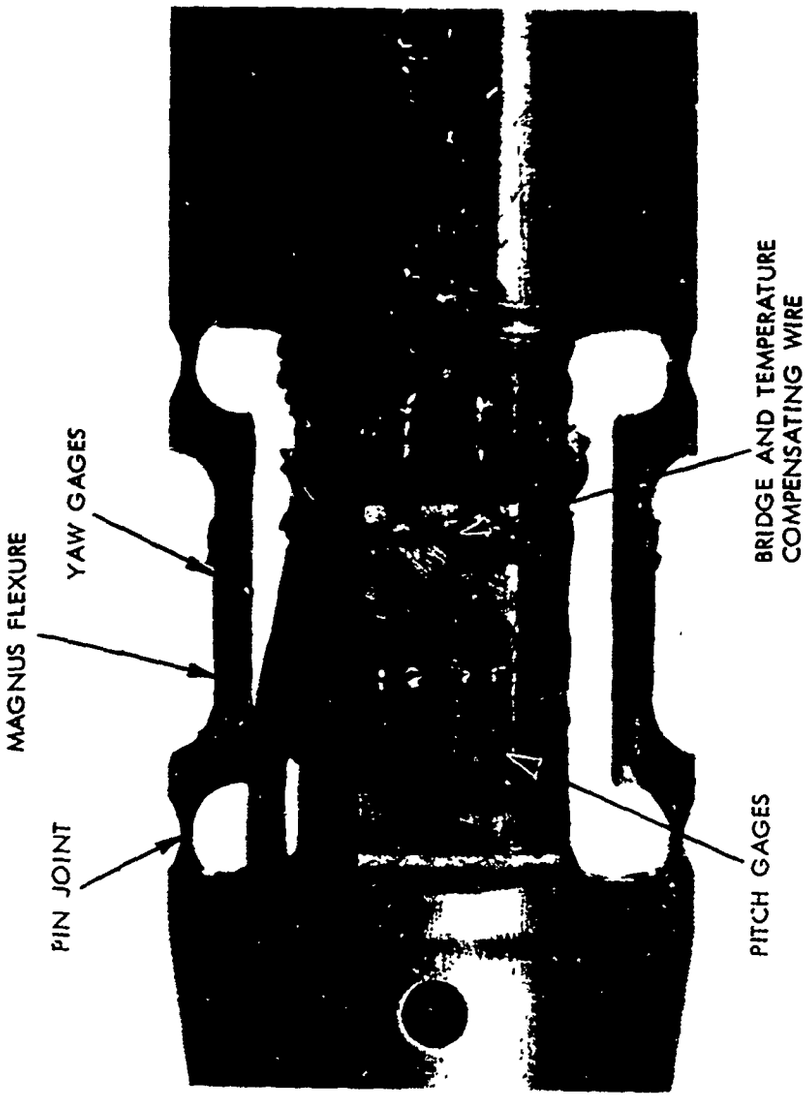

FIG. 5 DETAILS OF MAGNUS BRIDGE

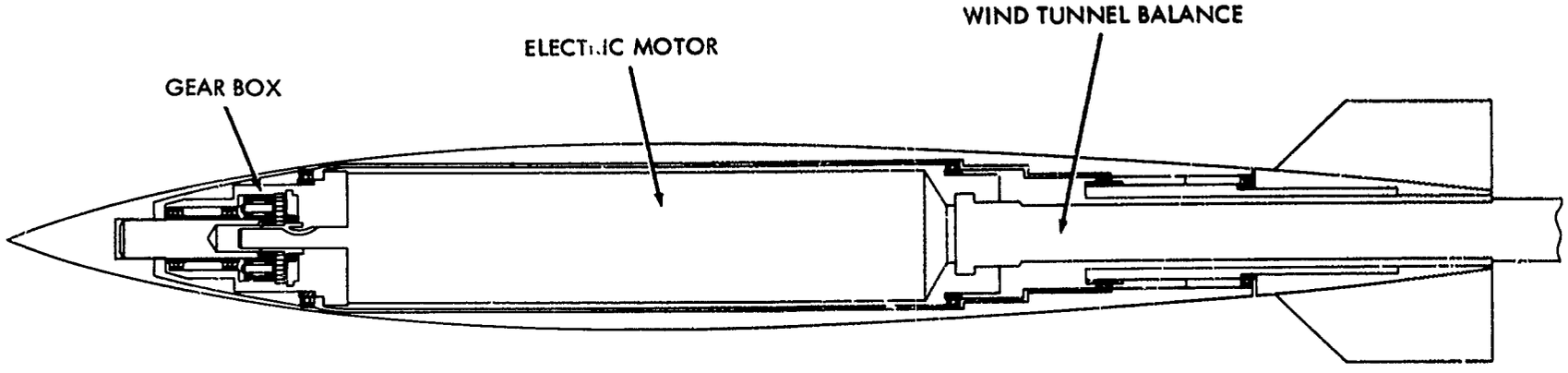

NOLTR 69-214

FIG. 6 MAGNUS WIND TUNNEL MODEL OF THE M823 FREE-FALL RESEARCH STORE WITH A FIXED CRUCIFORM STABILIZER

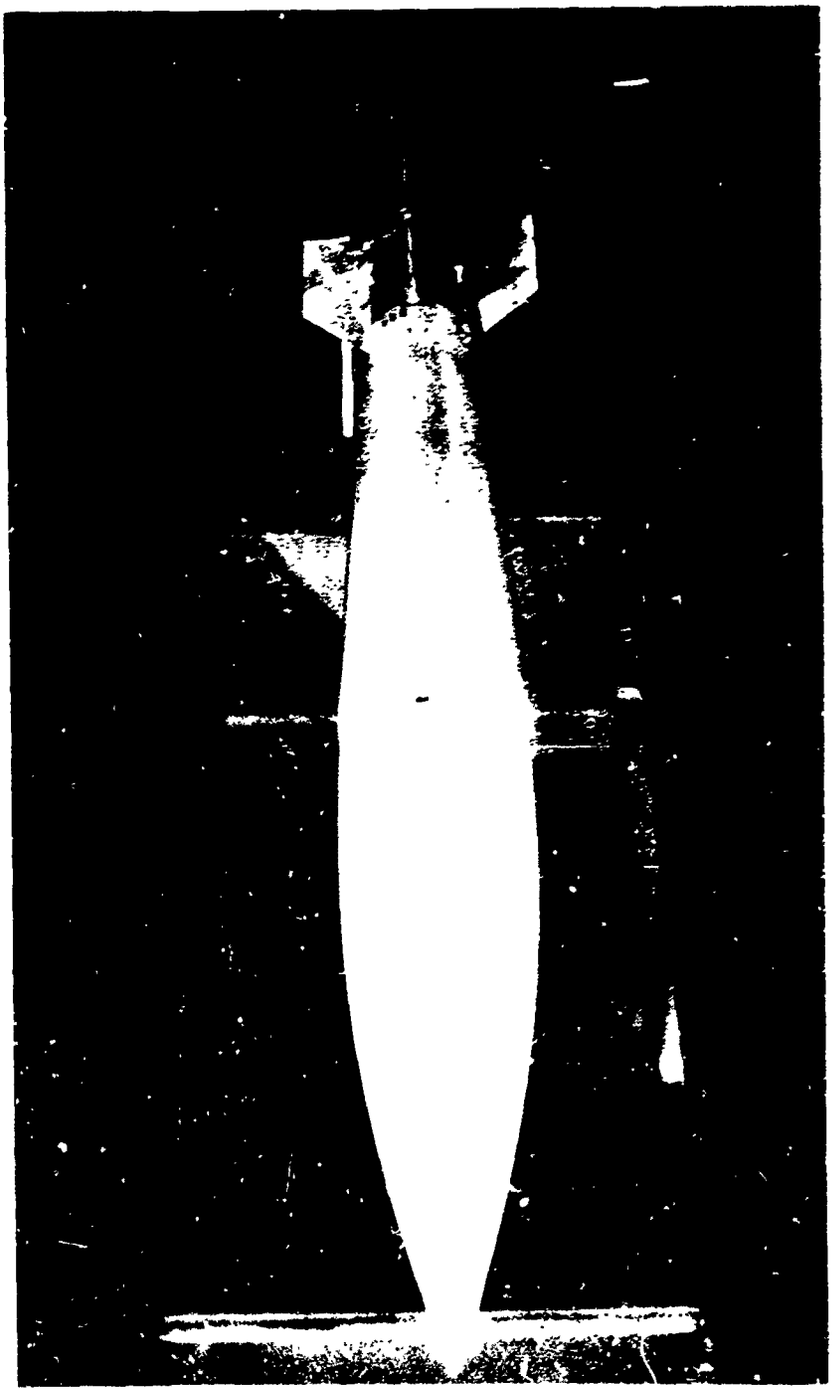

FIG. 7 MAGNUS MODEL OF M823 FREE-FALL RESEARCH STORE WITH A FIXED CRUCIFORM STABILIZER IN THE NSWDC TRANSONIC WIND TUNNEL

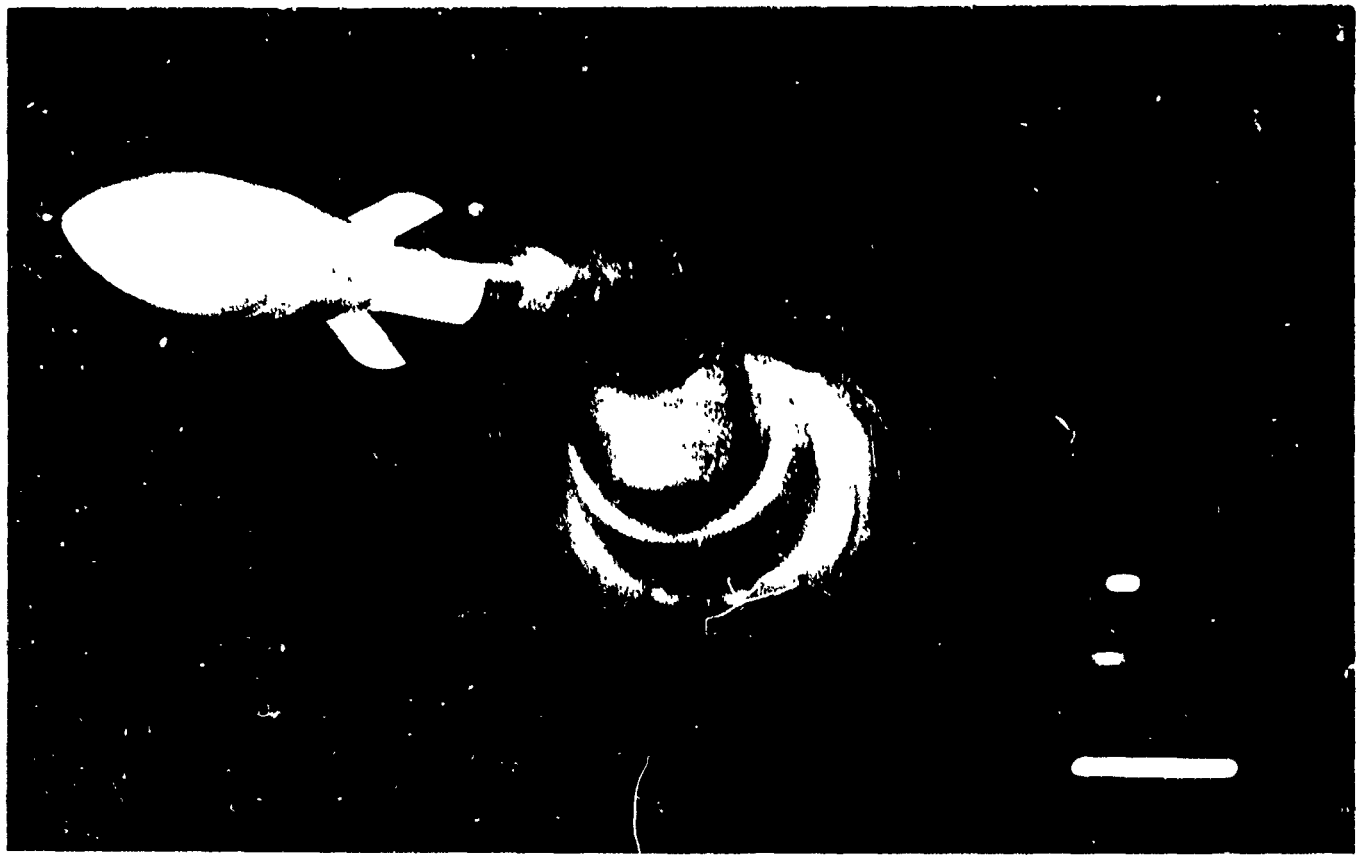

FIG. 8 MAGNUS MODEL OF M823 FREE-FALL RESEARCH STORE WITH SPLIT SKIRT STABILIZER IN THE NSRDC TRANSONIC WIND TUNNEL

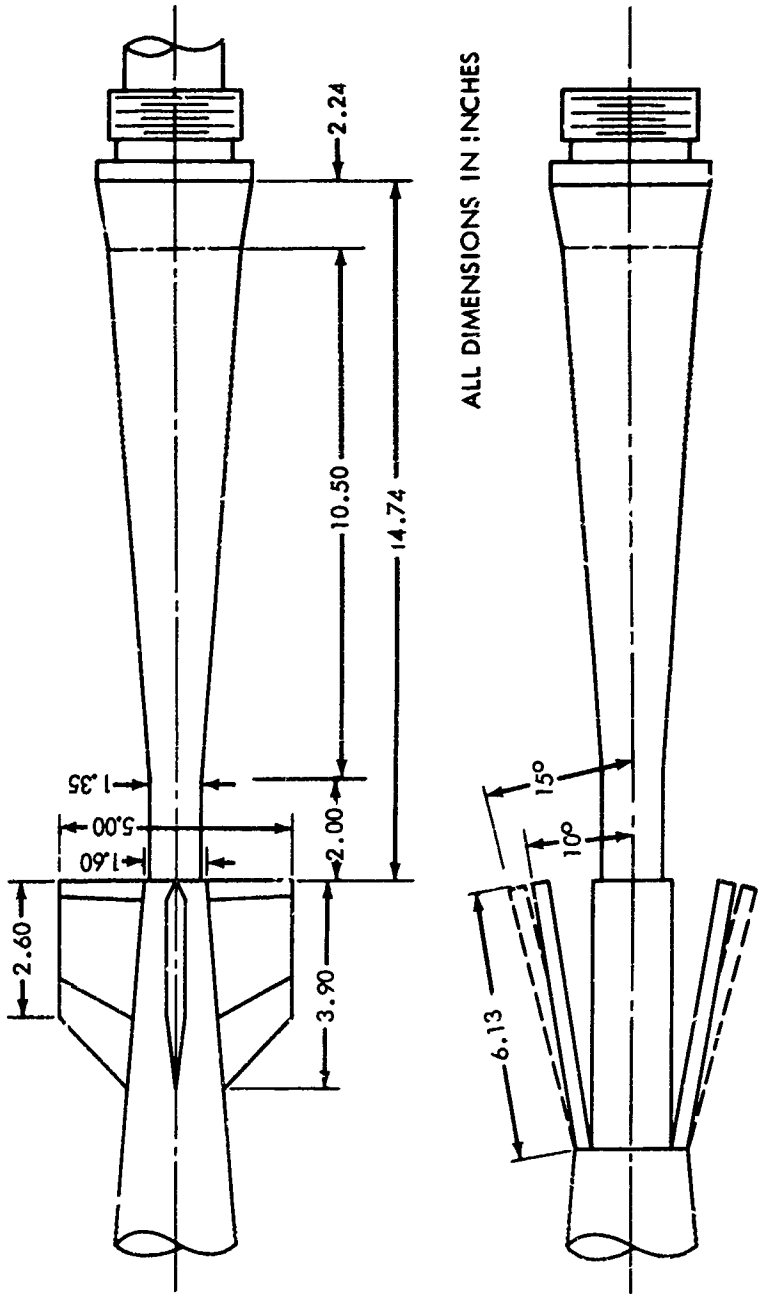

FIG. 9 STING GEOMETRY FOR CRUCIFORM AND SPLIT-SKIRT STABILIZERS

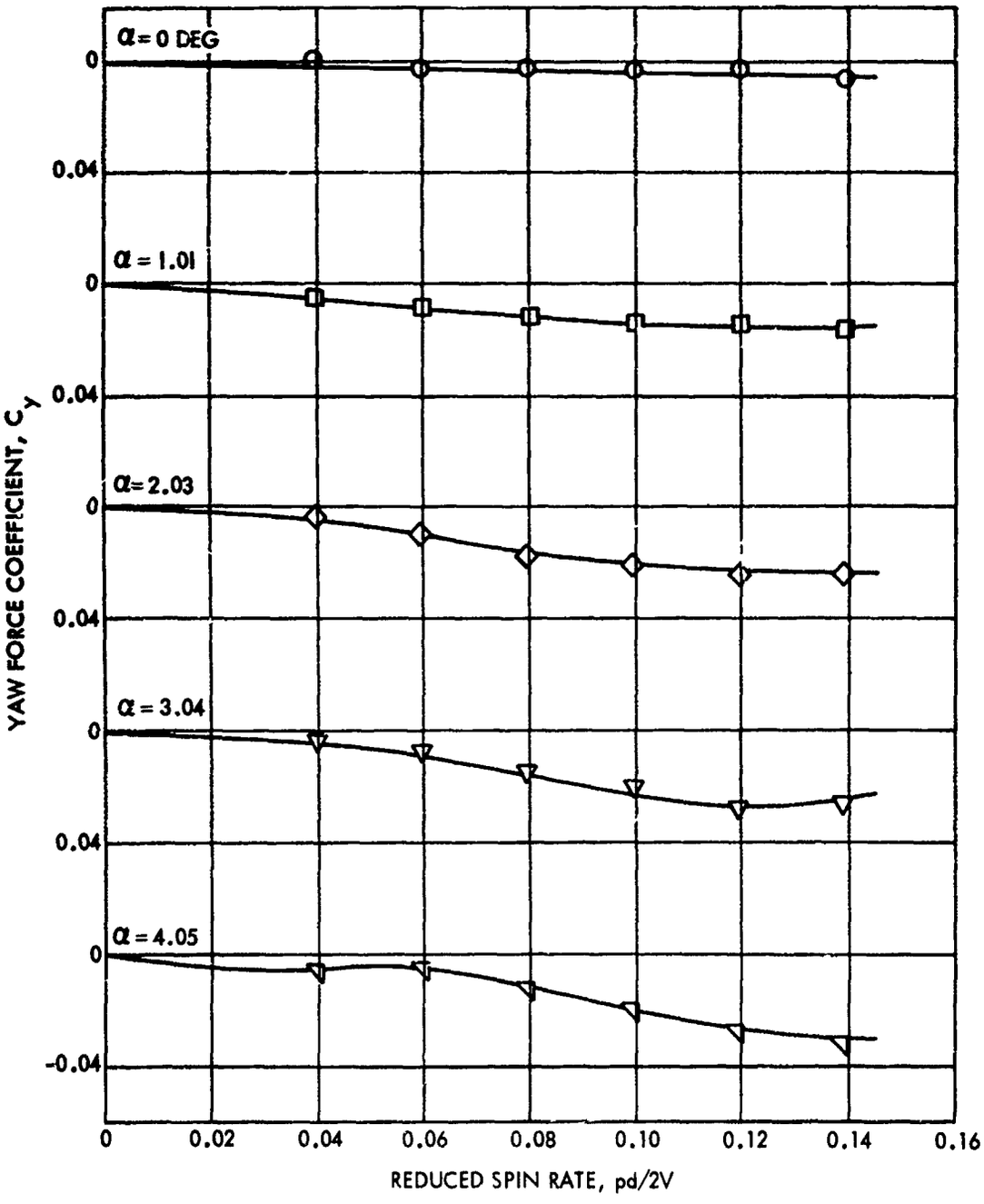

FIG. 10 YAW FORCE COEFFICIENT VERSUS REDUCED SPIN RATE AS A FUNCTION OF ANGLE OF ATTACK FOR CONFIGURATION Aδ0 AT A MACH NUMBER OF 0.70 AND A REYNOLDS NUMBER OF 0.545×10^6

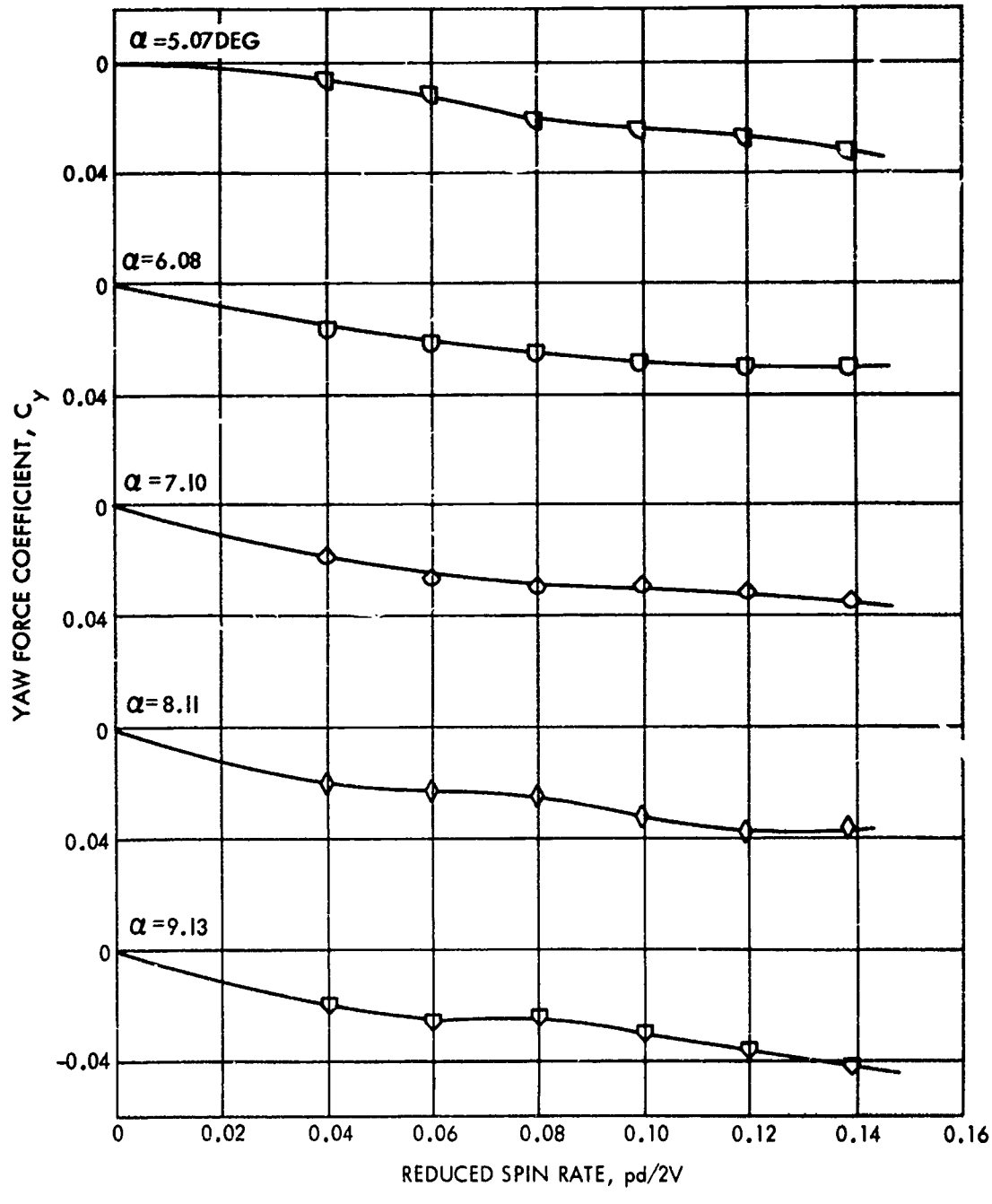

FIG. 11 YAW FORCE COEFFICIENT VERSUS REDUCED SPIN RATE AS A FUNCTION OF ANGLE OF ATTACK FOR CONFIGURATION Aδ0 AT A MACH NUMBER OF 0.70 AND A REYNOLDS NUMBER OF 0.545×10^6

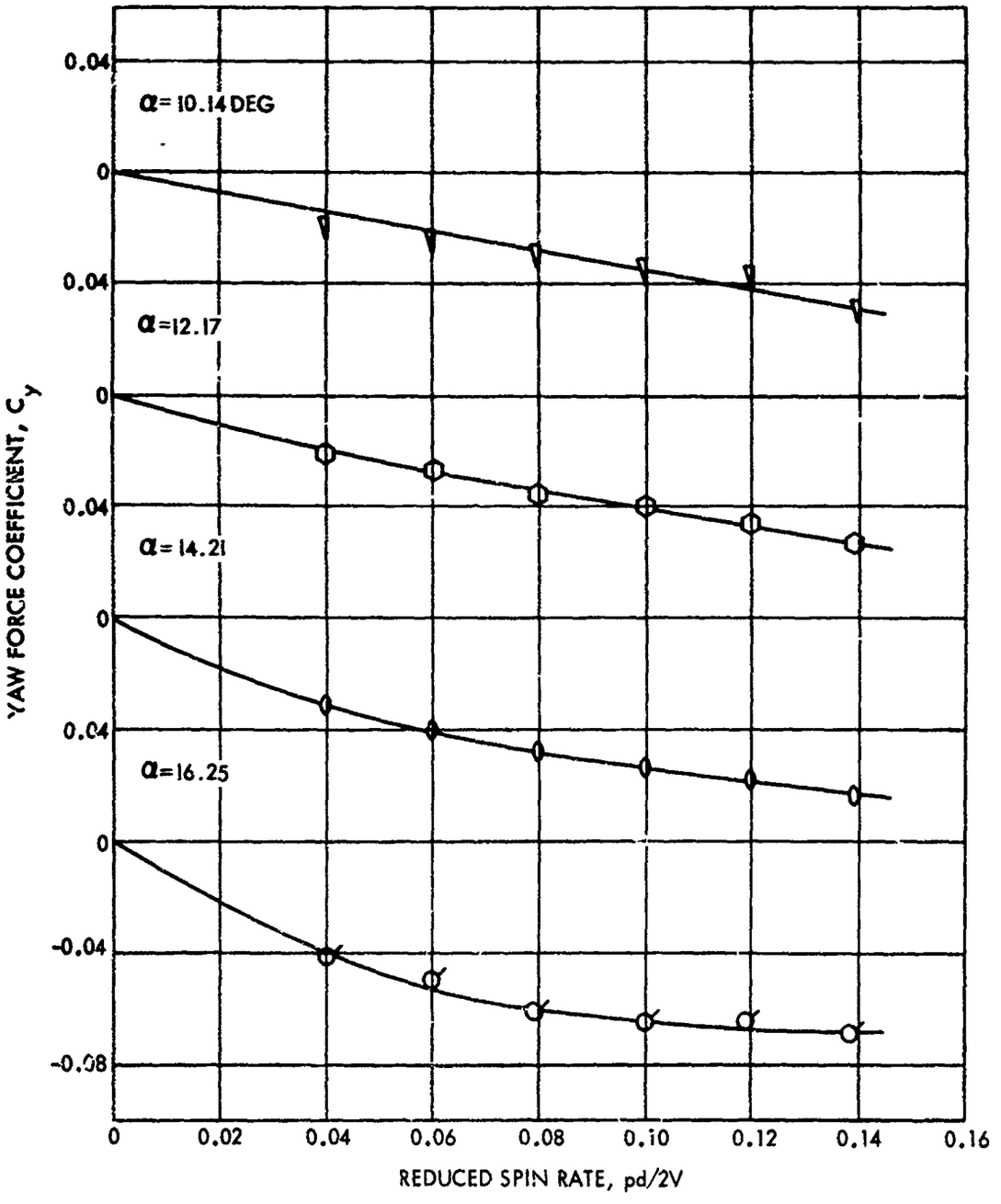

FIG. 12 YAW FORCE COEFFICIENT VERSUS REDUCED SPIN RATE AS A FUNCTION OF ANGLE OF ATTACK FOR CONFIGURATION Aδ0 AT A MACH NUMBER OF 0.70 AND A REYNOLDS NUMBER OF 0.545×10^6

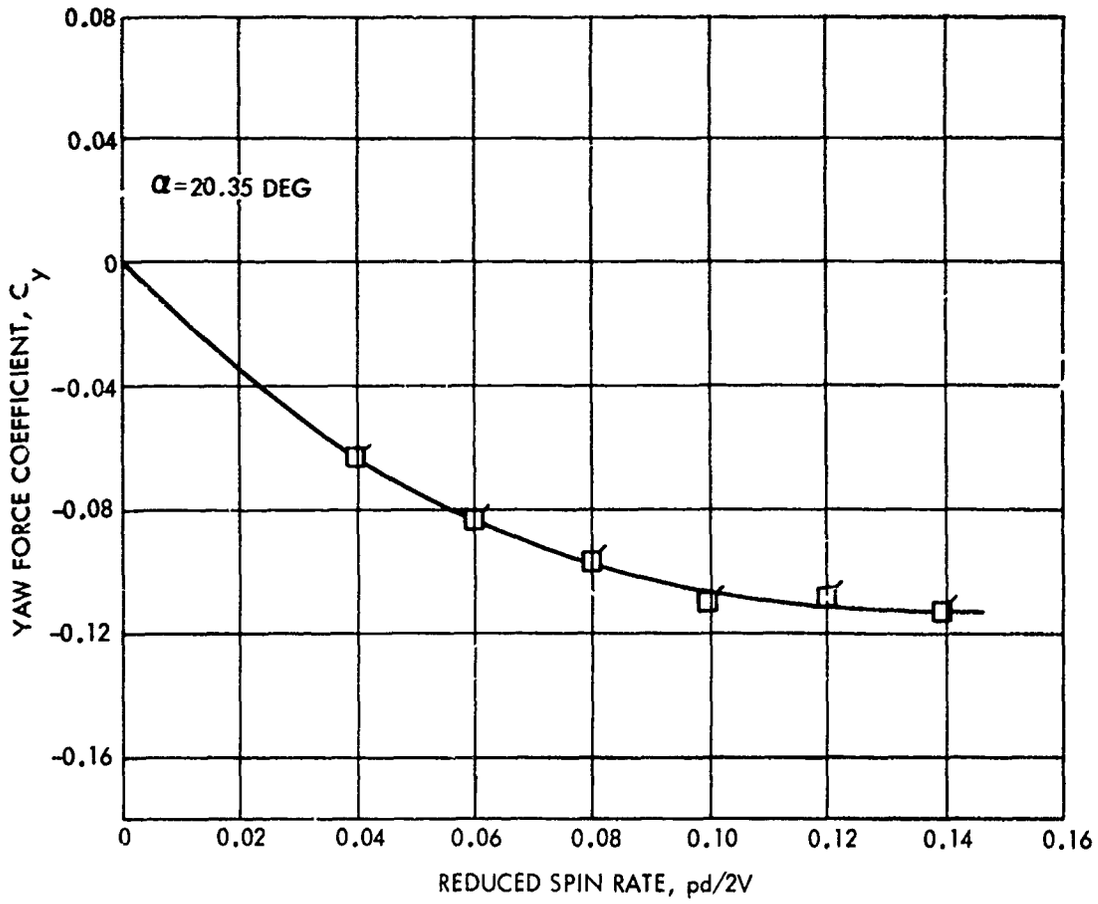

FIG. 13 YAW FORCE COEFFICIENT VERSUS REDUCED SPIN RATE AS A FUNCTION OF ANGLE OF ATTACK FOR CONFIGURATION Aδ0 AT A MACH NUMBER OF 0.70 AND A REYNOLDS NUMBER OF 0.545×10^6

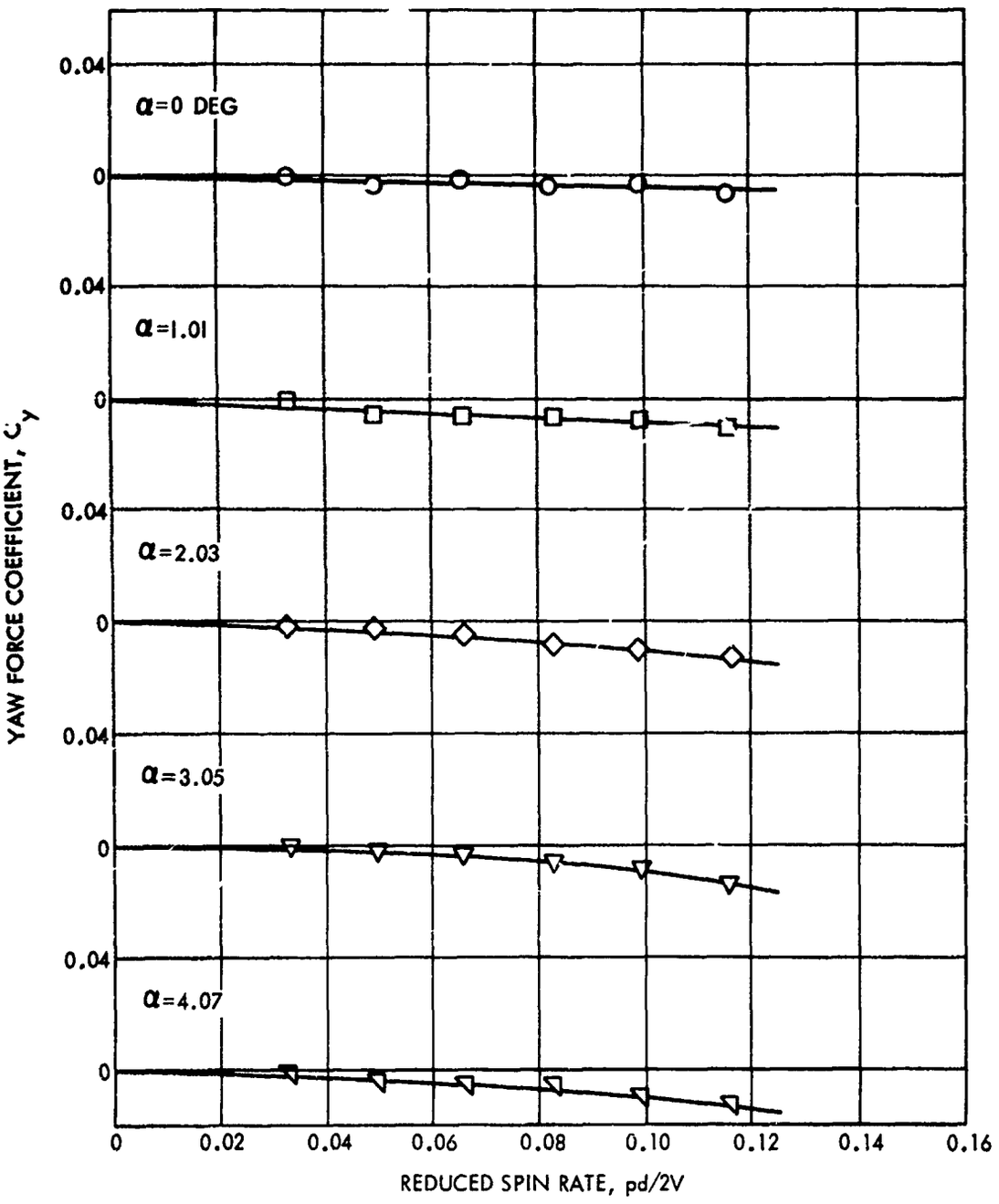

FIG. 14 YAW FORCE COEFFICIENT VERSUS REDUCED SPIN RATE AS A FUNCTION OF ANGLE OF ATTACK FOR CONFIGURATION Aδ0 AT A MACH NUMBER OF 0.85 AND A REYNOLDS NUMBER OF 0.587×10^6

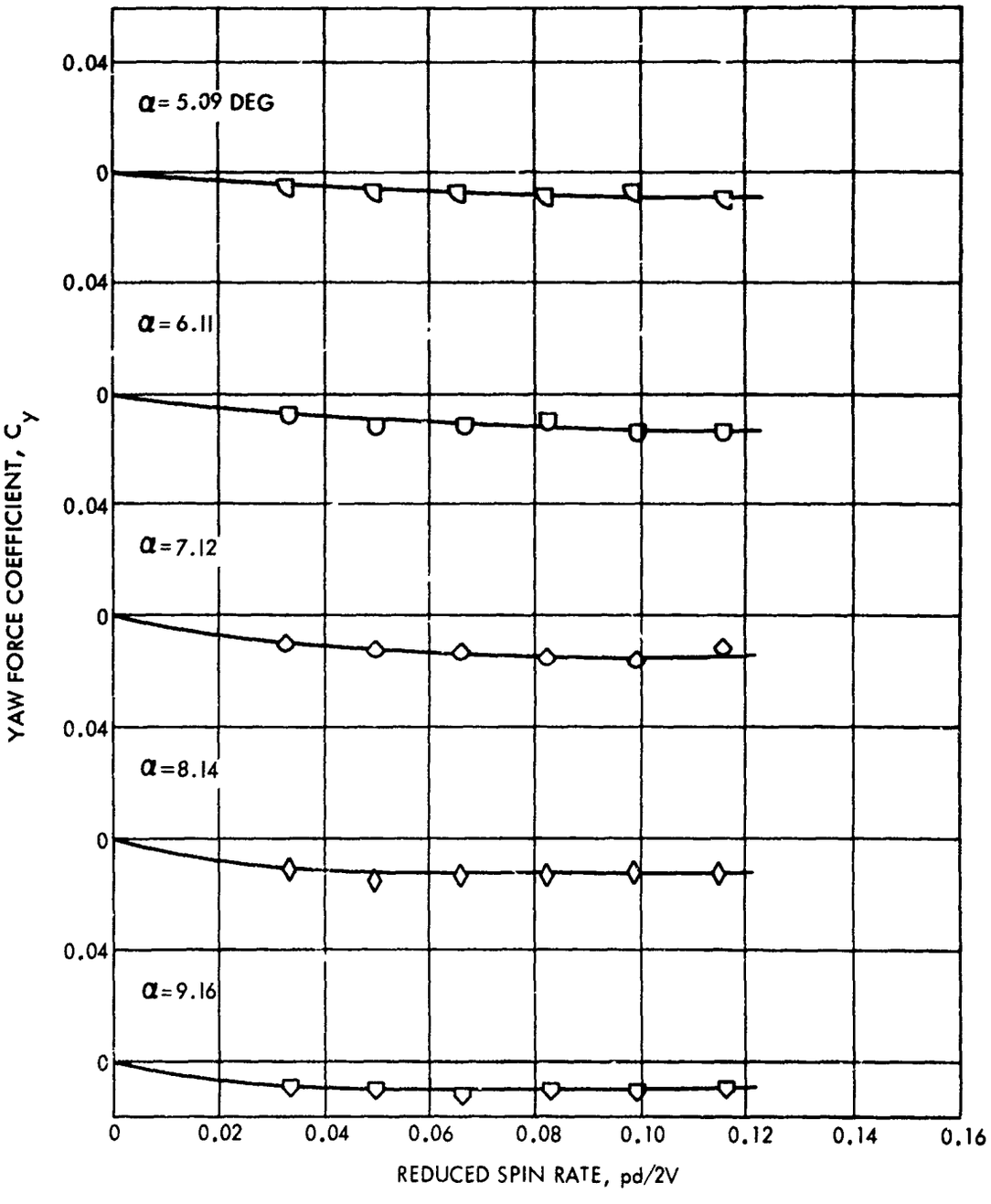

FIG. 15 YAW FORCE COEFFICIENT VERSUS REDUCED SPIN RATE AS A FUNCTION OF ANGLE OF ATTACK FOR CONFIGURATION Aδ 0 AT A MACH NUMBER OF 0.85 AND A REYNOLDS NUMBER OF 0.587×10^6

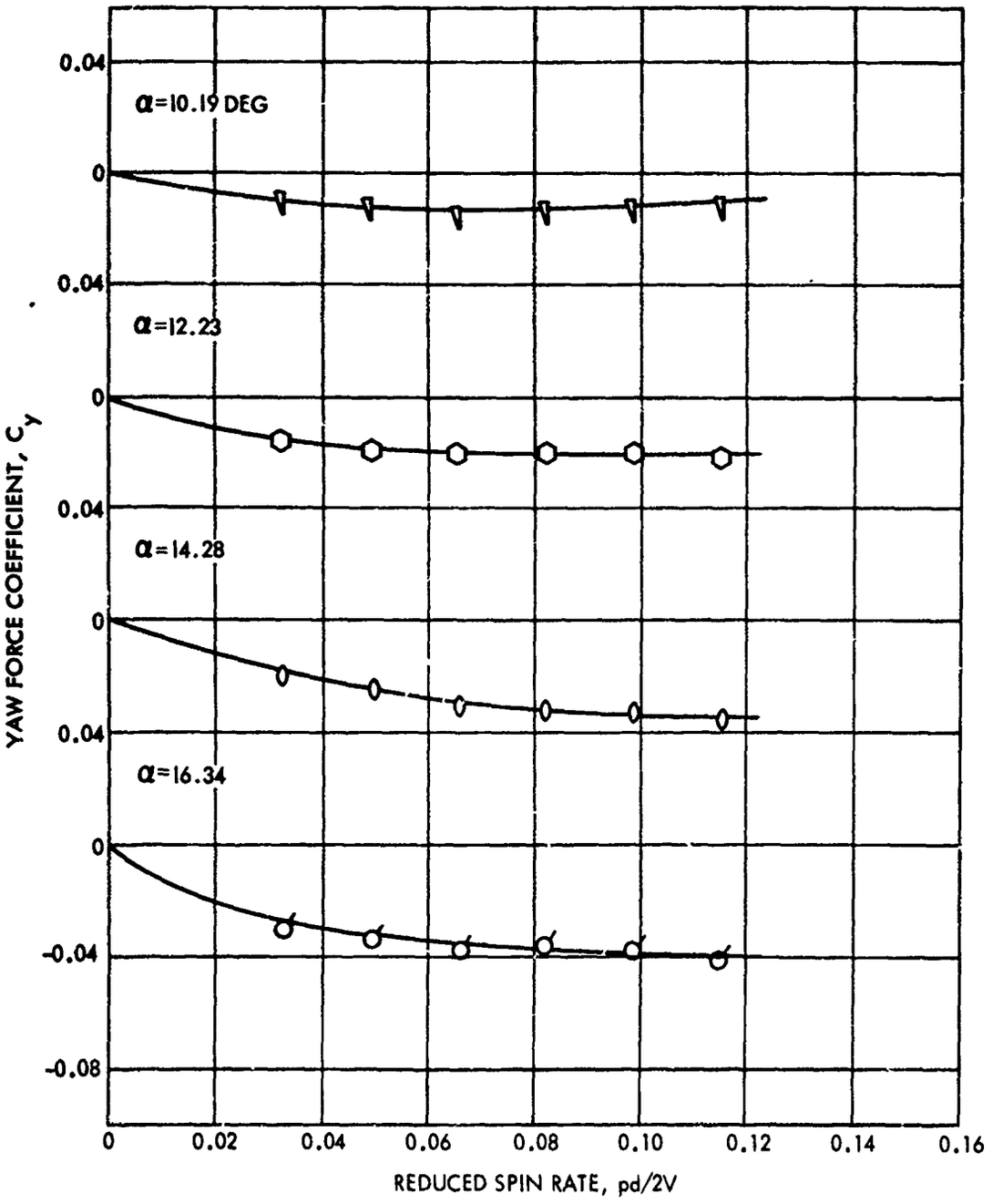

FIG. 16 YAW FORCE COEFFICIENT VERSUS REDUCED SPIN RATE AS A FUNCTION OF ANGLE OF ATTACK FOR CONFIGURATION Aδ0 AT A MACH NUMBER OF 0.85 AND A REYNOLDS NUMBER OF 9.587 x 10^6

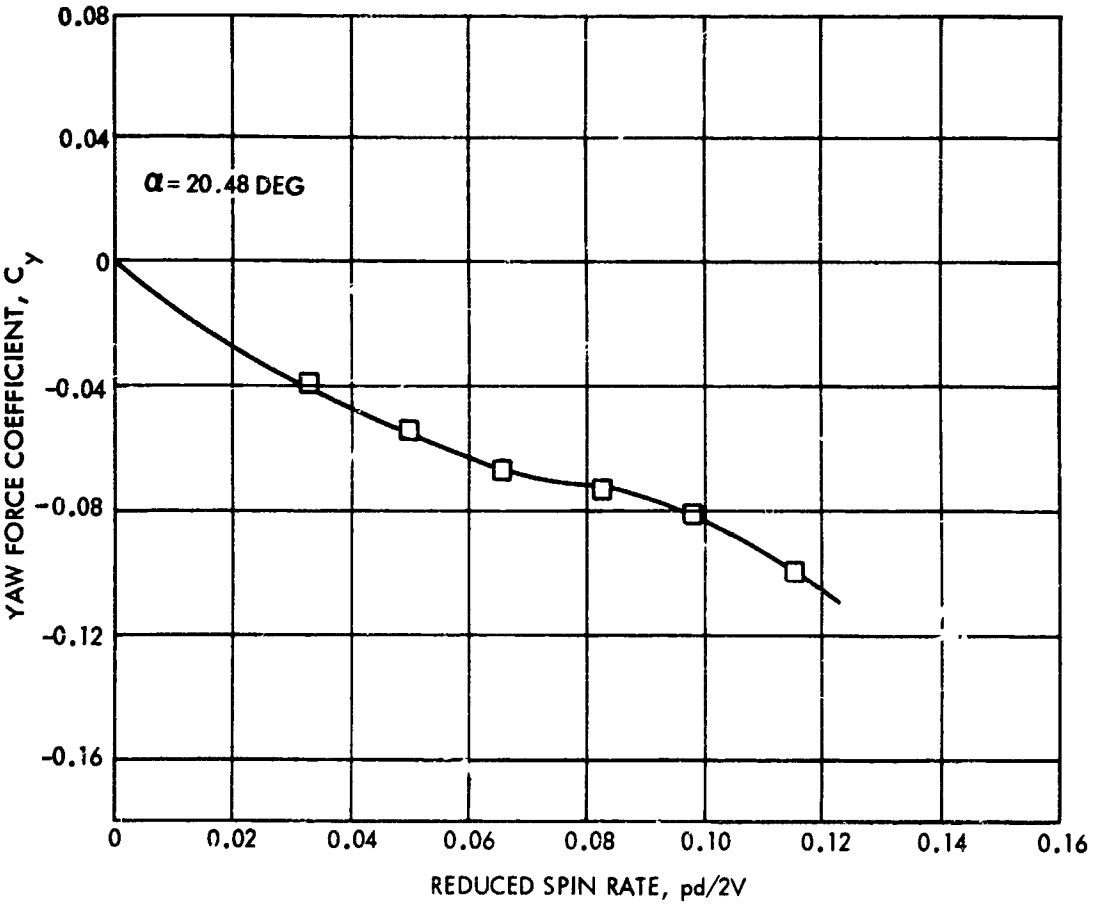

FIG. 17 YAW FORCE COEFFICIENT VERSUS REDUCED SPIN RATE AS A FUNCTION OF ANGLE OF ATTACK FOR CONFIGURATION Aδ0 AT A MACH NUMBER OF 0.85 AND A REYNOLDS NUMBER OF 0.587×10^6

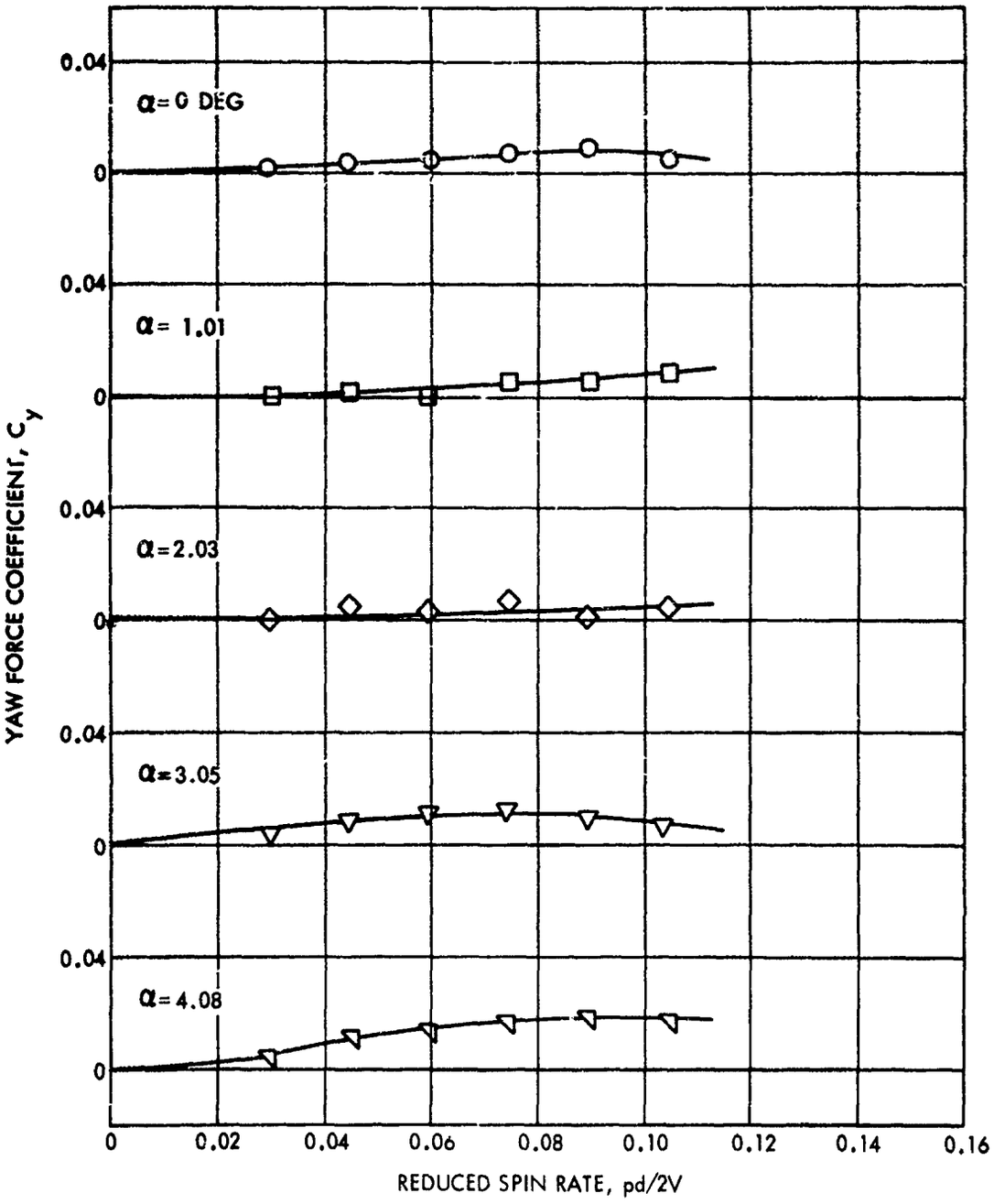

FIG. 18 YAW FORCE COEFFICIENT VERSUS REDUCED SPIN RATE AS A FUNCTION OF ANGLE OF ATTACK FOR CONFIGURATION Aδ0 AT A MACH NUMBER OF 0.95 AND A REYNOLDS NUMBER OF 0.600×10^6

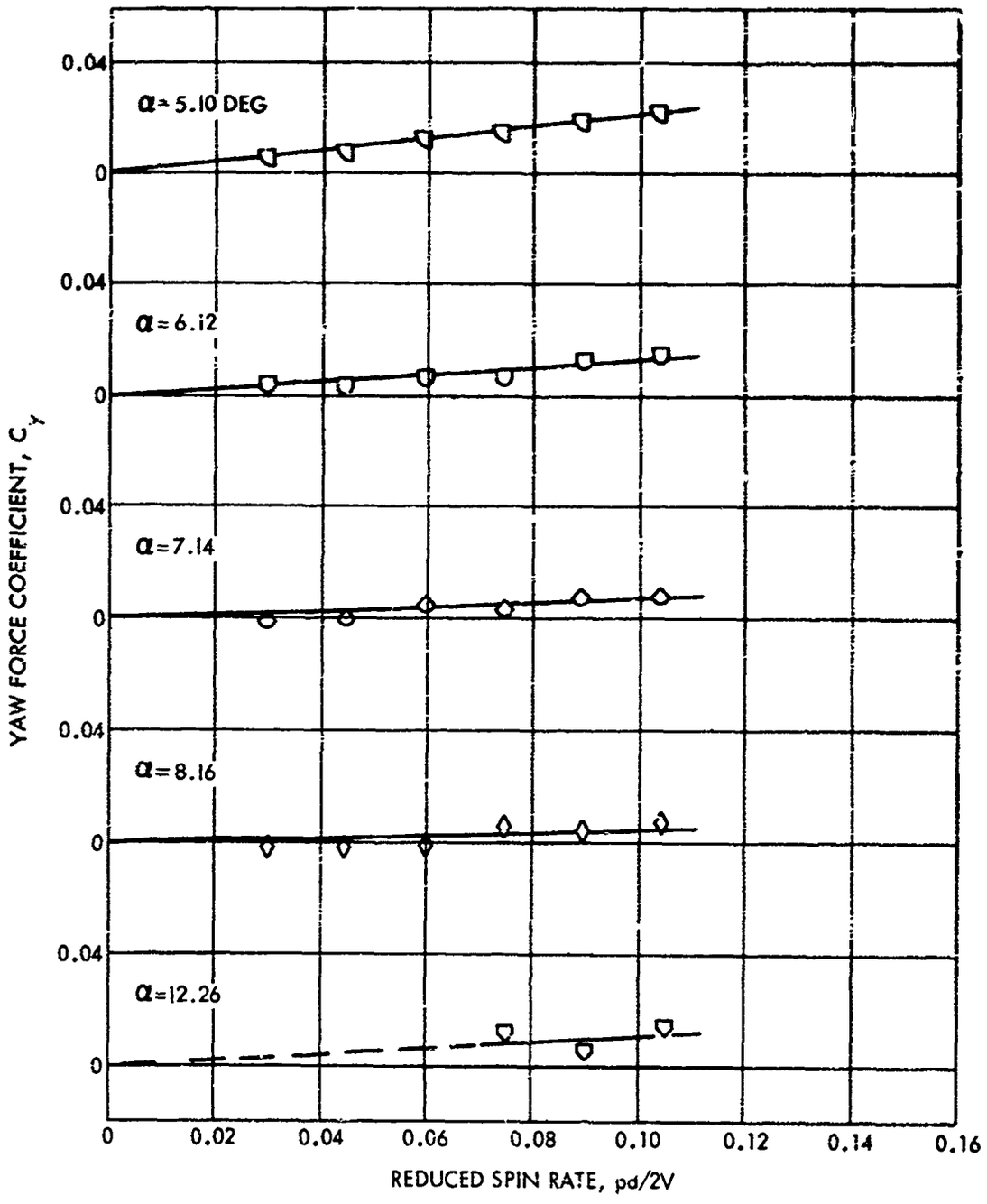

FIG. 19 YAW FORCE COEFFICIENT VERSUS REDUCED SPIN RATE AS A FUNCTION OF ANGLE OF ATTACK FOR CONFIGURATION Aδ0 AT A MACH NUMBER OF 0.95 AND A REYNOLDS NUMBER OF 0.600×10^6

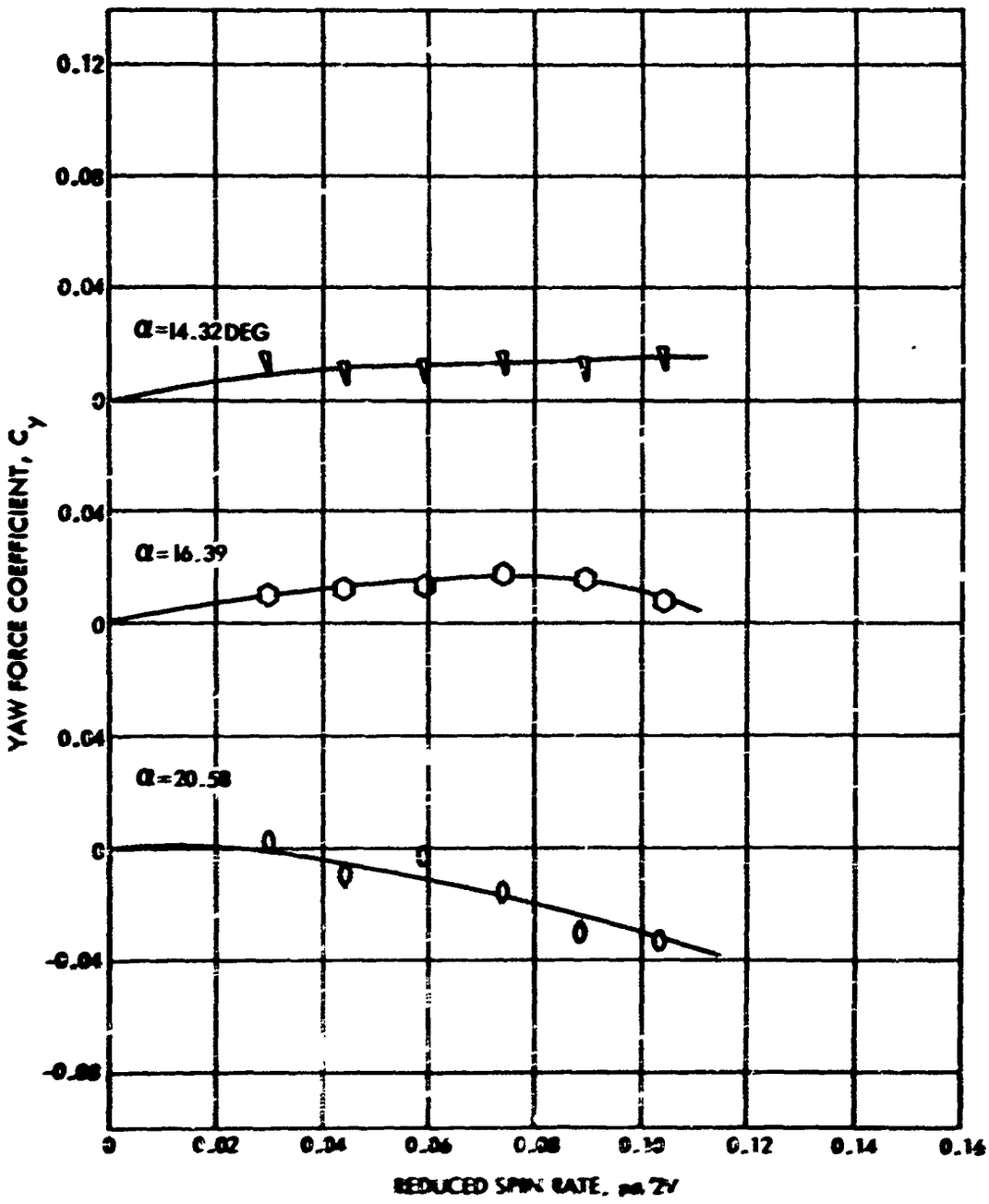

FIG. 25 YAW FORCE COEFFICIENT VERSUS REDUCED SPIN RATE AS A FUNCTION OF ANGLE OF ATTACK FOR CONFIGURATION A3B AT A MACH NUMBER OF 2.15 AND A REYNOLDS NUMBER OF 9.680 x 10^6

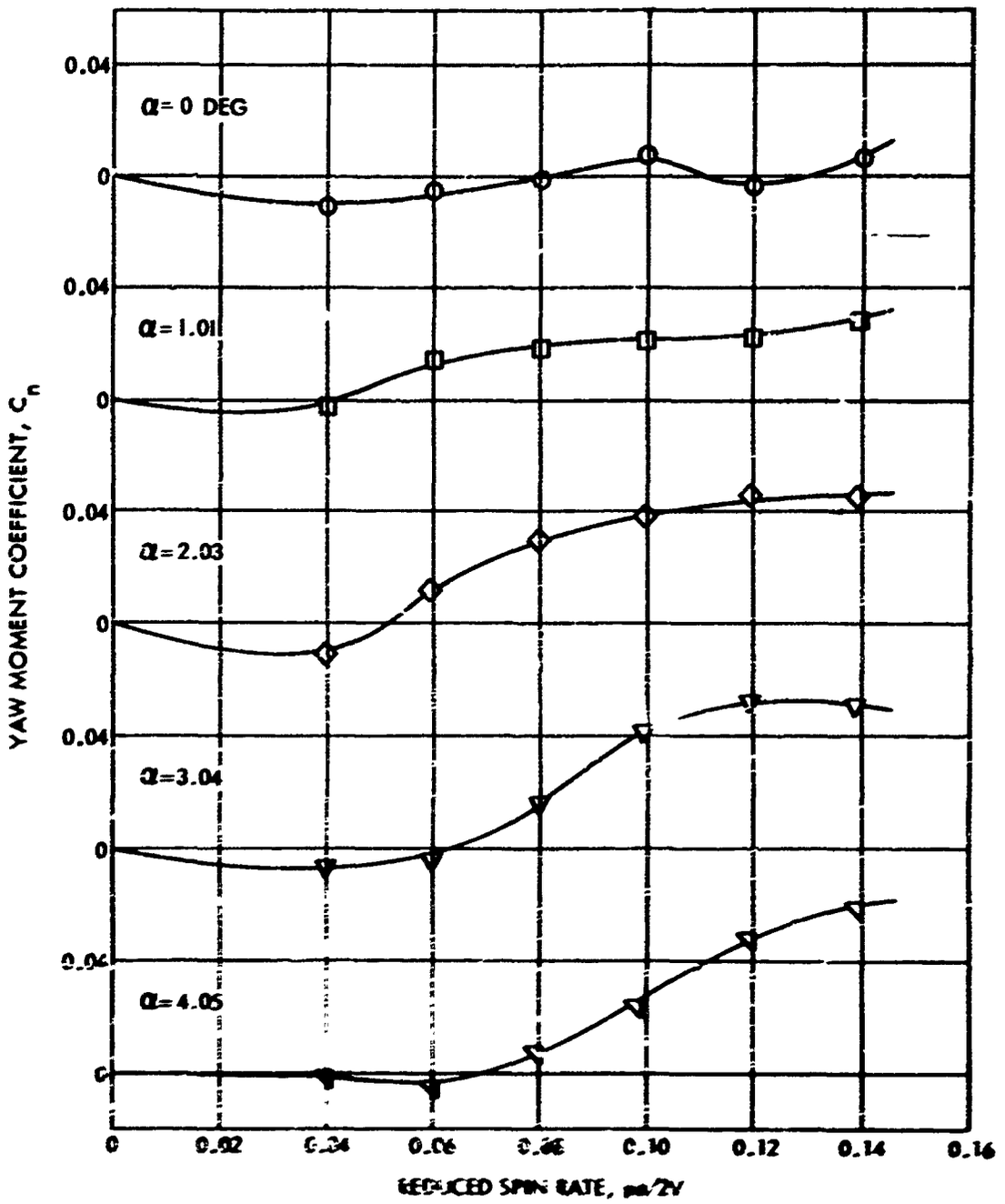

FIG. 21 YAW MOMENT COEFFICIENT VERSUS REDUCED SPIN RATE AS A FUNCTION OF ANGLE OF ATTACK FOR CONFIGURATION ABC AT A MACH NUMBER OF 3.75 AND A REYNOLDS NUMBER OF 3.545 x 10^6

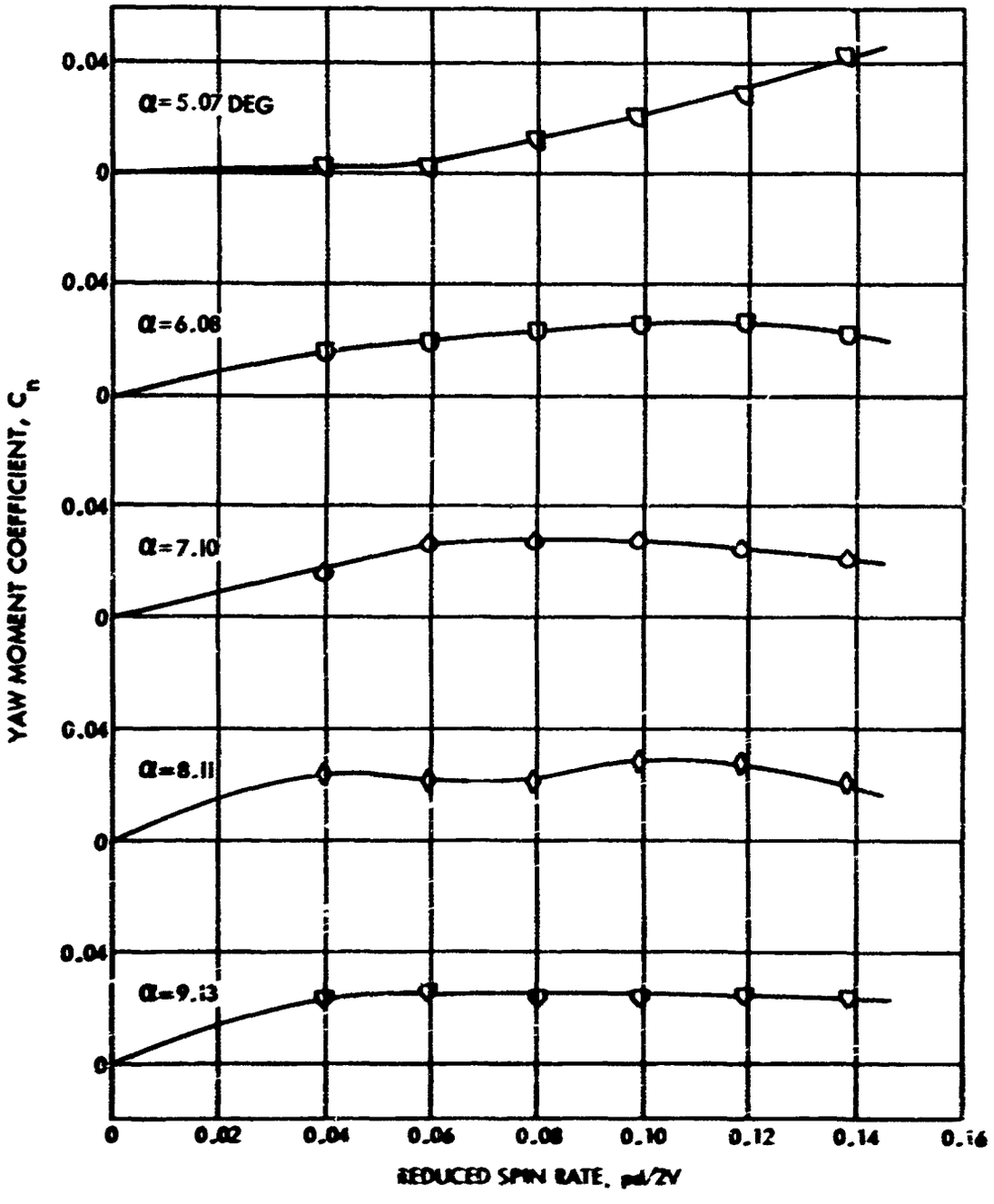

FIG. 22 YAW MOMENT COEFFICIENT VERSUS REDUCED SPIN RATE AS A FUNCTION OF ANGLE OF ATTACK FOR CONFIGURATION A3 0 AT A MACH NUMBER OF 0.70 AND A REYNOLDS NUMBER OF 0.565 x 10^6

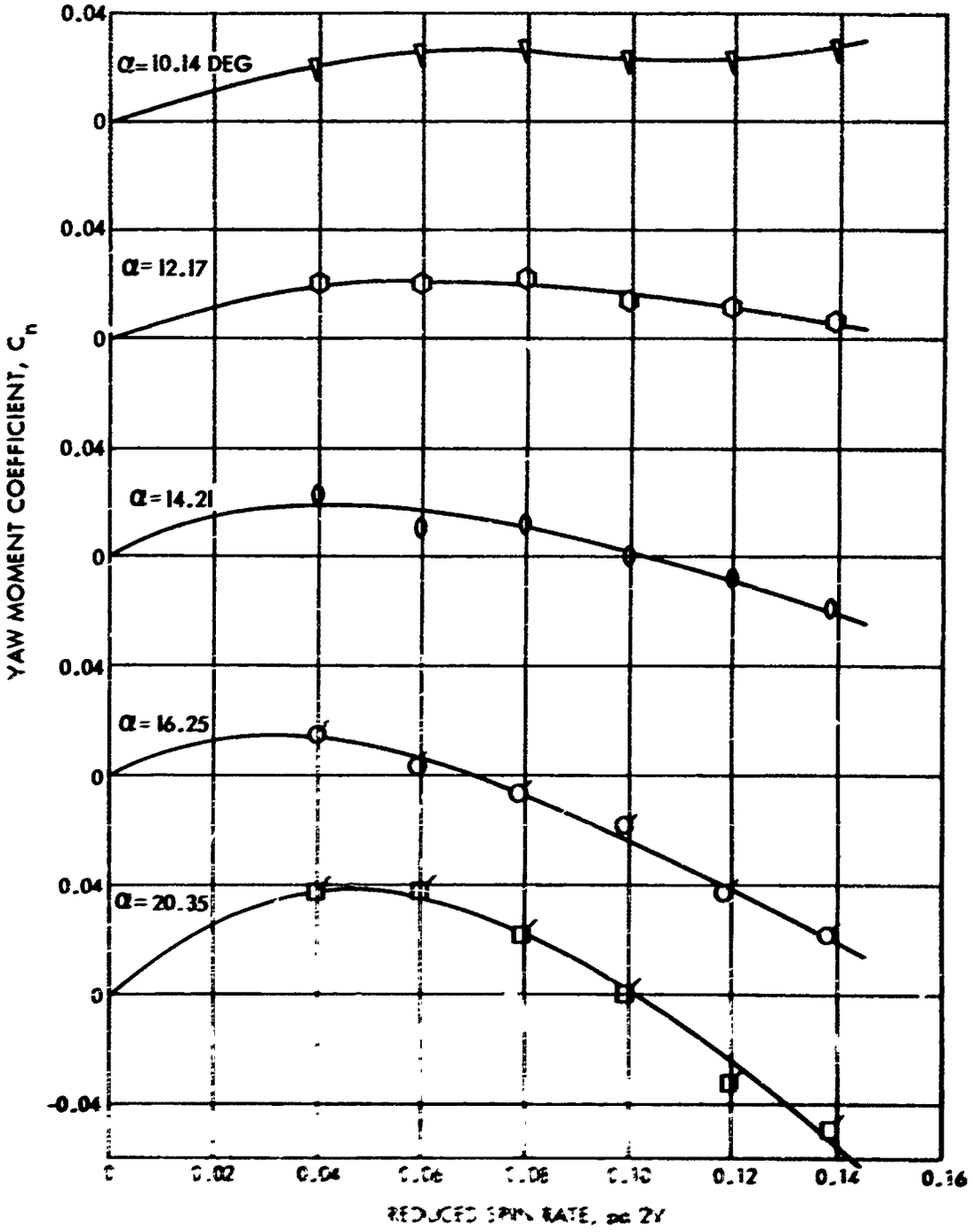

FIG. 23 YAW MOMENT COEFFICIENT VERSUS REDUCED SPIN RATE AS A FUNCTION OF ANGLE OF ATTACK FOR CONFIGURATION ABC AT A MACH NUMBER OF 2.70 AND A REYNOLDS NUMBER OF 2.545 x 10^6

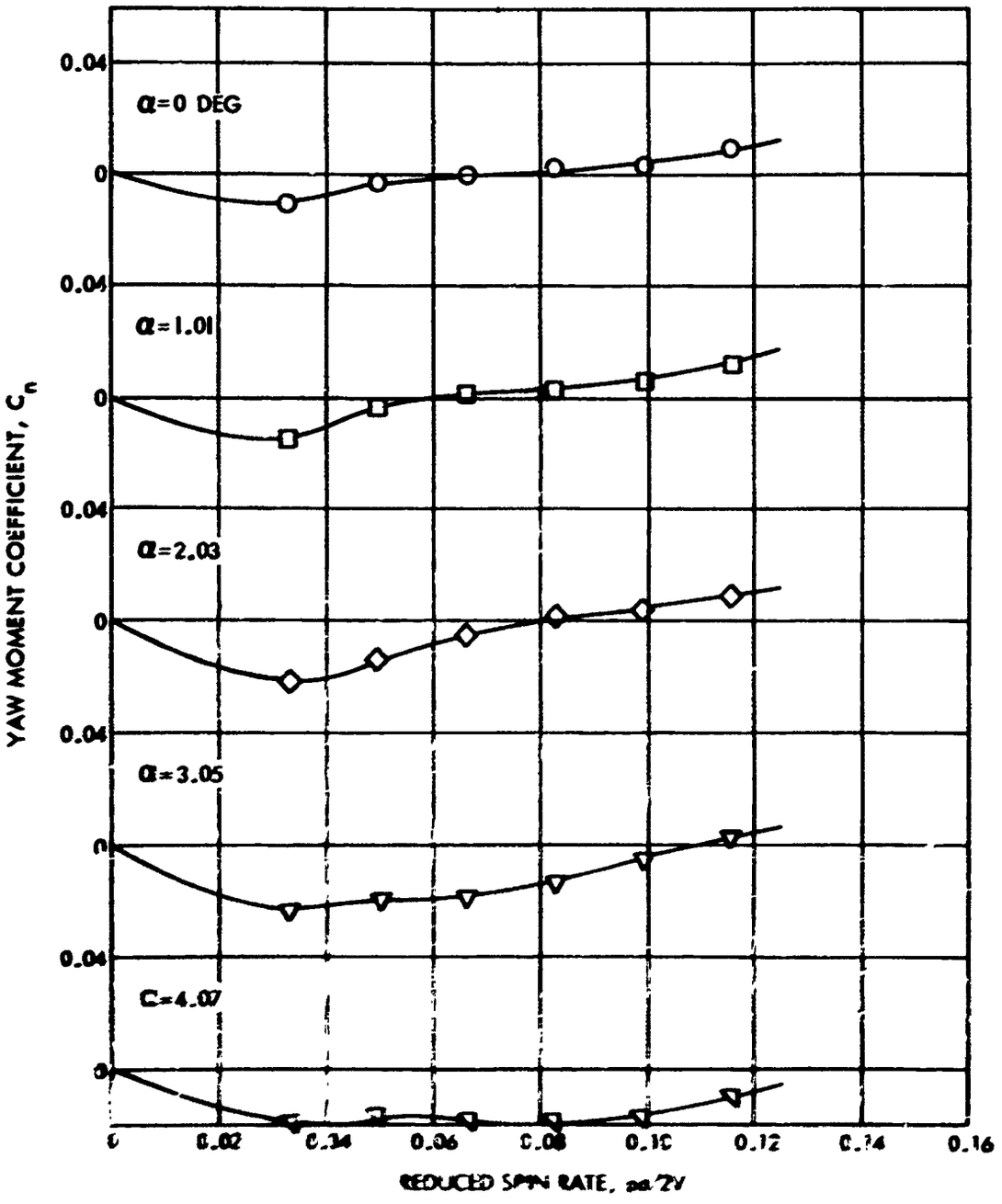

FIG 24 YAW MOMENT COEFFICIENT VERSUS REDUCED SPIN RATE AS A FUNCTION OF ANGLE OF ATTACK FOR CONFIGURATION ABB AT A MACH NUMBER OF 2.85 AND A REYNOLDS NUMBER OF 3.587 x 10^6

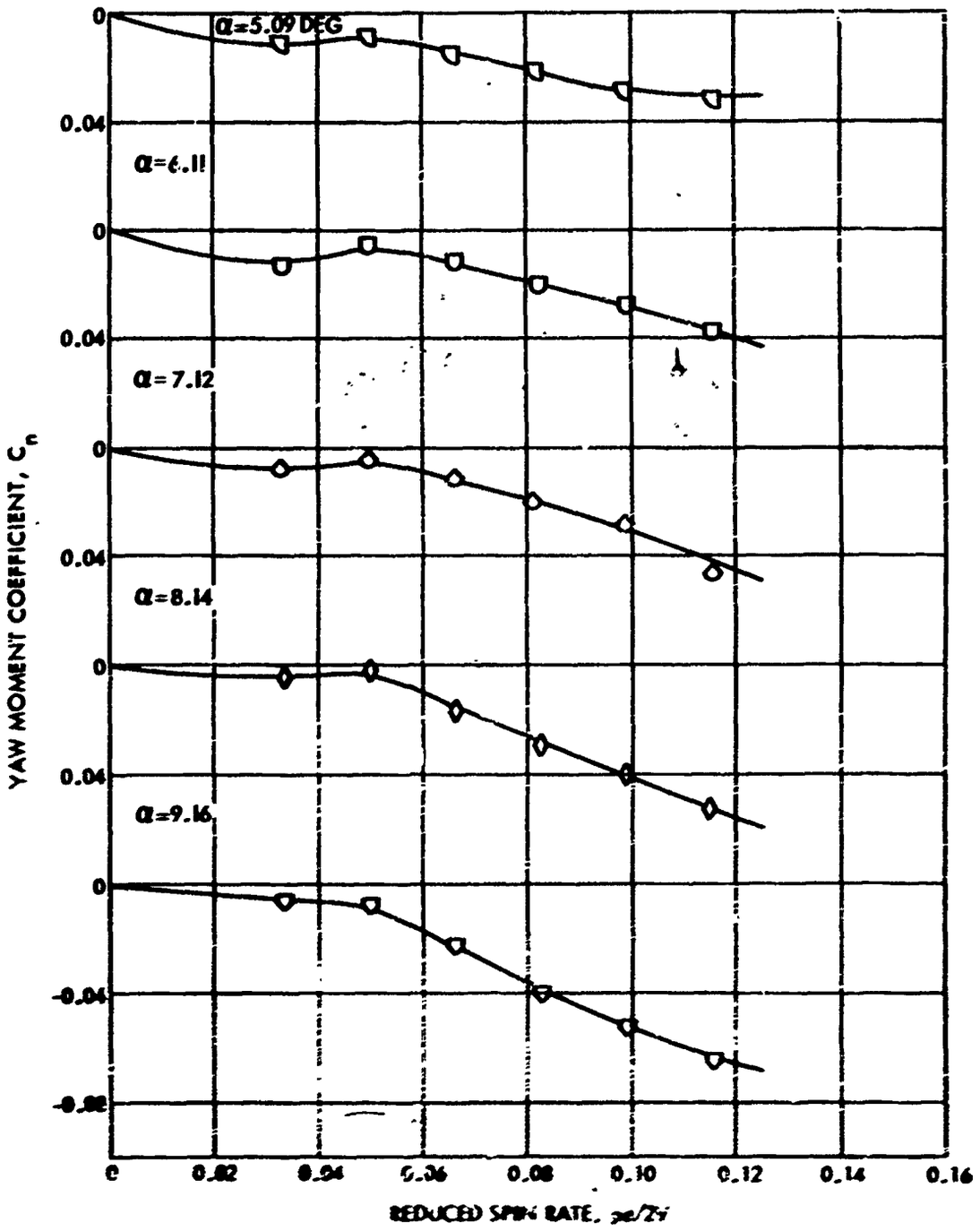

FIG. 25 YAW MOMENT COEFFICIENT VERSUS REDUCED SPIN RATE AS A FUNCTION OF ANGLE OF ATTACK FOR CONFIGURATION A3C AT A MACH NUMBER OF 0.85 AND A REYNOLDS NUMBER OF 0.587 x 10^6

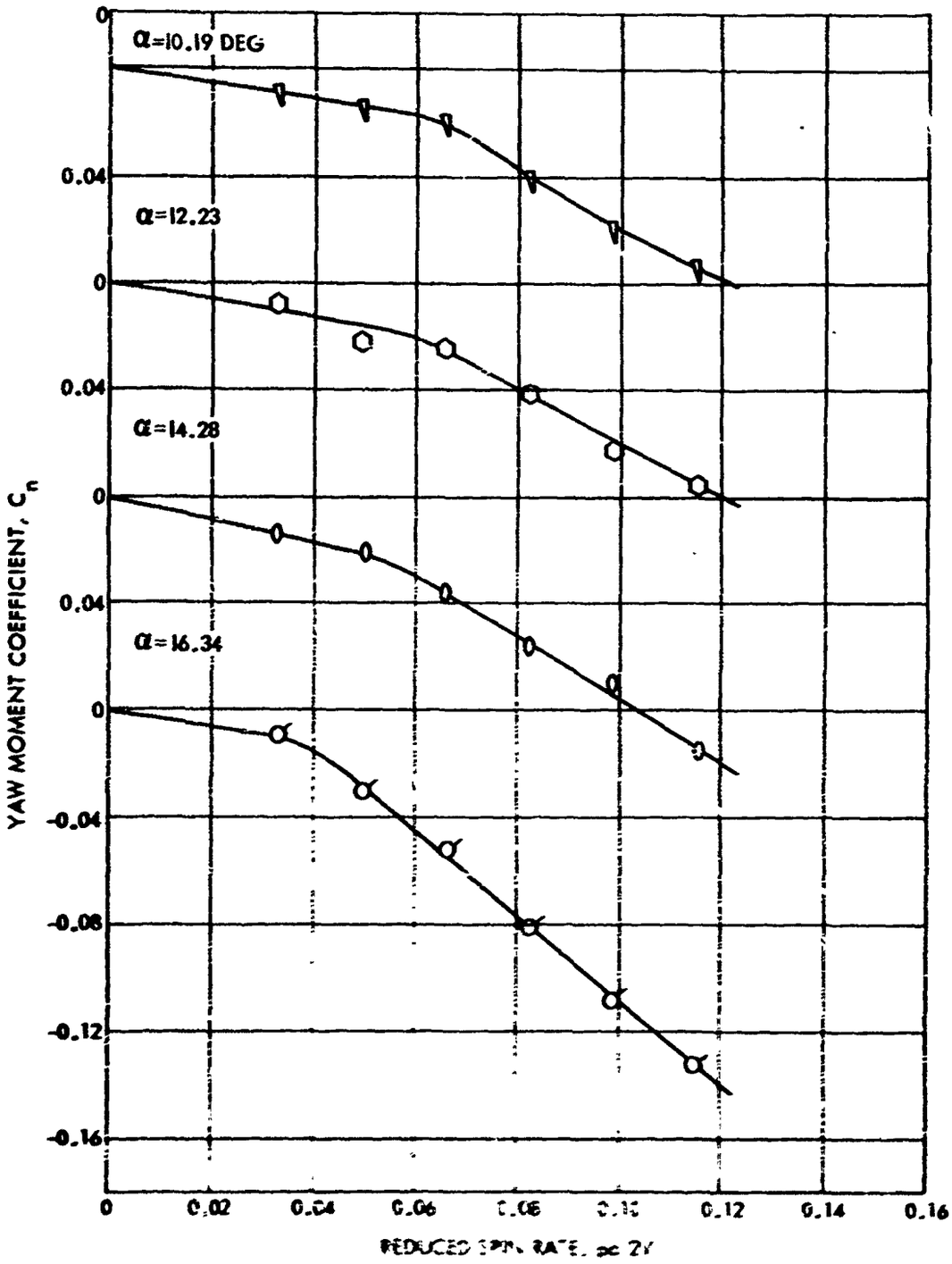

FIG. 26 YAW MOMENT COEFFICIENT VERSUS REDUCED SPIN RATE AS A FUNCTION OF ANGLE OF ATTACK FOR CONFIGURATION 2B AT A MACH NUMBER OF 0.85 AND A REYNOLDS NUMBER OF 2.387 x 10^6

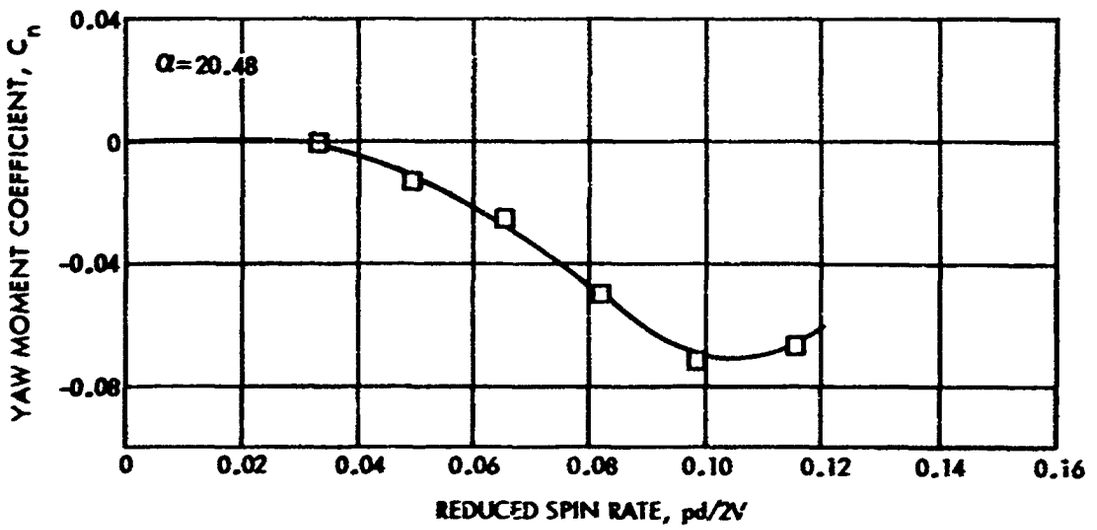

FIG. 27 YAW MOMENT COEFFICIENT VERSUS REDUCED SPIN RATE AS A FUNCTION OF ANGLE OF ATTACK FOR CONFIGURATION A3O AT A MACH NUMBER OF 0.85 AND A REYNOLDS NUMBER OF 0.587×10^6

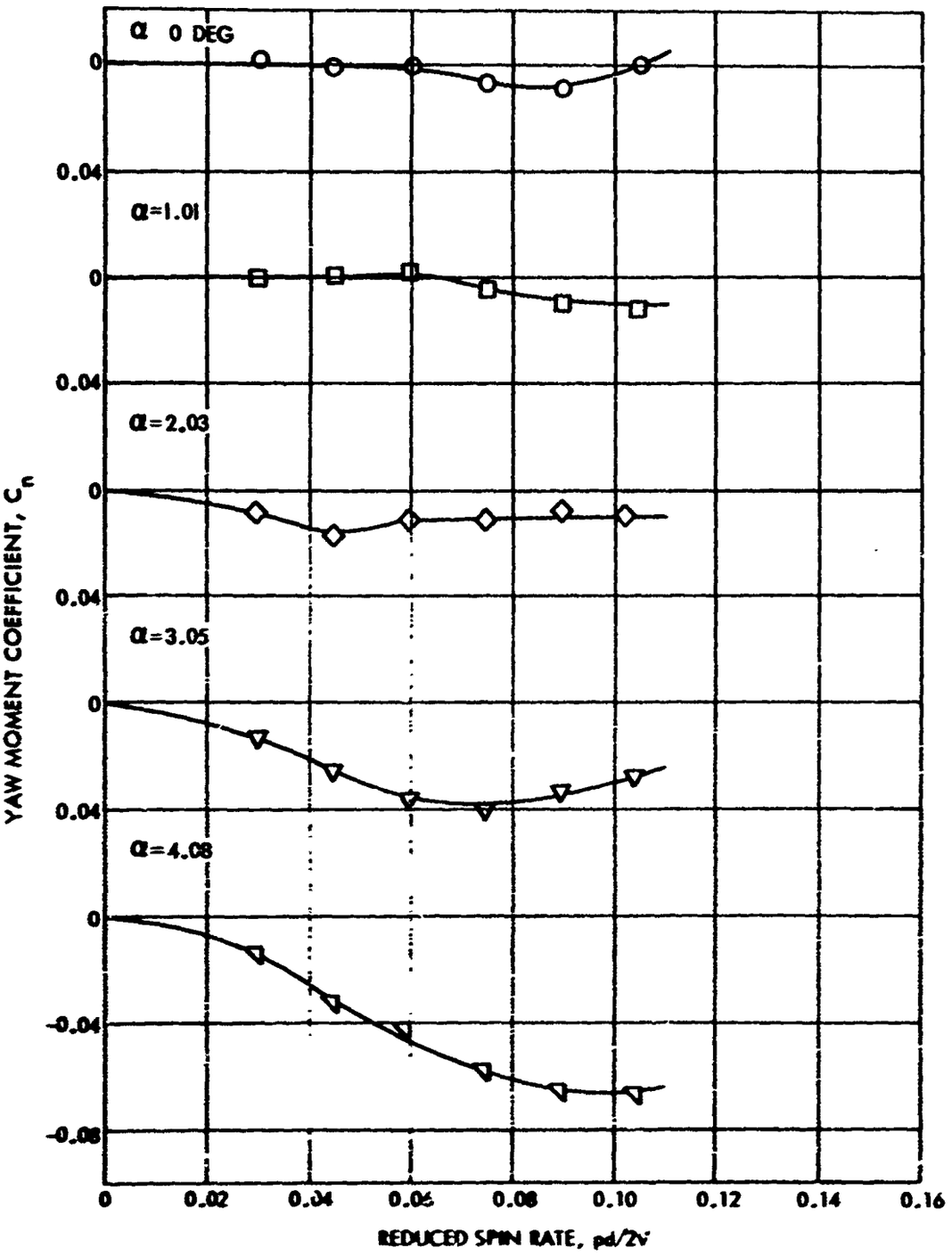

FIG. 28 YAW MOMENT COEFFICIENT VERSUS REDUCED SPIN RATE AS A FUNCTION OF ANGLE OF ATTACK FOR CONFIGURATION A$\hat{8}$0 AT A MACH NUMBER OF 0.95 AND A REYNOLDS NUMBER OF 0.600 x 10^6

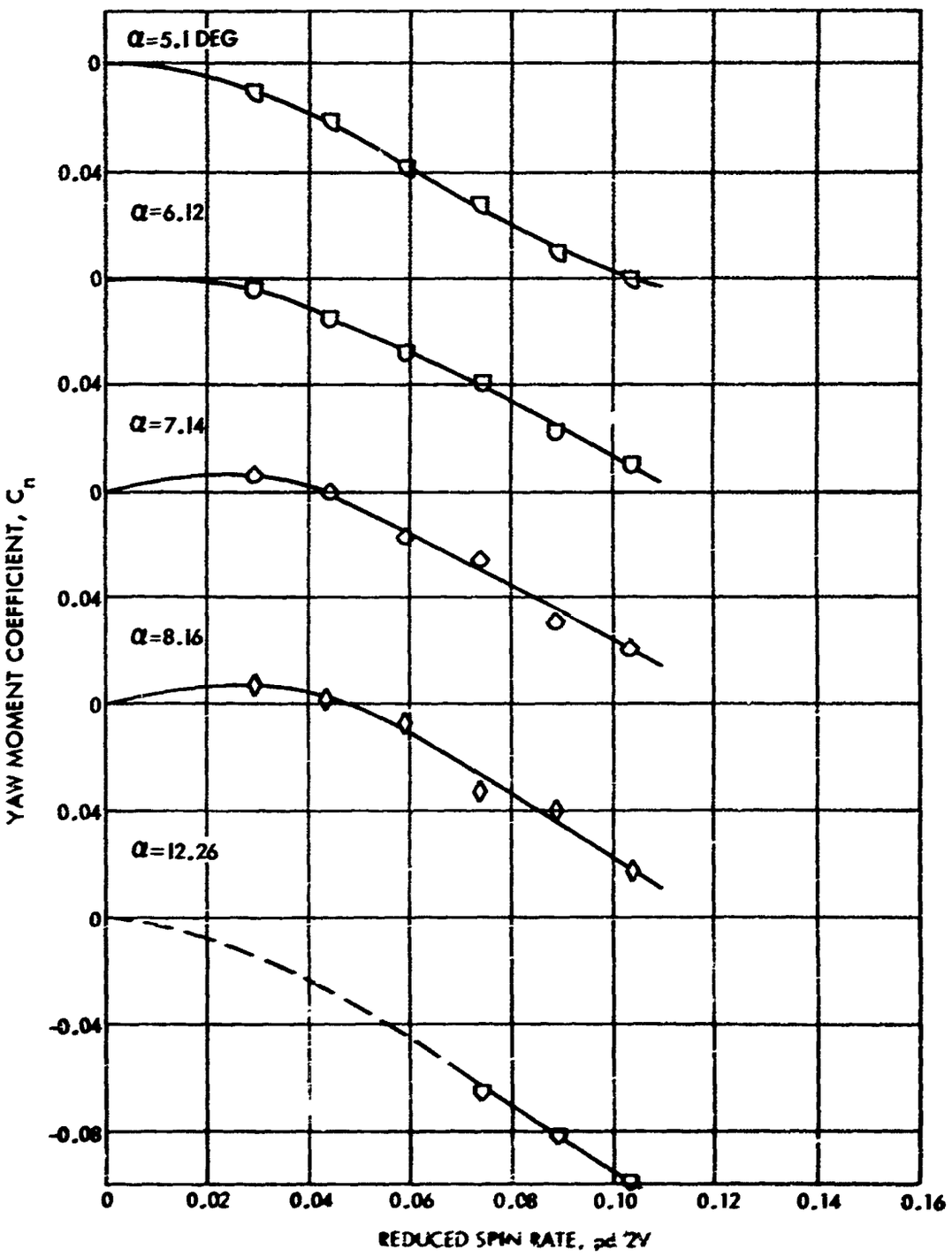

FIG. 29 YAW MOMENT COEFFICIENT VERSUS REDUCED SPIN RATE AS A FUNCTION OF ANGLE OF ATTACK FOR CONFIGURATION AB̄0 AT A MACH NUMBER OF 0.95 AND A REYNOLDS NUMBER OF 0.600 x 10^6

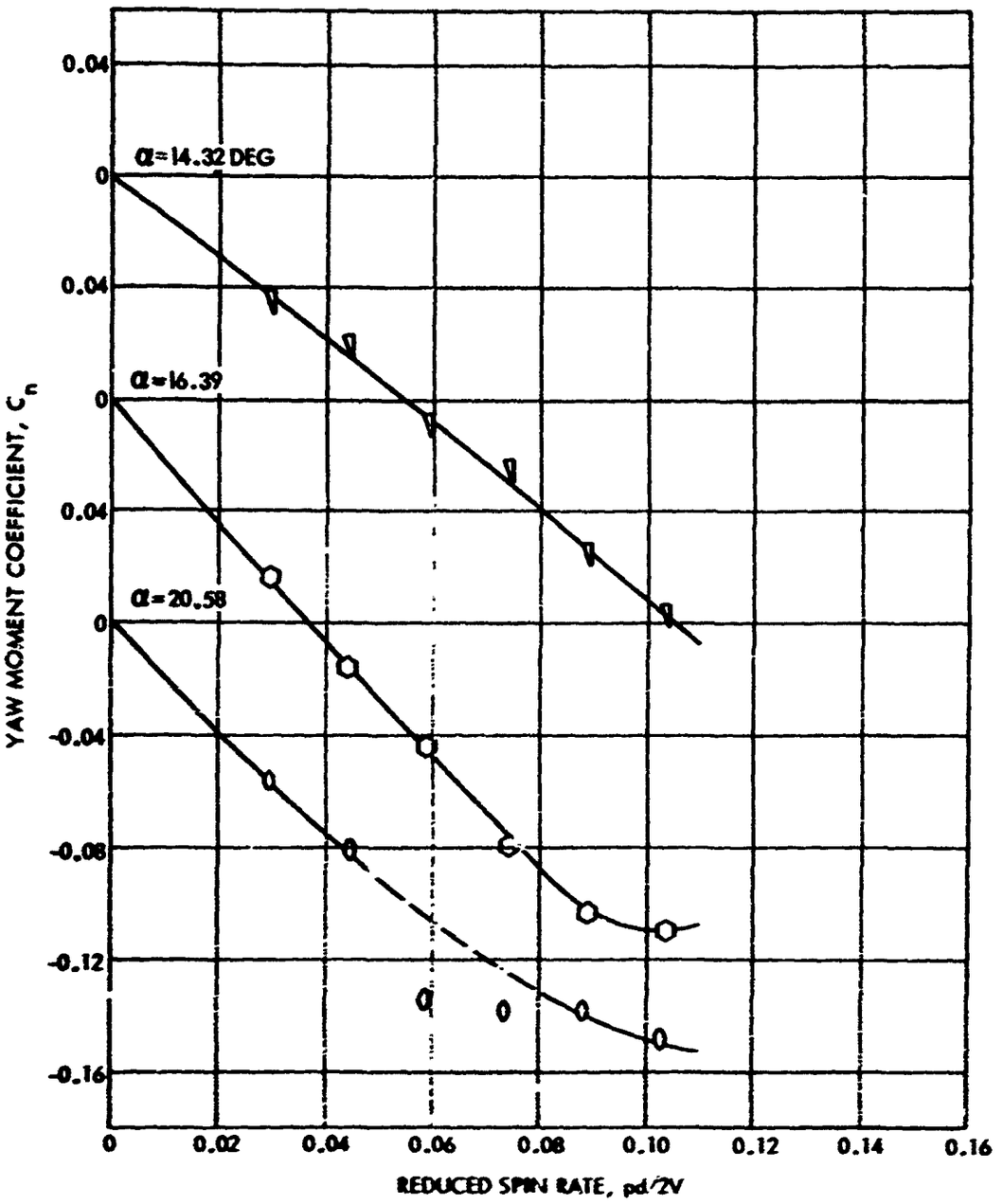

FIG. 30 YAW MOMENT COEFFICIENT VERSUS REDUCED SPIN RATE AS A FUNCTION OF ANGLE OF ATTACK FOR CONFIGURATION A$\bar{8}$0 AT A MACH NUMBER OF 0.95 AND A REYNOLDS NUMBER OF 0.600×10^6

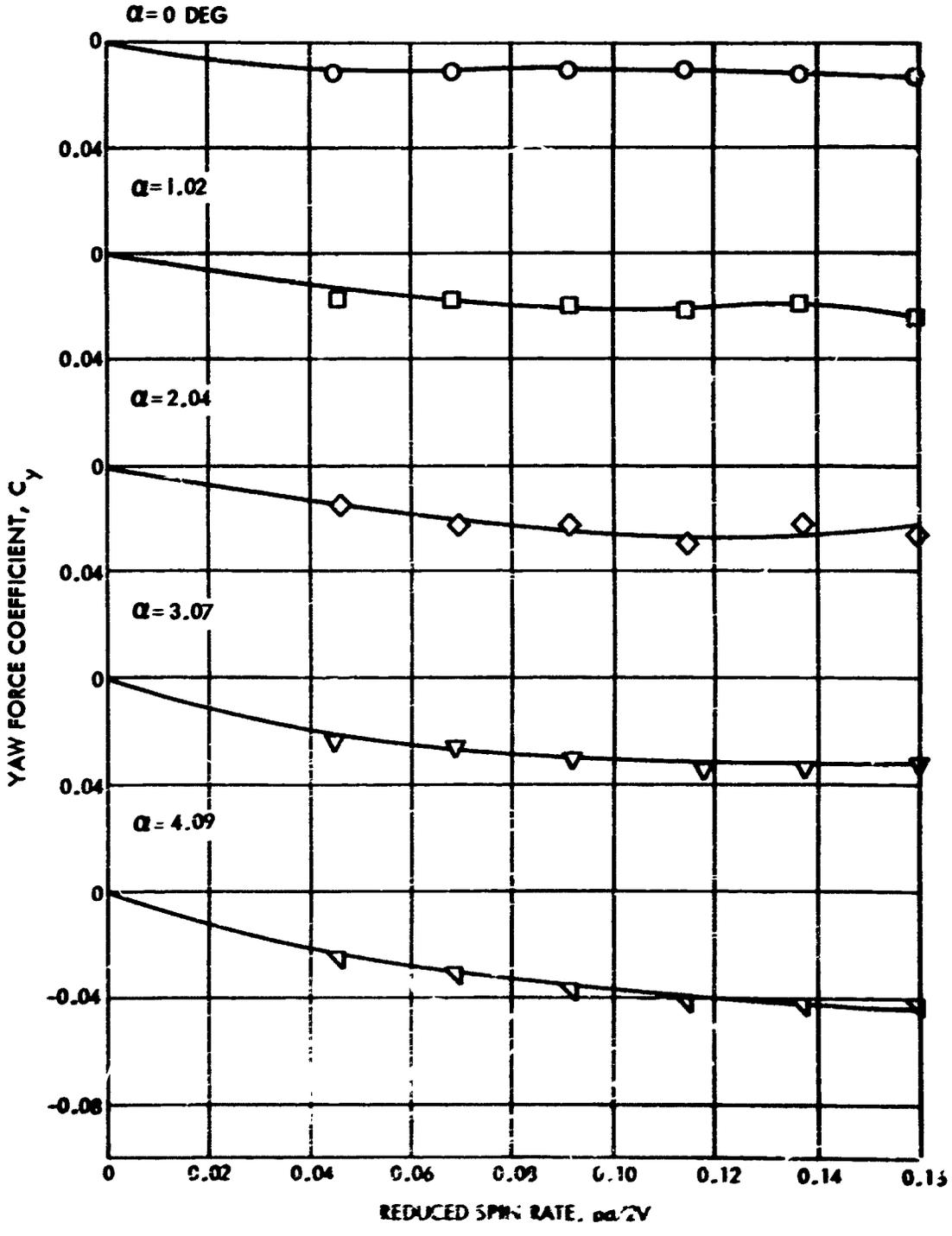

FIG. 31 YAW FORCE COEFFICIENT VERSUS REDUCED SPIN RATE AS A FUNCTION OF ANGLE OF ATTACK FOR CONFIGURATION AB 0 AT A MACH NUMBER OF 0.60 AND A REYNOLDS NUMBER OF 0.97 x 10^6

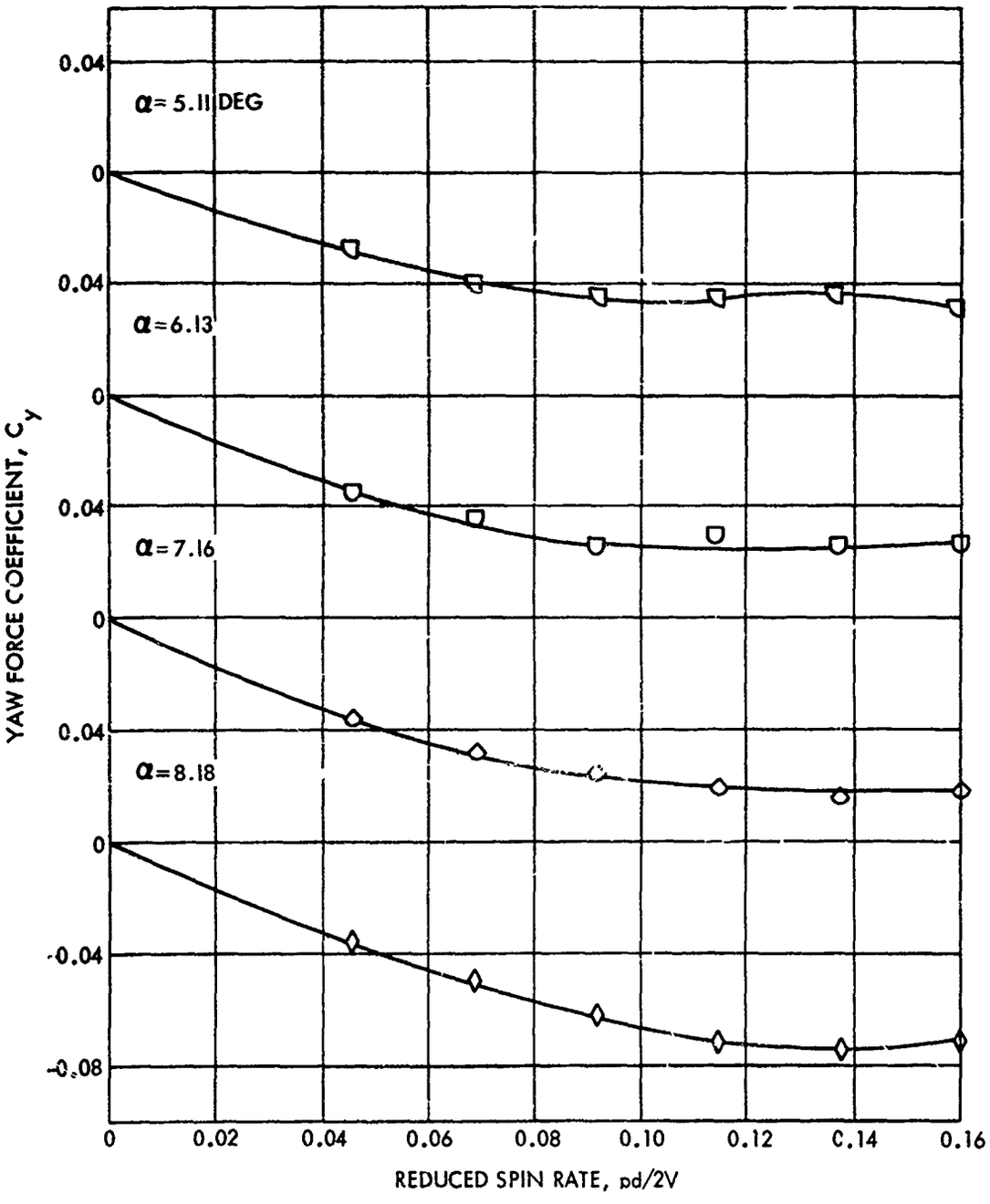

FIG. 32 YAW FORCE COEFFICIENT VERSUS REDUCED SPIN RATE AS A FUNCTION OF ANGLE OF ATTACK FOR CONFIGURATION Aδ0 AT A MACH NUMBER OF 0.60 AND A REYNOLDS NUMBER OF 0.971×10^6

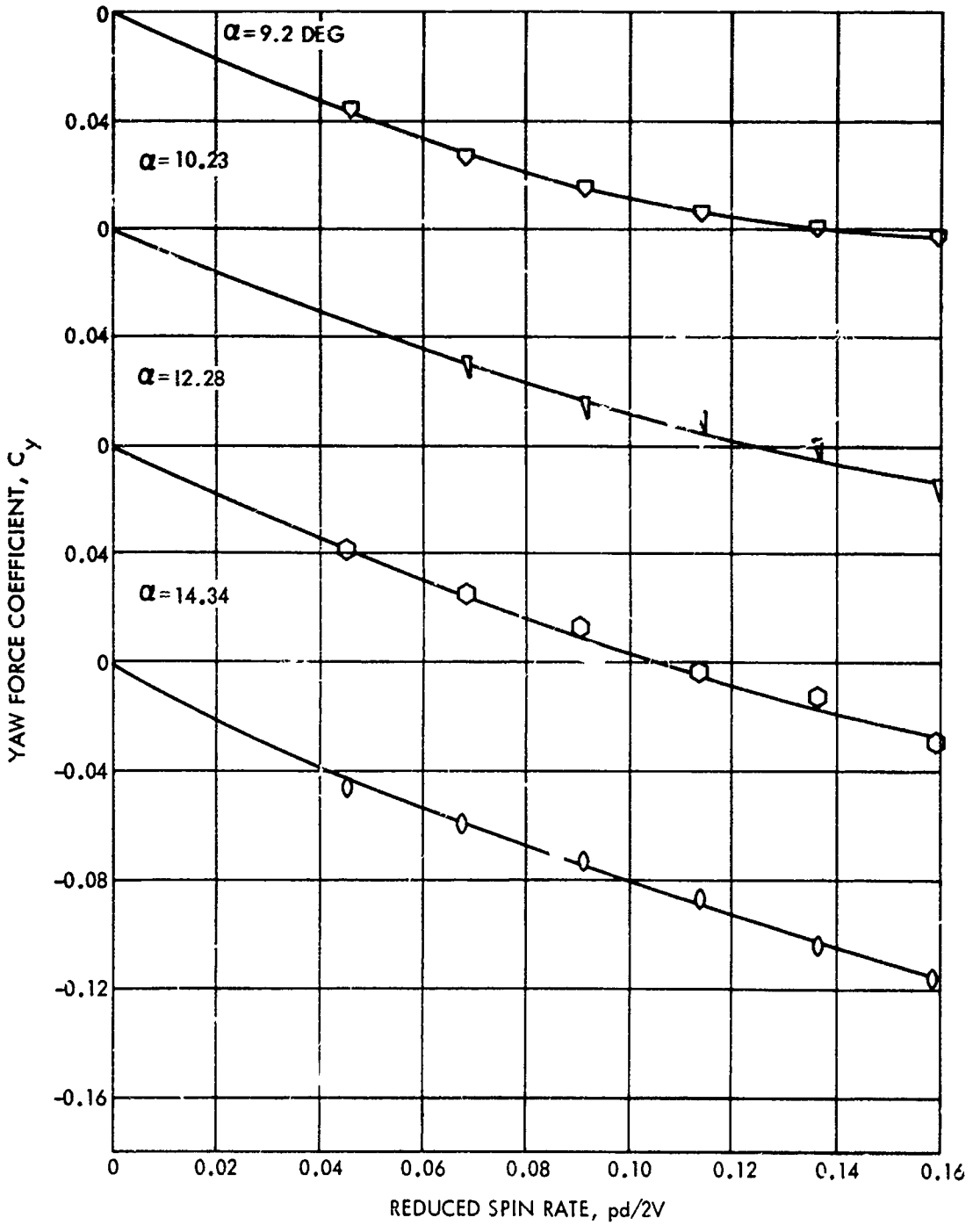

FIG. 33 YAW FORCE COEFFICIENT VERSUS REDUCED SPIN RATE AS A FUNCTION OF ANGLE OF ATTACK FOR CONFIGURATION Aδ0 AT A MACH NUMBER OF 0.60 AND A REYNOLDS NUMBER OF 0.971×10^6

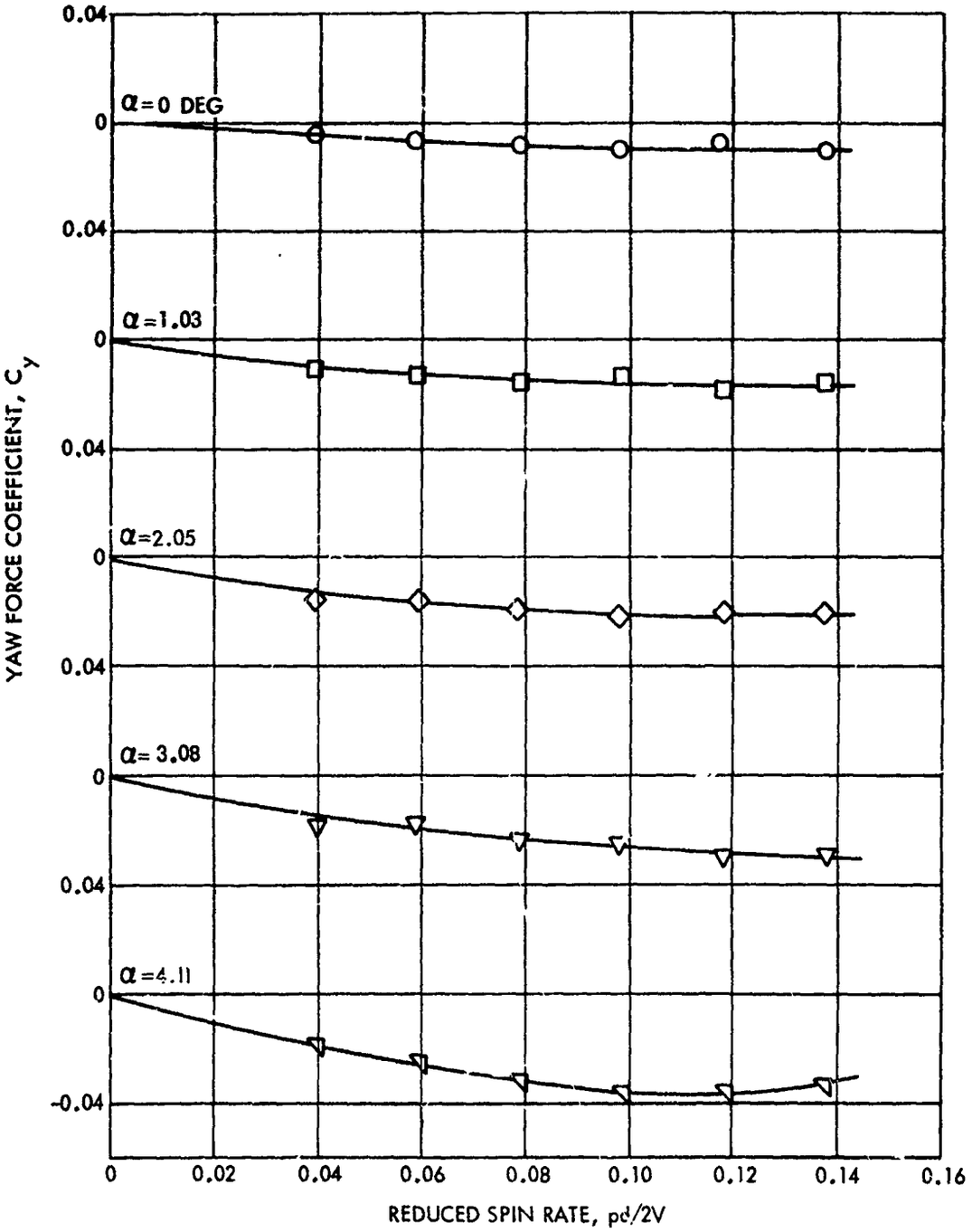

FIG. 34 YAW FORCE COEFFICIENT VERSUS REDUCED SPIN RATE AS A FUNCTION OF ANGLE OF ATTACK FOR CONFIGURATION A3 0 AT A MACH NUMBER OF 0.70 AND A REYNOLDS NUMBER OF 1.072×10^6

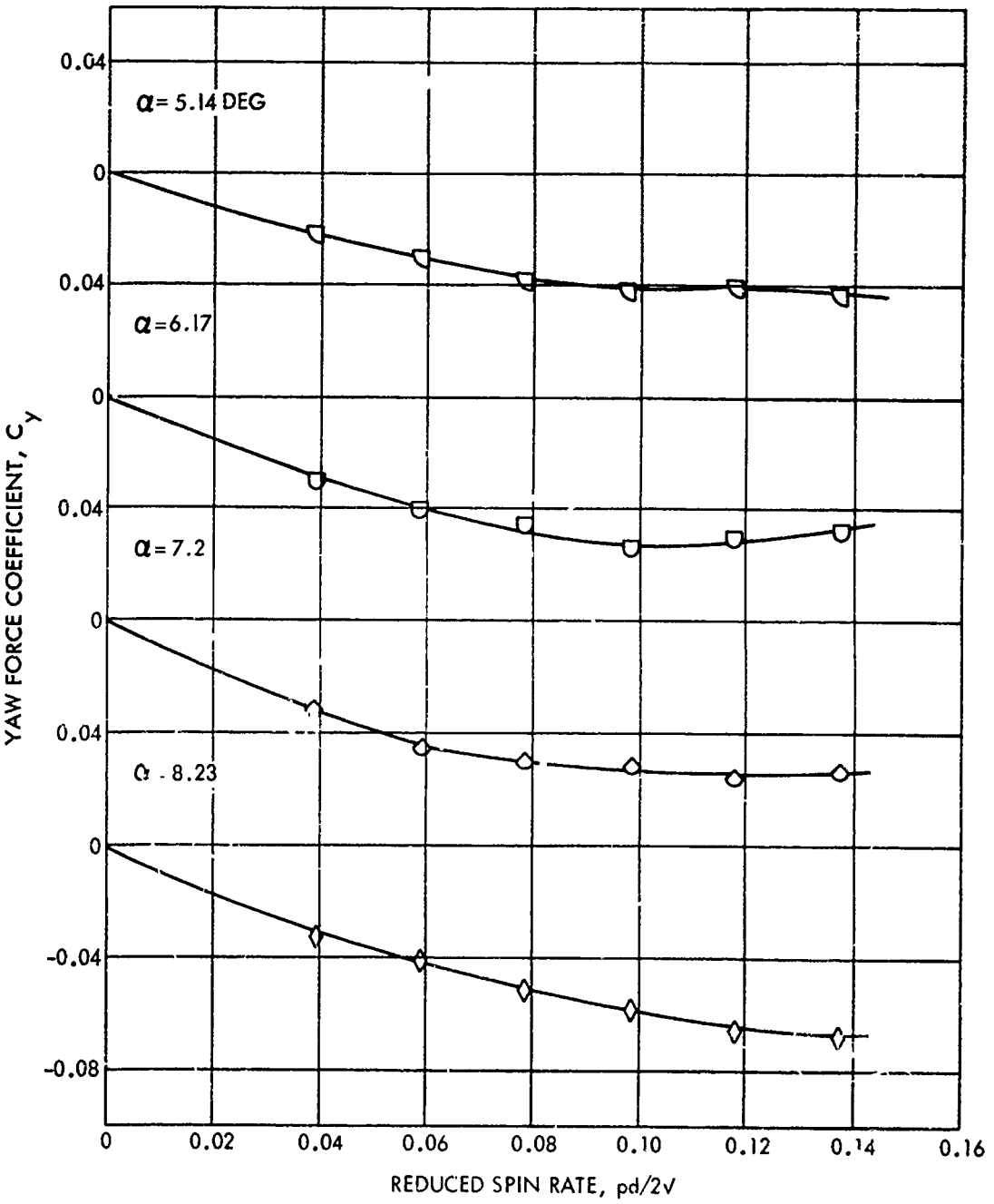

FIG. 35 YAW FORCE COEFFICIENT VERSUS REDUCED SPIN RATE AS A FUNCTION OF ANGLE OF ATTACK FOR CONFIGURATION A3O AT A MACH NUMBER OF 0.70 AND A REYNOLDS NUMBER OF 1.072×10^6

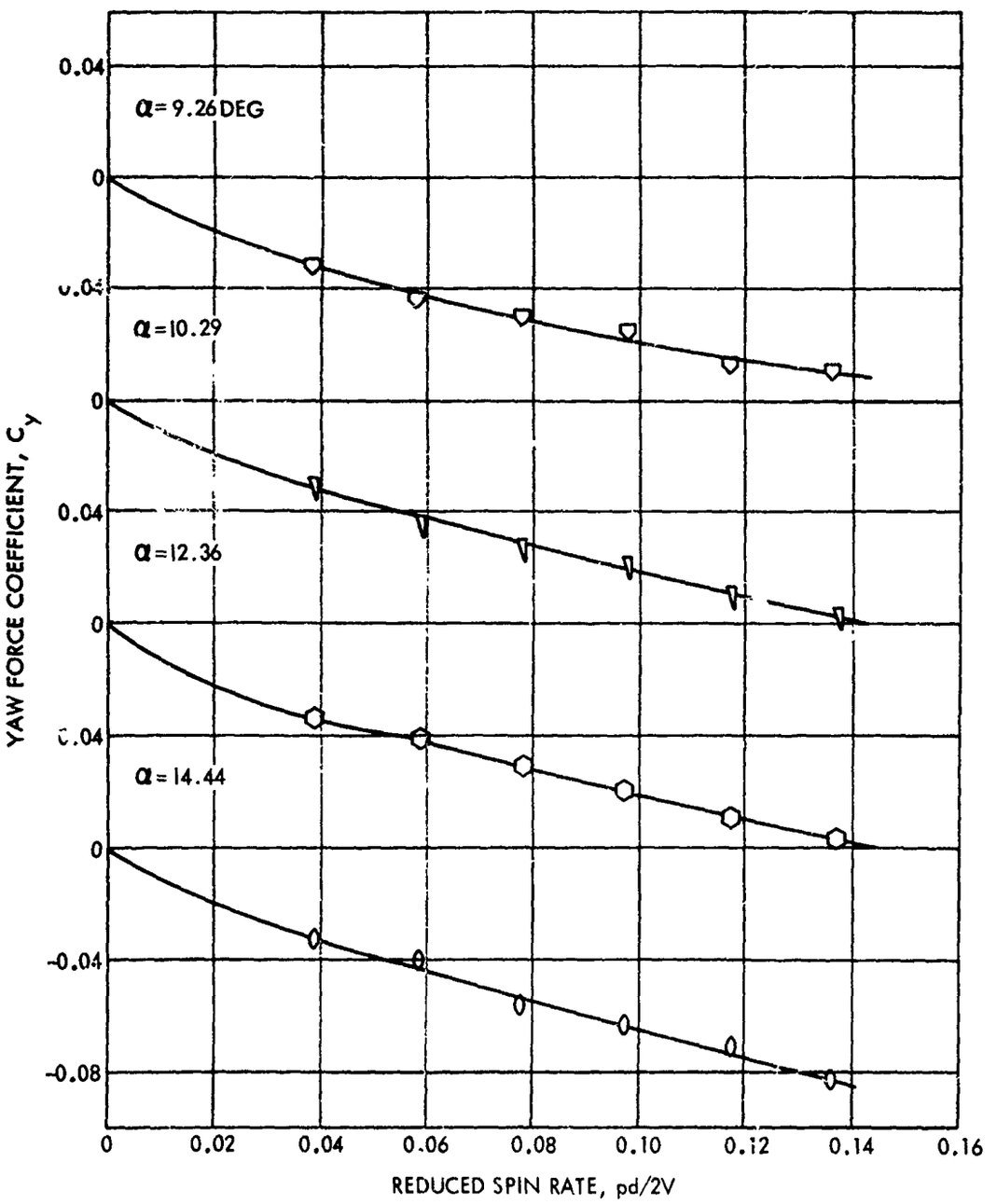

FIG. 36 YAW FORCE COEFFICIENT VERSUS REDUCED SPIN RATE AS A FUNCTION OF ANGLE OF ATTACK FOR CONFIGURATION Aδ_0 AT A MACH NUMBER OF 0.70 AND A REYNOLDS NUMBER OF 1.072×10^6

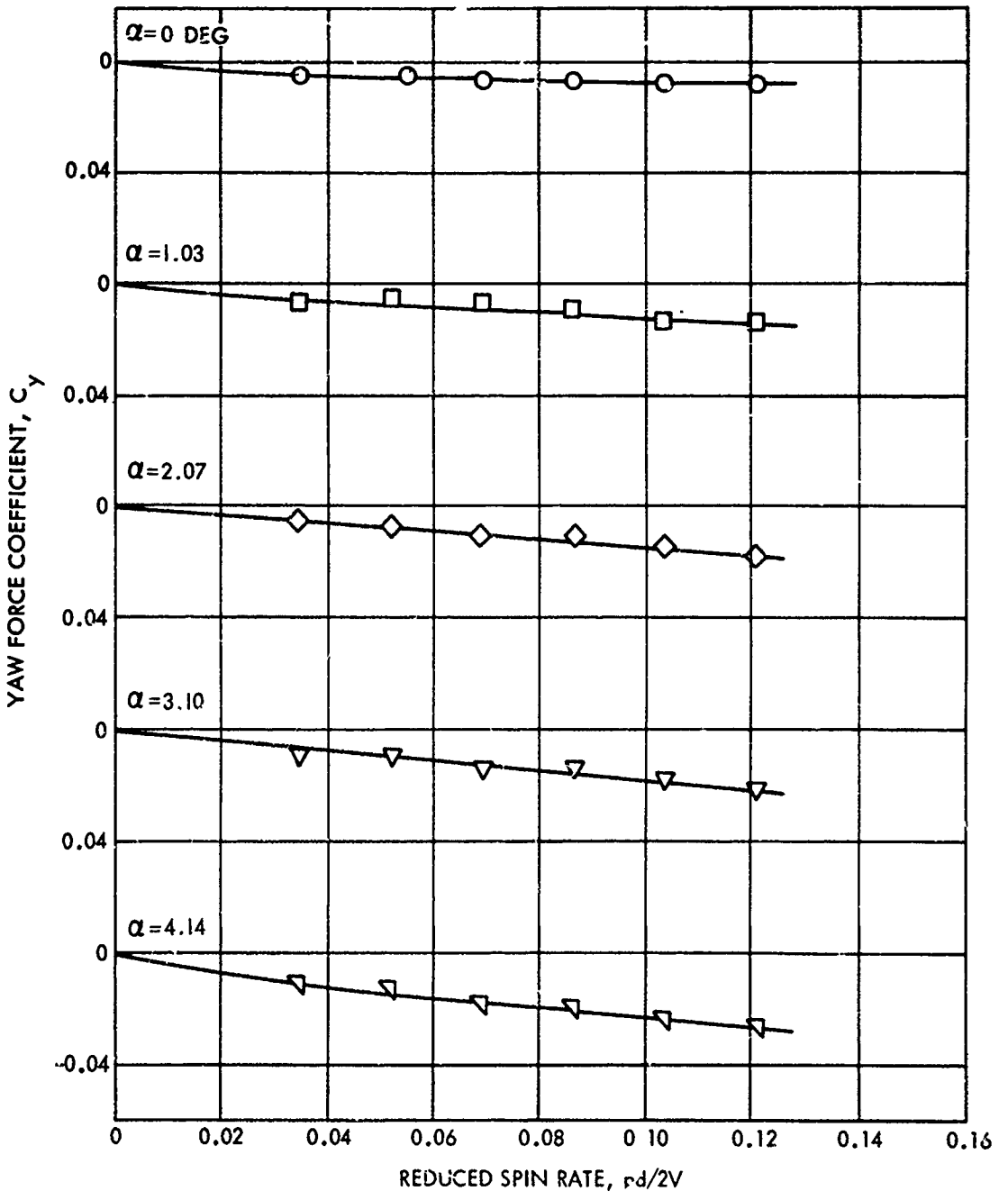

FIG. 37 YAW FORCE COEFFICIENT VERSUS REDUCED SPIN RATE AS A FUNCTION OF ANGLE OF ATTACK FOR CONFIGURATION Aδ0 AT A MACH NUMBER OF 0.80 AND A REYNOLDS NUMBER OF 1.098×10^6

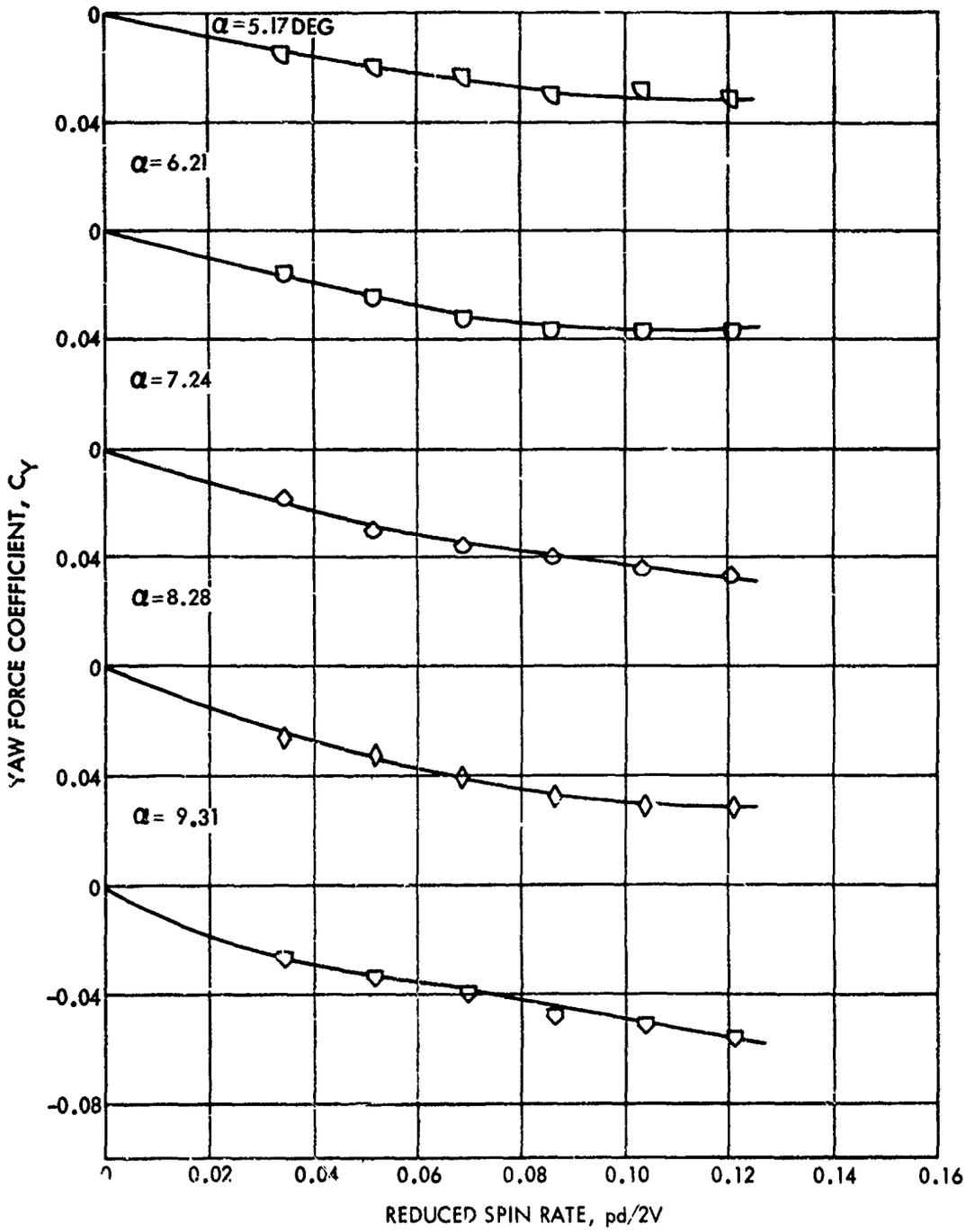

FIG. 38 YAW FORCE COEFFICIENT VERSUS REDUCED SPIN RATE AS A FUNCTION OF ANGLE OF ATTACK FOR CONFIGURATION A8 0 AT A MACH NUMBER OF 0.80 AND A REYNOLDS NUMBER OF 1.098×10^6

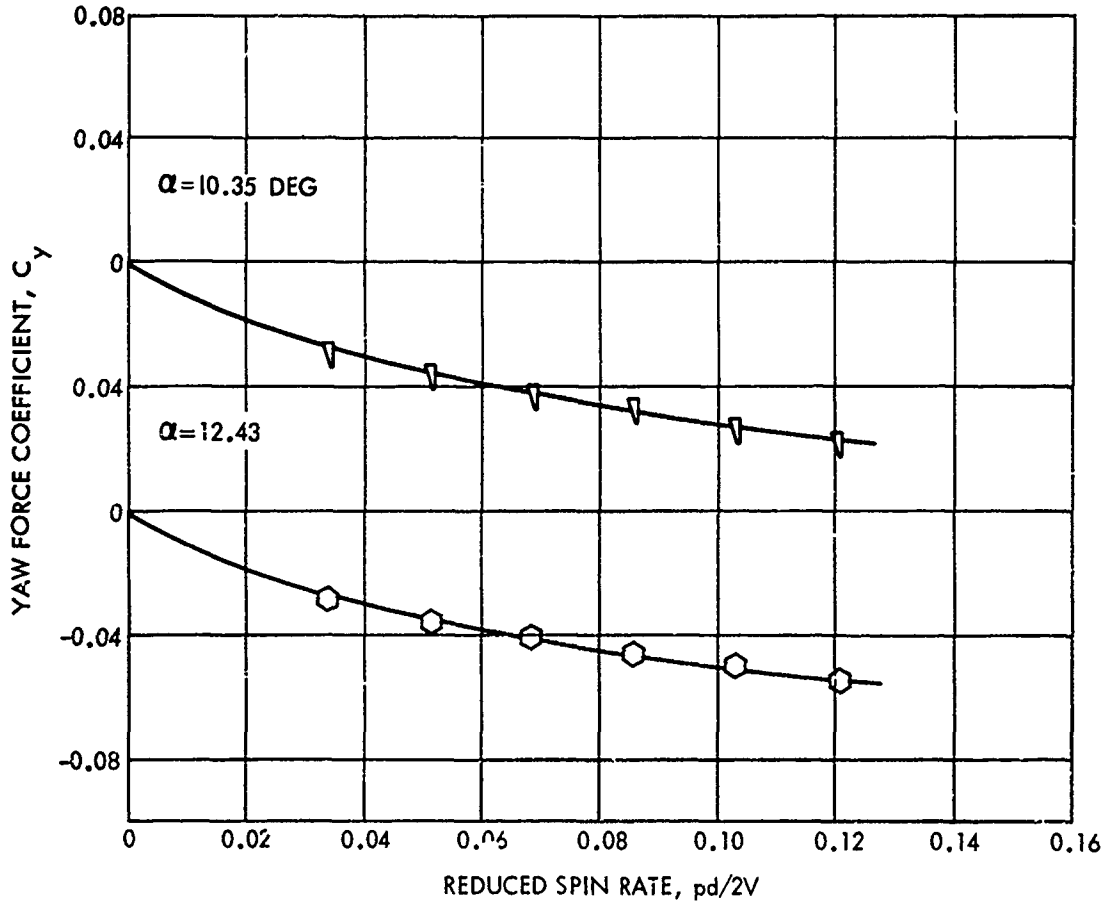

FIG. 39 YAW FORCE COEFFICIENT VERSUS REDUCED SPIN RATE AS A FUNCTION OF ANGLE OF ATTACK FOR CONFIGURATION Aδ0 AT A MACH NUMBER OF 0.80 AND A REYNOLDS NUMBER OF 1.098×10^6

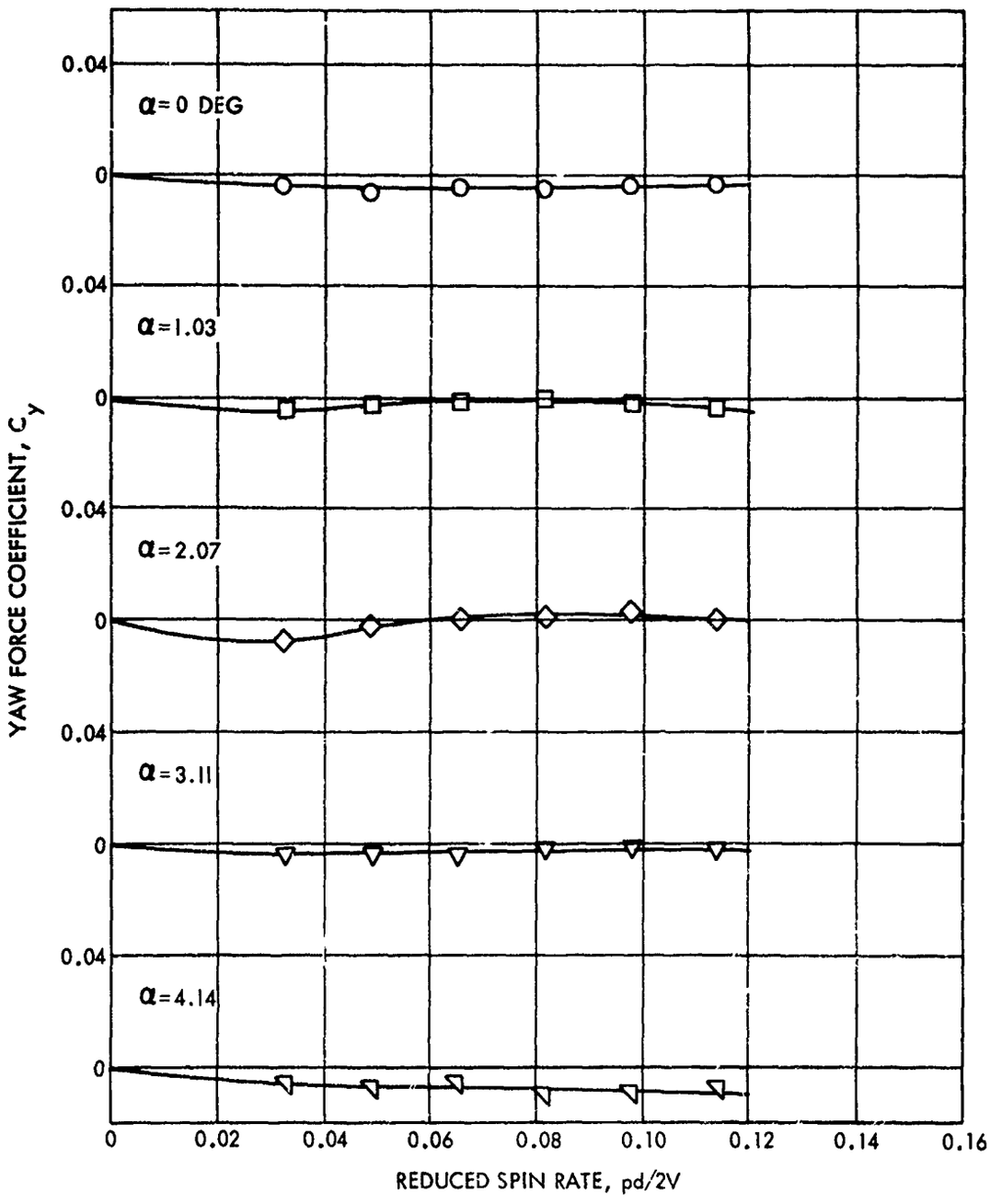

FIG. 40 YAW FORCE COEFFICIENT VERSUS REDUCED SPIN RATE AS A FUNCTION OF ANGLE OF ATTACK FOR CONFIGURATION $A\delta_0$ AT A_6 MACH NUMBER OF 0.85 AND A REYNOLDS NUMBER OF 1.098×10^6

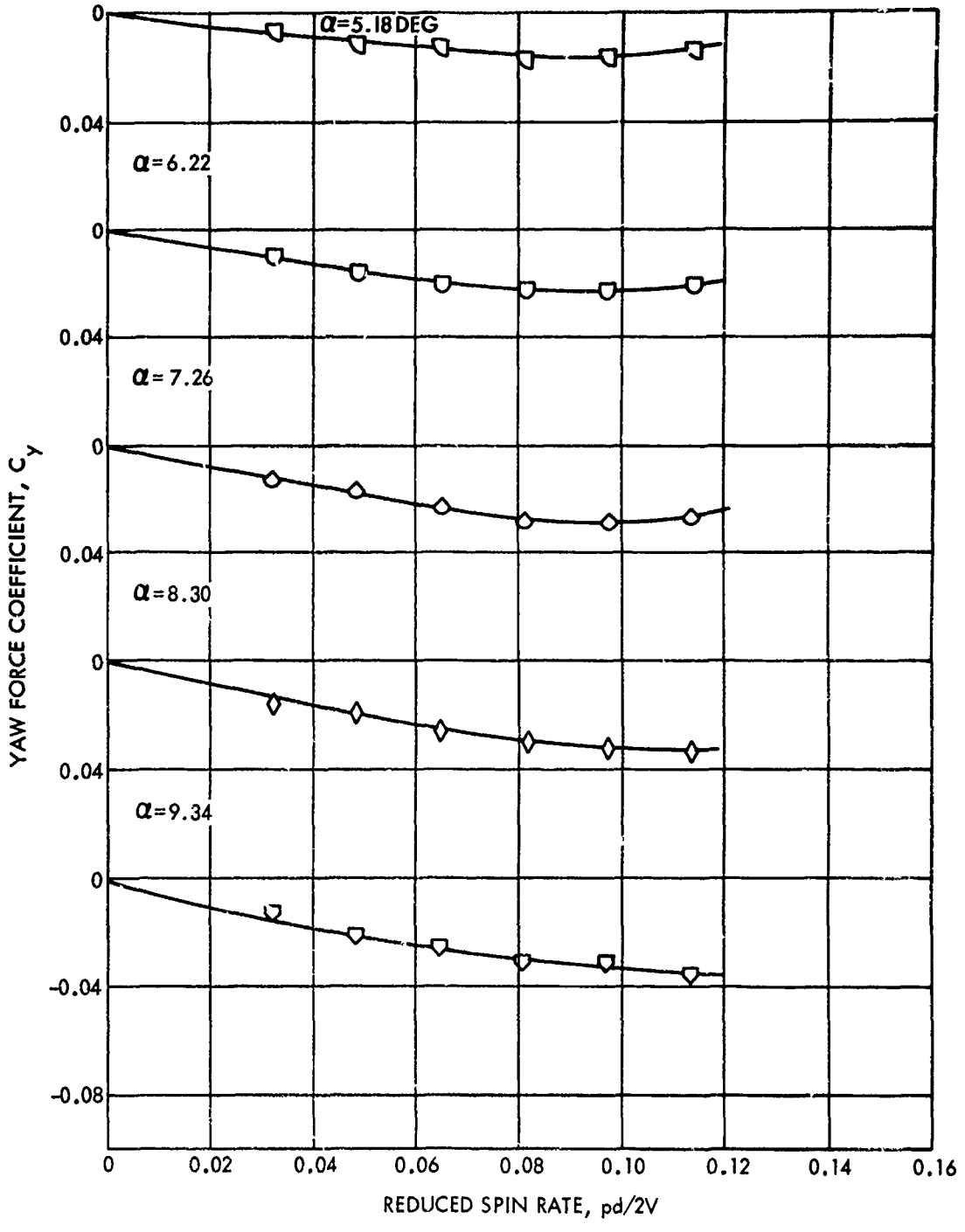

FIG. 41 YAW FORCE COEFFICIENT VERSUS REDUCED SPIN RATE AS A FUNCTION OF ANGLE OF ATTACK FOR CONFIGURATION Aδ0 AT A MACH NUMBER OF 0.85 AND A REYNOLDS NUMBER OF 1.098×10^6

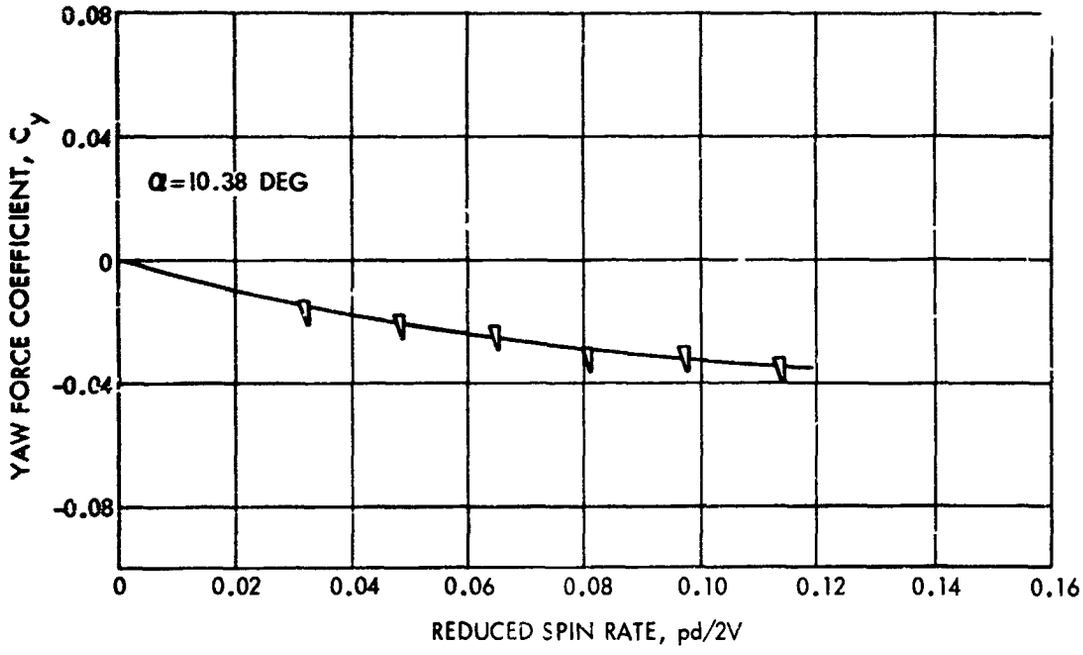

FIG. 42 YAW FORCE COEFFICIENT VERSUS REDUCED SPIN RATE AS A FUNCTION OF ANGLE OF ATTACK FOR CONFIGURATION Aδ0 AT A MACH NUMBER OF 0.85 AND A REYNOLDS NUMBER OF 1.098×10^6

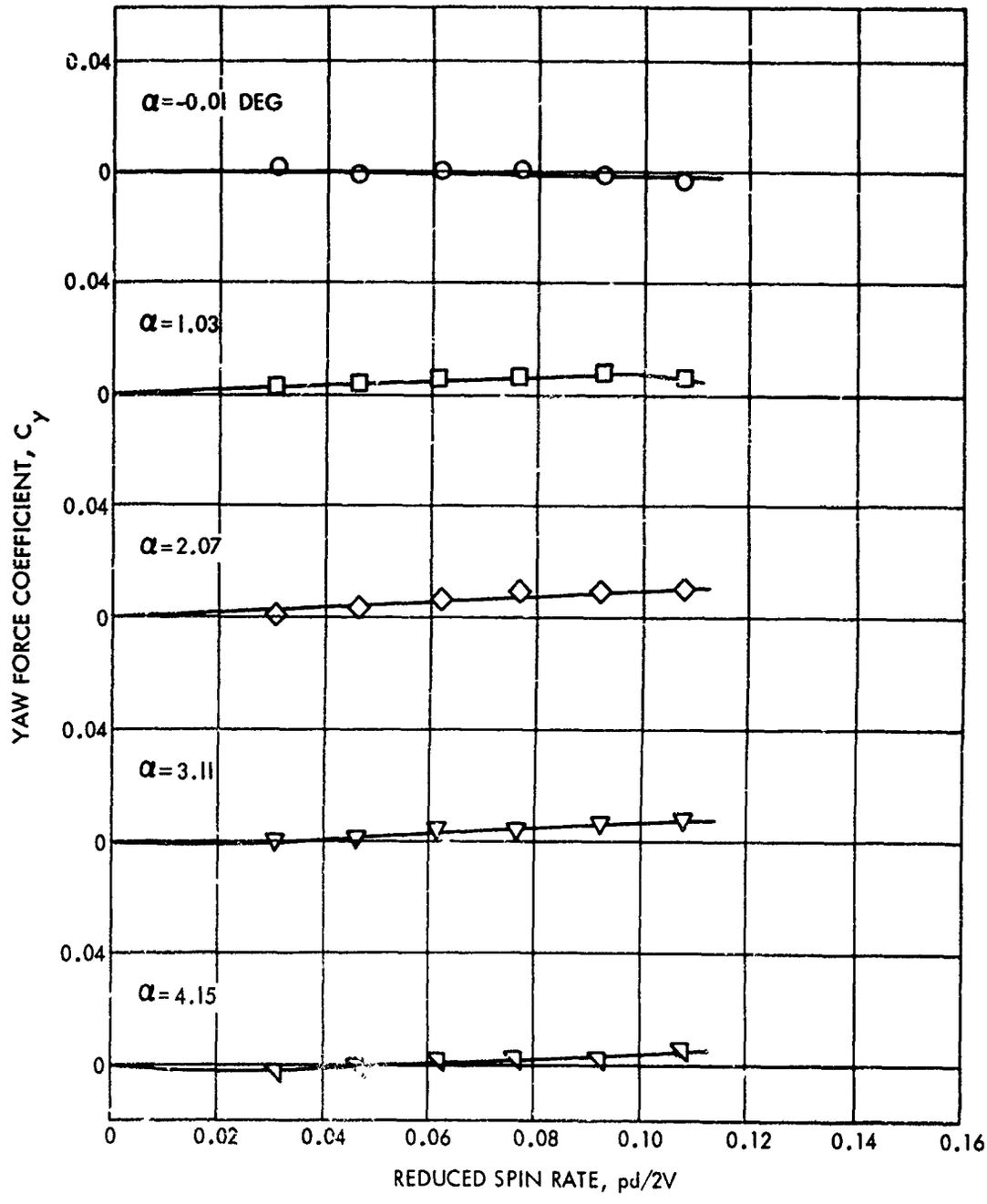

FIG. 43 YAW FORCE COEFFICIENT VERSUS REDUCED SPIN RATE AS A FUNCTION OF ANGLE OF ATTACK FOR CONFIGURATION Aδ0 AT A MACH NUMBER OF 0.90 AND A REYNOLDS NUMBER OF 1.151×10^6

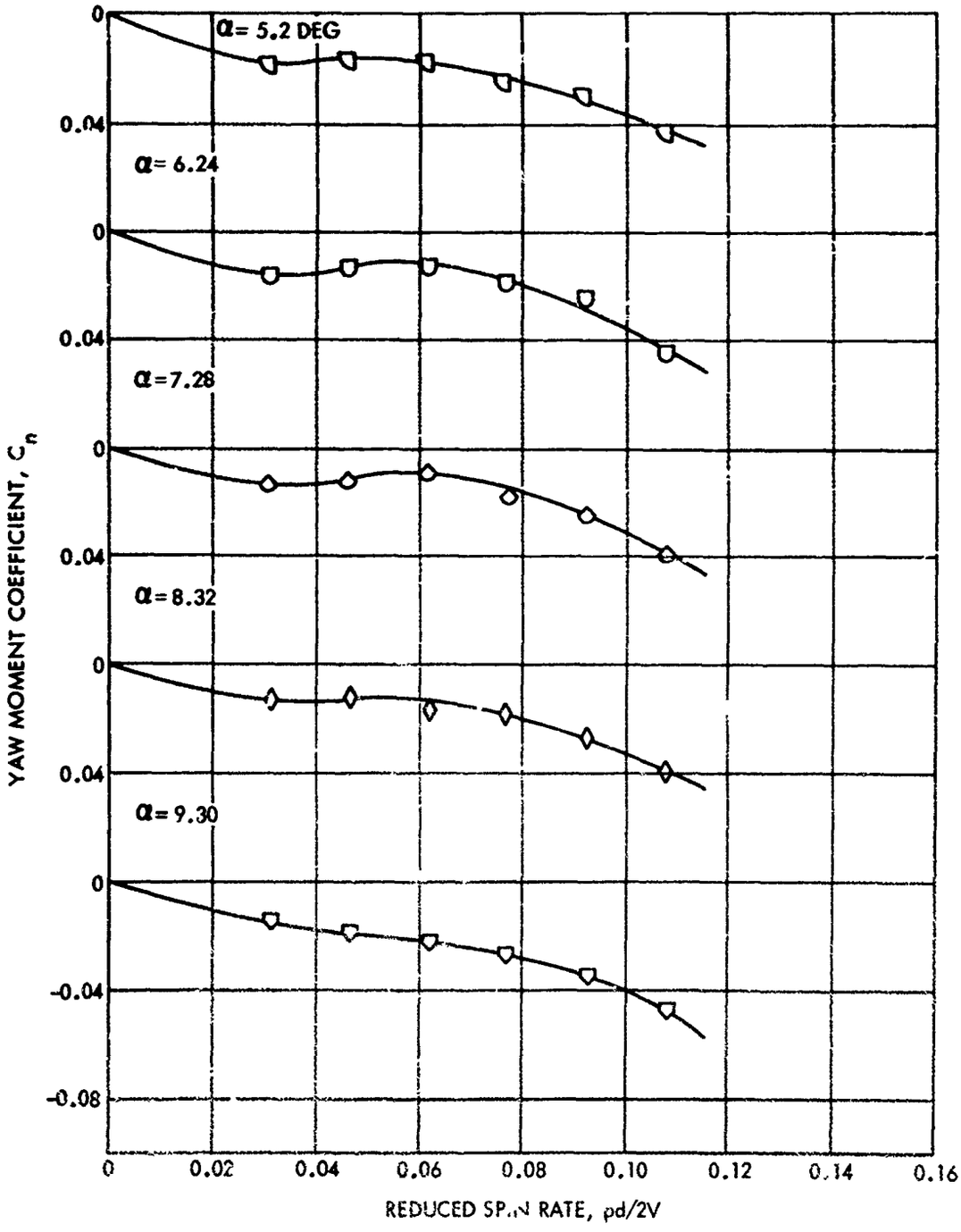

FIG. 44 YAW MOMENT COEFFICIENT VERSUS REDUCED SPIN RATE AS A FUNCTION OF ANGLE OF ATTACK FOR CONFIGURATION Aδ 0 AT A MACH NUMBER OF 0.90 AND A REYNOLDS NUMBER OF 1.151×10^6

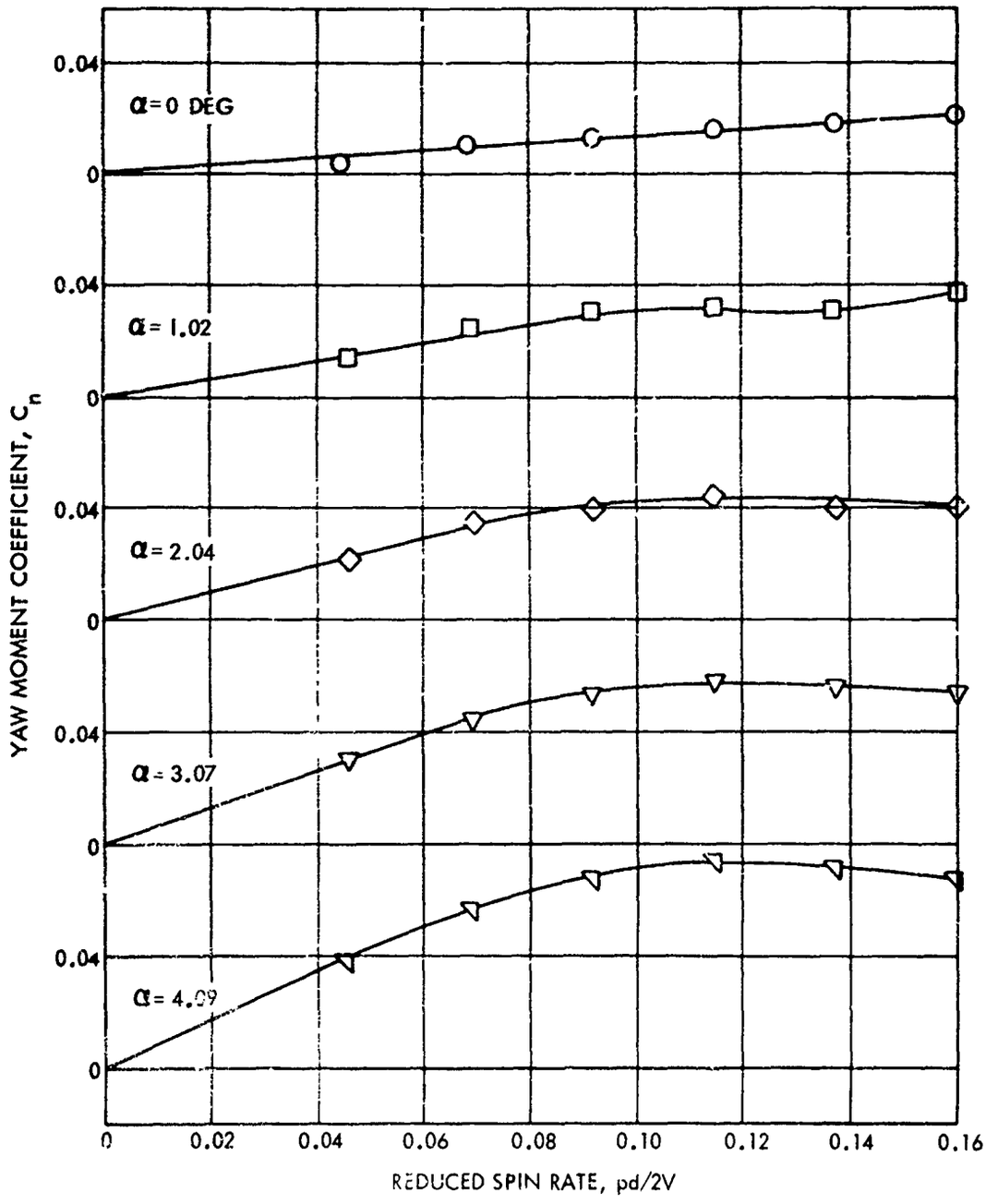

FIG. 45 YAW MOMENT COEFFICIENT VERSUS REDUCED SPIN RATE AS A FUNCTION OF ANGLE OF ATTACK FOR CONFIGURATION Aδ 0 AT A MACH NUMBER OF 0.60 AND A REYNOLDS NUMBER OF 0.971×10^6

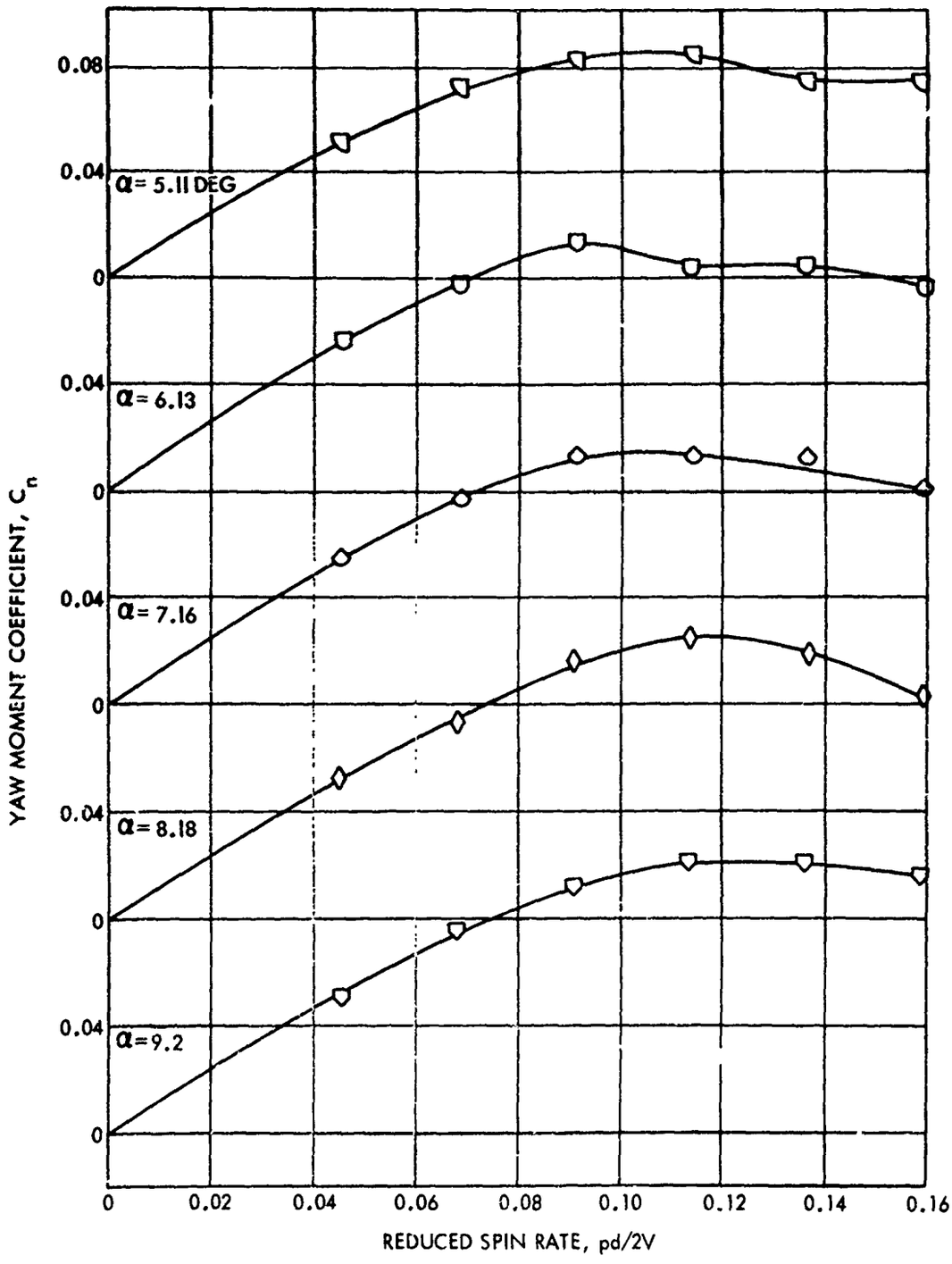

FIG. 46 YAW MOMENT COEFFICIENT VERSUS REDUCED SPIN RATE AS A FUNCTION OF ANGLE OF ATTACK FOR CONFIGURATION Aδ0 AT A MACH NUMBER OF 0.60 AND A REYNOLDS NUMBER OF 0.971×10^6

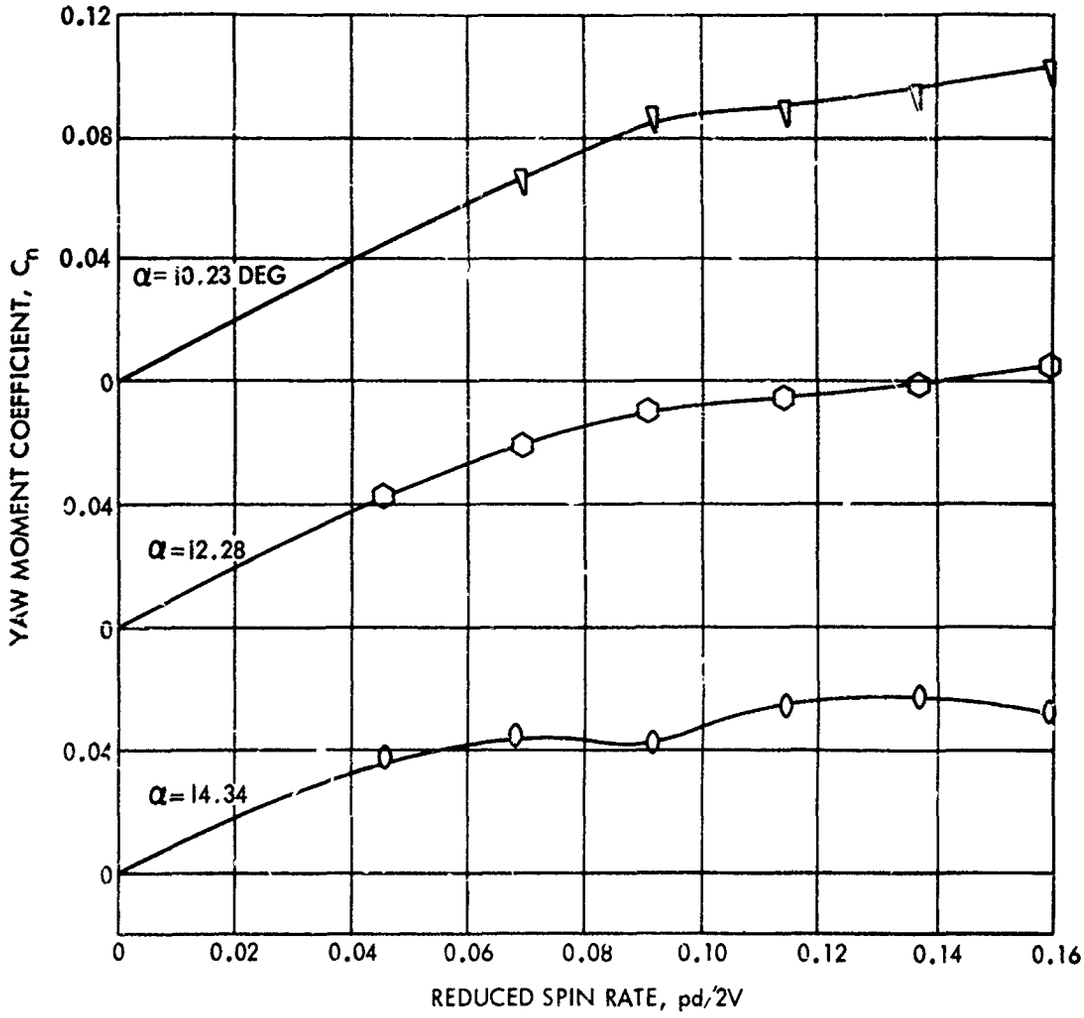

FIG. 47 YAW MOMENT COEFFICIENT VERSUS REDUCED SPIN RATE AS A FUNCTION OF ANGLE OF ATTACK FOR CONFIGURATION Aδ0 AT A MACH NUMBER OF 0.60 AND A REYNOLDS NUMBER OF 0.971×10^6

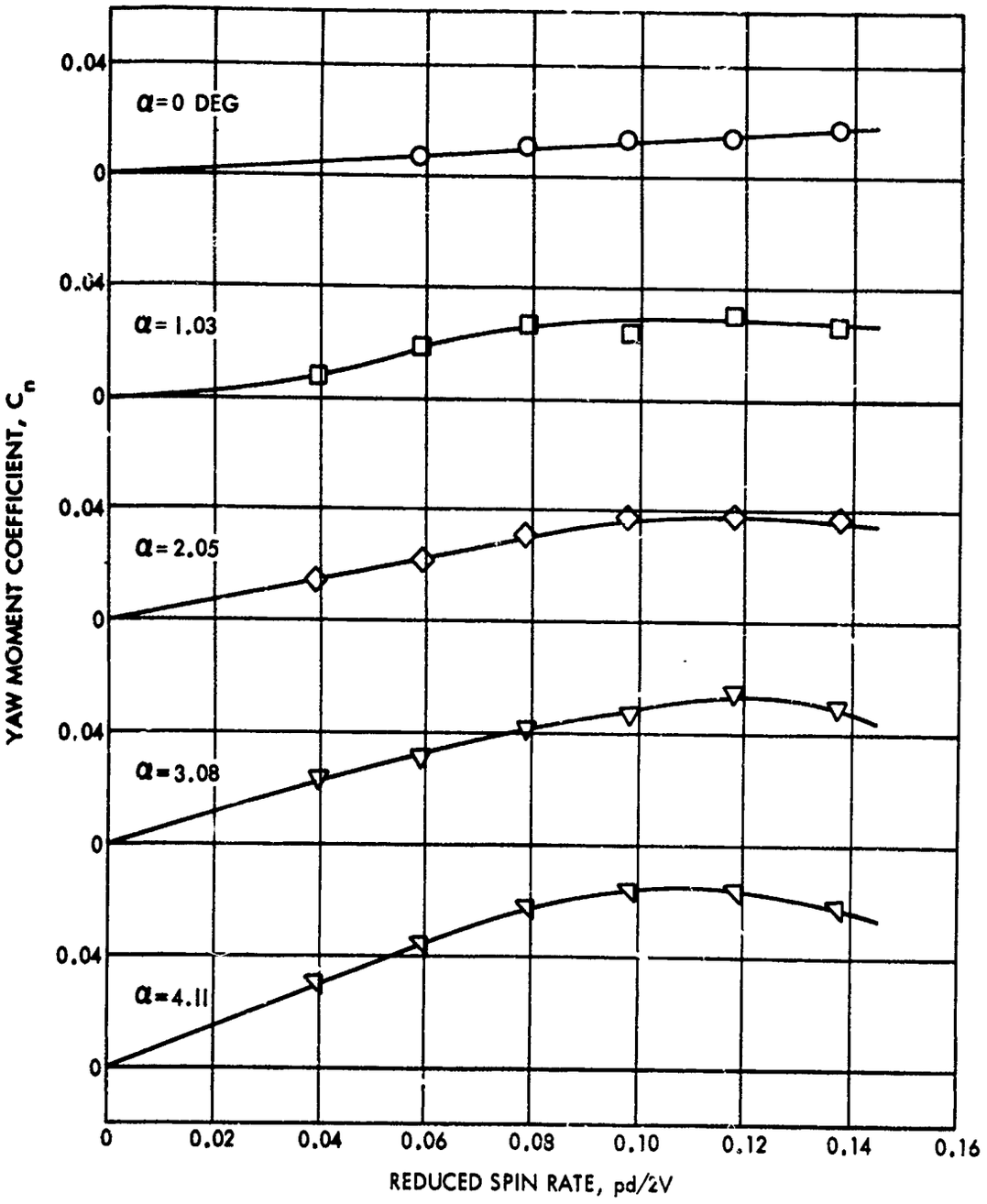

FIG. 48 YAW MOMENT COEFFICIENT VERSUS REDUCED SPIN RATE AS A FUNCTION OF ANGLE OF ATTACK FOR CONFIGURATION A3 0 AT A MACH NUMBER OF 0.70 AND A REYNOLDS NUMBER OF 1.072×10^6

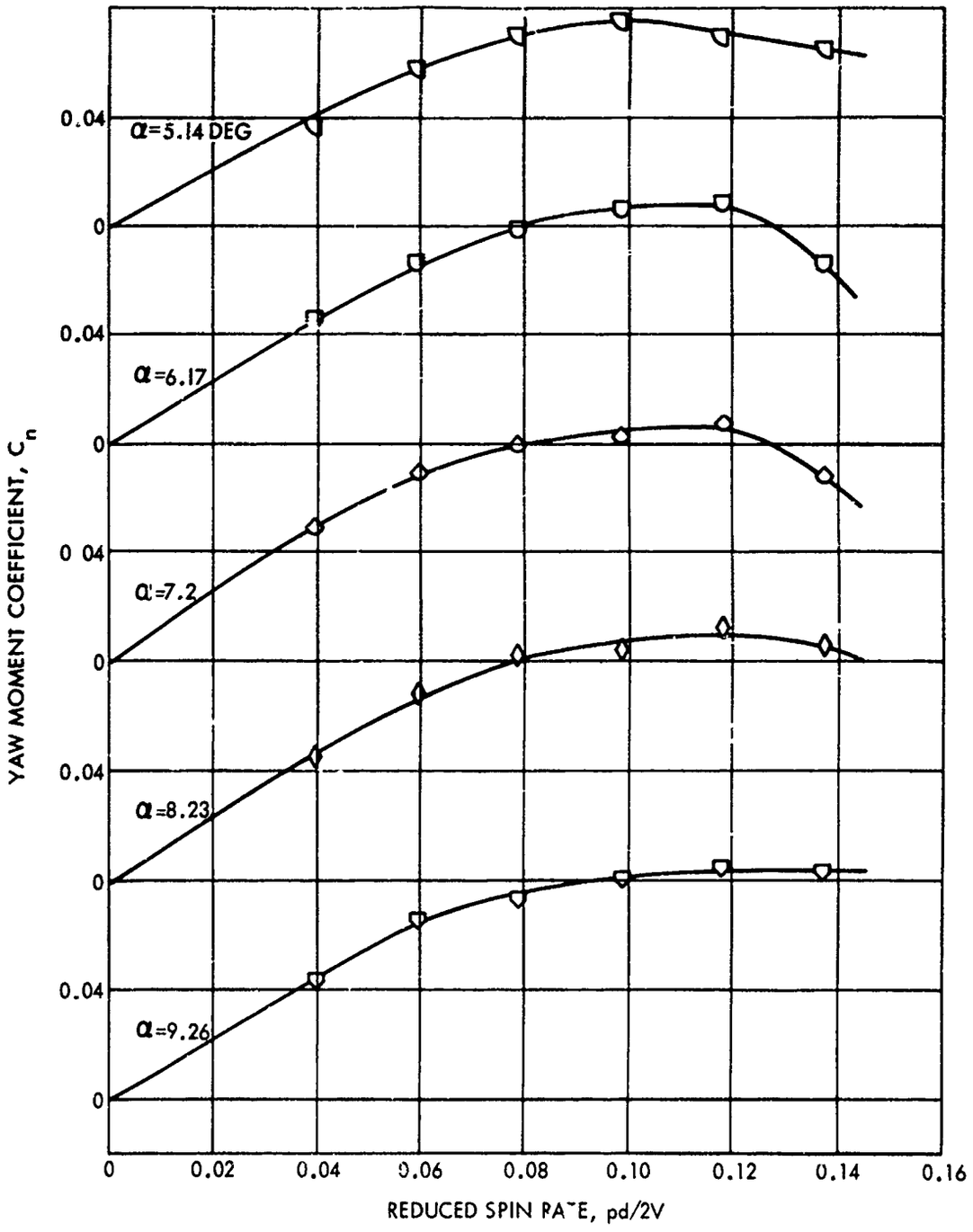

FIG. 49 YAW MOMENT COEFFICIENT VERSUS REDUCED SPIN RATE AS A FUNCTION OF ANGLE OF ATTACK FOR CONFIGURATION Aδ0 AT A MACH NUMBER OF 0.70 AND A REYNOLDS NUMBER OF 1.072×10^6

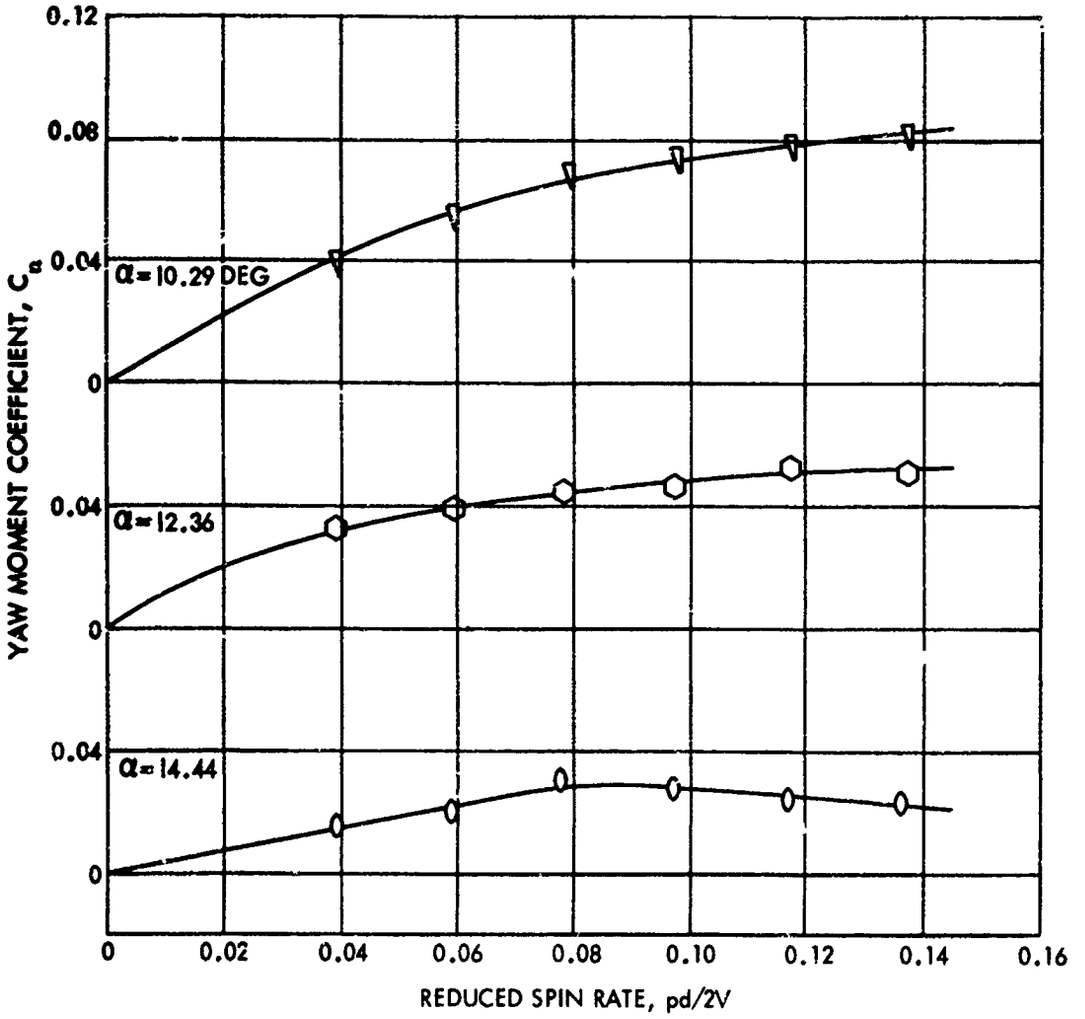

FIG. 50 YAW MOMENT COEFFICIENT VERSUS REDUCED SPIN RATE AS A FUNCTION OF ANGLE OF ATTACK FOR CONFIGURATION Aδ0 AT A MACH NUMBER OF 0.70 AND A REYNOLDS NUMBER OF 1.072×10^6

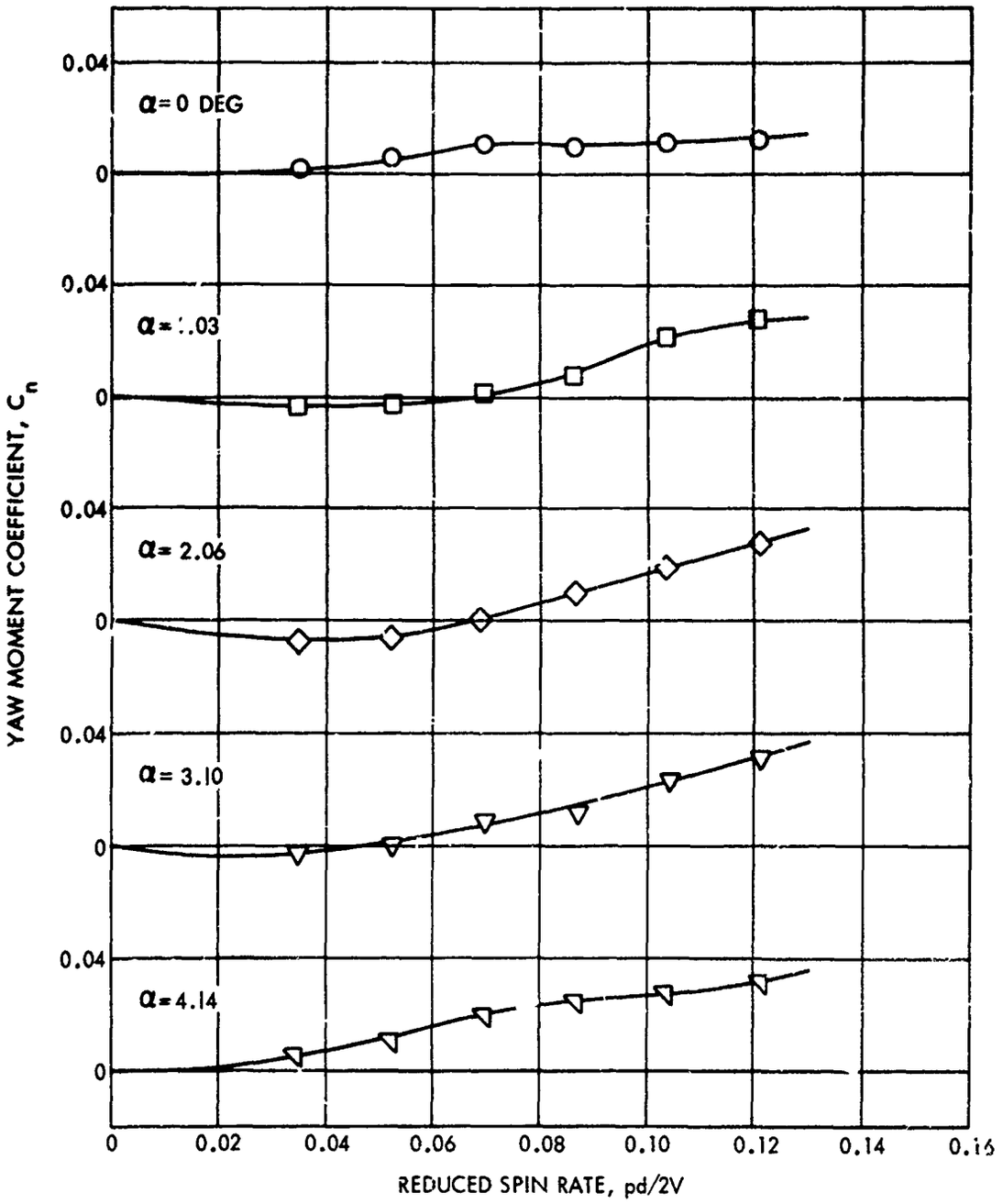

FIG. 51 YAW MOMENT COEFFICIENT VERSUS REDUCED SPIN RATE AS A FUNCTION OF ANGLE OF ATTACK FOR CONFIGURATION A8 0 AT A MACH NUMBER OF 0.80 AND A REYNOLDS NUMBER OF 1.098×10^6

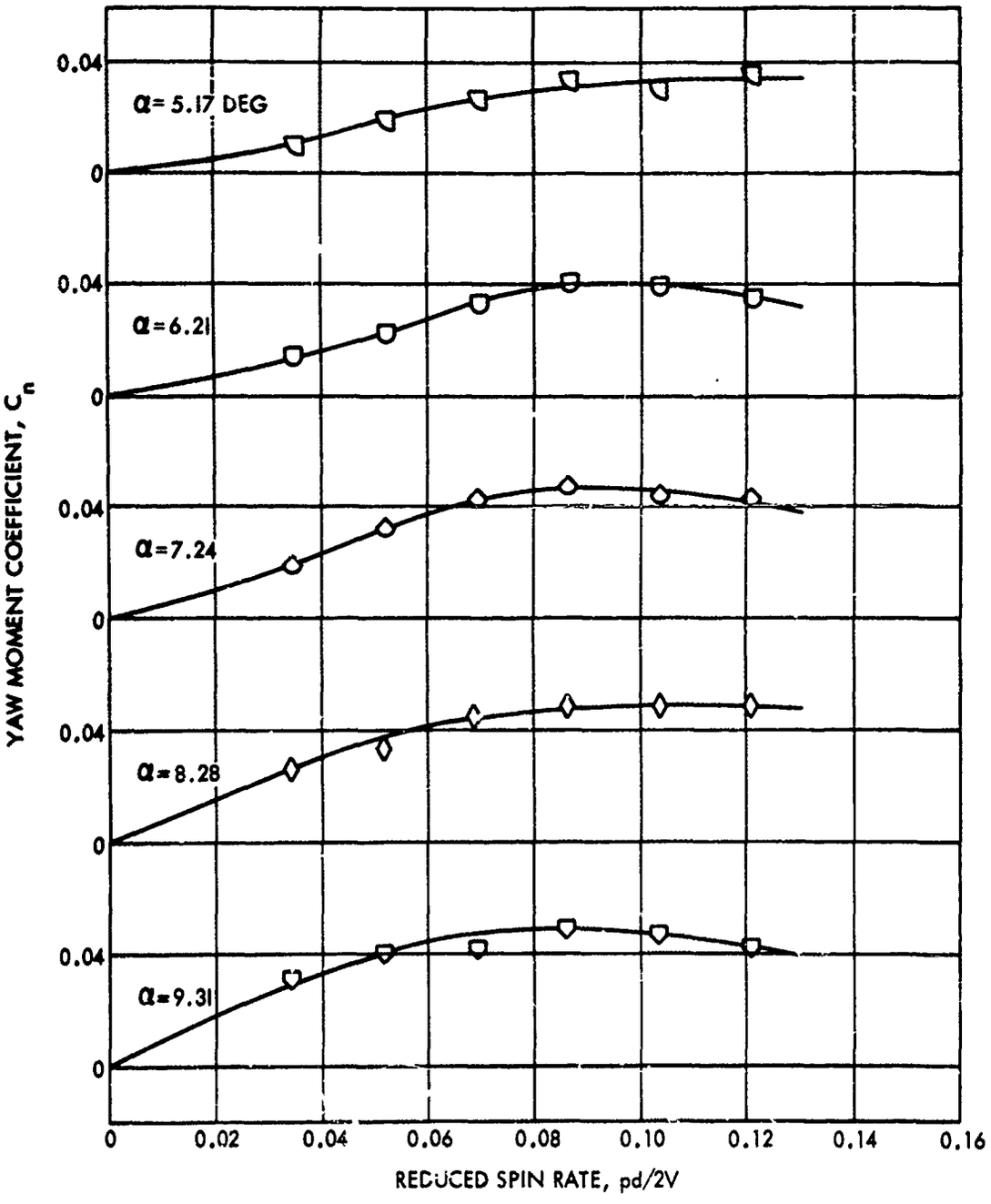

FIG. 52 YAW MOMENT COEFFICIENT VERSUS REDUCED SPIN RATE AS A FUNCTION OF ANGLE OF ATTACK FOR CONFIGURATION A8 0 AT A MACH NUMBER OF 0.80 AND A REYNOLDS NUMBER OF 1.098×10^6

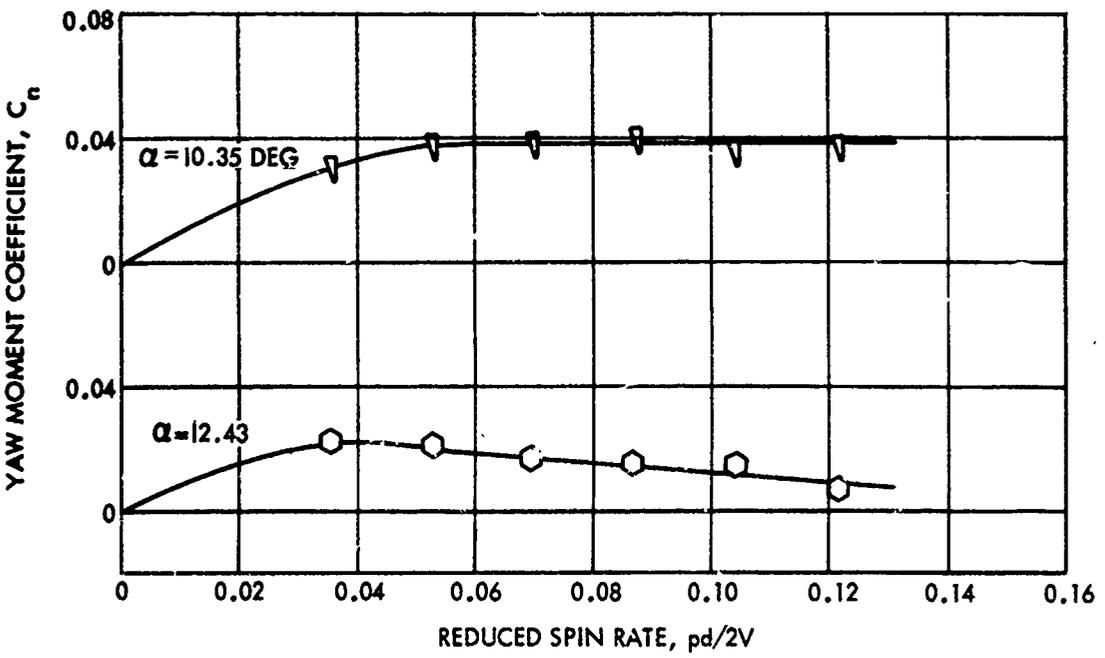

FIG. 53 YAW MOMENT COEFFICIENT VERSUS REDUCED SPIN RATE AS A FUNCTION OF ANGLE OF ATTACK FOR CONFIGURATION $A\delta_0$ AT A_6 MACH NUMBER OF 0.80 AND A REYNOLDS NUMBER OF 1.098×10^6

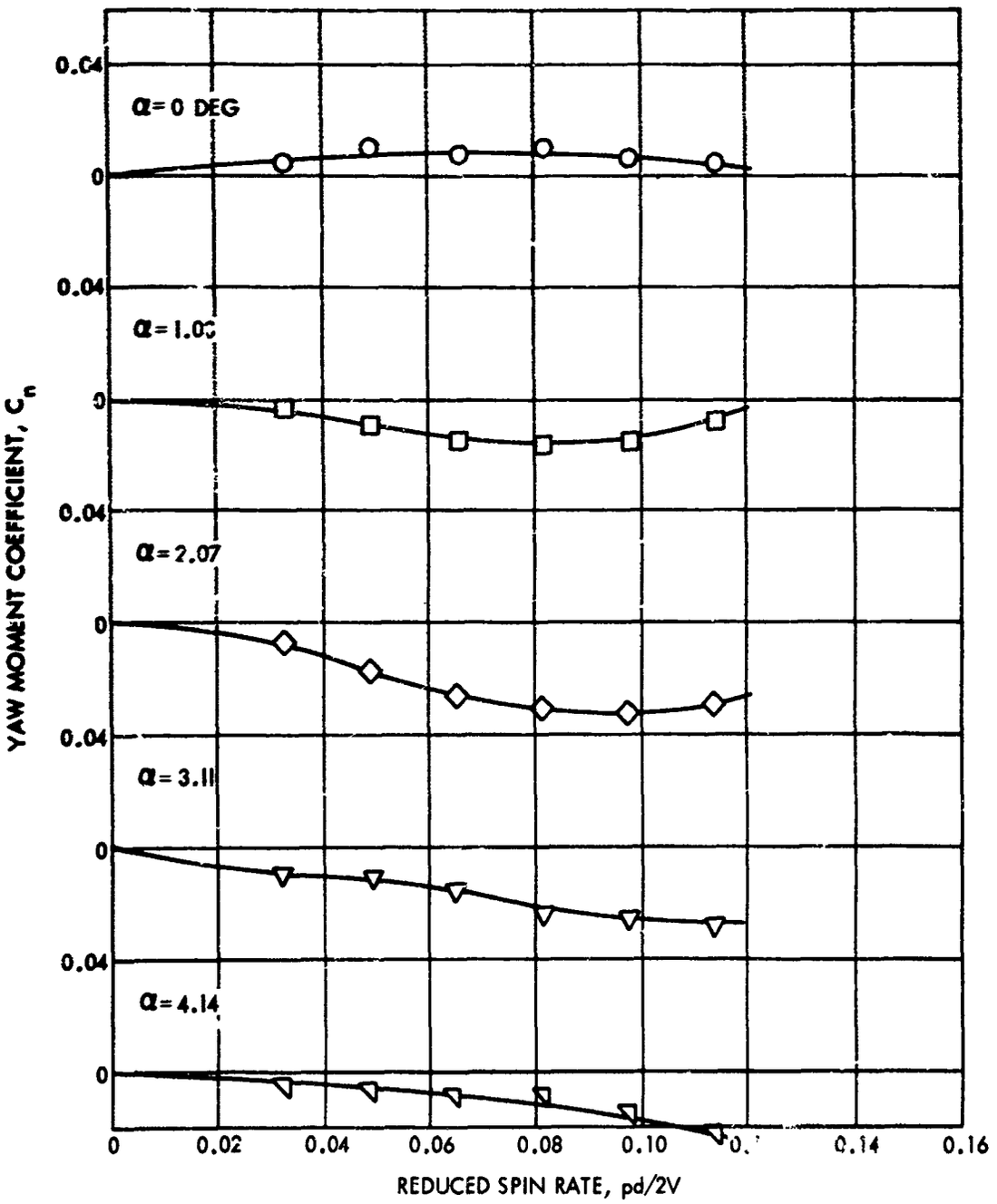

FIG. 54 YAW MOMENT COEFFICIENT VERSUS REDUCED SPIN RATE AS A FUNCTION OF ANGLE OF ATTACK FOR CONFIGURATION A8 0 AT A MACH NUMBER OF 0.85 AND A REYNOLDS NUMBER OF 1.098×10^6

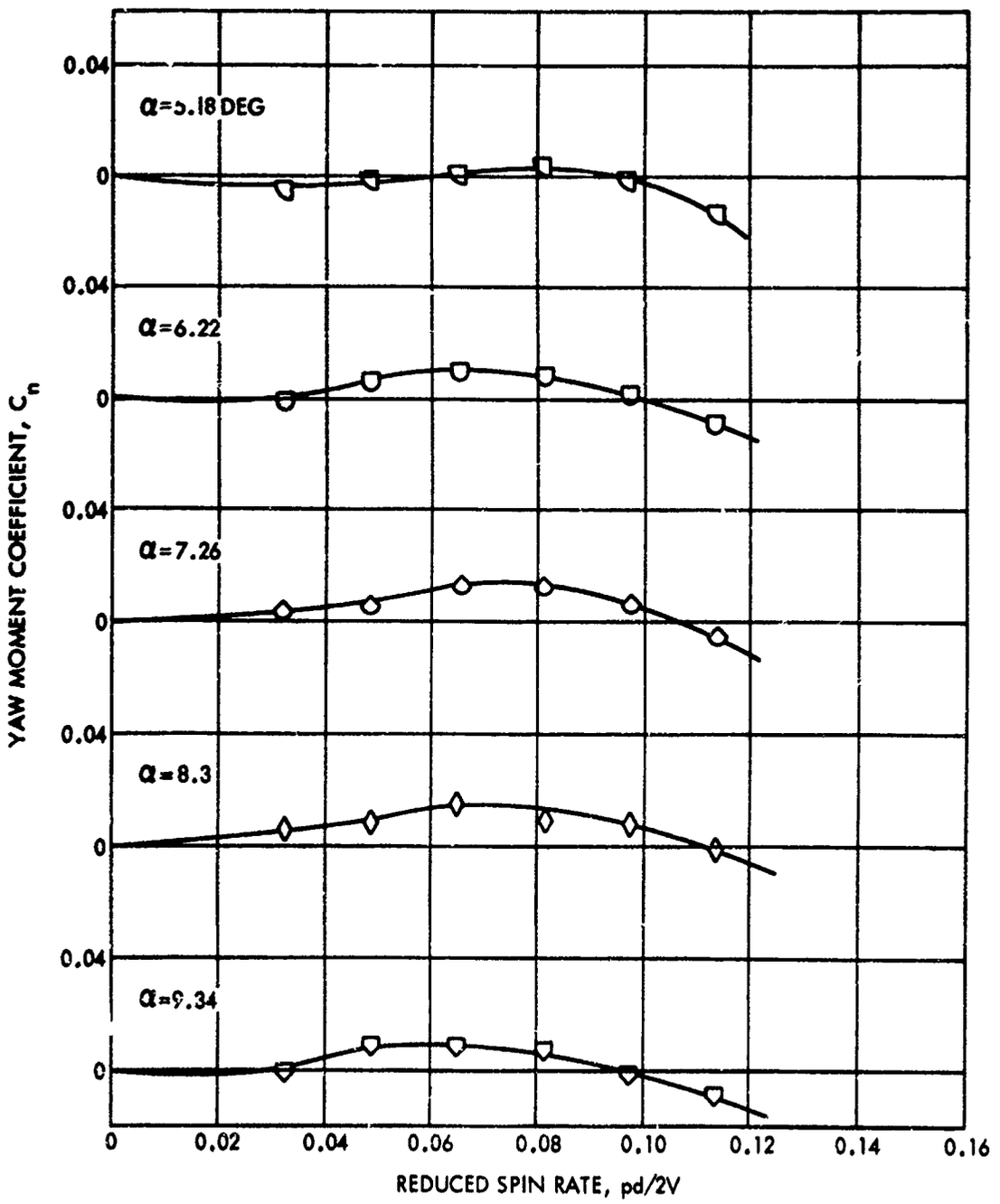

FIG. 55 YAW MOMENT COEFFICIENT VERSUS REDUCED SPIN RATE AS A FUNCTION OF ANGLE OF ATTACK FOR CONFIGURATION A8 0 AT A6 MACH NUMBER OF 0.85 AND A REYNOLDS NUMBER OF 1.098×10^6

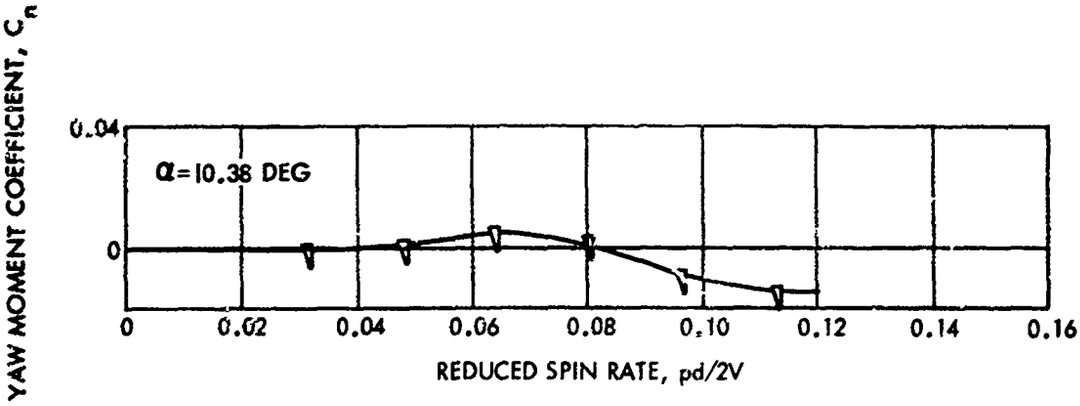

FIG. 56 YAW MOMENT COEFFICIENT VERSUS REDUCED SPIN RATE AS A FUNCTION OF ANGLE OF ATTACK FOR CONFIGURATION A8 0 AT A MACH NUMBER OF 0.85 AND A REYNOLDS NUMBER OF 1.098×10^6

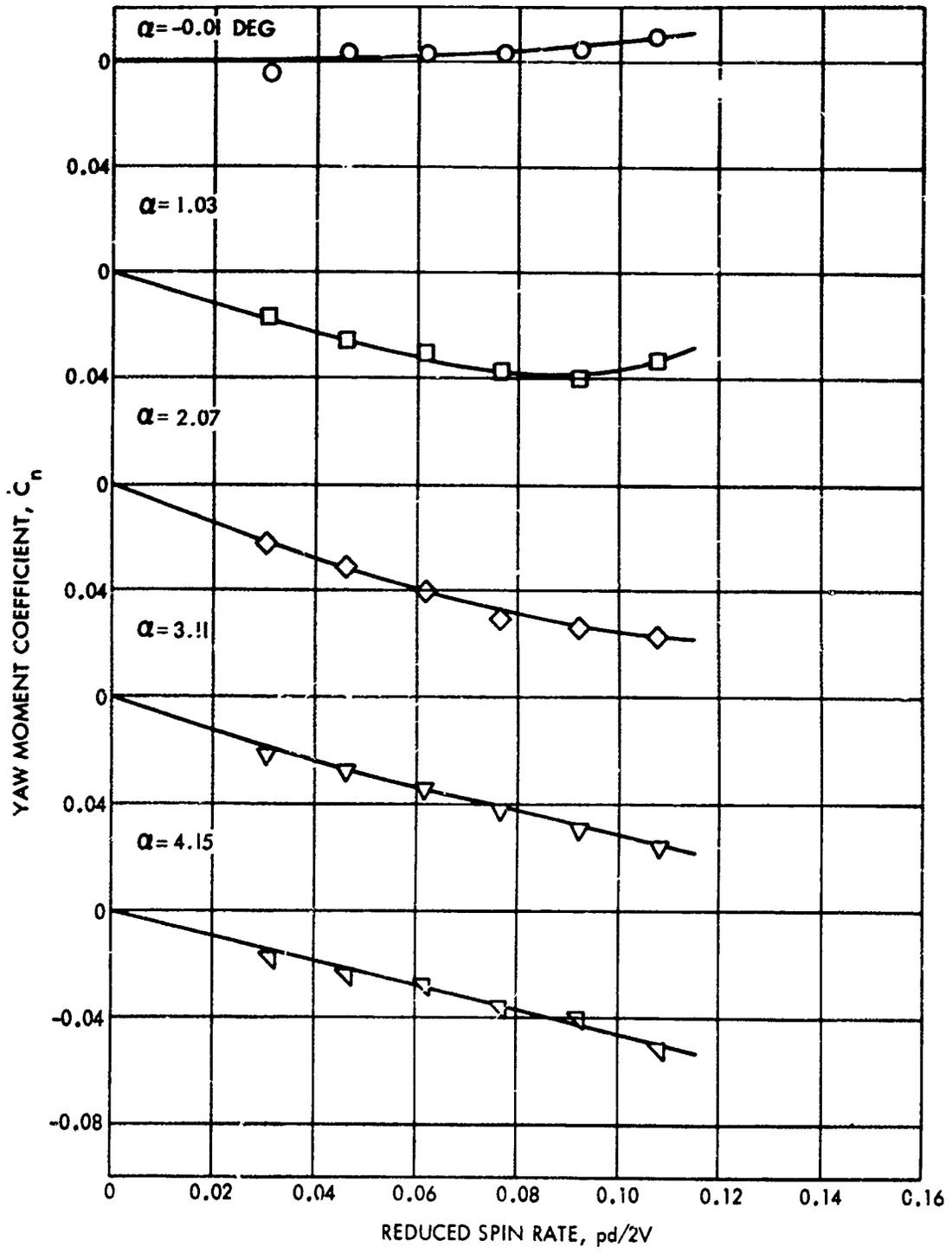

FIG. 57 YAW MOMENT COEFFICIENT VERSUS REDUCED SPIN RATE AS A FUNCTION OF ANGLE OF ATTACK FOR CONFIGURATION A8 0 AT A MACH NUMBER OF 0.90 AND A REYNOLDS NUMBER OF 1.151 x 10^6

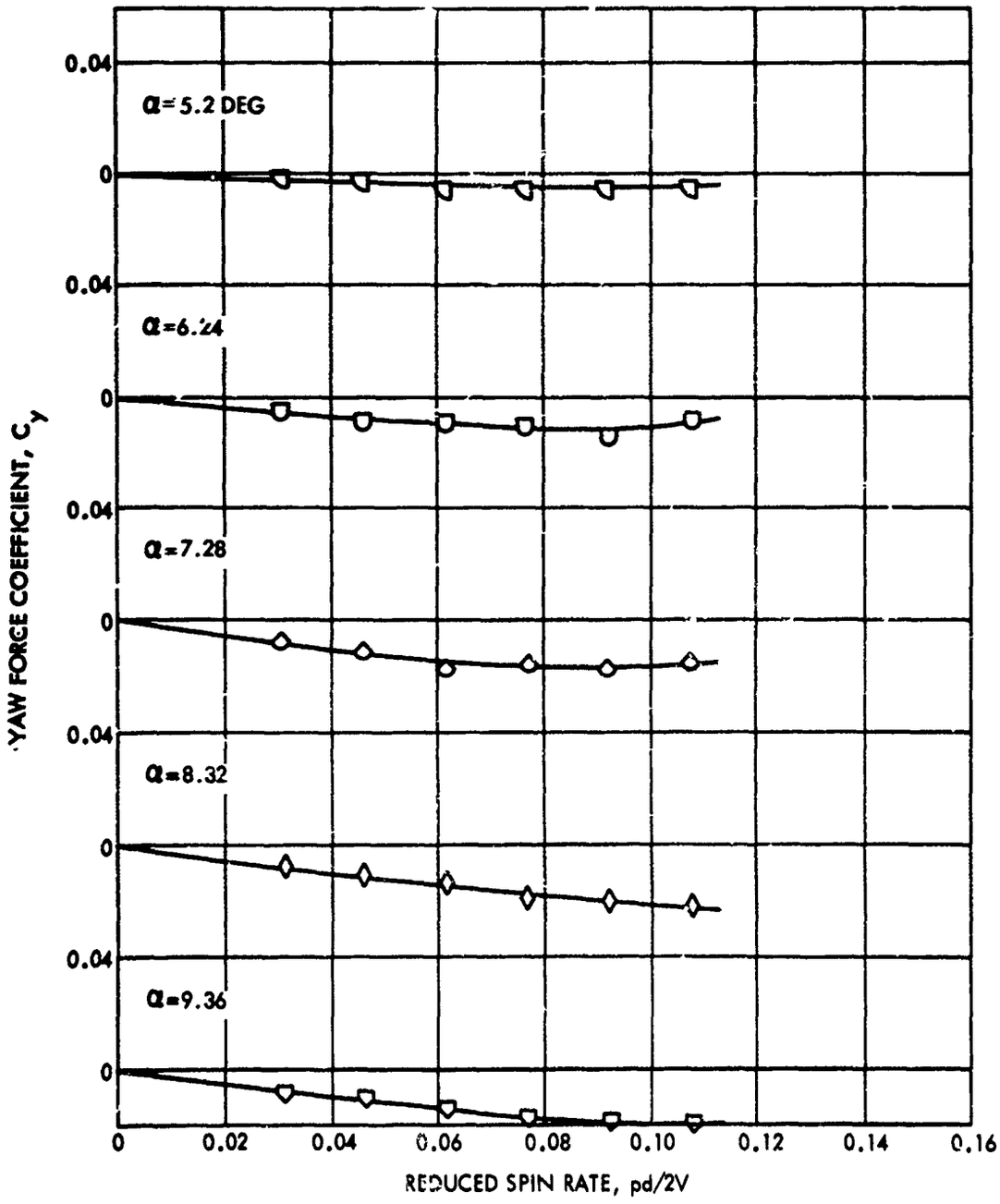

FIG. 58 YAW FORCE COEFFICIENT VERSUS REDUCED SPIN RATE AS A FUNCTION OF ANGLE OF ATTACK FOR CONFIGURATION A8 0 AT A MACH NUMBER OF 0.90 AND A REYNOLDS NUMBER OF 1.151 x 10^6

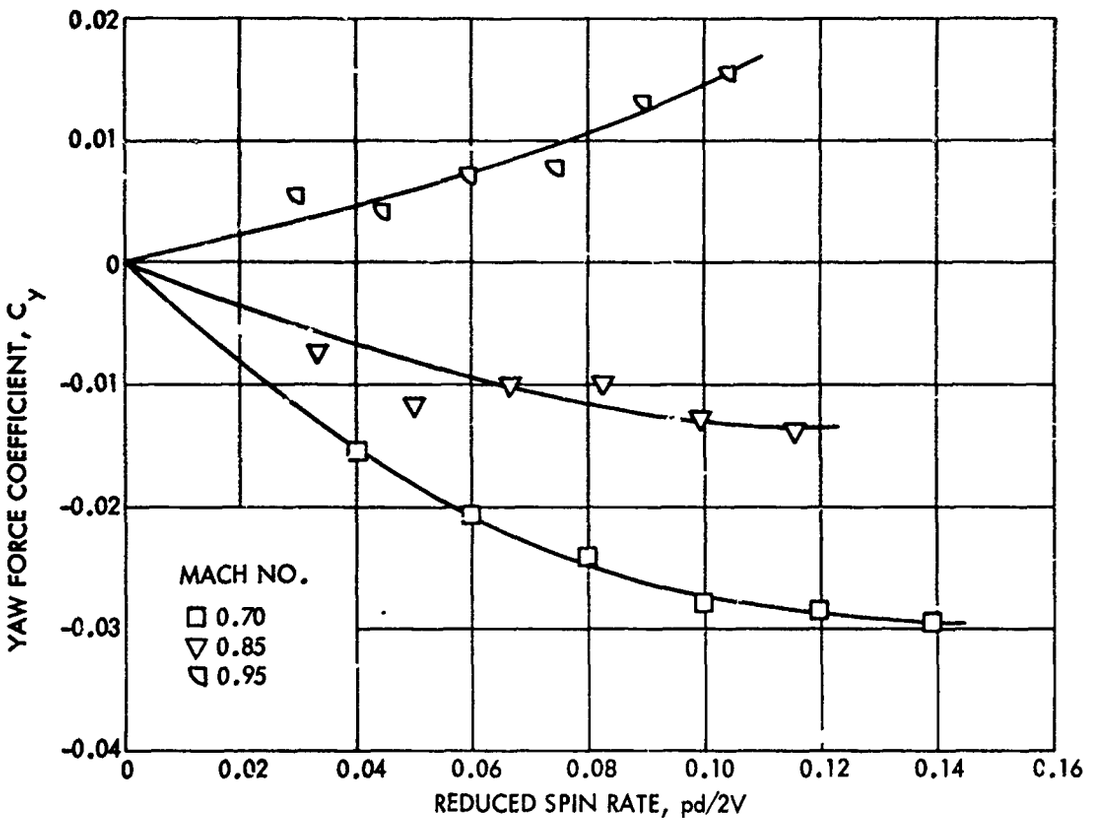

FIG. 59 YAW FORCE COEFFICIENT VERSUS REDUCED SPIN RATE AS A FUNCTION OF MACH NUMBER FOR CONFIGURATION Aδ 0 AT AN ANGLE OF ATTACK OF SIX DEGREES AND AN APPROXIMATE REYNOLDS NUMBER OF 0.58×10^6

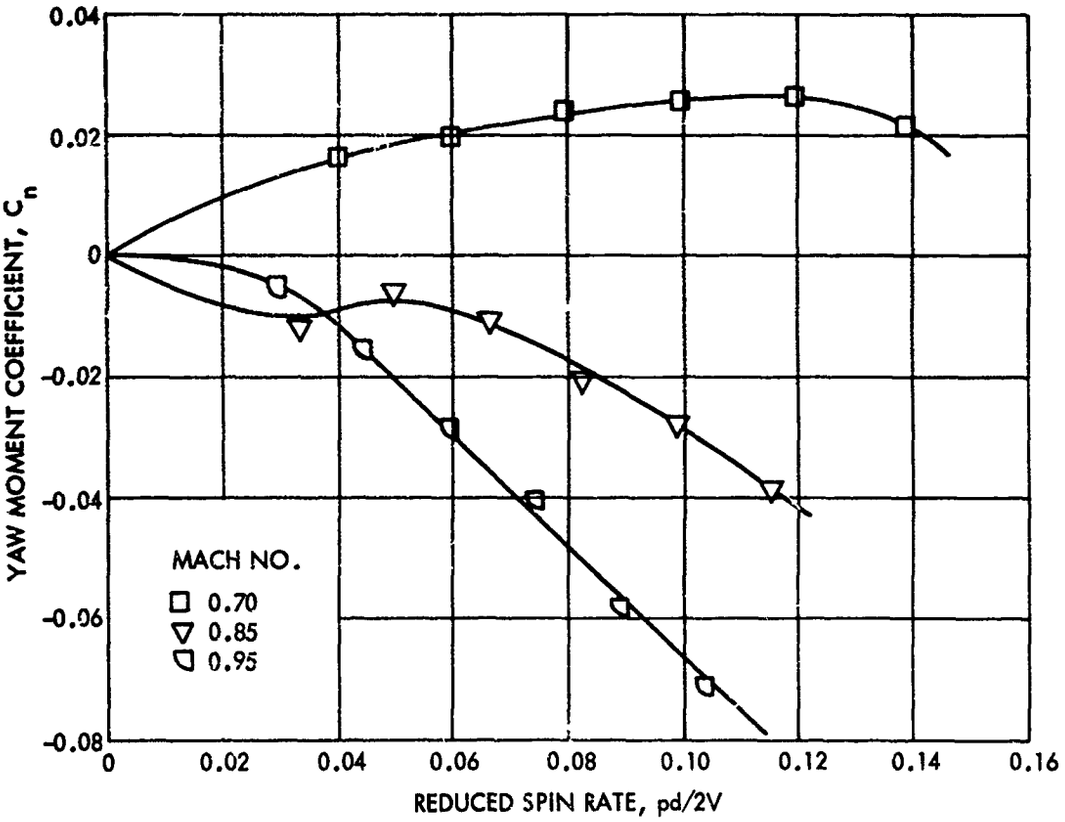

FIG. 60 YAW MOMENT COEFFICIENT VERSUS REDUCED SPIN RATE AS A FUNCTION OF MACH NUMBER FOR CONFIGURATION Aδ0 AT AN ANGLE OF ATTACK OF SIX DEGREES AND AN APPROXIMATE REYNOLDS NUMBER OF 0.58×10^6

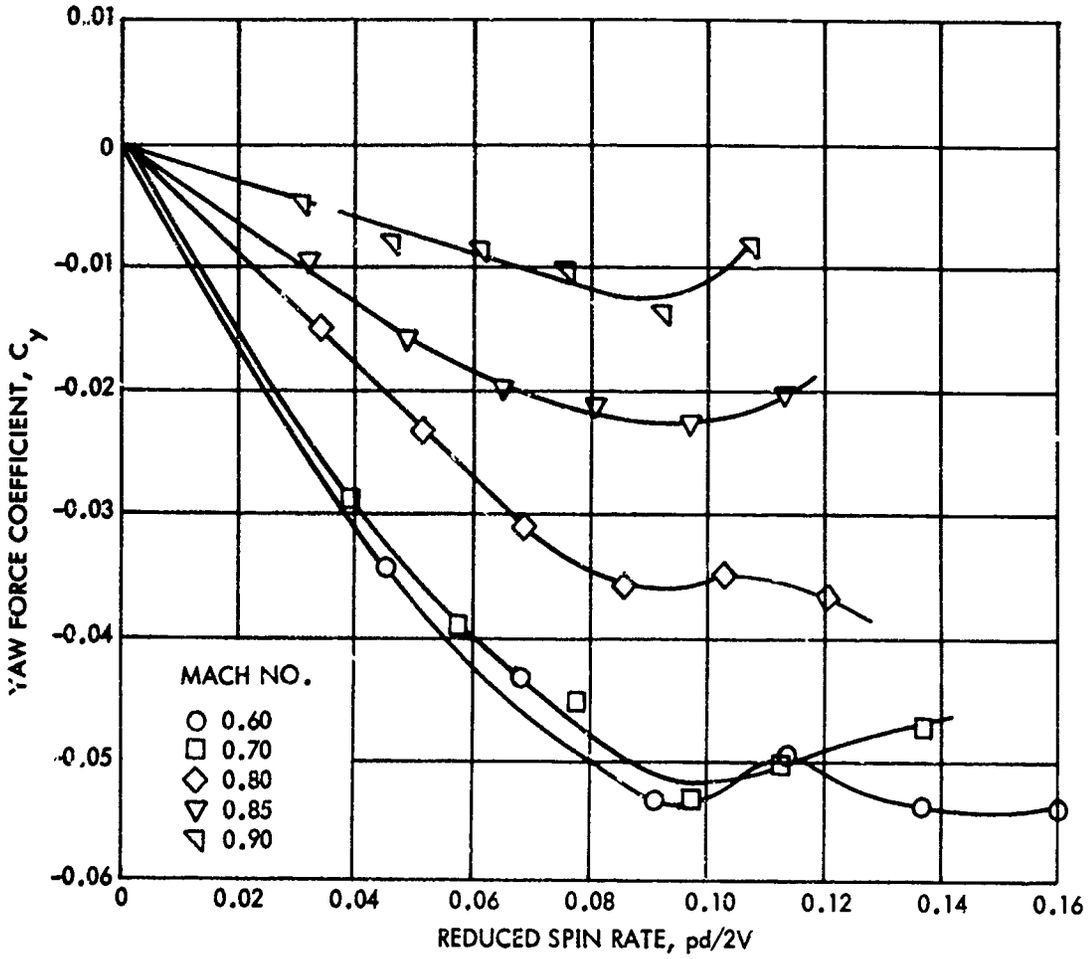

FIG. 61 YAW FORCE COEFFICIENT VERSUS REDUCED SPIN RATE AS A FUNCTION OF MACH NUMBER FOR CONFIGURATION Aδ0 AT AN ANGLE OF ATTACK OF SIX DEGREES AND AN APPROXIMATE REYNOLDS NUMBER OF 1×10^6

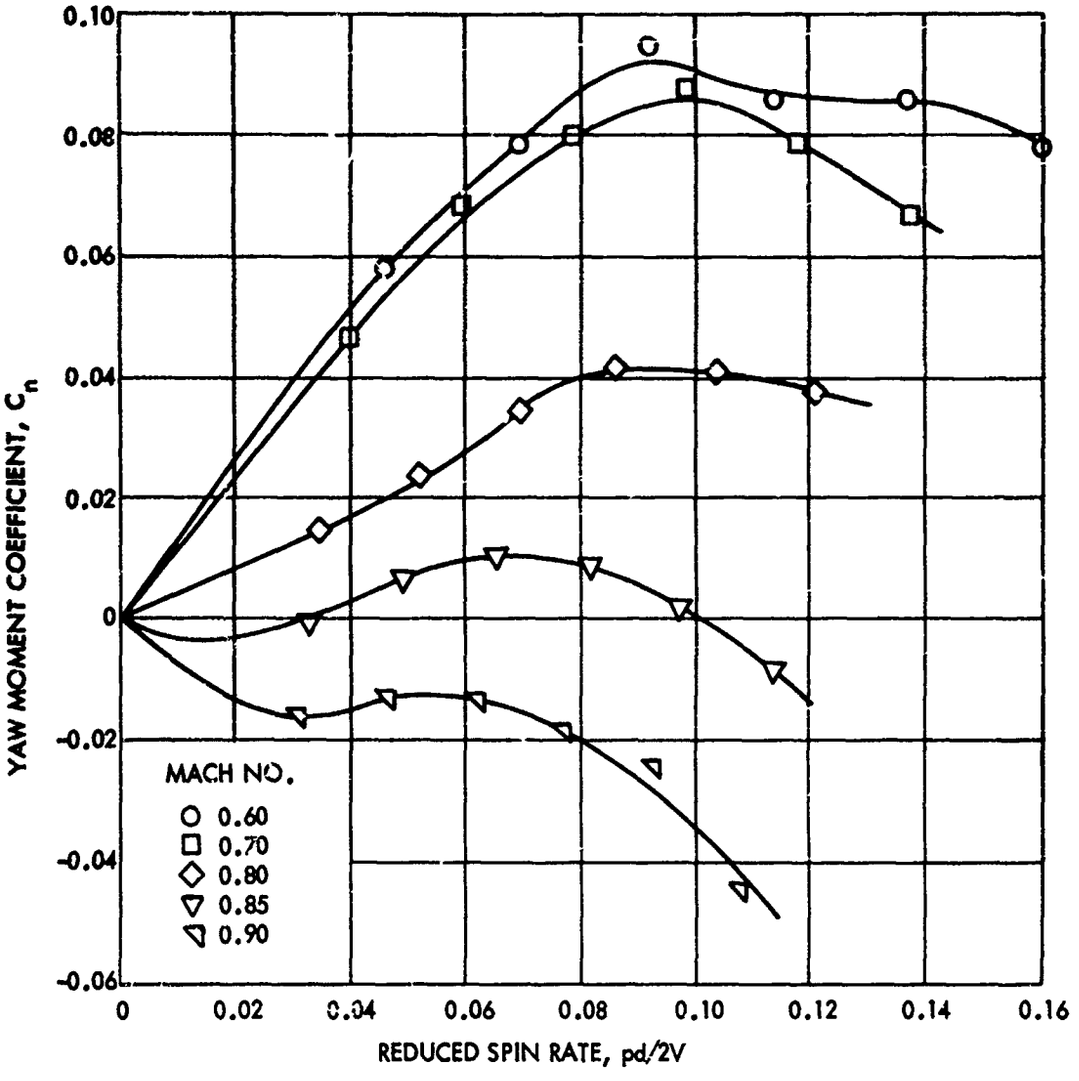

FIG. 62 YAW MOMENT COEFFICIENT VERSUS REDUCED SPIN RATE AS A FUNCTION OF MACH NUMBER FOR CONFIGURATION Aδ0 AT AN ANGLE OF ATTACK OF SIX DEGREES AND AN APPROXIMATE REYNOLDS NUMBER OF 1 x 10^6

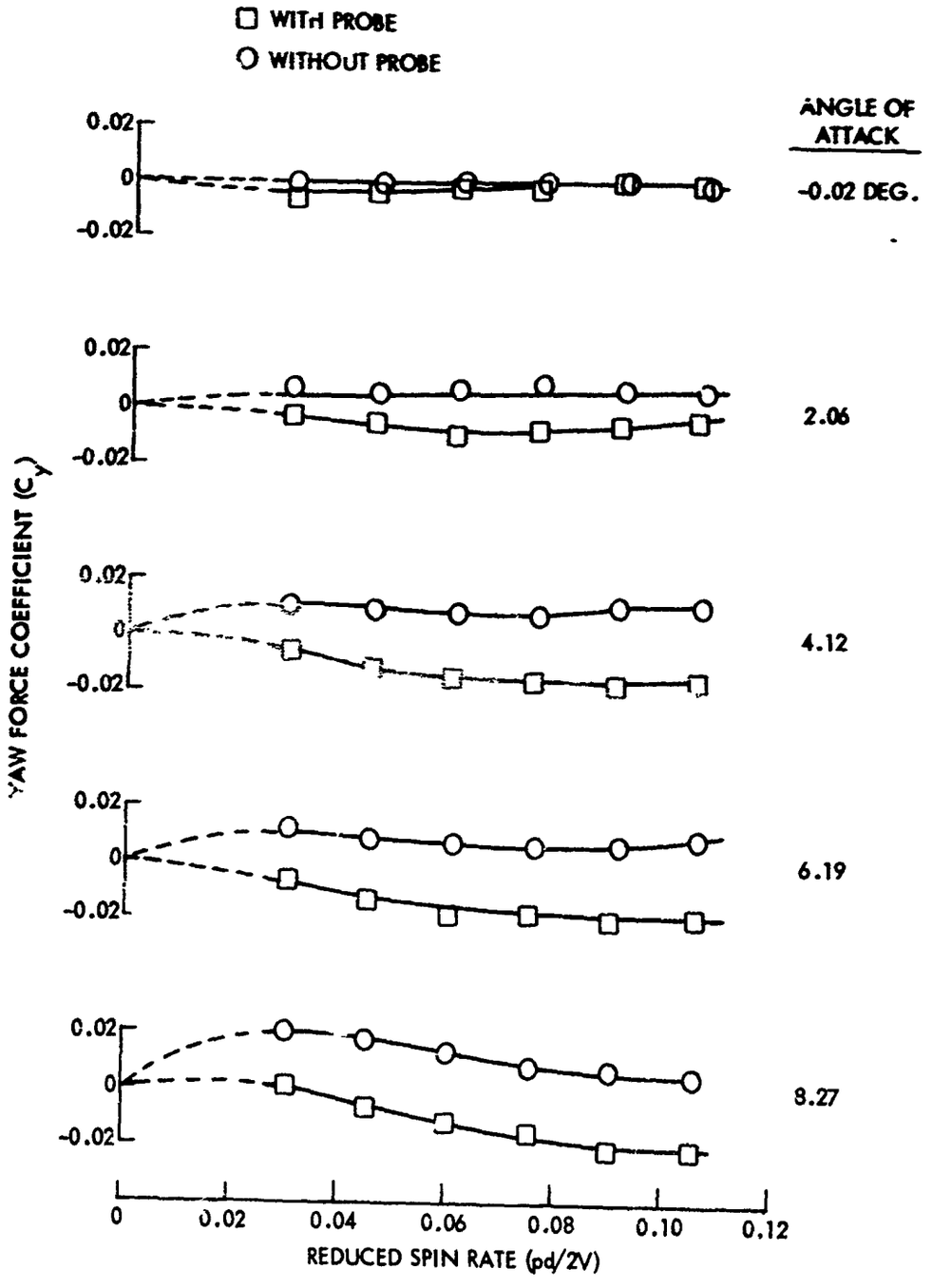

FIG. 63 YAW FORCE COEFFICIENT VERSUS REDUCED SPIN RATE FOR THE M823 RESEARCH STORE, CONFIGURATION A8O, AT A MACH NUMBER OF 0.85 WITH AND WITHOUT A YAW PROBE.

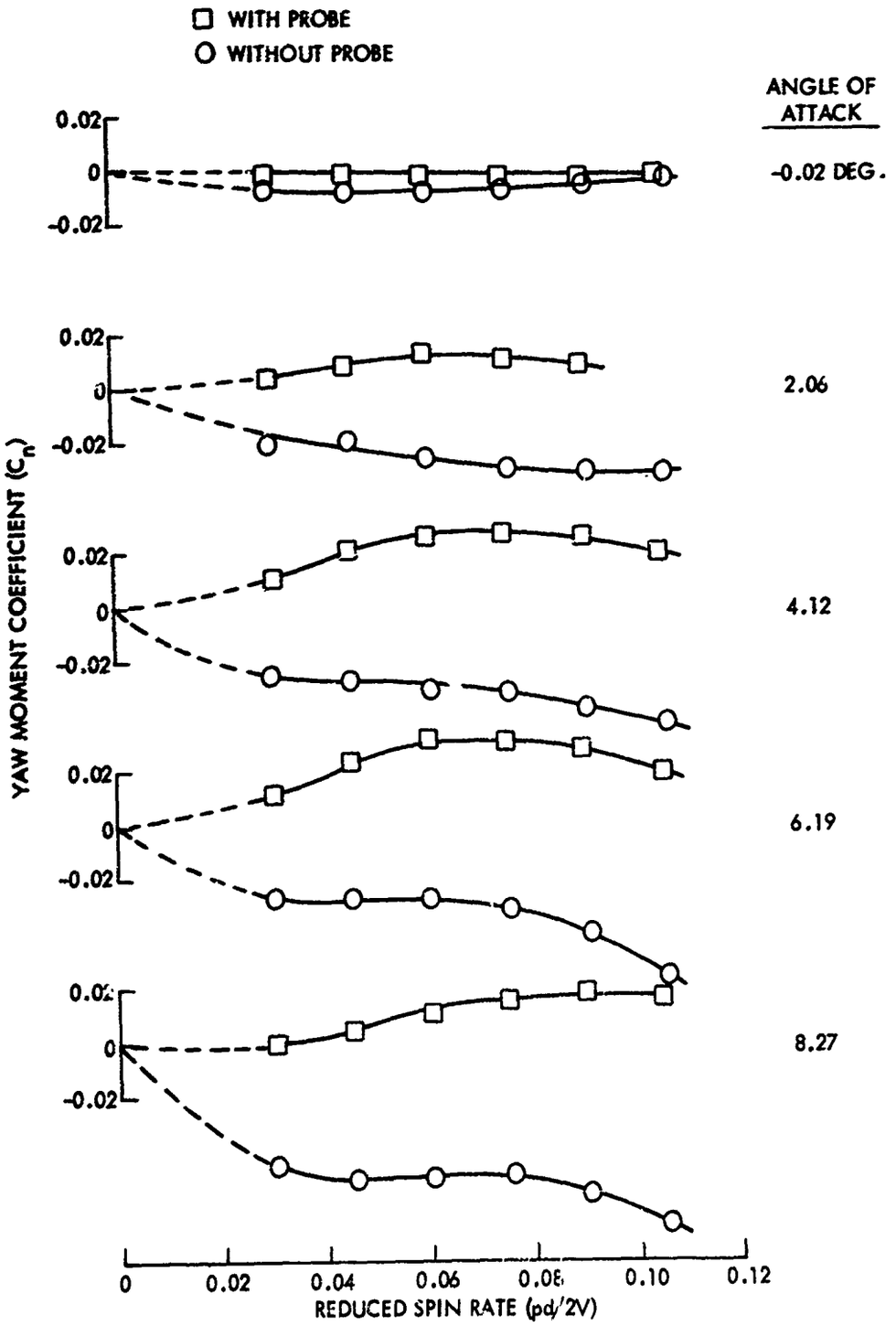

FIG. 64 YAW MOMENT COEFFICIENT VERSUS REDUCED SPIN RATE FOR THE M823 RESEARCH STORE, CONFIGURATION A8O, AT A MACH NUMBER OF 0.85 WITH AND WITHOUT A YAW PROBE.

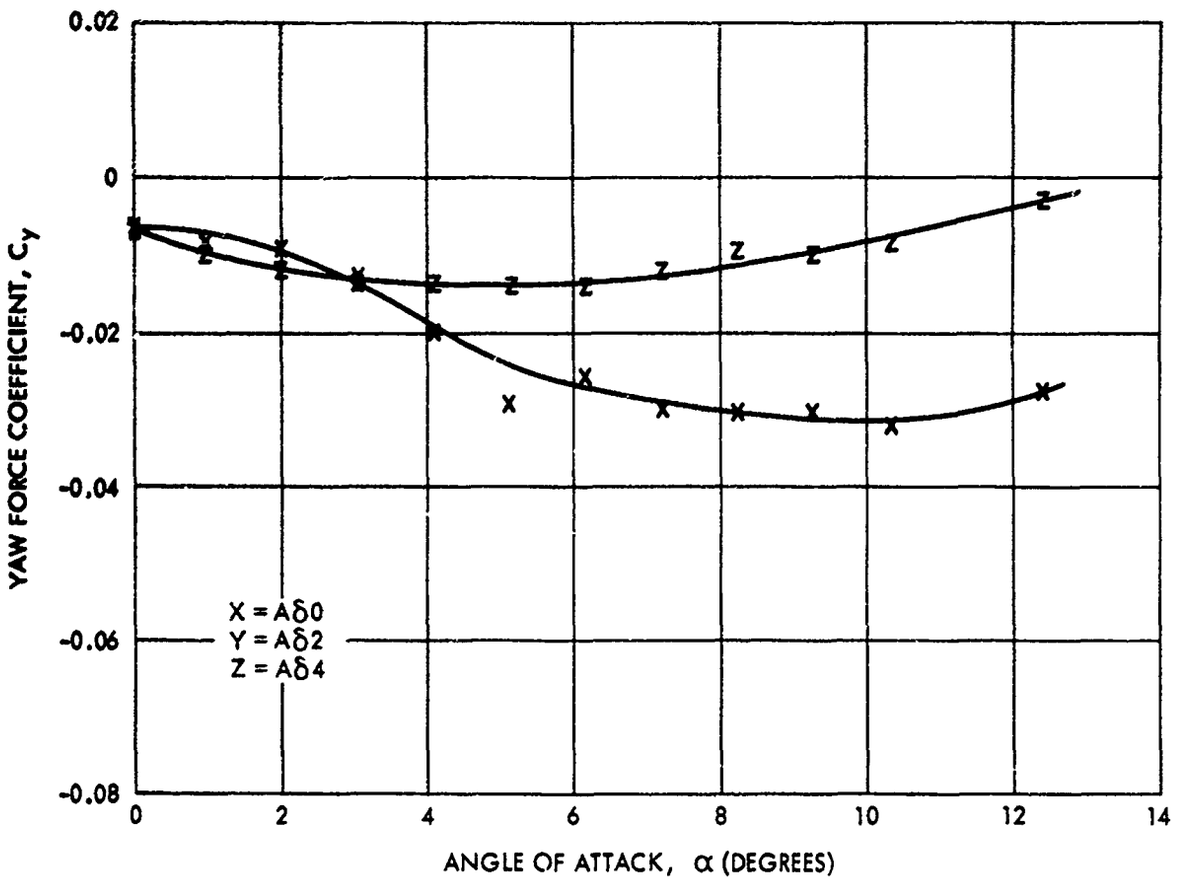

FIG. 65 YAW FORCE COEFFICIENT VERSUS ANGLE OF ATTACK FOR THE FIXED CRUCIFORM CONFIGURATION WITHOUT YAW PROBE AT A MACH NO. OF 0.70 AND A REDUCED SPIN RATE OF 0.040

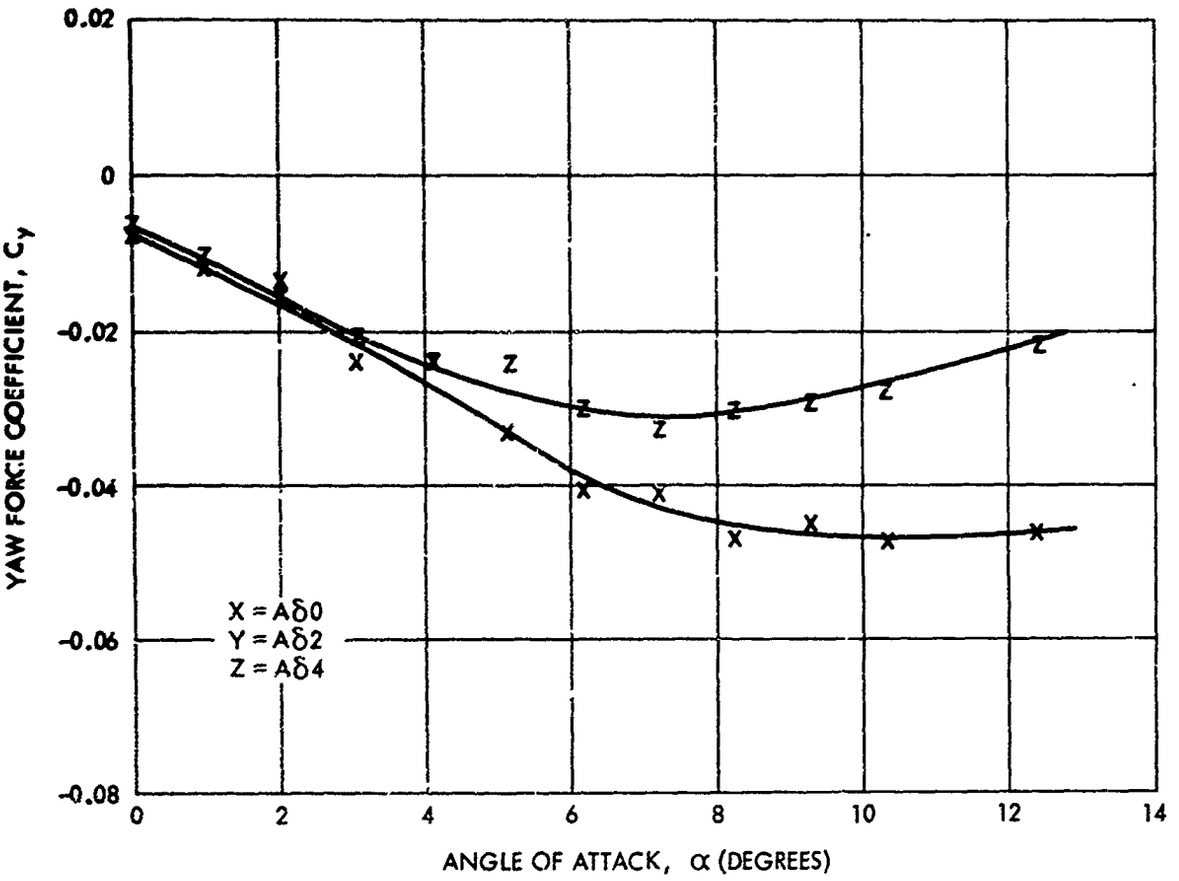

FIG. 66 YAW FORCE COFFFICIENT VERSUS ANGLE OF ATTACK FOR THE FIXED CRUCIFORM CONFIGURATION WITHOUT YAW PROBE AT A MACH NO. OF 0.70 AND A REDUCED SPIN RATE OF 0.072

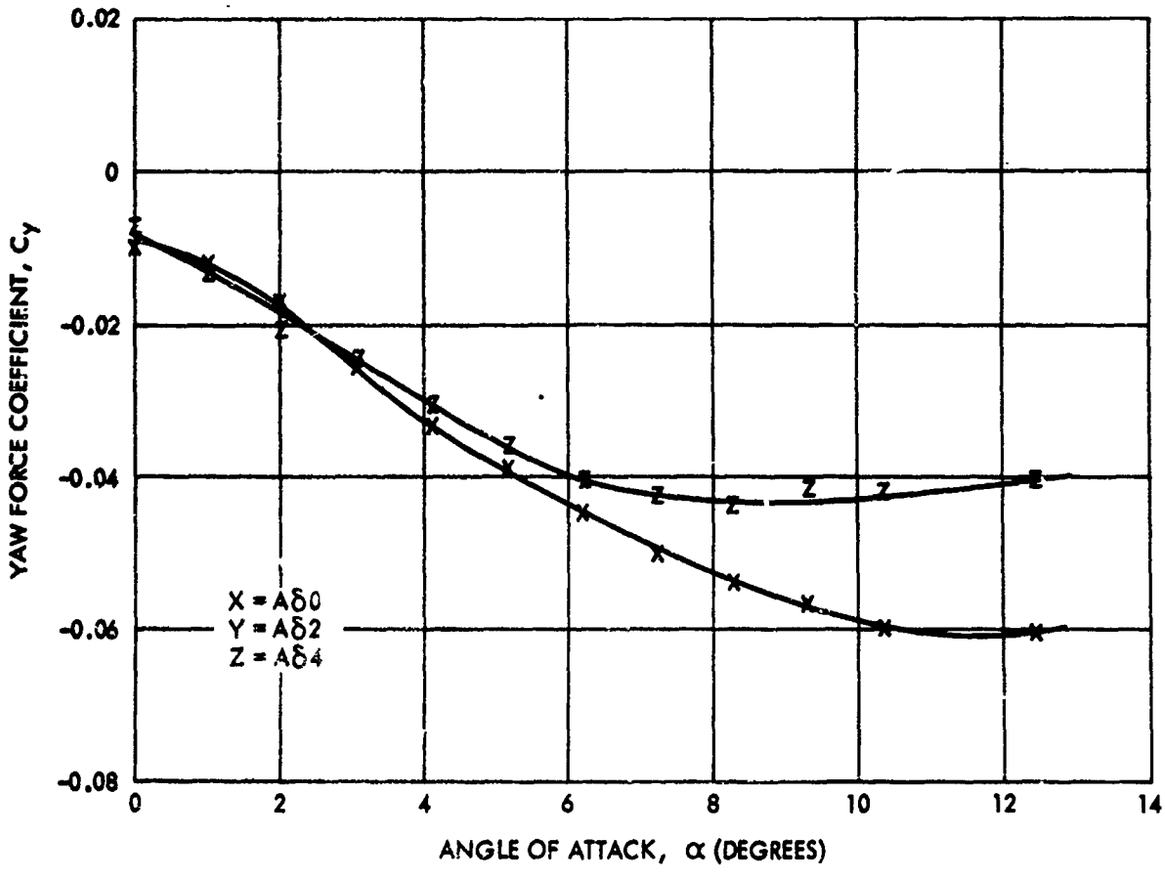

FIG. 67 YAW FORCE COEFFICIENT VERSUS ANGLE OF ATTACK FOR THE FIXED CRUCIFORM CONFIGURATION WITHOUT YAW PROBE AT A MACH NO. OF 0.70 AND A REDUCED SPIN RATE OF 0.100

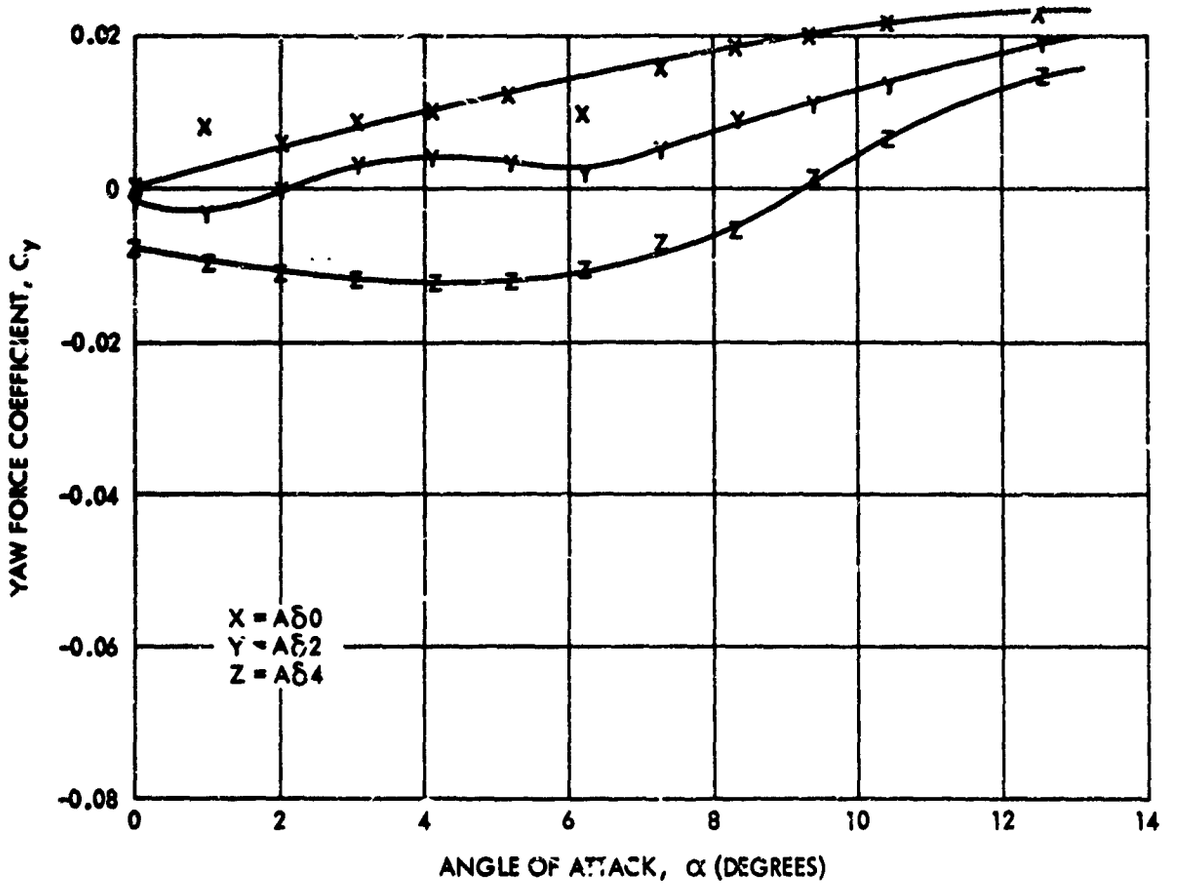

FIG. 68 YAW FORCE COEFFICIENT VERSUS ANGLE OF ATTACK FOR THE FIXED CRUCIFORM CONFIGURATION WITHOUT YAW PROBE AT A MACH NO. OF 0.85 AND A REDUCED SPIN RATE OF 0.040

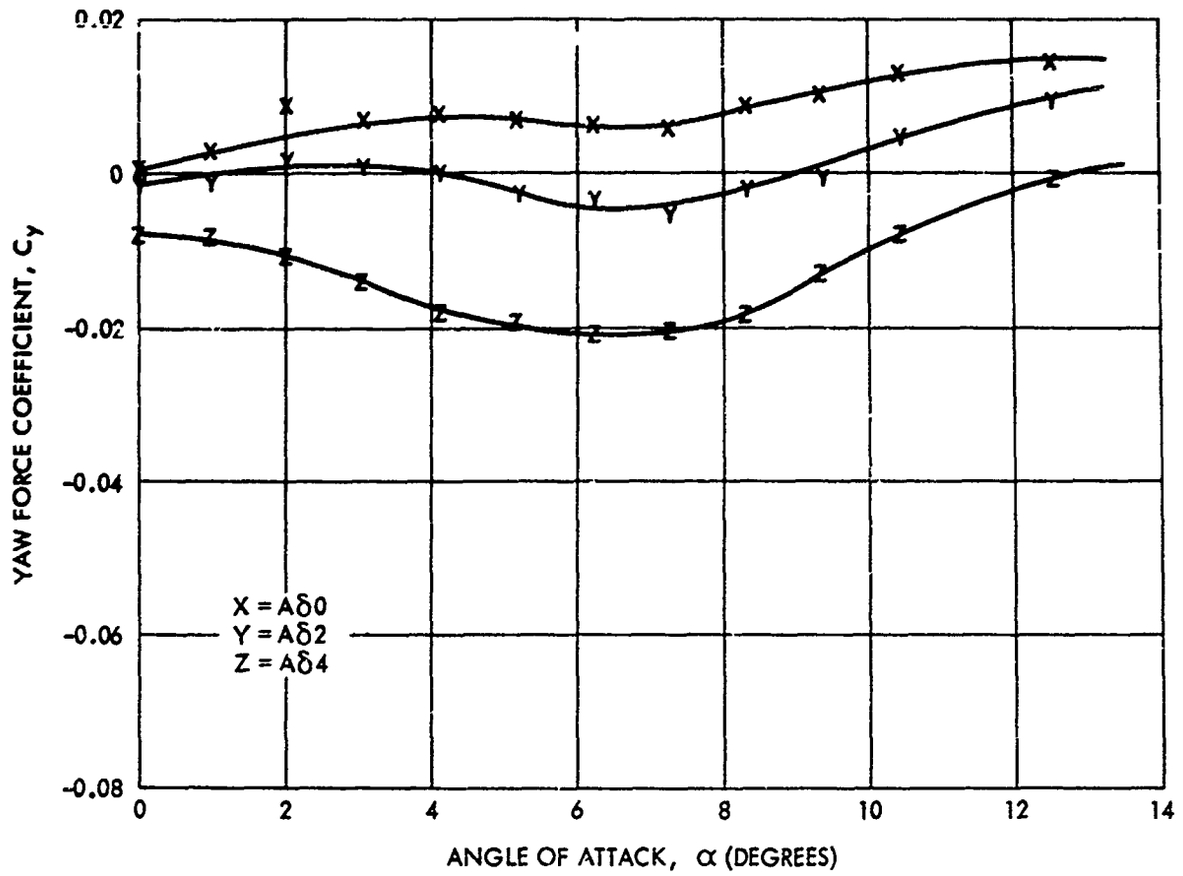

FIG. 69 YAW FORCE COEFFICIENT VERSUS ANGLE OF ATTACK FOR THE FIXED CRUCIFORM CONFIGURATION WITHOUT YAW PROBE AT A MACH NO. OF 0.85 AND A REDUCED SPIN RATE OF 0.072

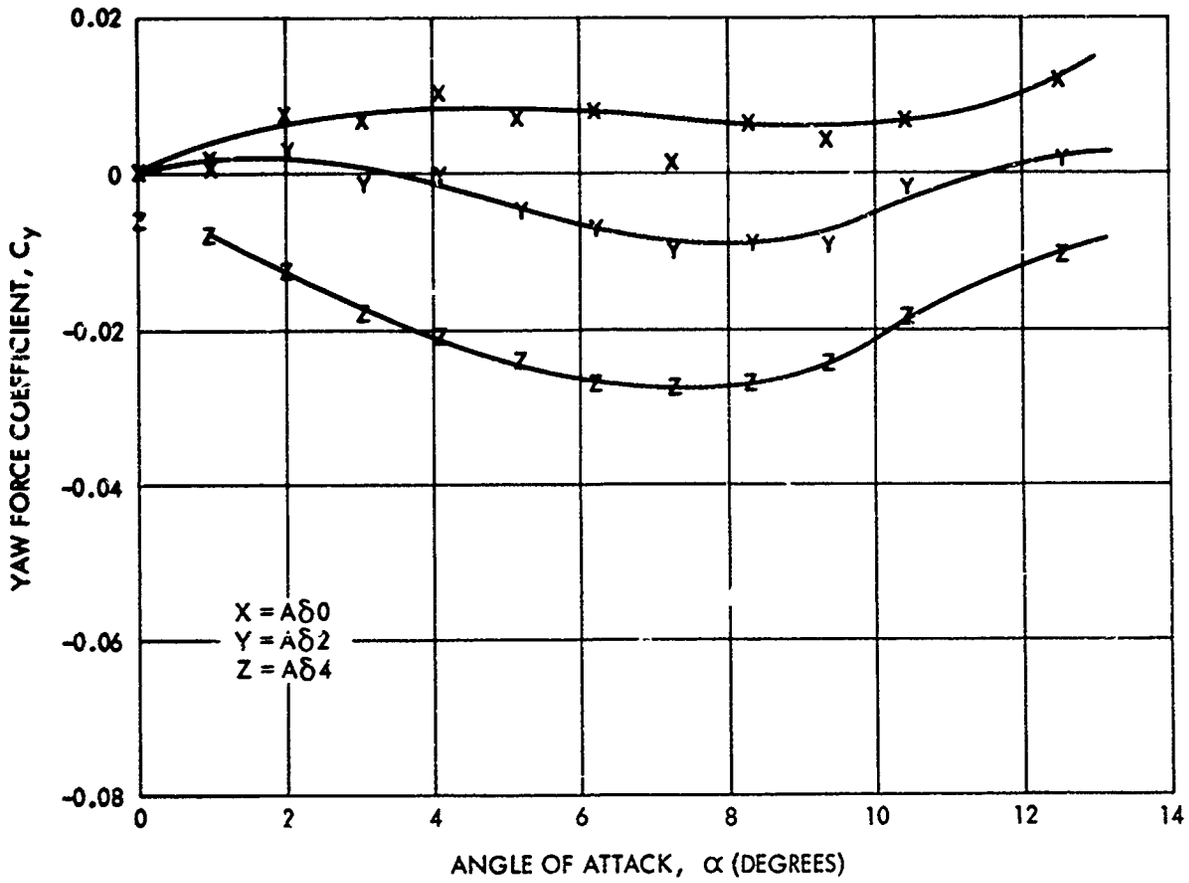

FIG. 70 YAW FORCE COEFFICIENT VERSUS ANGLE OF ATTACK FOR THE FIXED CRUCIFORM CONFIGURATION WITHOUT YAW PROBE AT A MACH NO. OF 0.85 AND A REDUCED SPIN RATE OF 0.100

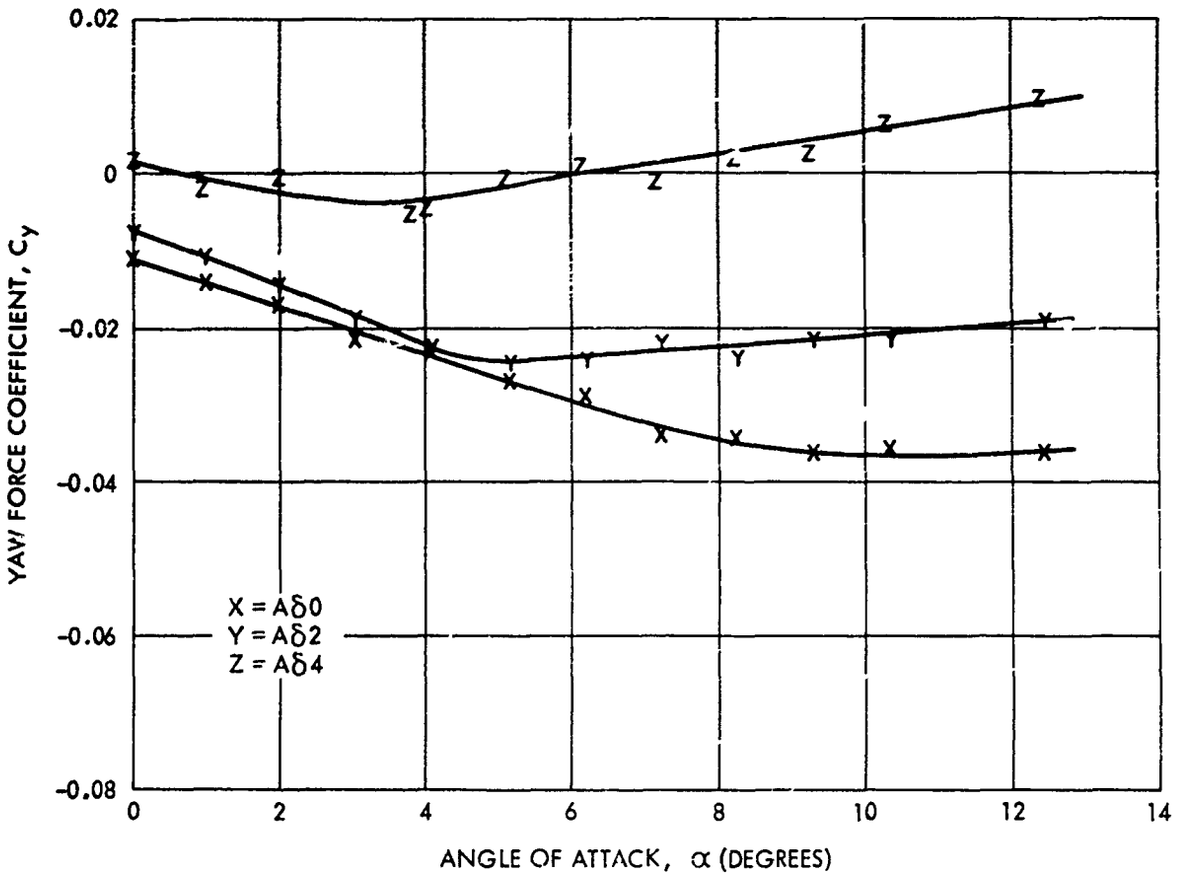

FIG. 71 YAW FORCE COEFFICIENT VERSUS ANGLE OF ATTACK FOR THE FIXED CRUCIFORM CONFIGURATION WITH YAW PROBE AT A MACH NO. OF 0.70 AND A REDUCED SPIN RATE OF 0.040

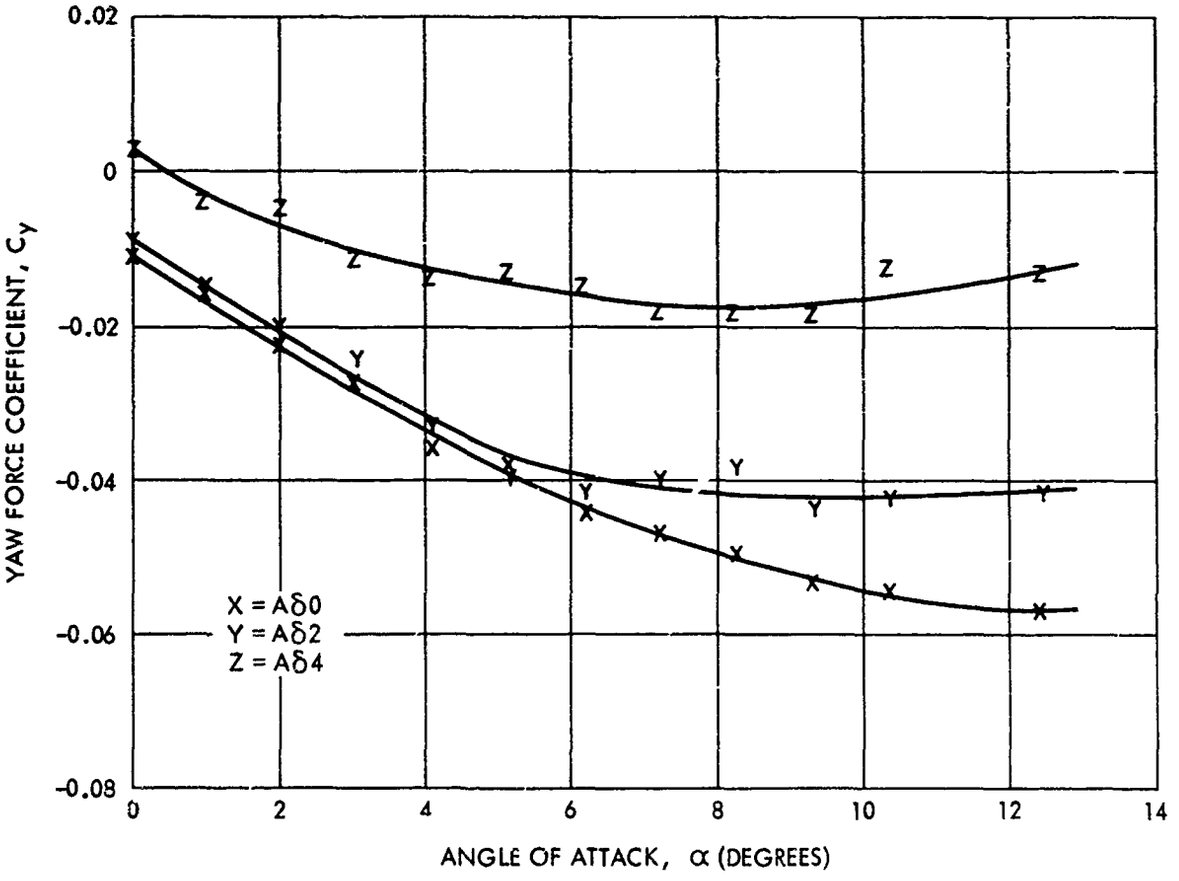

FIG. 72 YAW FORCE COEFFICIENT VERSUS ANGLE OF ATTACK FOR THE FIXED CRUCIFORM CONFIGURATION WITH YAW PROBE AT A MACH NO. OF 0.70 AND A REDUCED SPIN RATE OF 0.072

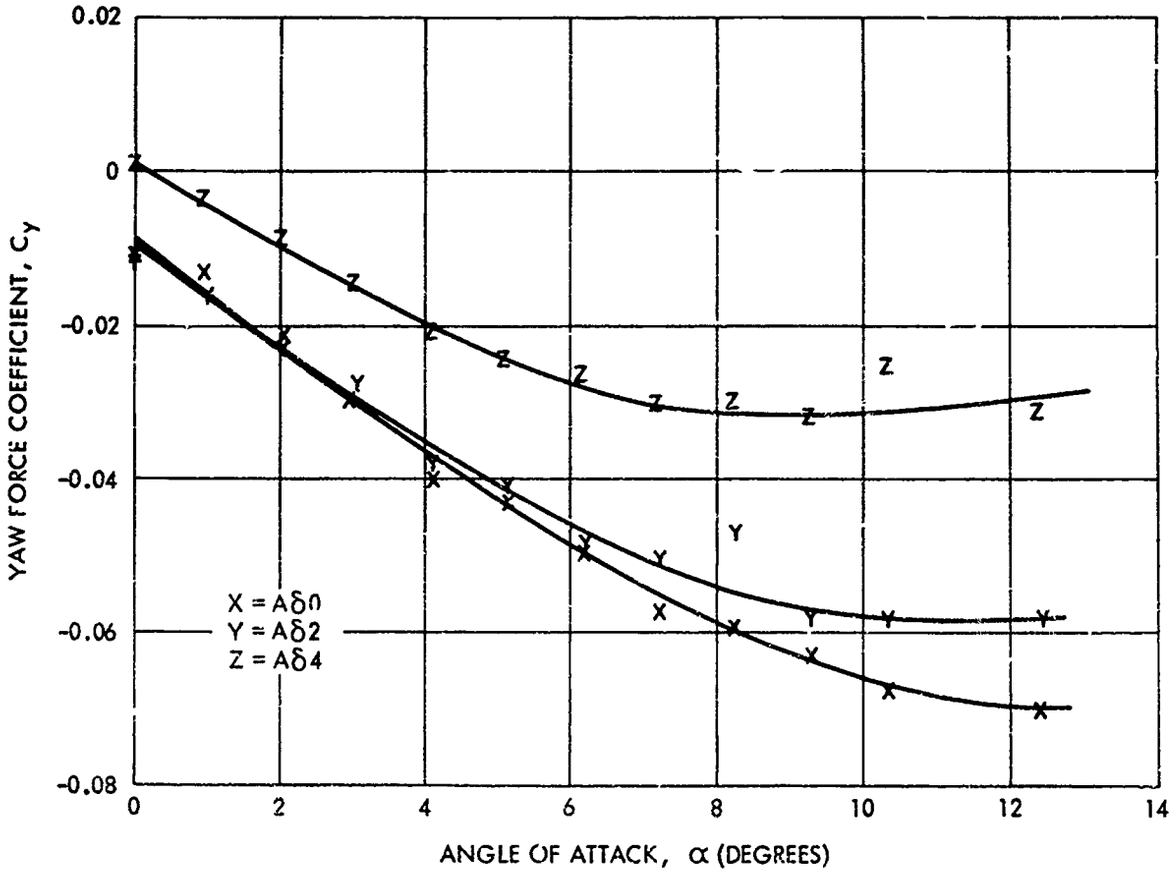

FIG. 73 YAW FORCE COEFFICIENT VERSUS ANGLE OF ATTACK FOR THE FIXED CRUCIFORM CONFIGURATION WITH YAW PROBE AT A MACH NO. OF 0.70 AND A REDUCED SPIN RATE OF 0.100

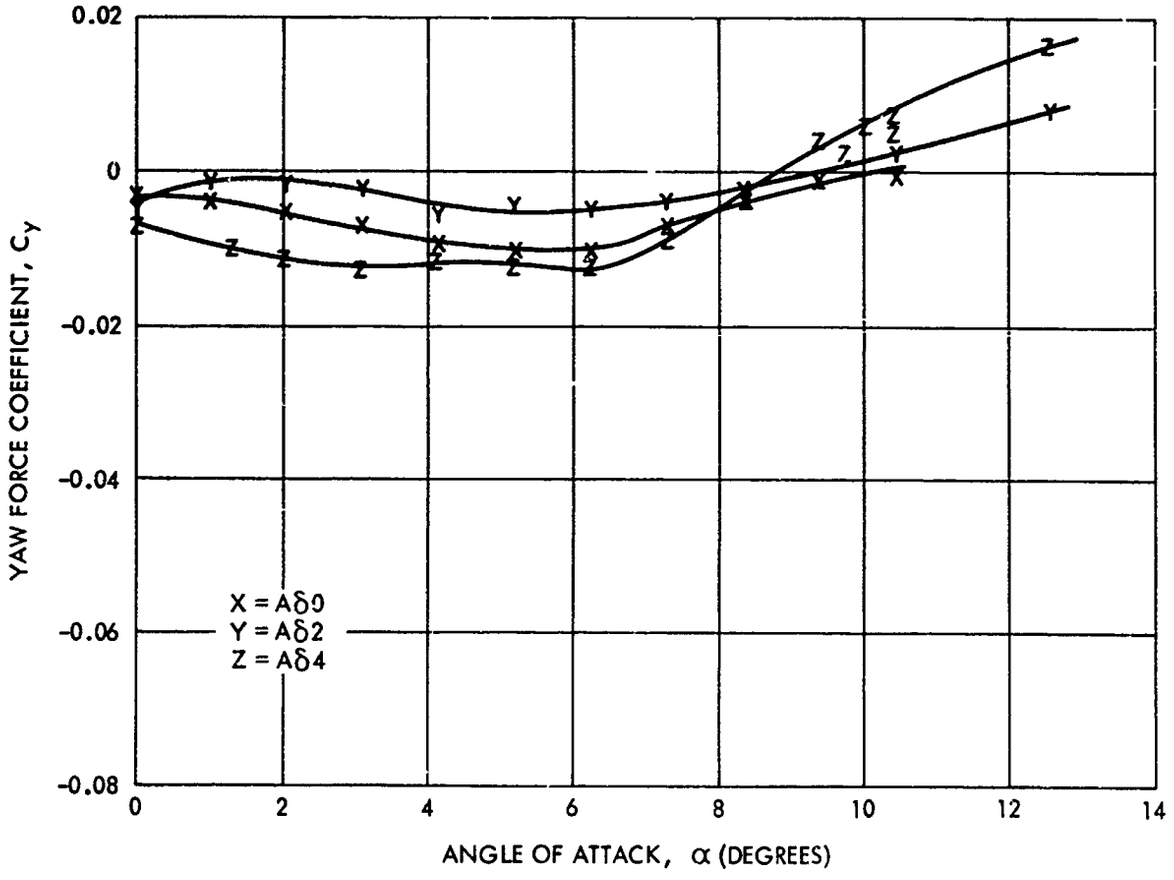

FIG. 74 YAW FORCE COEFFICIENT VERSUS ANGLE OF ATTACK FOR THE FIXED CRUCIFORM CONFIGURATION WITH YAW PROBE AT A MACH NO. OF 0.85 AND A REDUCED SPIN RATE OF 0.040

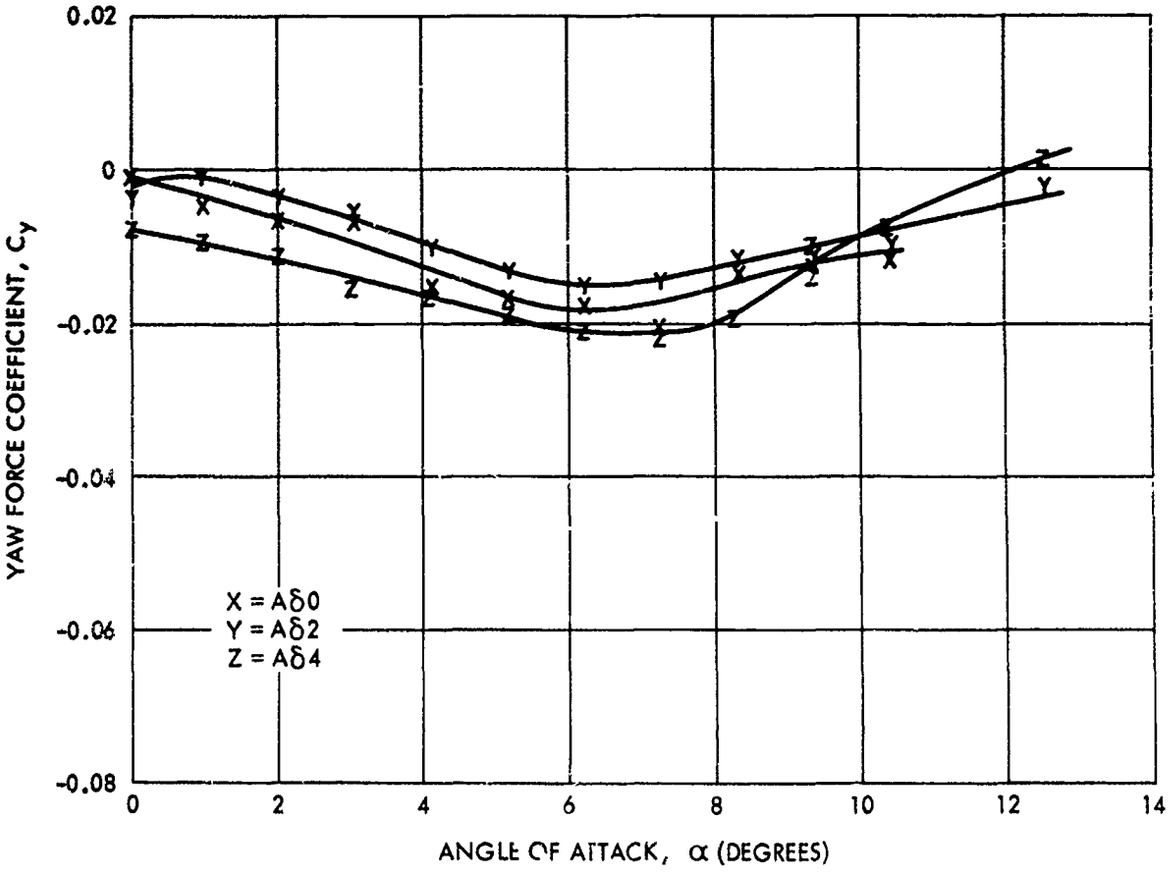

FIG. 75 YAW FORCE COEFFICIENT VERSUS ANGLE OF ATTACK FOR THE FIXED CRUCIFORM CONFIGURATION WITH YAW PROBE AT A MACH NO. OF 0.85 AND A REDUCED SPIN RATE OF 0.072

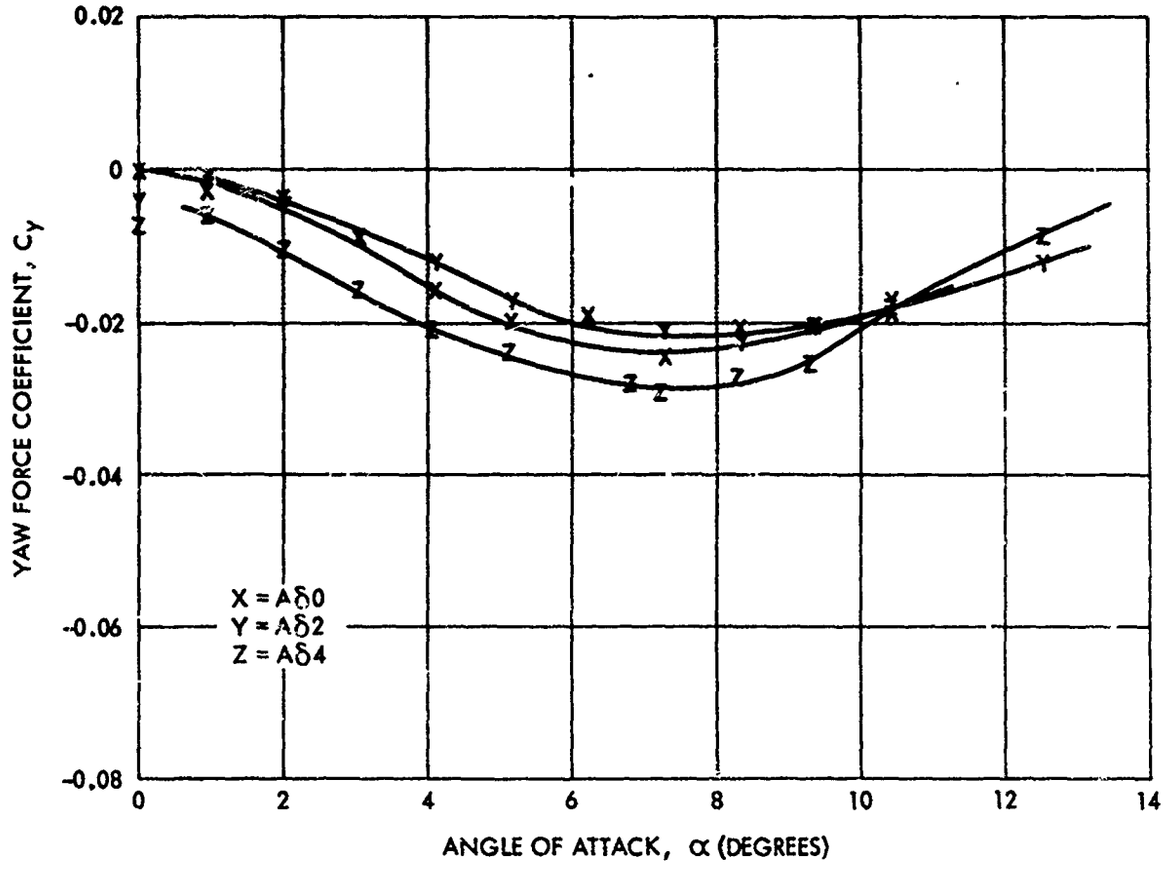

FIG. 76 YAW FORCE COEFFICIENT VERSUS ANGLE OF ATTACK FOR THE FIXED CRUCIFORM CONFIGURATION WITH YAW PROBE AT A MACH NO. OF 0.85 AND A REDUCED SPIN RATE OF 0.100

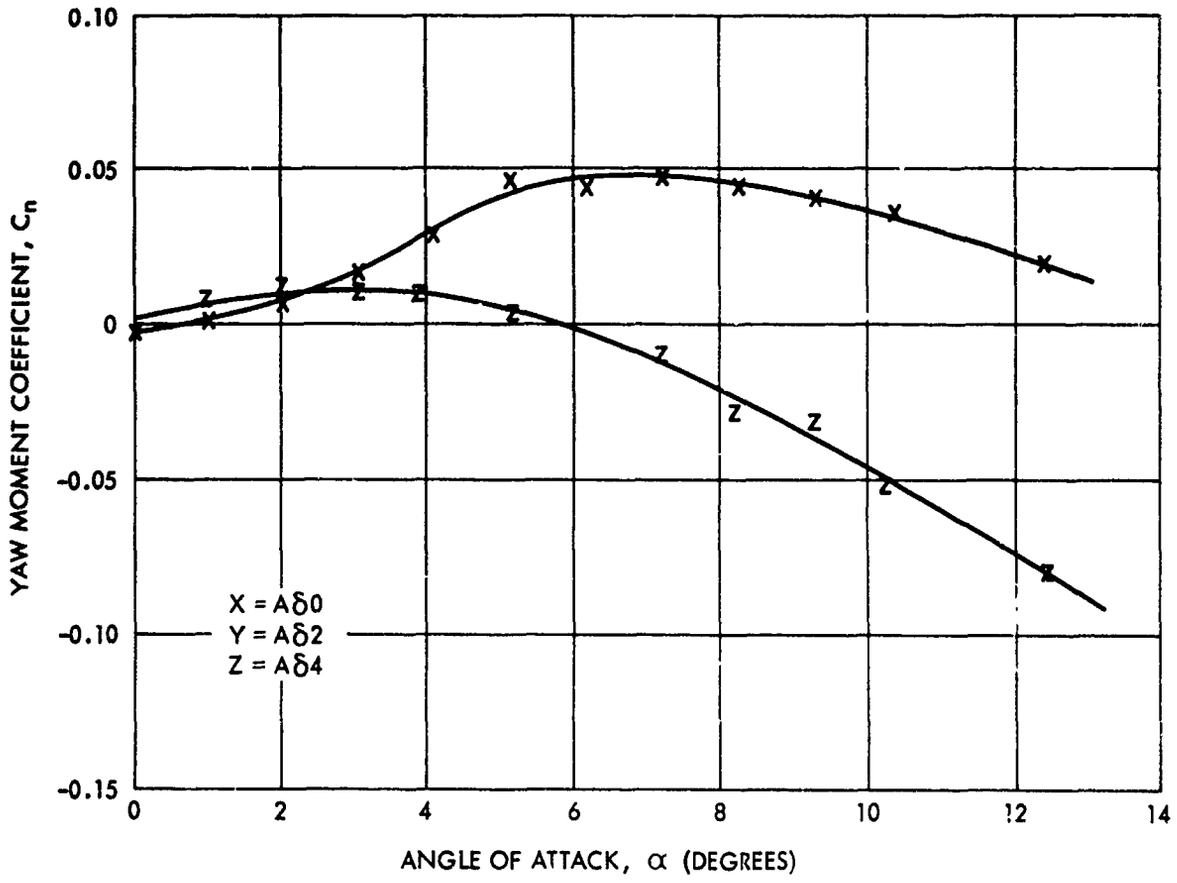

FIG. 77 YAW MOMENT COEFFICIENT VERSUS ANGLE OF ATTACK FOR THE FIXED CRUCIFORM CONFIGURATION WITHOUT YAW PROBE AT A MACH NO. OF 0.70 AND A REDUCED SPIN RATE OF 0.040

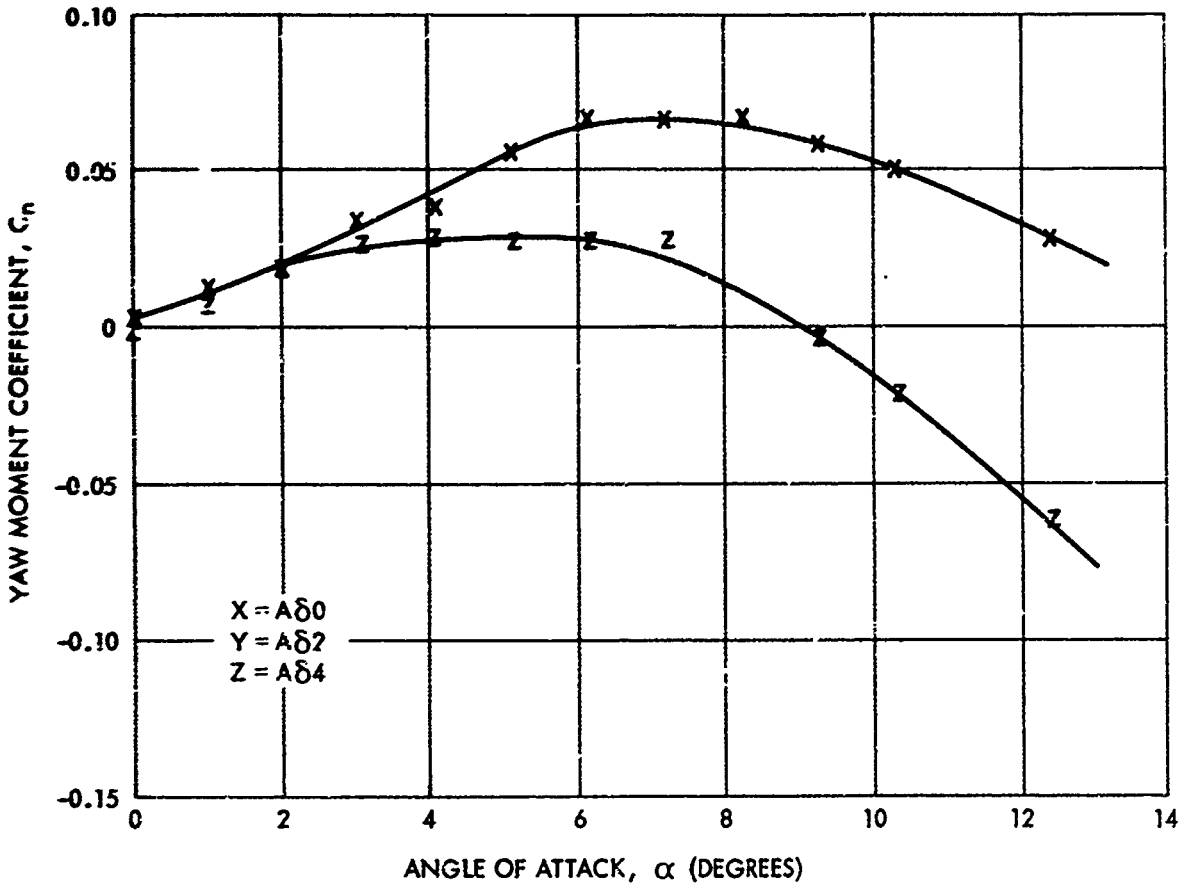

FIG. 78 YAW MOMENT COEFFICIENT VERSUS ANGLE OF ATTACK FOR THE FIXED CRUCIFORM CONFIGURATION WITHOUT YAW PROBE AT A MACH NO. OF 0.70 AND A REDUCED SPIN RATE OF 0.072

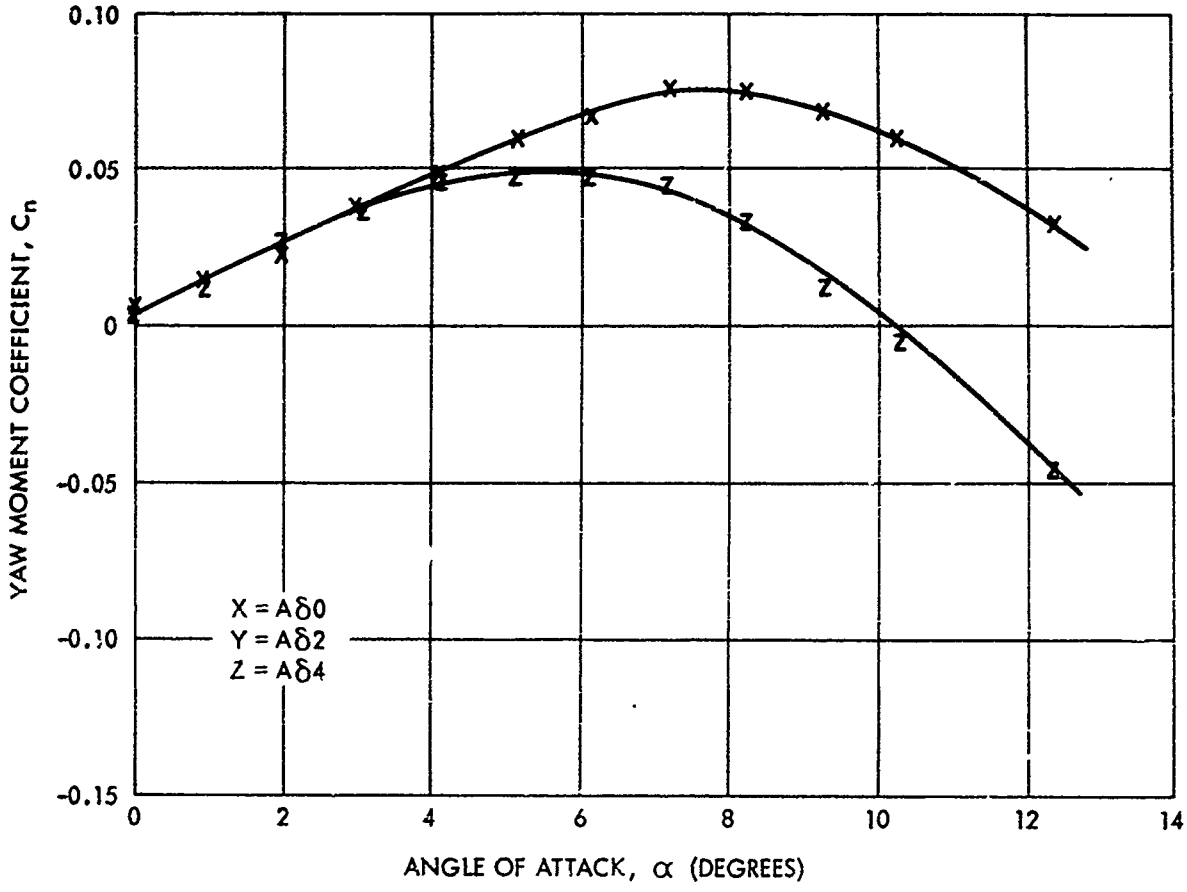

FIG. 79 YAW MOMENT COEFFICIENT VERSUS ANGLE OF ATTACK FOR THE FIXED CRUCIFORM CONFIGURATION WITHOUT YAW PROBE AT A MACH NO. OF 0.70 AND A REDUCED SPIN RATE OF 0.100

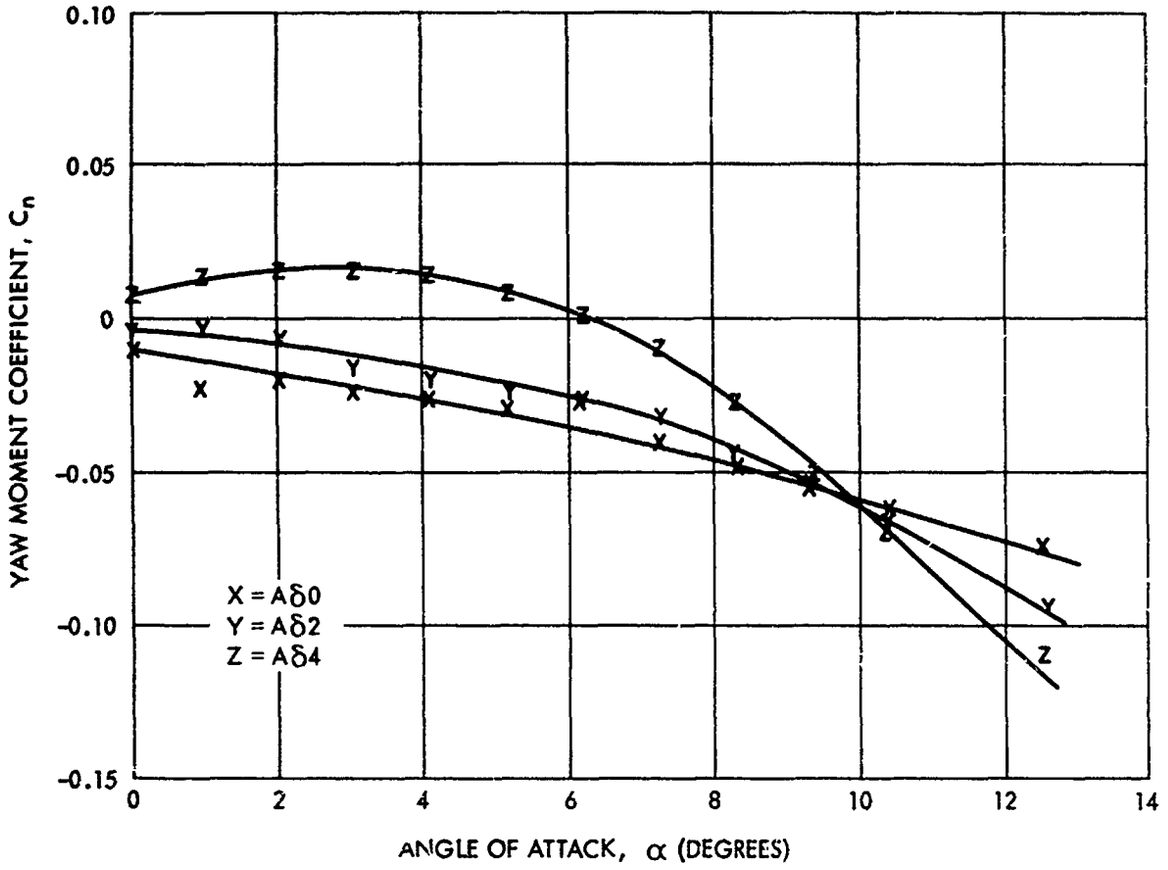

FIG. 80 YAW MOMENT COEFFICIENT VERSUS ANGLE OF ATTACK FOR THE FIXED CRUCIFORM CONFIGURATION WITHOUT YAW PROBE AT A MACH NO. OF 0.85 AND A REDUCED SPIN RATE OF 0.040

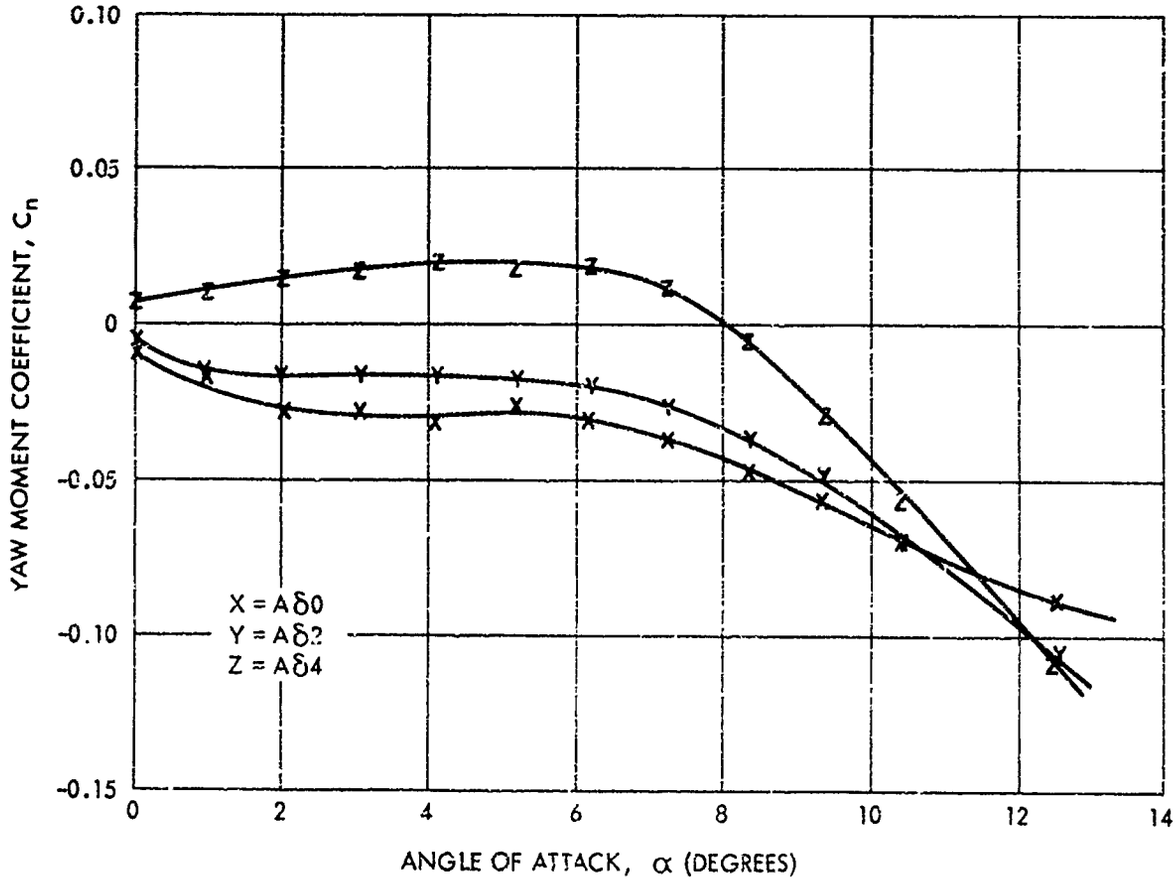

FIG. 81 YAW MOMENT COEFFICIENT VERSUS ANGLE OF ATTACK FOR THE FIXED CRUCIFORM CONFIGURATION WITHOUT YAW PROBE AT A MACH NO. OF 0.85 AND A REDUCED SPIN RATE OF 0.072

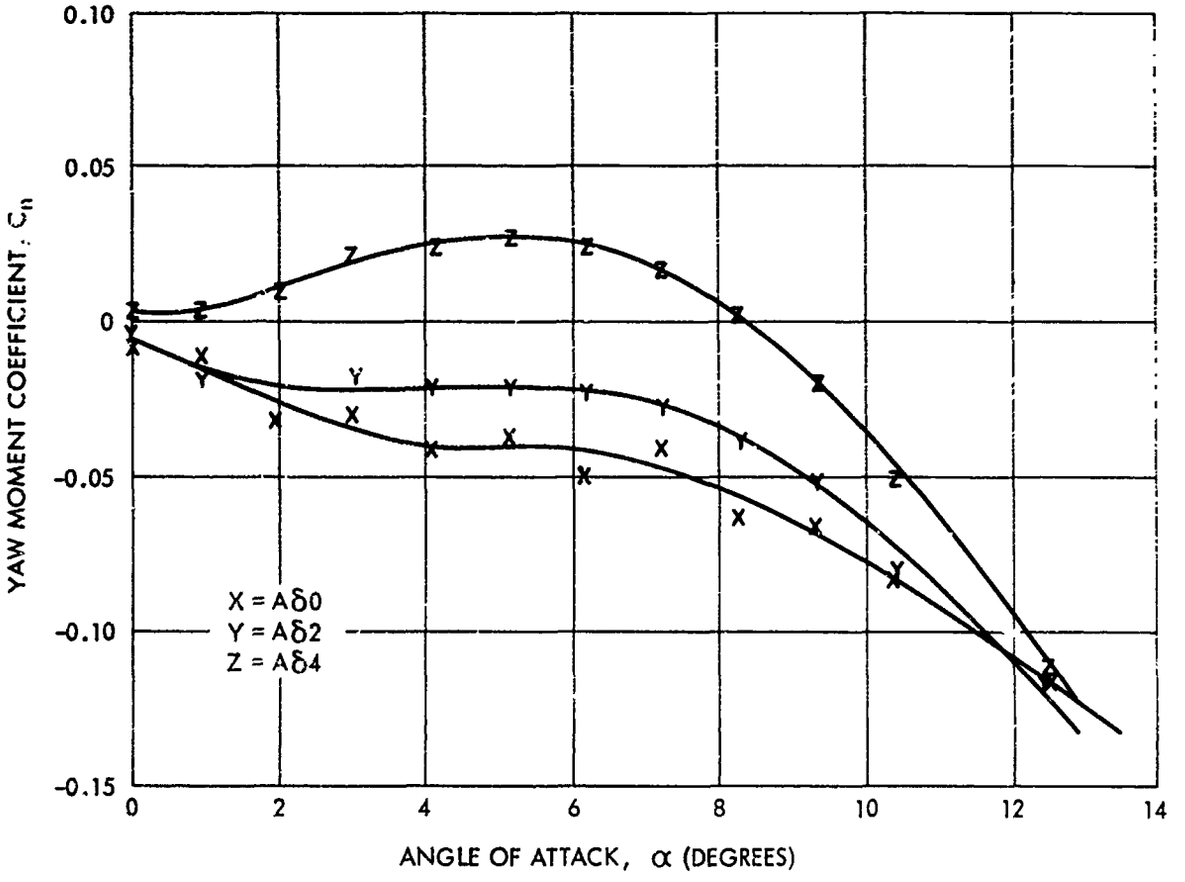

FIG. 82 YAW MOMENT COEFFICIENT VERSUS ANGLE OF ATTACK FOR THE FIXED CRUCIFORM CONFIGURATION WITHOUT YAW PROBE AT A MACH NO. OF 0.85 AND A REDUCED SPIN RATE OF 0.100

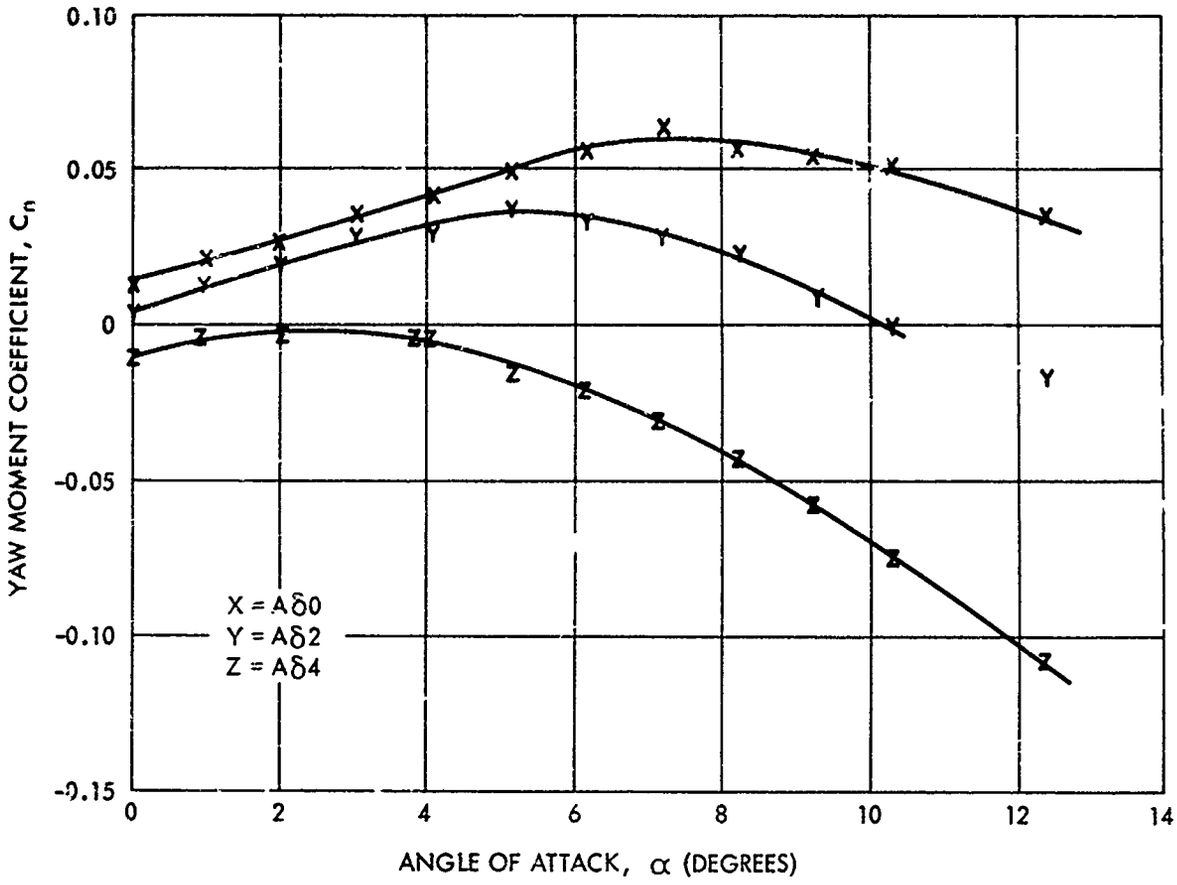

FIG. 83 YAW MOMENT COEFFICIENT VERSUS ANGLE OF ATTACK FOR THE FIXED CRUCIFORM CONFIGURATION WITH YAW PROBE AT A MACH NO. OF 0.70 AND A REDUCED SPIN RATE OF 0.040

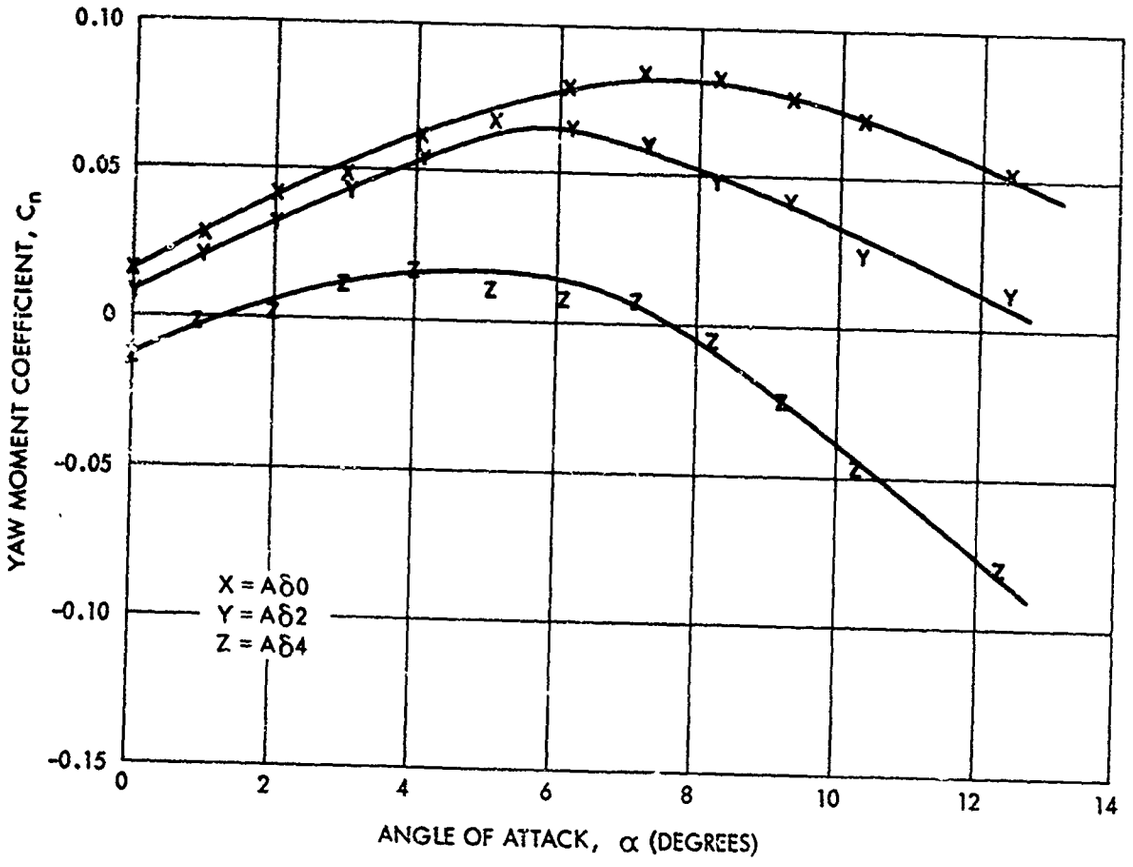

FIG. 84 YAW MOMENT COEFFICIENT VERSUS ANGLE OF ATTACK FOR THE FIXED CRUCIFORM CONFIGURATION WITH YAW PROBE AT A MACH NO. OF 0.70 AND A REDUCED SPIN RATE OF 0.072

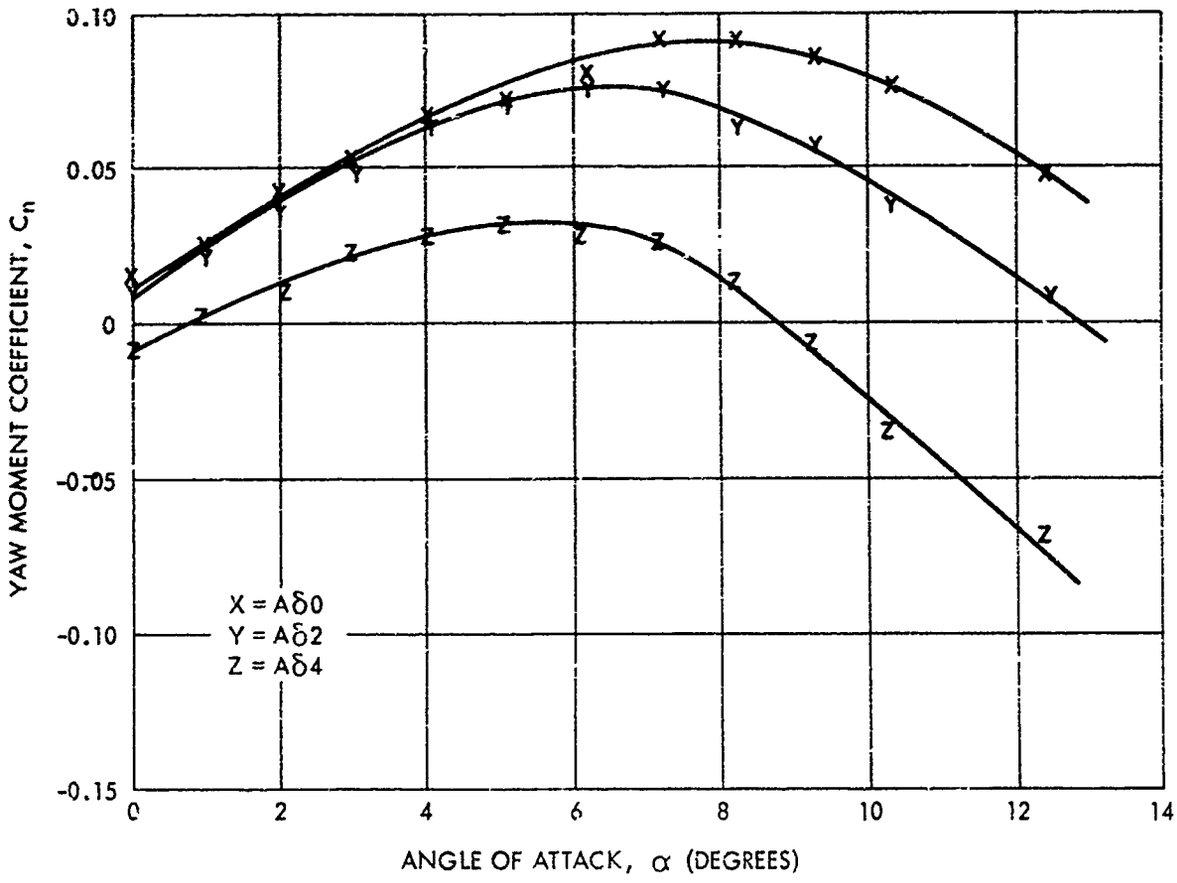

FIG. 85 YAW MOMENT COEFFICIENT VERSUS ANGLE OF ATTACK FOR THE FIXED CRUCIFORM CONFIGURATION WITH YAW PROBE AT A MACH NO. OF 0.70 AND A REDUCED SPIN RATE OF 0.100

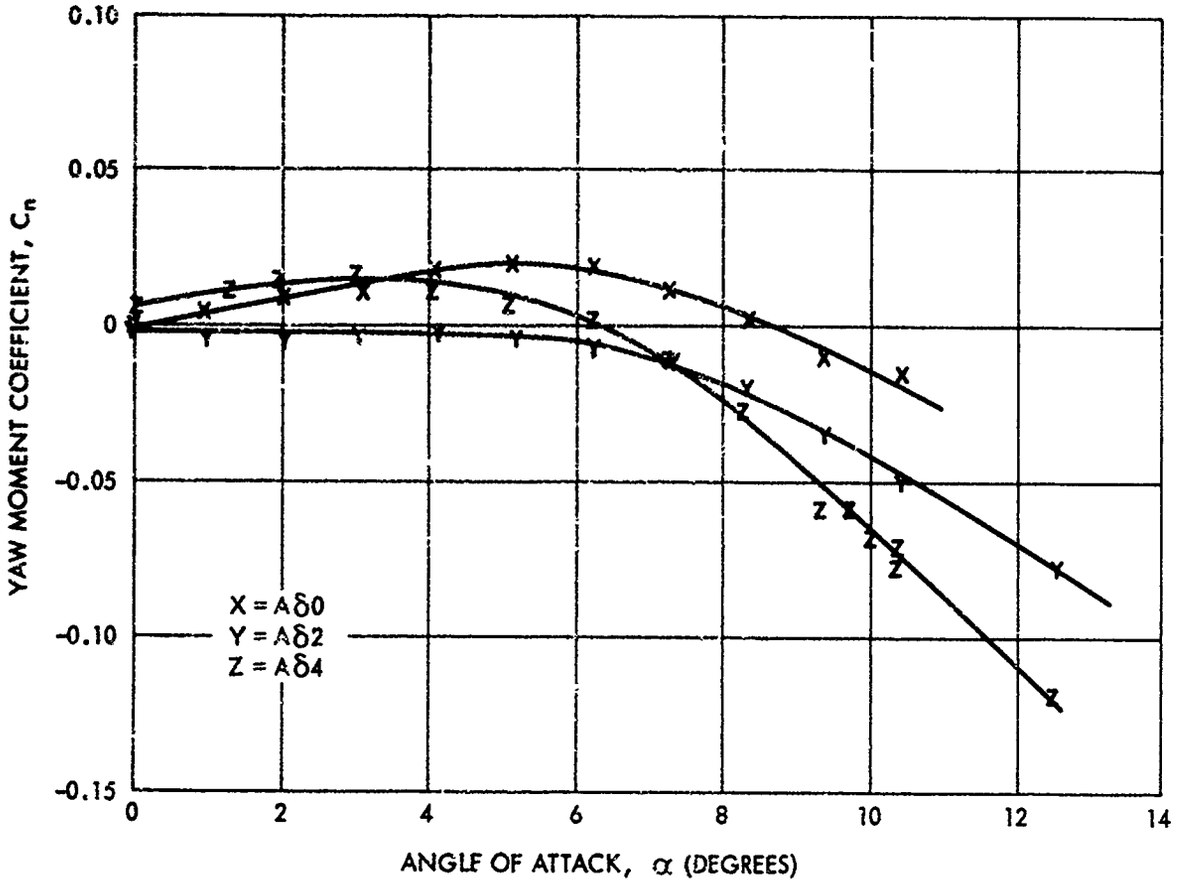

FIG. 86 YAW MOMENT COEFFICIENT VERSUS ANGLE OF ATTACK FOR THE FIXED CRUCIFORM CONFIGURATION WITH YAW PROBE AT A MACH NO. OF 0.85 AND A REDUCED SPIN RATE OF 0.040

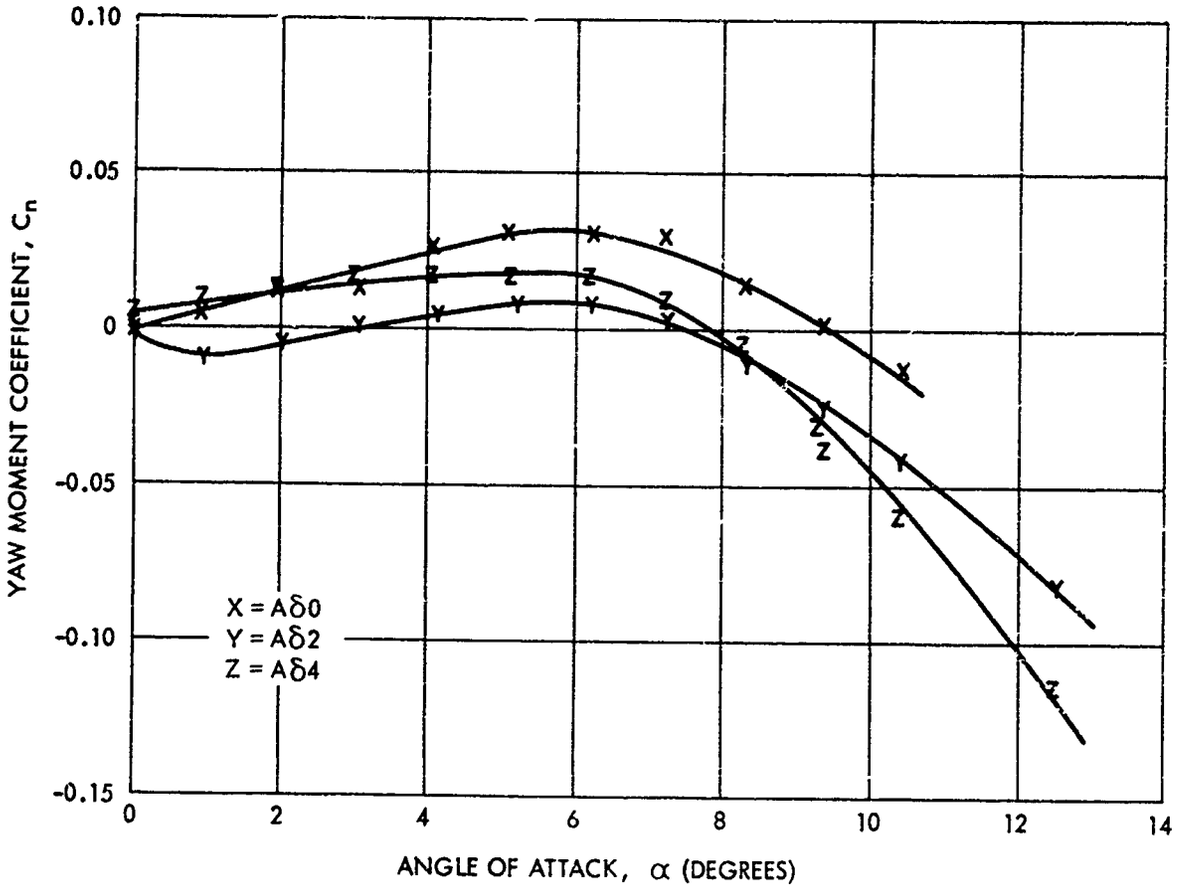

FIG. 87 YAW MOMENT COEFFICIENT VERSUS ANGLE OF ATTACK FOR THE FIXED CRUCIFORM CONFIGURATION WITH YAW PROBE AT A MACH NO. OF 0.85 AND A REDUCED SPIN RATE OF 0.072

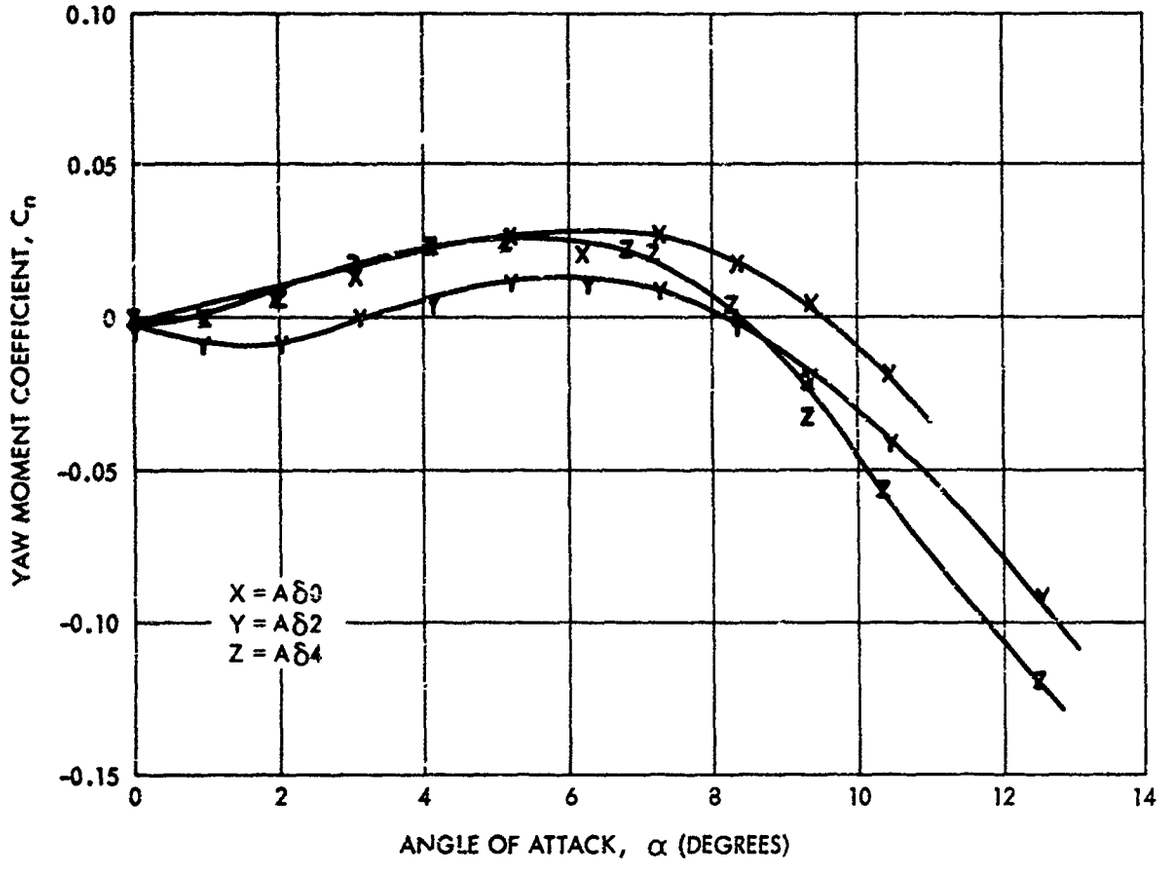

FIG. 88 YAW MOMENT COEFFICIENT VERSUS ANGLE OF ATTACK FOR THE FIXED CRUCIFORM CONFIGUPATION WITH YAW PROBE AT A MACH NO. OF 0.85 AND A REDUCED SPIN RATE OF 0.100

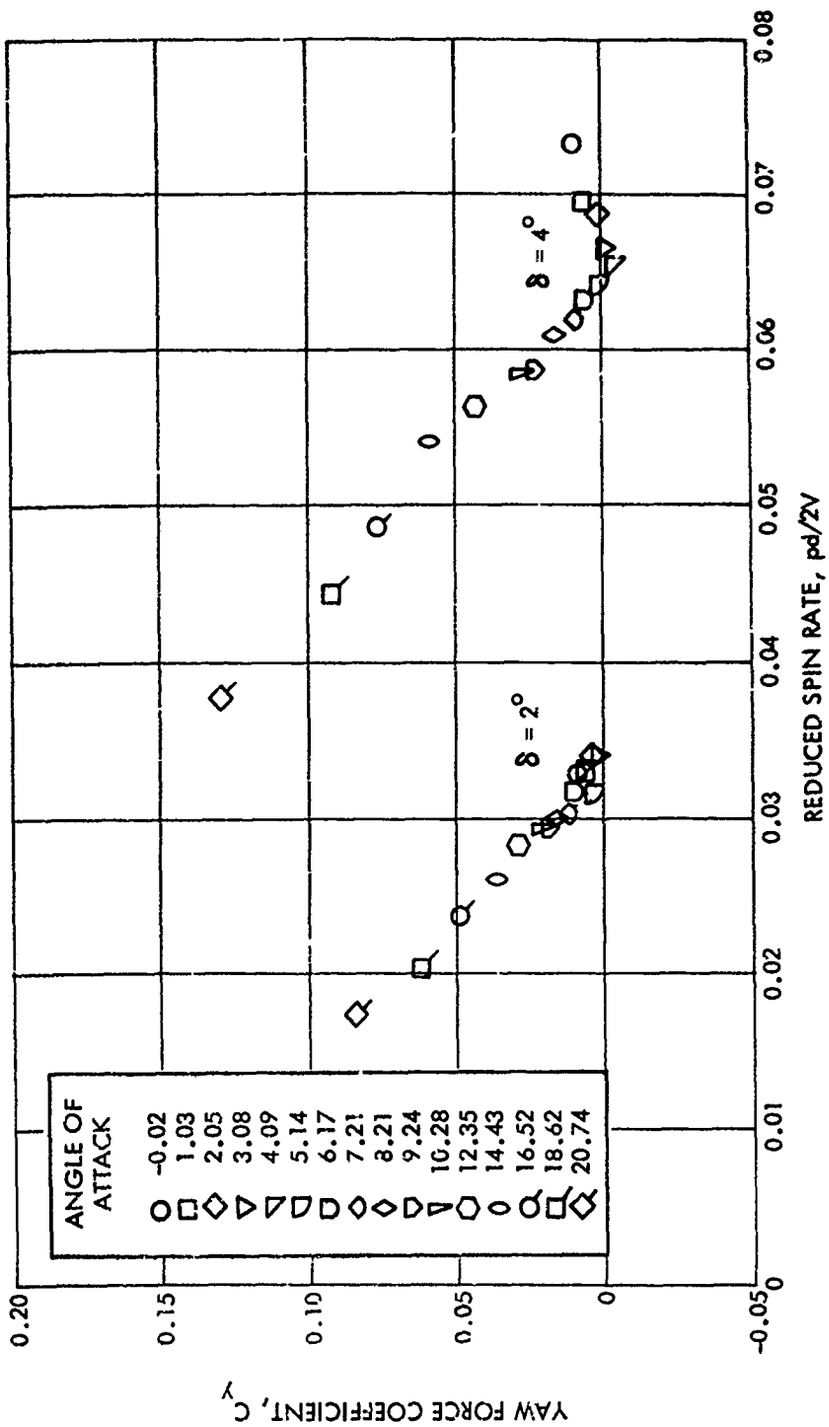

FIG. 89 YAW FORCE COEFFICIENT VERSUS REDUCED SPIN RATE FOR THE M823 RESEARCH STORE WITH A FREELY SPINNING CRUCIFORM STABILIZER AND YAW PROBE AT A MACH NUMBER OF 0.70

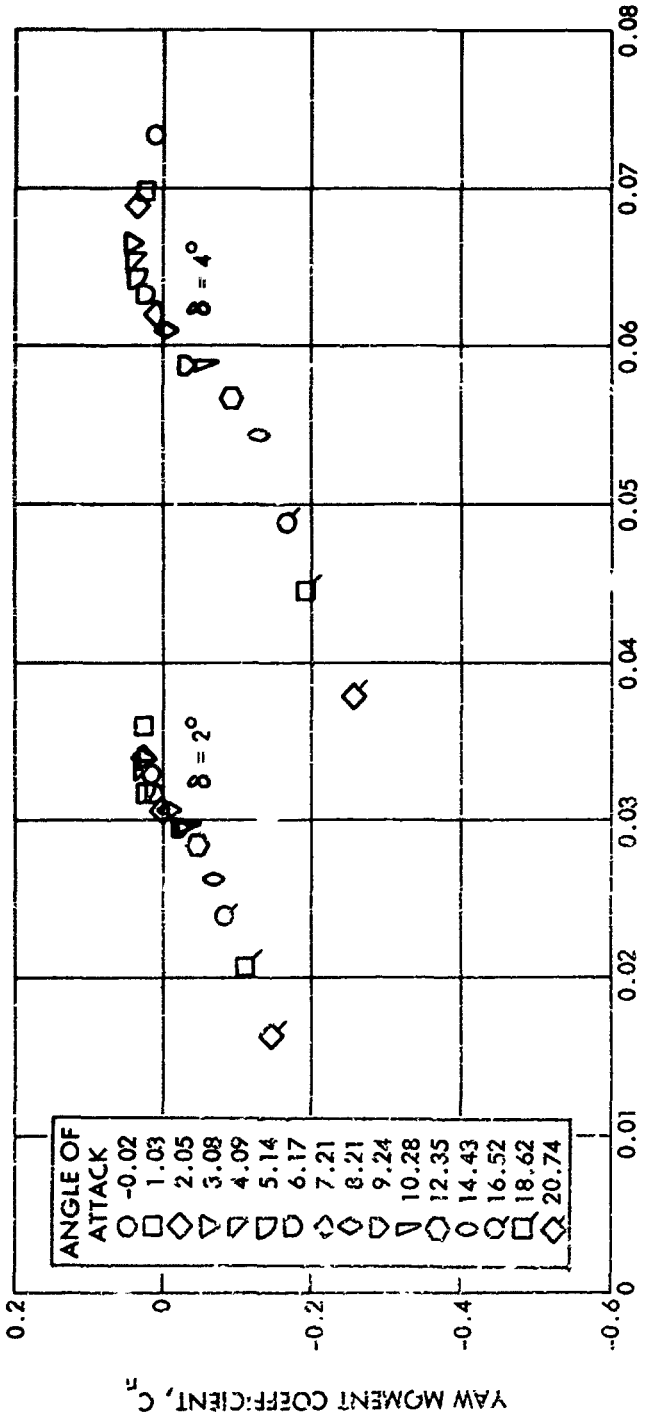

FIG. 90 YAW MOMENT COEFFICIENT VERSUS REDUCED SPIN RATE FOR THE M823 RESEARCH STORE WITH A FREELY SPINNING CRUCIFORM STABILIZER AND YAW PROBE AT A MACH NUMBER OF 0.70

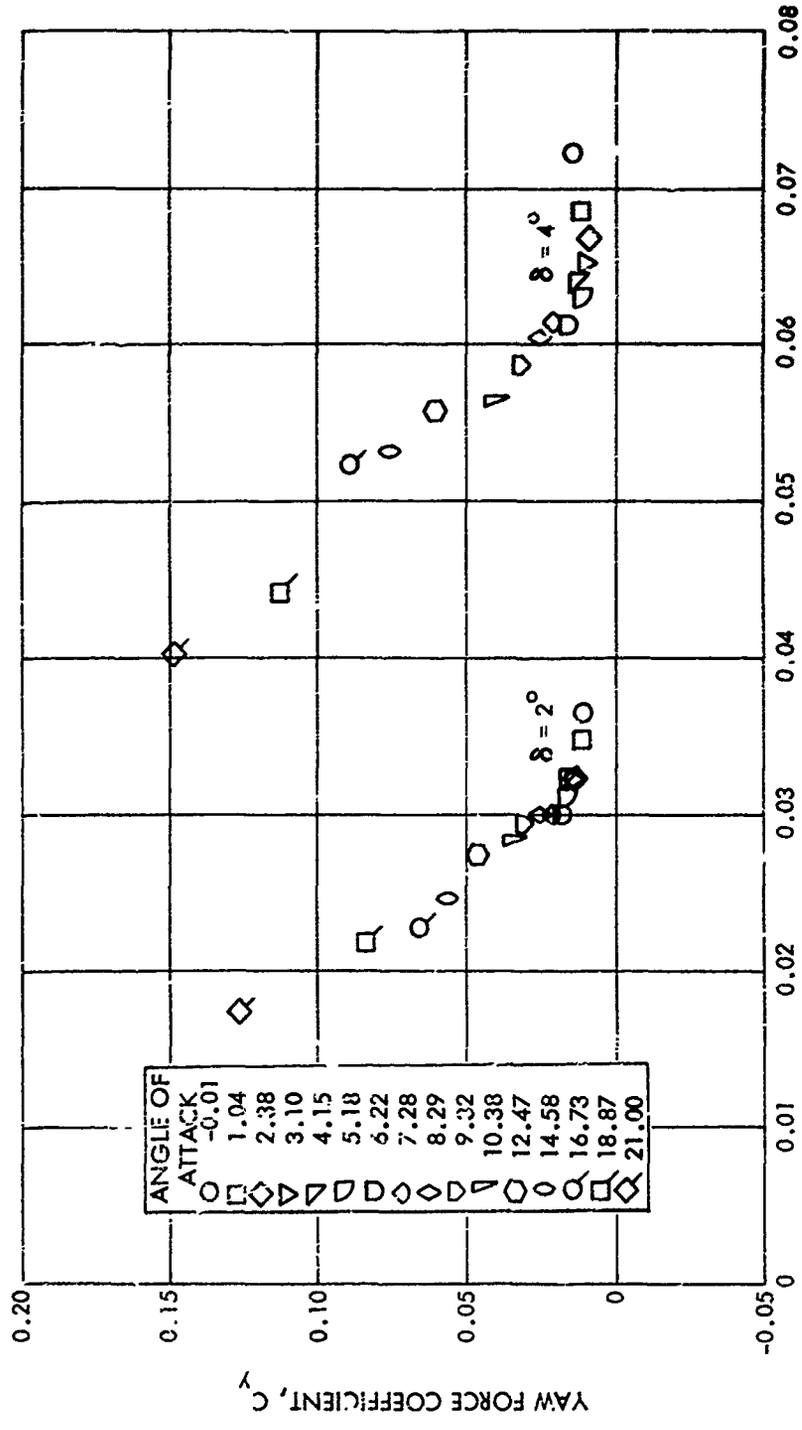

FIG. 91 YAW FORCE COEFFICIENT VERSUS REDUCED SPIN RATE FOR THE M823 RESEARCH STORE WITH A FREELY SPINNING CRUCIFORM STABILIZER AND YAW PROBE AT A MACH NUMBER OF 0.85

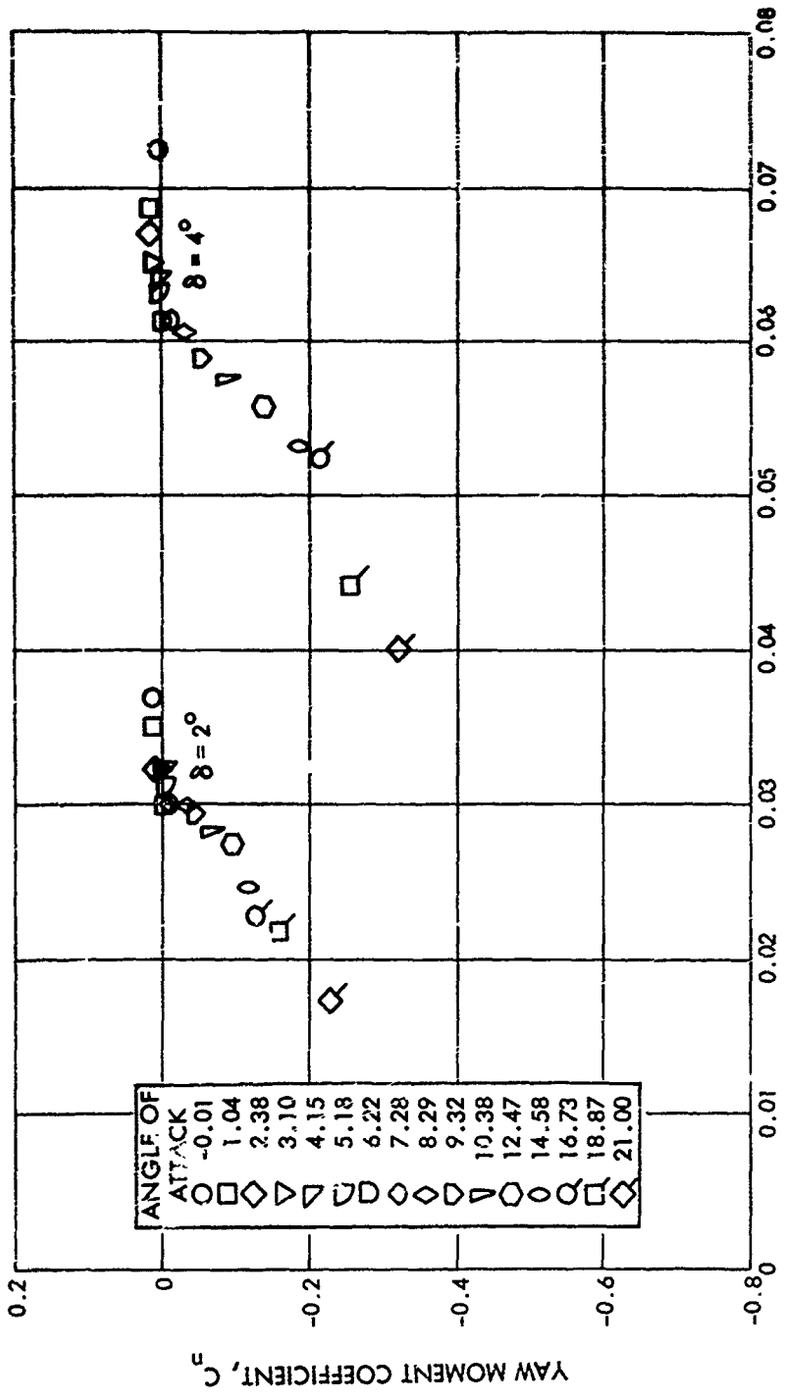

FIG. 92 YAW MOMENT COEFFICIENT VERSUS REDUCED SPIN RATE FOR THE M823 RESEARCH STORE WITH A FREELY SPINNING CRUCIFORM STABILIZER AND YAW PROBE AT A MACH NUMBER OF 0.85

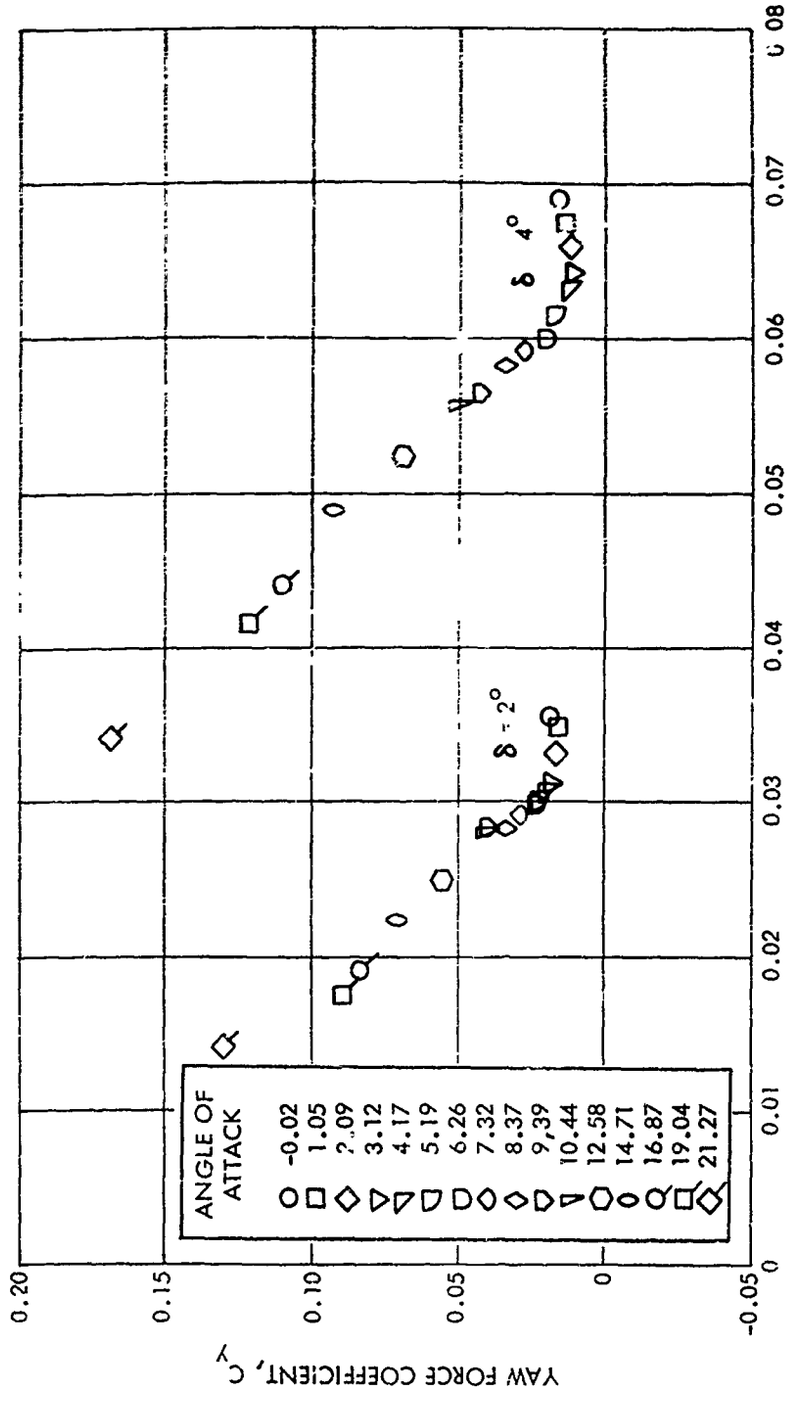

FIG. 93 YAW FORCE COEFFICIENT VERSUS REDUCED SPIN RATE FOR THE M823 RESEARCH STORE WITH A FREELY SPINNING CRUCIFORM STABILIZER AND YAW PROBE AT A MACH NUMBER OF 0.95

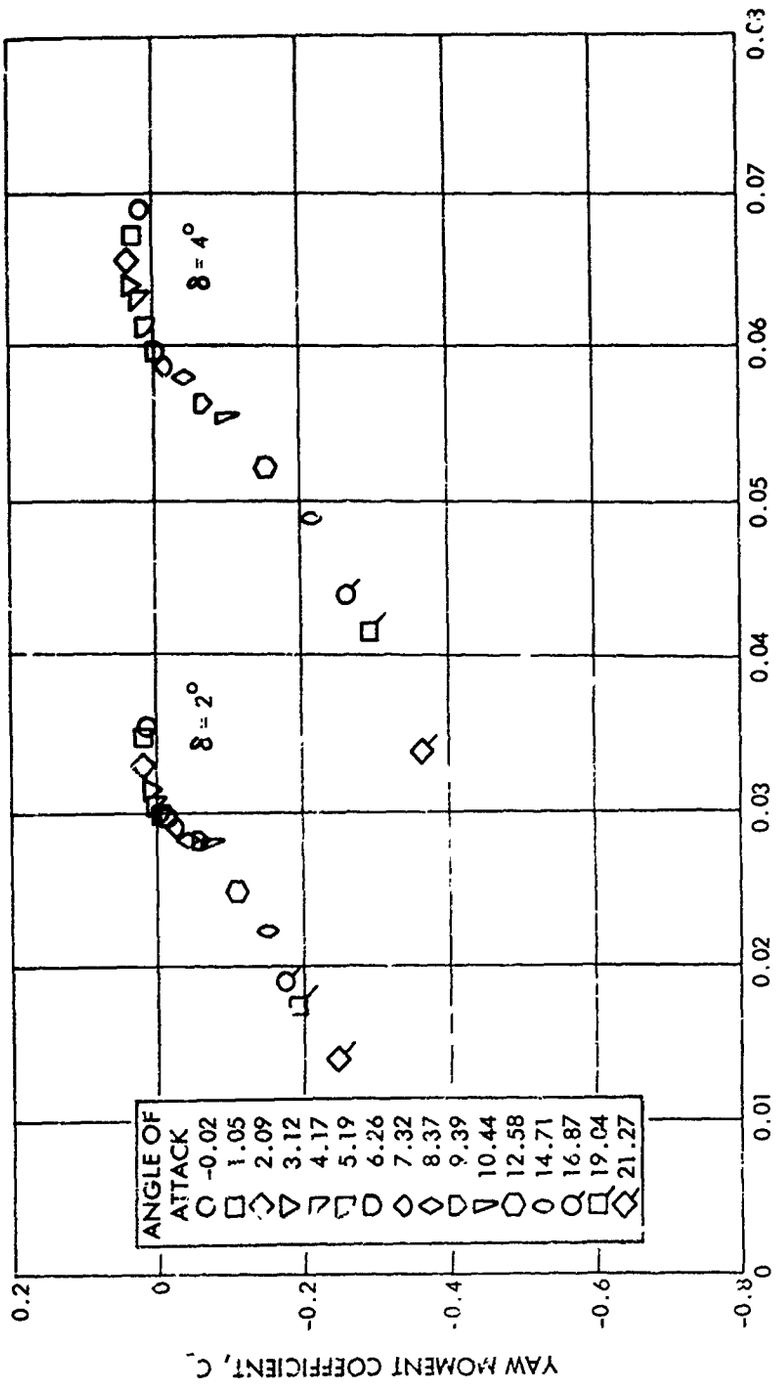

FIG. 94 YAW MOMENT COEFFICIENT VERSUS REDUCED SPIN RATE FOR THE M823 RESEARCH STORE WITH A FREELY SPINNING CRUCIFORM STABILIZER AND YAW PROBE AT A MACH NUMBER OF 0.95

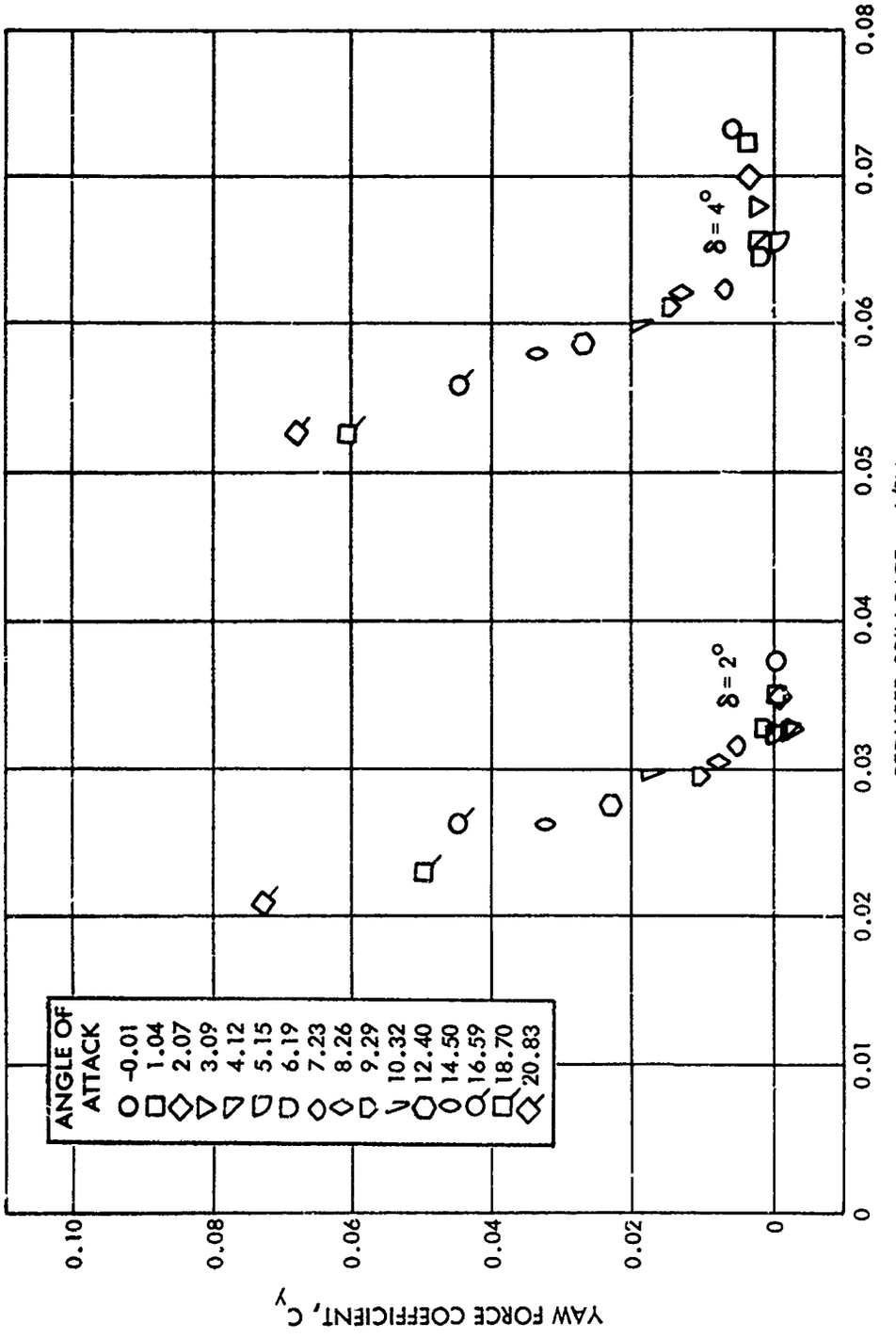

FIG. 95 YAW FORCE COEFFICIENT VERSUS REDUCED SPIN RATE FOR THE M823 RESEARCH STORE WITH A MONOPLANE STABILIZER AND YAW PROBE AT A MACH NUMBER OF 0.70

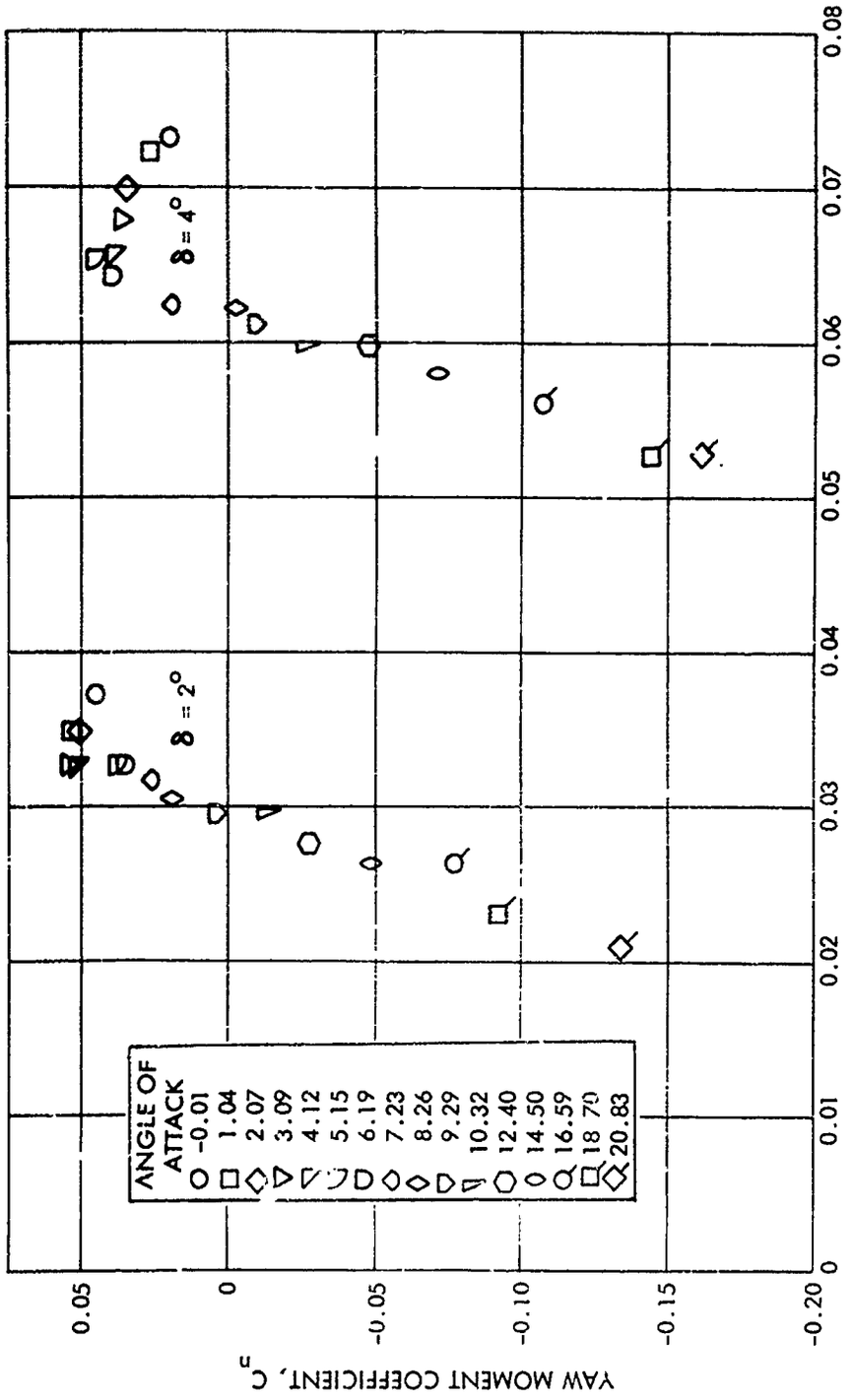

FIG. 96 YAW MOMENT COEFFICIENT VERSUS REDUCED SPIN RATE FOR THE M823 RESEARCH STORE WITH A MONOPLANE STABILIZER AND YAW PROBE AT A MACH NUMBER OF 0.70

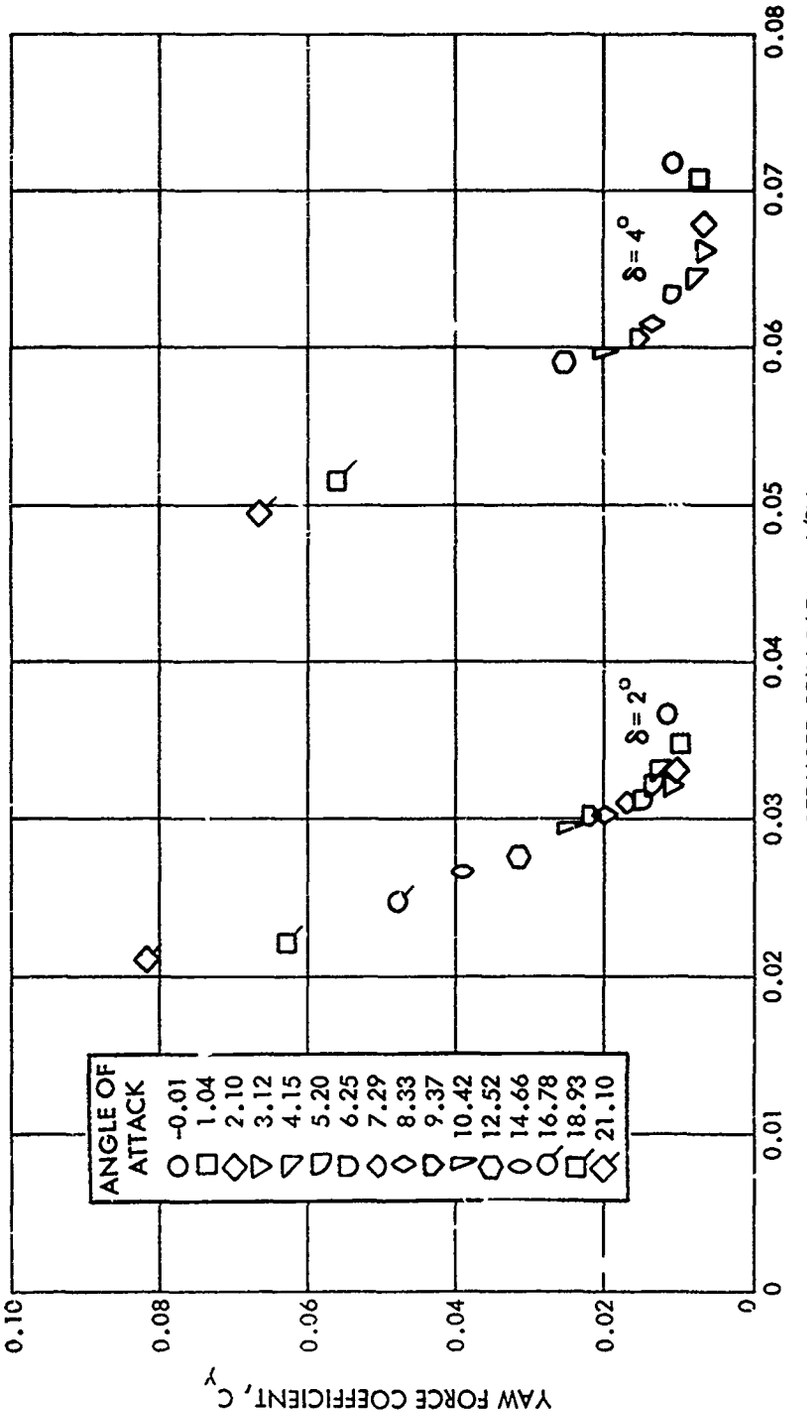

FIG. 97 YAW FORCE COEFFICIENT VERSUS REDUCED SPIN RATE FOR THE M823 RESEARCH STORE WITH A MONOPLANE STABILIZER AND YAW PROBE AT A MACH NUMBER OF 0.85

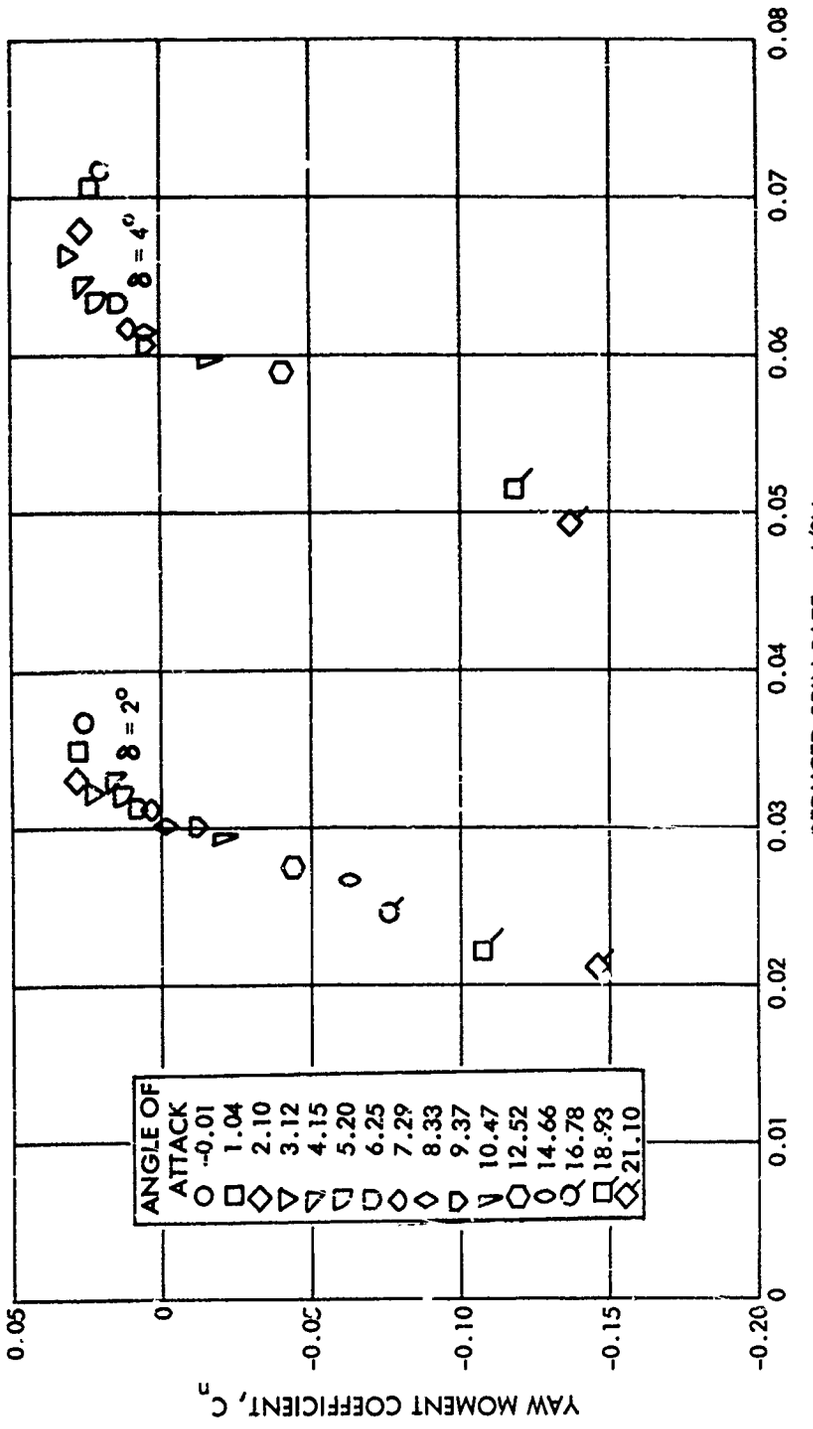

FIG. 98 YAW MOMENT COEFFICIENT VERSUS REDUCED SPIN RATE FOR THE M823 RESEARCH STORE WITH A MONOPLANE STABILIZER AND YAW PROBE AT A MACH NUMBER OF 0.85

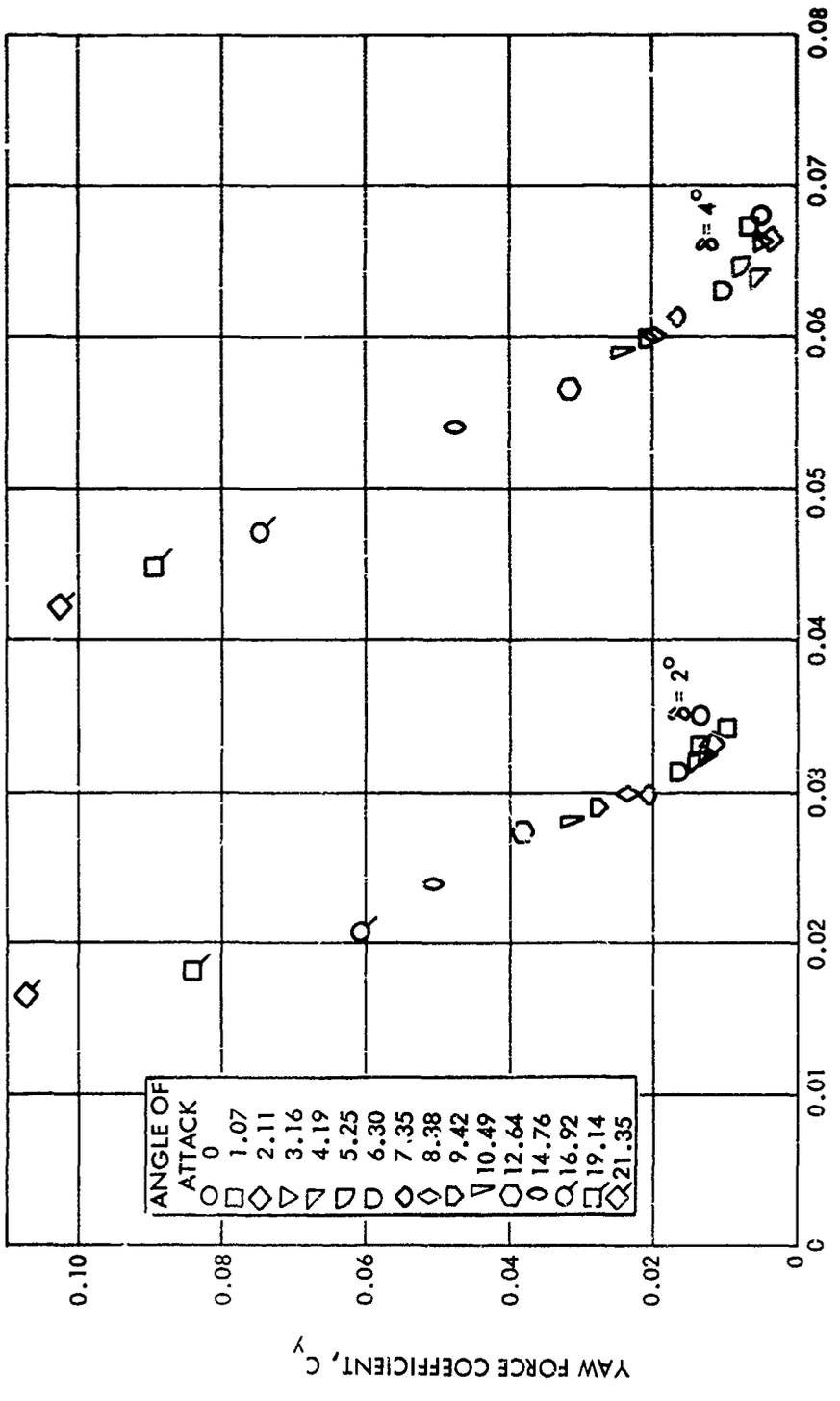

FIG. 99 YAW FORCE COEFFICIENT VERSUS REDUCED SPIN RATE FOR THE M823 RESEARCH STORE WITH A MONOPLANE STABILIZER AND YAW PROBE AT A MACH NUMBER OF 0.95

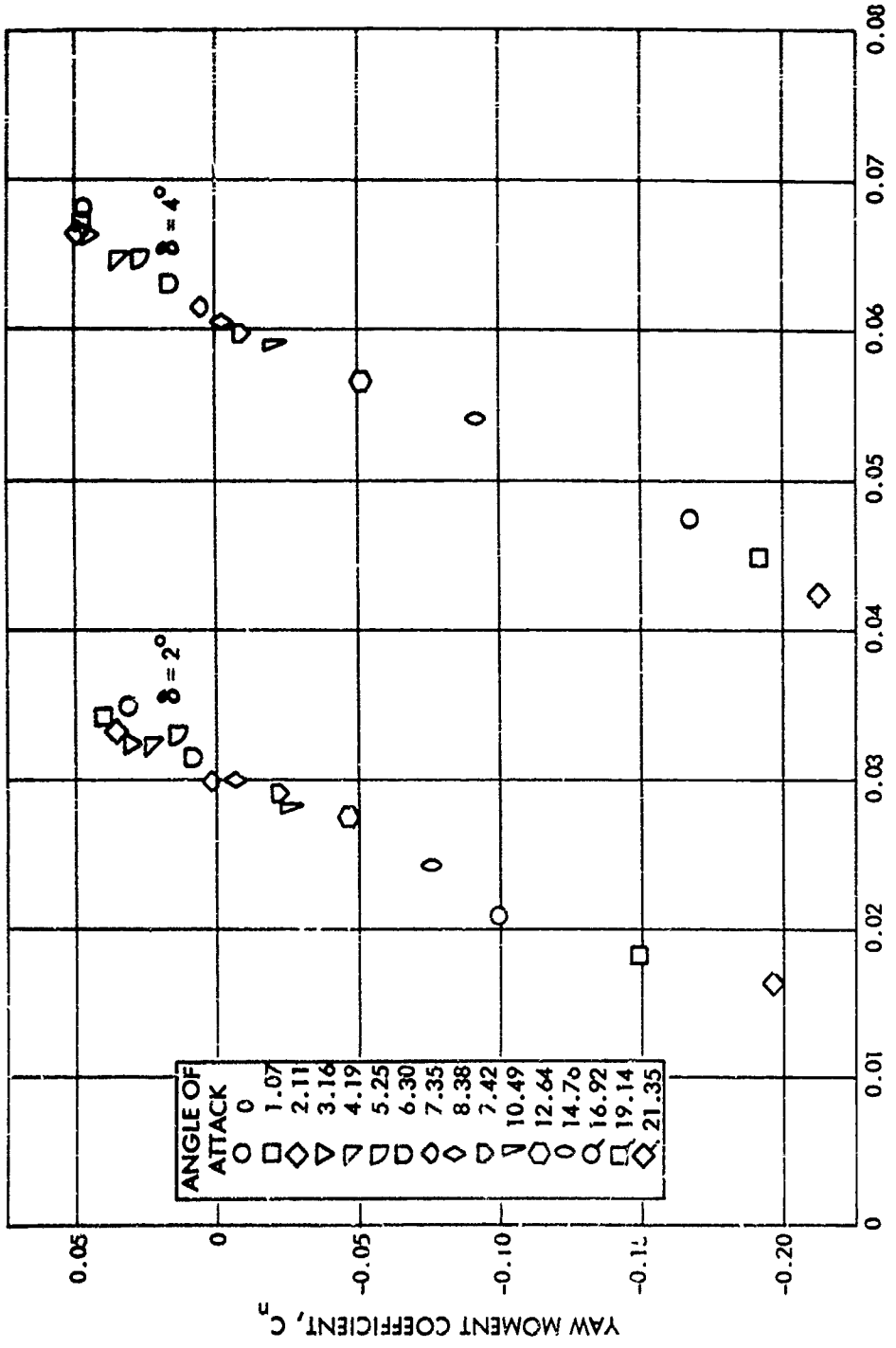

FIG. 100 YAW MOMENT COEFFICIENT VERSUS REDUCED SPIN RATE FOR THE M823 RESEARCH STORE WITH A MONOPLANE STABILIZER AND YAW PROBE AT A MACH NUMBER OF 0.95

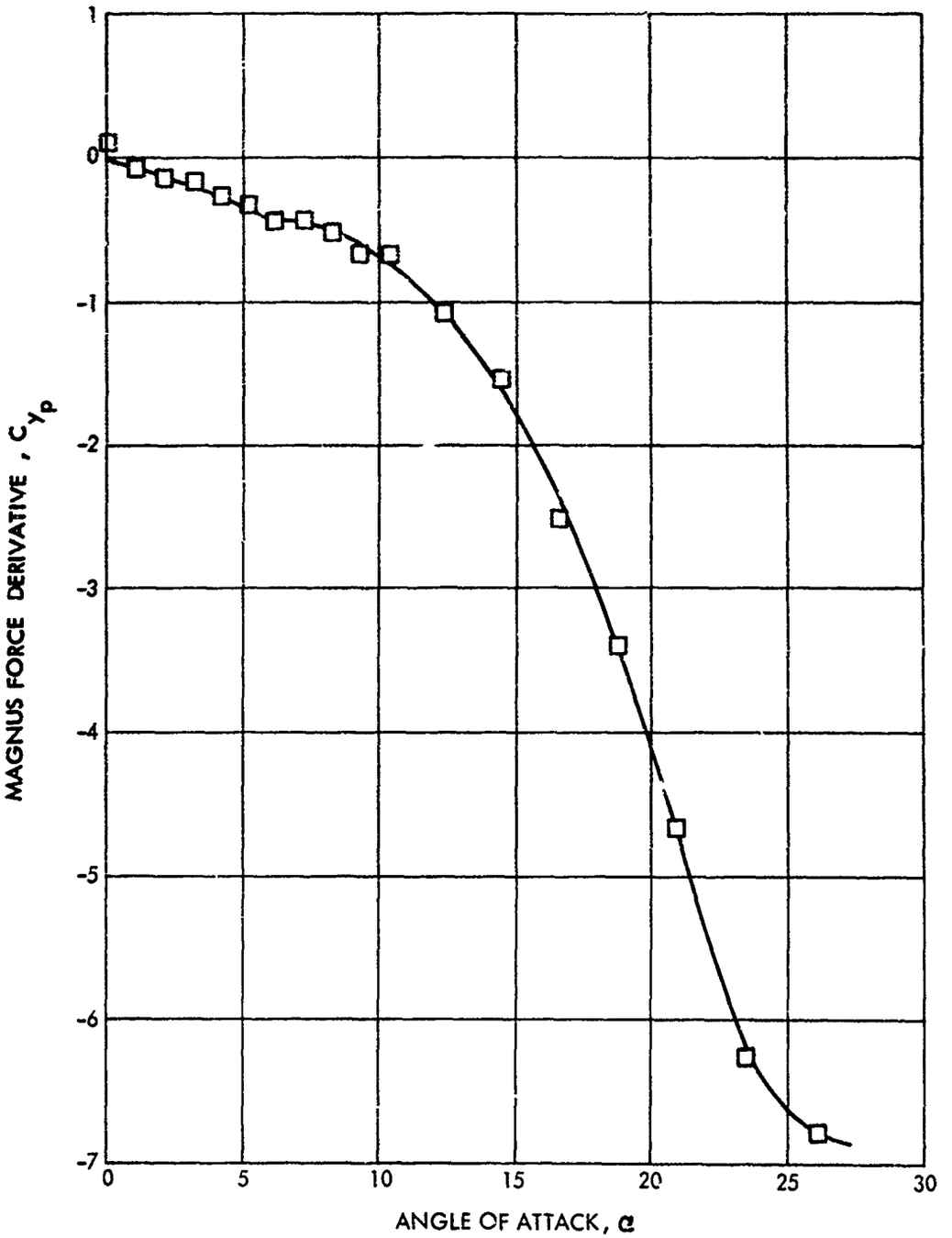

FIG. 101 MAGNUS FORCE DERIVATIVE VERSUS ANGLE OF ATTACK FOR THE M823 RESEARCH STORE WITH A TEN DEGREE SPLIT-SKIRT STABILIZER AND YAW PROBE AT A MACH NUMBER OF 0.70

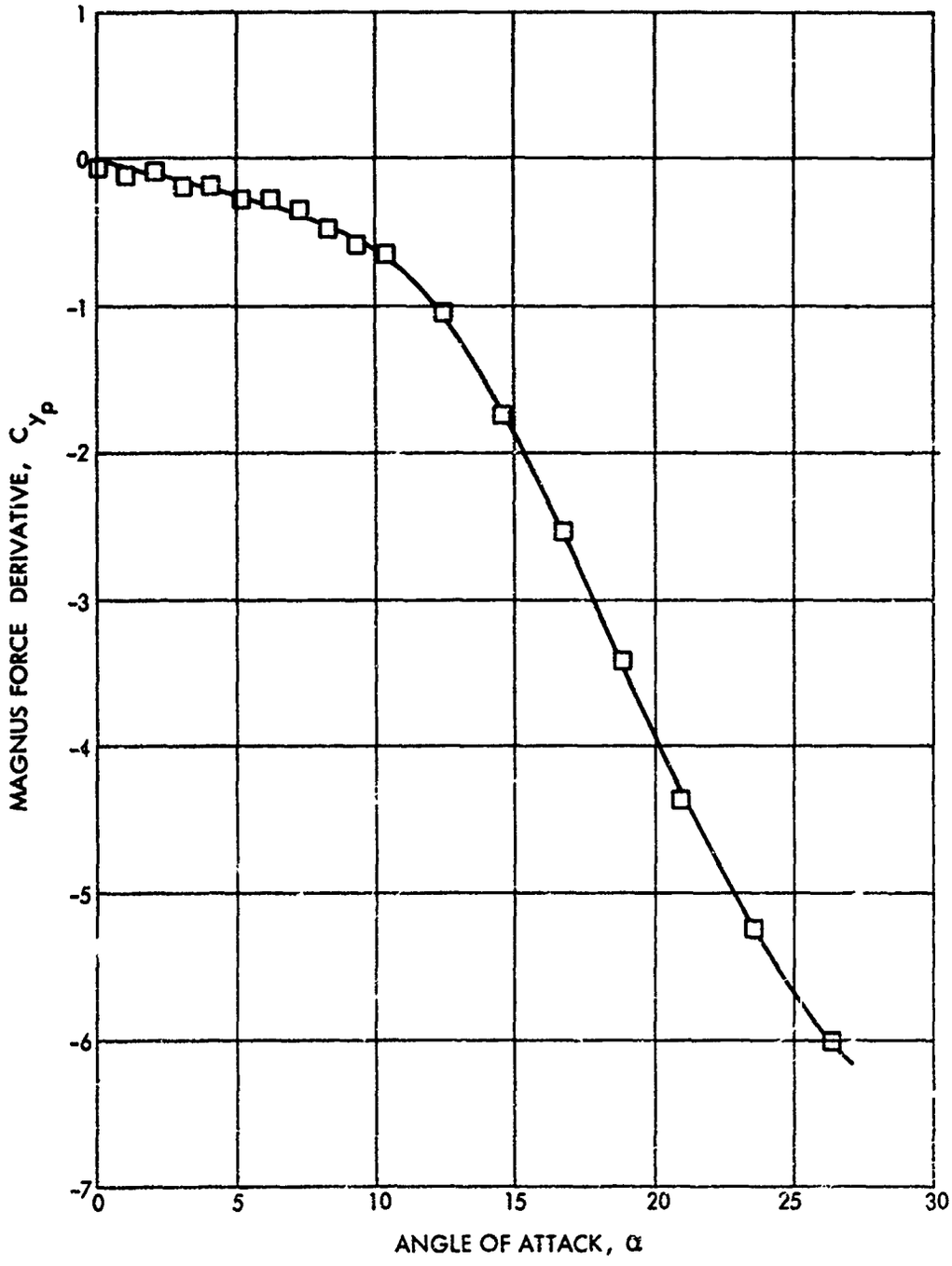

FIG. 102 MAGNUS FORCE DERIVATIVE VERSUS ANGLE OF ATTACK FOR THE M823 RESEARCH STORE WITH A TEN DEGREE SPLIT-SKIRT STABILIZER AND YAW PROBE AT A MACH NUMBER OF 0.80

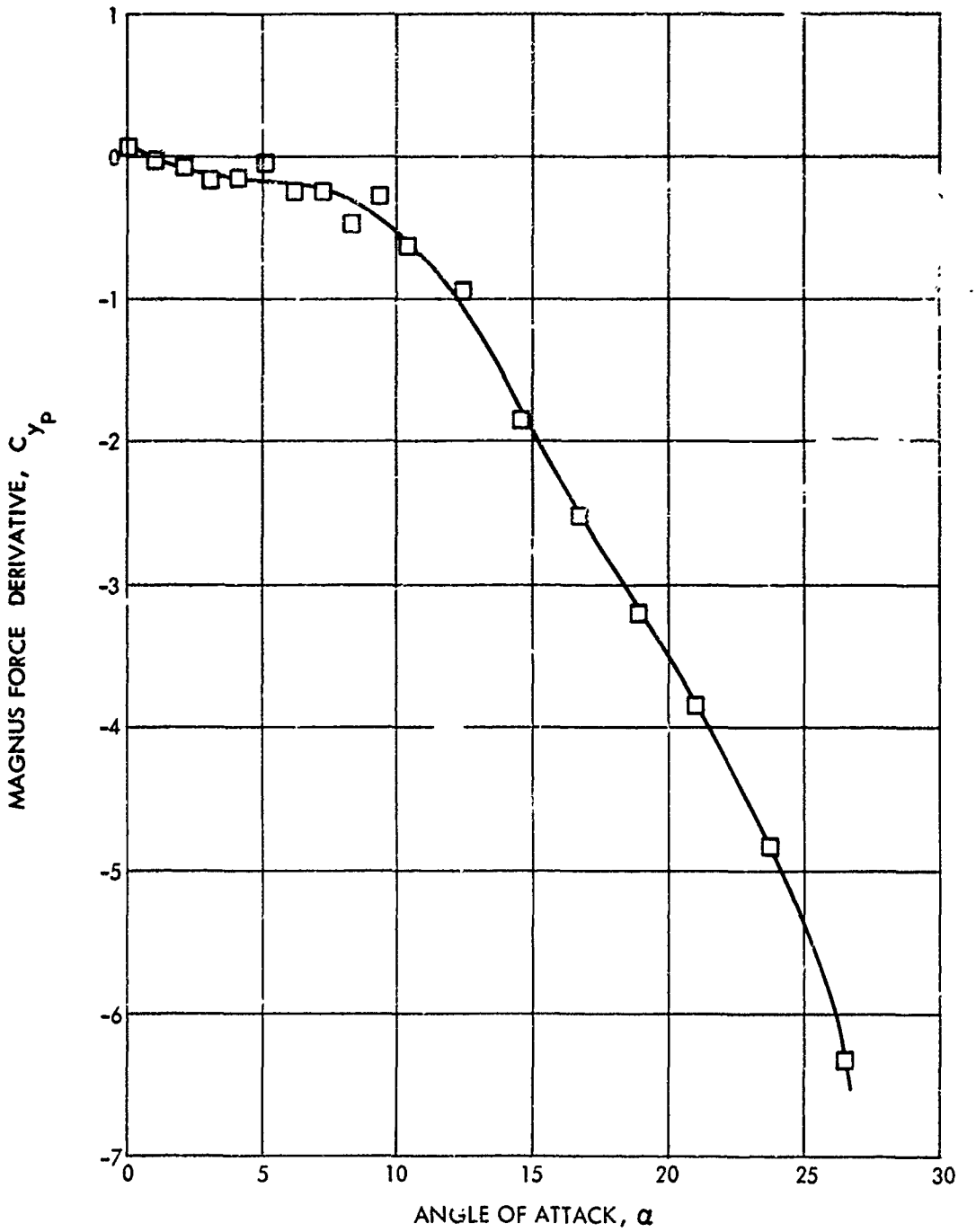

FIG. 103 MAGNUS FORCE DERIVATIVE VERSUS ANGLE OF ATTACK FOR THE M823 RESEARCH STORE WITH A TEN DEGREE SPLIT-SKIRT STABILIZER AND YAW PROBE AT A MACH NUMBER OF 0.85

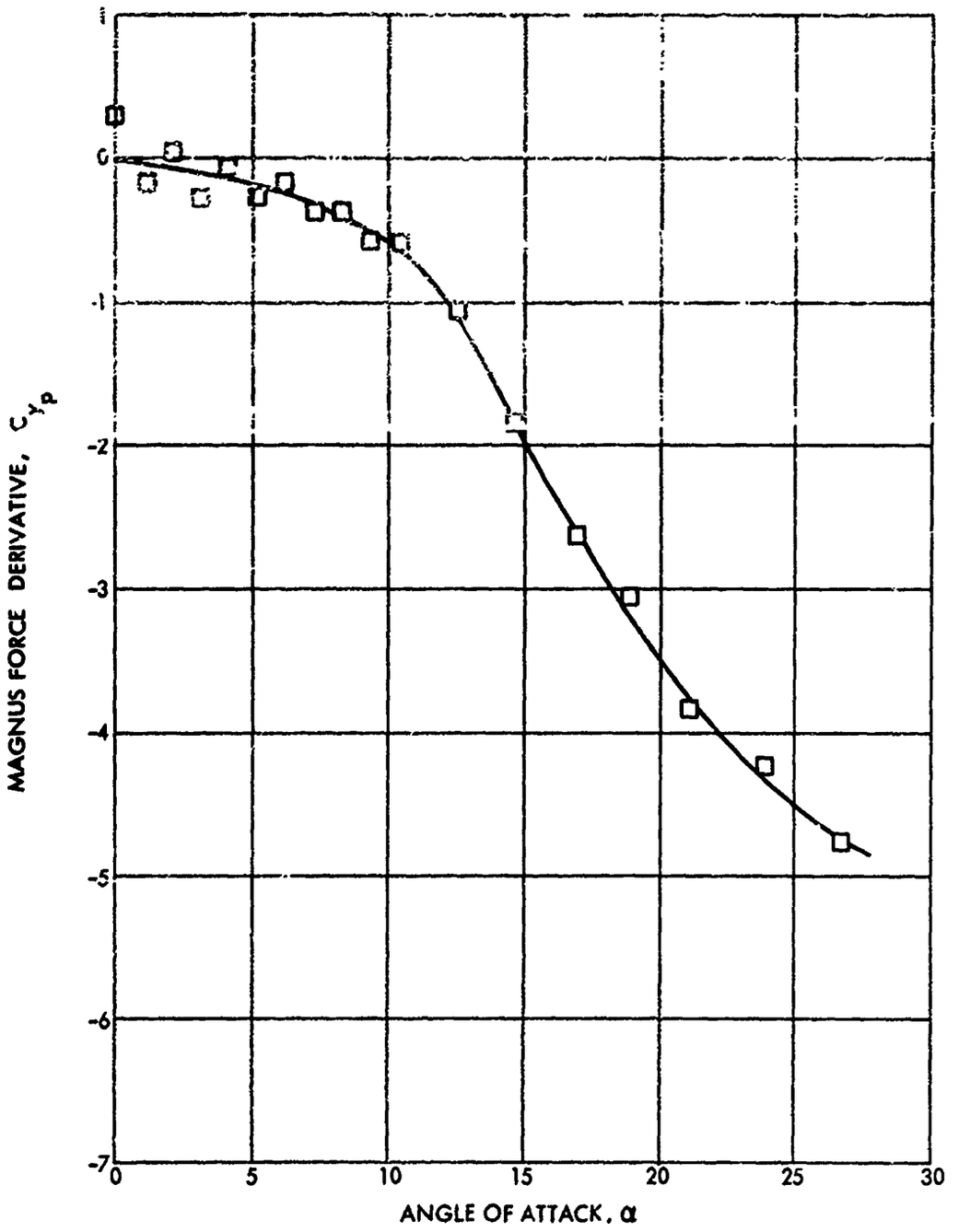

FIG. 104 MAGNUS FORCE DERIVATIVE VERSUS ANGLE OF ATTACK FOR THE M823 RESEARCH STORE WITH A TEN DEGREE SPLIT-SKIRT STABILIZER AND YAW PROBE AT A MACH NUMBER OF 0.90

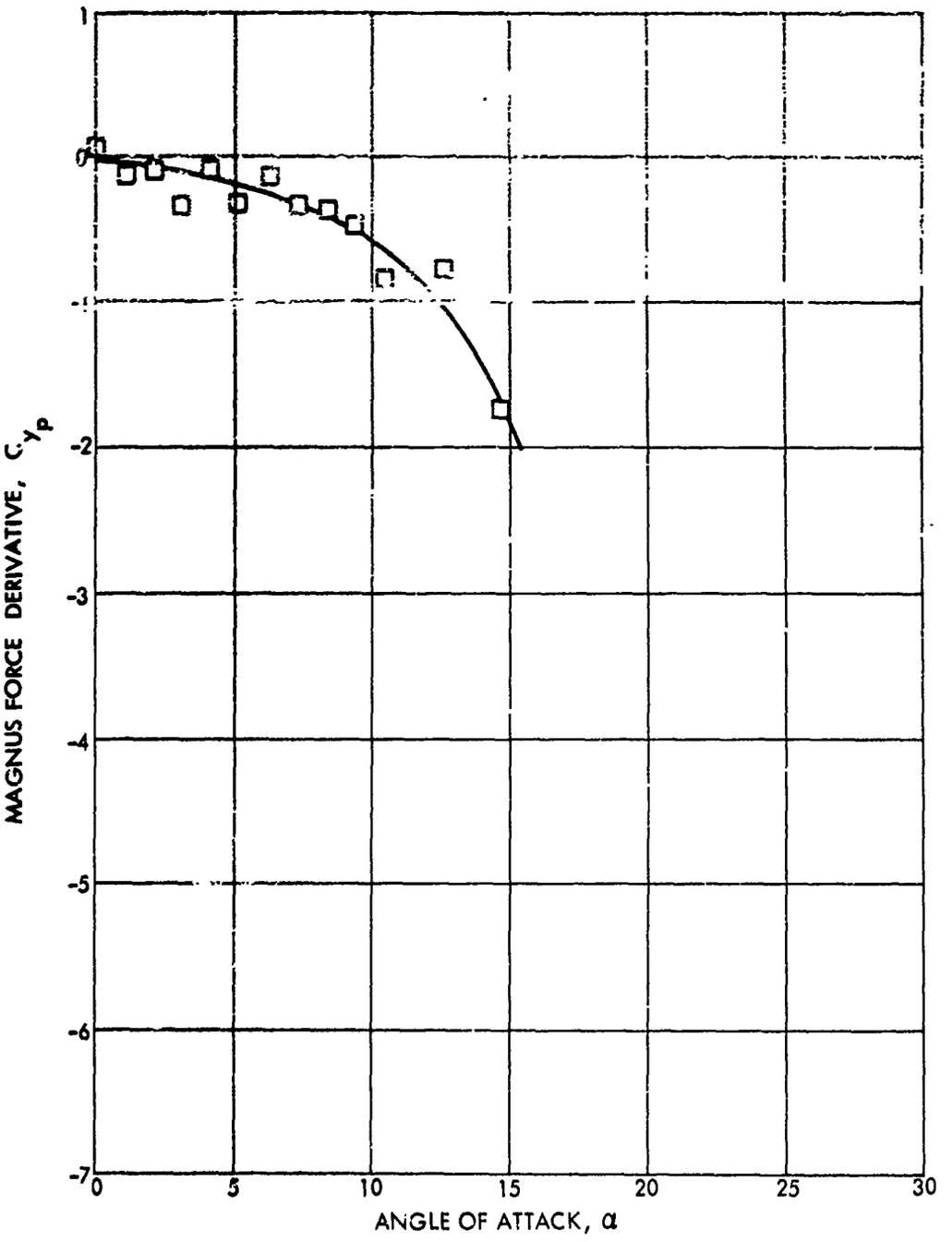

FIG. 105 MAGNUS FORCE DERIVATIVE VERSUS ANGLE OF ATTACK FOR THE M823 RESEARCH STORE WITH A TEN DEGREE SPLIT-SKIRT STABILIZER AND YAW PROBE AT A MACH NUMBER OF 0.95

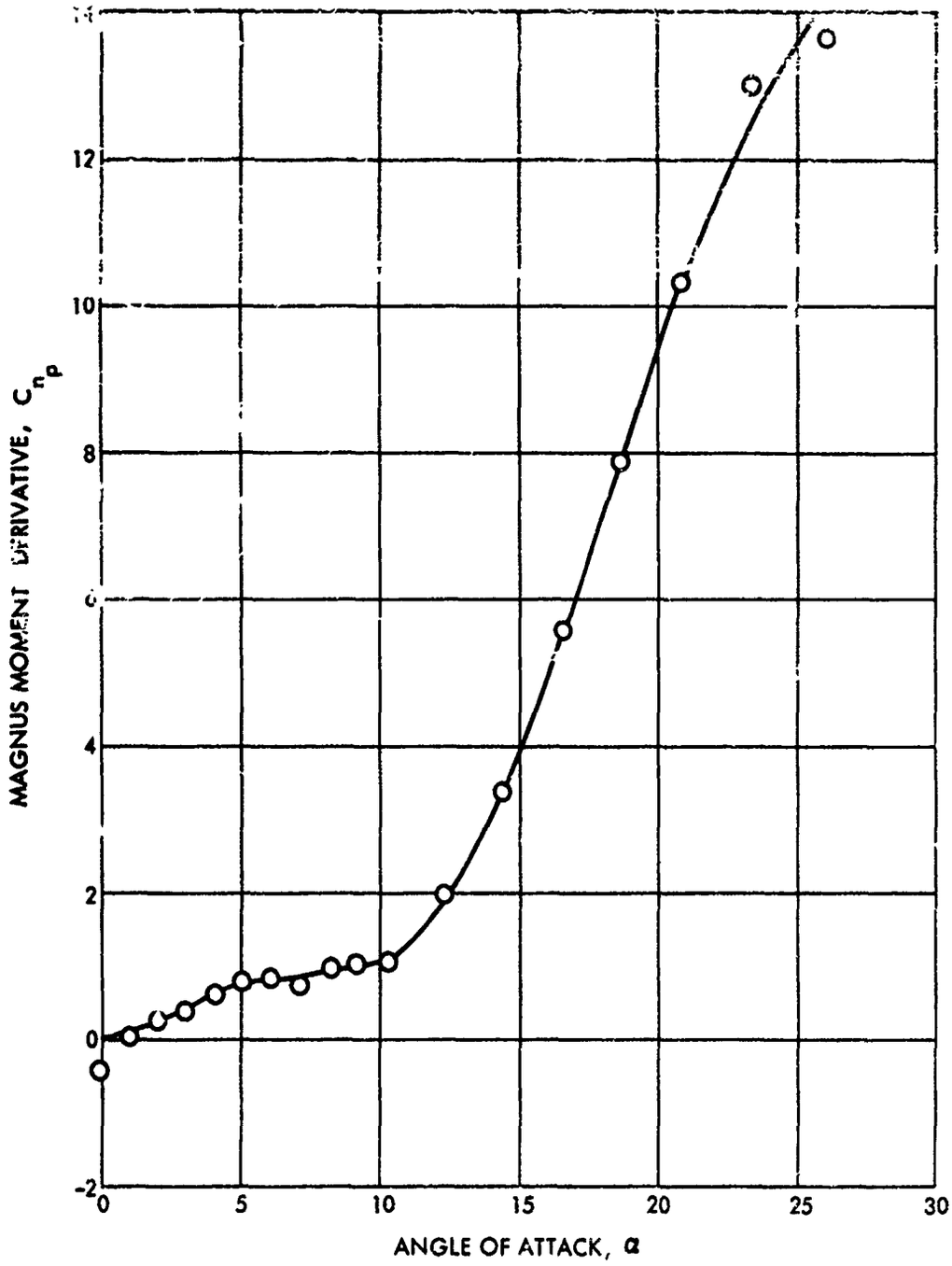

FIG. 106 MAGNUS MOMENT DERIVATIVE VERSUS ANGLE OF ATTACK FOR THE M823 RESEARCH STORE WITH A TEN DEGREE SPLIT-SKIRT STABILIZER AND YAW PROBE AT A MACH NUMBER OF 0.70

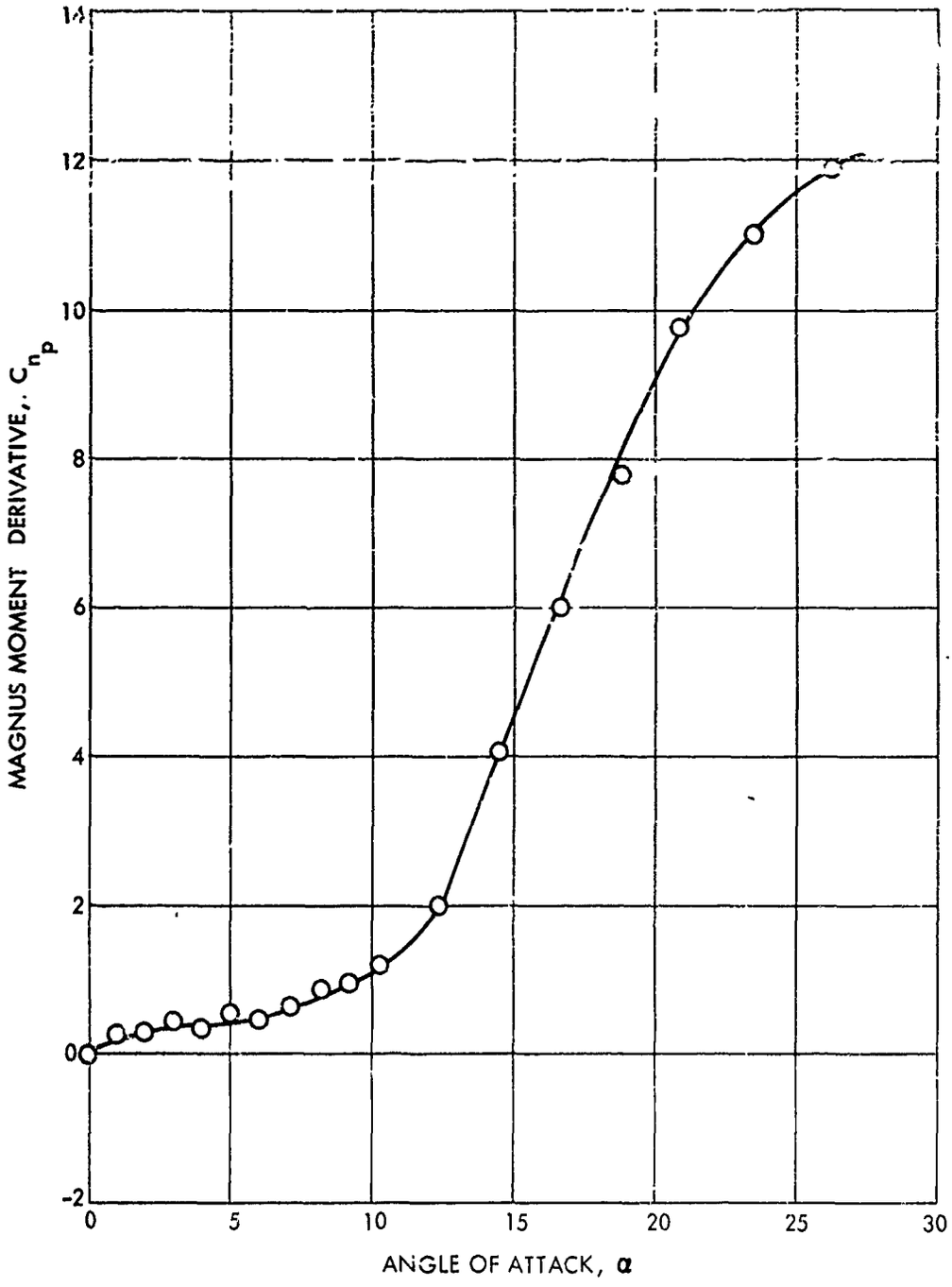

FIG. 107 MAGNUS MOMENT DERIVATIVE VERSUS ANGLE OF ATTACK FOR THE M823 RESEARCH STORE WITH A TEN DEGREE SPLIT-SKIRT STABILIZER AND YAW PROBE AT A MACH NUMBER OF 0.80

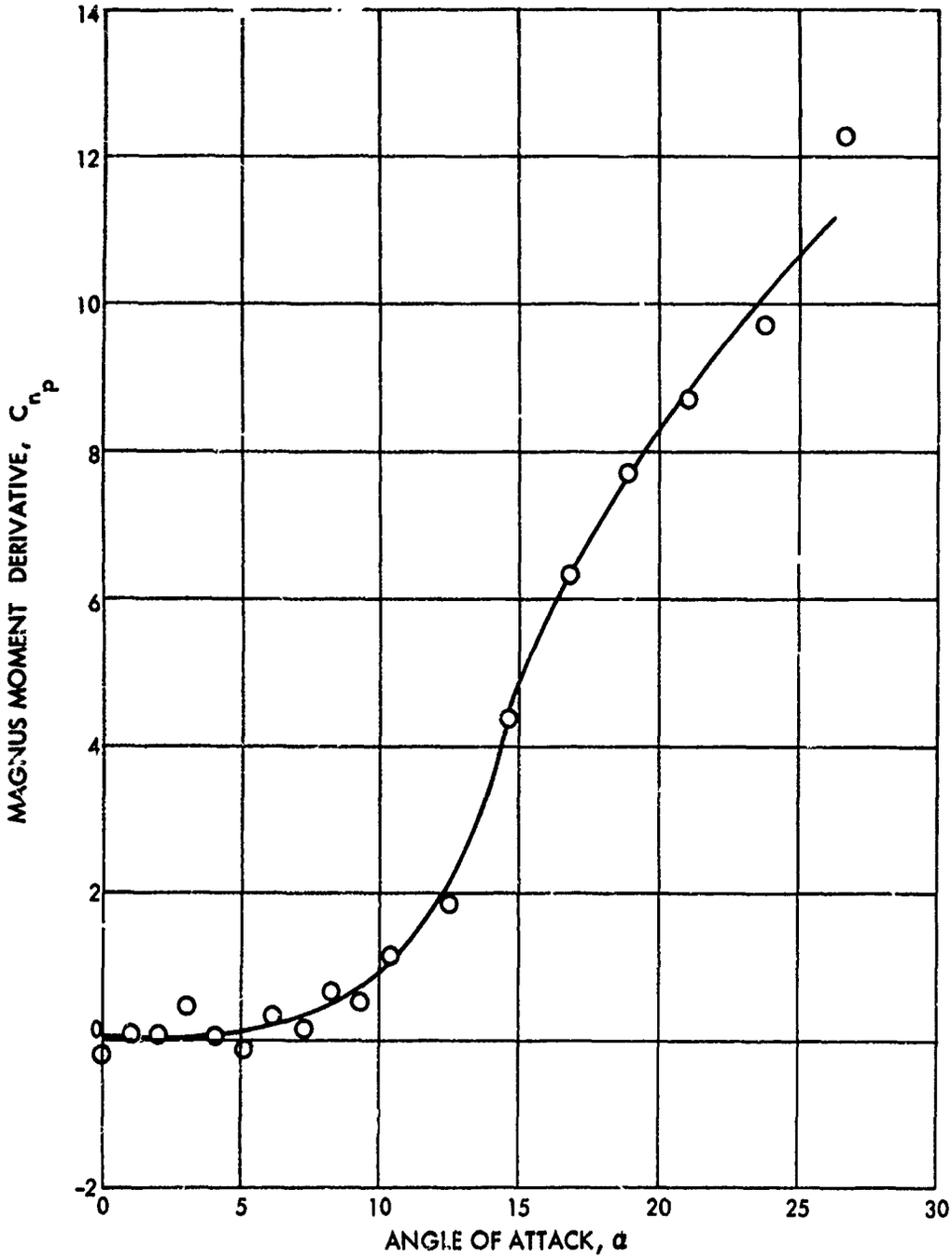

FIG. 108 MAGNUS MOMENT DERIVATIVE VERSUS ANGLE OF ATTACK FOR THE M823 RESEARCH STORE WITH A TEN DEGREE SPLIT-SKIRT STABILIZER AND YAW PROBE AT A MACH NUMBER OF 0.85

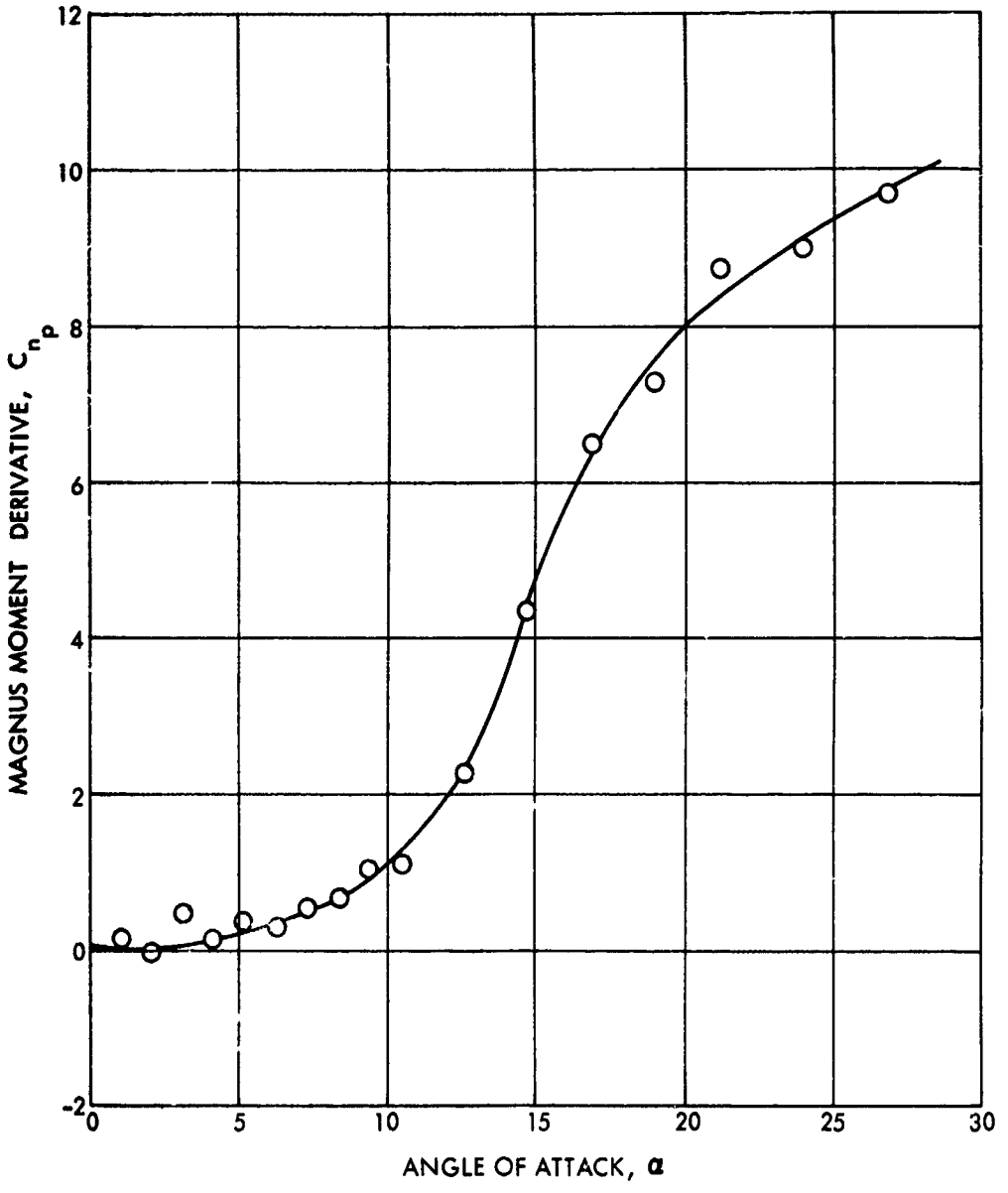

FIG. 109 MAGNUS MOMENT DERIVATIVE VERSUS ANGLE OF ATTACK FOR THE M823 RESEARCH STORE WITH A TEN DEGREE SPLIT-SKIRT STABILIZER AND YAW PROBE AT A MACH NUMBER OF 0.90

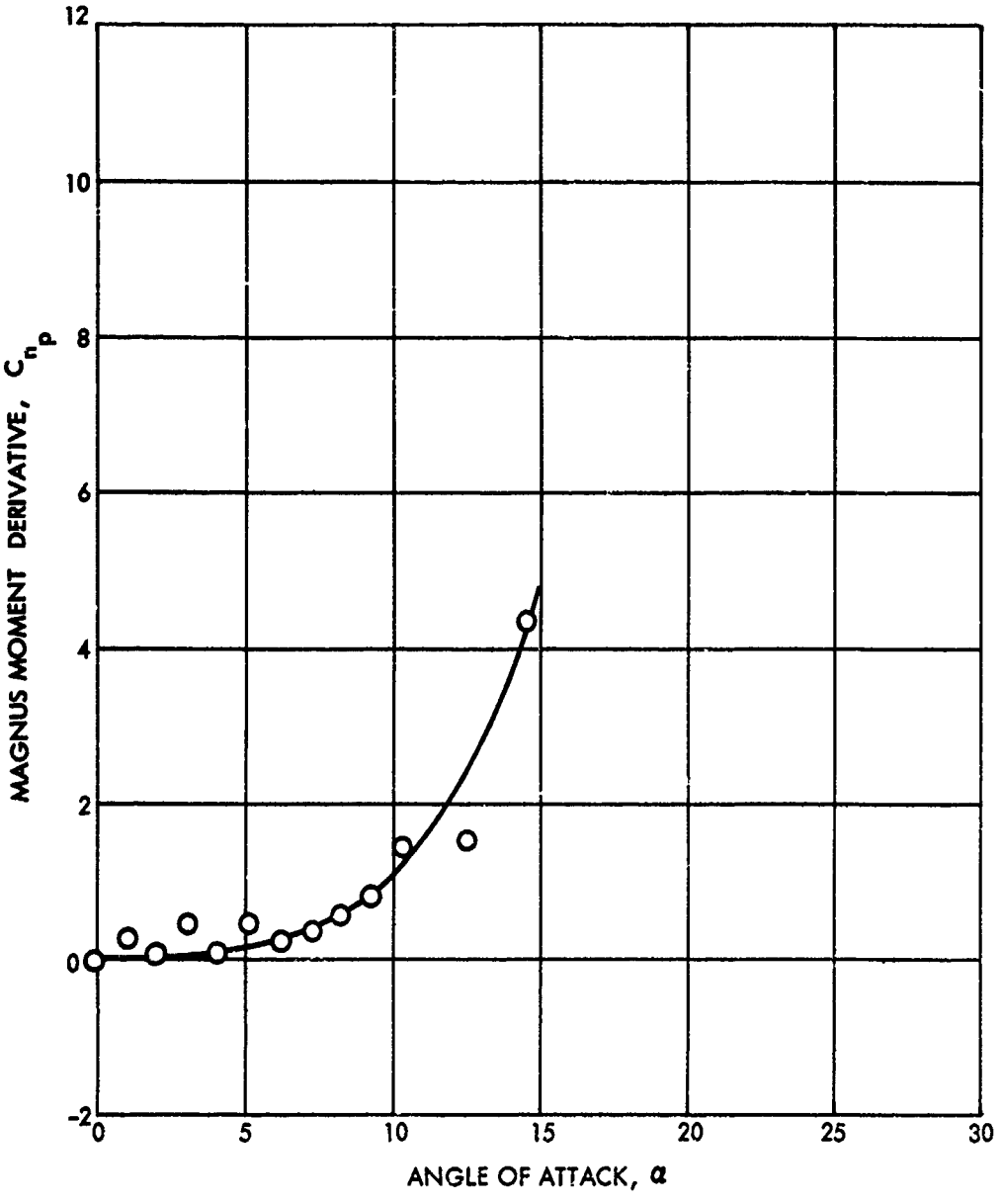

FIG. 110 MAGNUS MOMENT DERIVATIVE VERSUS ANGLE OF ATTACK FOR THE M823 RESEARCH STORE WITH A TEN DEGREE SPLIT-SKIRT STABILIZER AND YAW PROBE AT A MACH NUMBER OF 0.95

UNCLASSIFIED
Security Classification

DOCUMENT CONTROL DATA - R&D

(Security classification of title, body of abstract and indexing annotation must be entered when the overall report is classified)

1. ORIGINATING ACTIVITY (Corporate author)

U. S. Naval Ordnance Laboratory
White Oak, Silver Spring, Maryland

2a. REPORT SECURITY CLASSIFICATION
UNCLASSIFIED

2b GROUP

3. REPORT TITLE

Magnus Measurements on the M823 Research Store with Fixed and Freely Spinning Cruciform Stabilizers, Freely Spinning Monoplane Stabilizers and Split-Skirt Stabilizers

4. DESCRIPTIVE NOTES (Type of report and inclusive dates)

5. AUTHOR(S) (Last name, first name, initial)

Frank J. Regan, John E. Holmes, Mary Ellen Falusi

6. REPORT DATE	7a. TOTAL NO. OF PAGES	7b. NO. OF REFS
25 November 1969	134	6

8a. CONTRACT OR GRANT NO.

b. PROJECT NO.
RMMO-42-005/212-1/F 008-09-001

c.

d.

9a. ORIGINATOR'S REPORT NUMBER(S)
NOLTR 69-214

9b. OTHER REPORT NO(S) (Any other numbers that may be assigned this report)

10. AVAILABILITY/LIMITATION NOTICES
This document is subject to special export controls and each transmittal to foreign governments or foreign nationals may be made only with prior approval of NOL.

11. SUPPLEMENTARY NOTES

12. SPONSORING MILITARY ACTIVITY
Naval Ordnance Systems Command
Washington, D. C.

13. ABSTRACT

The M823 configuration is an instrumented free-fall store used in bomb stability research programs. This report presents the results of Magnus wind-tunnel tests on the basic forebody with fixed and freely spinning cruciform stabilizers, freely spinning monoplane stabilizers and split-skirt stabilizers.

DD FORM 1 JAN 64 1473

UNCLASSIFIED
Security Classification

UNCLASSIFIED

Security Classification

14. KEY WORDS	LINK A		LINK B		LINK C	
	ROLE	WT	ROLE	WT	ROLE	WT
Magnus **Aerodynamics** **Wind tunnel** **freely spinning stabilizers**						

INSTRUCTIONS

1. ORIGINATING ACTIVITY: Enter the name and address of the contractor, subcontractor, grantee, Department of Defense activity or other organization *(corporate author)* issuing the report.

2a. REPORT SECURITY CLASSIFICATION: Enter the overall security classification of the report. Indicate whether "Restricted Data" is included. Marking is to be in accordance with appropriate security regulations.

2b. GROUP: Automatic downgrading is specified in DoD Directive 5200.10 and Armed Forces Industrial Manual. Enter the group number. Also, when applicable, show that optional markings have been used for Group 3 and Group 4 as authorized.

3. REPORT TITLE: Enter the complete report title in all capital letters. Titles in all cases should be unclassified. If a meaningful title cannot be selected without classification, show title classification in all capitals in parenthesis immediately following the title.

4. DESCRIPTIVE NOTES: If appropriate, enter the type of report, e.g., interim, progress, summary, annual, or final. Give the inclusive dates when a specific reporting period is covered.

5. AUTHOR(S): Enter the name(s) of author(s) as shown on or in the report. Enter last name, first name, middle initial. If military, show rank and branch of service. The name of the principal author is an absolute minimum requirement.

6. REPORT DATE: Enter the date of the report as day, month, year; or month, year. If more than one date appears on the report, use date of publication.

7a. TOTAL NUMBER OF PAGES: The total page count should follow normal pagination procedures, i.e., enter the number of pages containing information.

7b. NUMBER OF REFERENCES: Enter the total number of references cited in the report.

8a. CONTRACT OR GRANT NUMBER: If appropriate, enter the applicable number of the contract or grant under which the report was written.

8b, 8c, & 8d. PROJECT NUMBER: Enter the appropriate military department identification, such as project number, subproject number, system numbers, task number, etc.

9a. ORIGINATOR'S REPORT NUMBER(S): Enter the official report number by which the document will be identified and controlled by the originating activity. This number must be unique to this report.

9b. OTHER REPORT NUMBER(S): If the report has been assigned any other report numbers *(either by the originator or by the sponsor)*, also enter this number(s).

10. AVAILABILITY/LIMITATION NOTICES: Enter any limitations on further dissemination of the report, other than those imposed by security classification, using standard statements such as:

(1) "Qualified requesters may obtain copies of this report from DDC."

(2) "Foreign announcement and dissemination of this report by DDC is not authorized."

(3) "U. S. Government agencies may obtain copies of this report directly from DDC. Other qualified DDC users shall request through

_____."

(4) "U. S. military agencies may obtain copies of this report directly from DDC. Other qualified users shall request through

_____."

(5) "All distribution of this report is controlled. Qualified DDC users shall request through

_____."

If the report has been furnished to the Office of Technical Services, Department of Commerce, for sale to the public, indicate this fact and enter the price, if known.

11. SUPPLEMENTARY NOTES: Use for additional explanatory notes.

12. SPONSORING MILITARY ACTIVITY: Enter the name of the departmental project office or laboratory sponsoring *(paying for)* the research and development. Include address.

13. ABSTRACT: Enter an abstract giving a brief and factual summary of the document indicative of the report, even though it may also appear elsewhere in the body of the technical report. If additional space is required, a continuation sheet shall be attached.

It is highly desirable that the abstract of classified reports be unclassified. Each paragraph of the abstract shall end with an indication of the military security classification of the information in the paragraph, represented as *(TS), (S), (C), or (U)*.

There is no limitation on the length of the abstract. However, the suggested length is from 150 to 225 words.

14. KEY WORDS: Key words are technically meaningful terms or short phrases that characterize a report and may be used as index entries for cataloging the report. Key words must be selected so that no security classification is required. Identifiers, such as equipment model designation, trade name, military project code name, geographic location, may be used as key words but will be followed by an indication of technical context. The assignment of links, roles, and weights is optional.

UNCLASSIFIED

Security Classification